

**Some pages of this thesis may have been removed for copyright restrictions.**

If you have discovered material in Aston Research Explorer which is unlawful e.g. breaches copyright, (either yours or that of a third party) or any other law, including but not limited to those relating to patent, trademark, confidentiality, data protection, obscenity, defamation, libel, then please read our [Takedown policy](#) and contact the service immediately ([openaccess@aston.ac.uk](mailto:openaccess@aston.ac.uk))

VARIABLE IMPEDANCE BEARINGS FOR  
LARGE ROTATING MACHINERY

BY

MICHAEL JOHN GOODWIN BSc (HONS)

Submitted for consideration for the degree of  
Doctor of Philosophy  
of  
The University of Aston in Birmingham

DECEMBER 1981

ACKNOWLEDGMENTS

The author wishes to express his gratitude to:-

Dr J Penny, for acting as main supervisor and for his valuable guidance throughout the project.

Mr M Mudge, associate supervisor, for his help with the finite difference work and the statistical analysis of results.

Mr D Hickson, IHD Department of the University of Aston, for acting as personal tutor throughout the project.

Dr C Hooke, Department of Mechanical Engineering of Birmingham University, for his help with the theoretical analysis.

GEC Turbine Generators Ltd, Stafford, for sponsoring the work described in this thesis and in particular to Dr R Whitelaw and Mr C Heathcote for acting as industrial supervisors.

THE UNIVERSITY OF ASTON IN BIRMINGHAM

Variable Impedance Bearings for Large Rotating Machinery

Submitted by Michael John Goodwin for consideration for the degree of Doctor of Philosophy in December 1981.

This thesis describes an investigation which was carried out under the Interdisciplinary Higher Degrees (IHD) Scheme of The University of Aston In Birmingham. The investigation, which involved joint collaboration between the IHD scheme, the Department of Mechanical Engineering, and G.E.C. Turbine Generators Limited, was concerned with hydrostatic bearing characteristics and of how hydrostatic bearings could be used to enable turbine generator rotor support impedances to be controlled to give an improved rotor dynamic response.

Turbine generator rotor critical speeds are determined not only by the mass and flexibility of the rotor itself, which are relatively easily predicted, but also by the dynamic characteristics of the bearing oil film, pedestal, and foundations. It is because of the difficulty in accurately predicting the rotor support characteristics that the designer has a problem in ensuring that a rotor's normal running speed is not close to one of its critical speeds. The consequence of this situation is that some rotors do have critical speeds close to their normal running speed and the resulting high levels of vibration cause noise, high rotor stresses, and a shortening of bearing life.

A combined theoretical and experimental investigation of the effects of mounting the normal rotor journal bearing in a hydrostatic bearing was carried out. The purpose of the work was to show that by changing the oil flow resistance offered by capillaries connecting accumulators to the hydrostatic bearing, the overall rotor support characteristics could be tuned to enable rotor critical speeds to be moved at will.

Testing of a combined journal and hydrostatic bearing has confirmed the theory of its operation and a theoretical study for a full size machine showed that its critical speed could be moved by over 350 rpm and that its rotor vibration at running speed could be reduced by 80%.

Key words: Bearing  
Dynamic  
Hydrostatic  
Mechanical Impedance  
Turbogenerator

LIST OF CONTENTS

	<u>Page</u>
Acknowledgments	i
Summary	ii
List of Contents	iii
List of Figures	viii
Notation	xv
 <u>Chapter One : Introduction</u>	
1.1 Background to the problem	1
1.2 The proposed new design of rotor support	8
1.3 Project specifications and objectives	12
 <u>Chapter Two : Literature Survey</u>	
2.1 Journal bearings, their foundation and rotor response	14
2.2 Oil lubricated hydrostatic bearings	18
2.3 Modifications to bearing characteristics	26
 <u>Chapter Three : Theoretical Analysis of the Hydrostatic Bearing</u>	
3.1 Static characteristics of one hydrostatic bearing pad	41
3.2 Dynamic characteristics of one hydrostatic bearing pad	45
3.3 Operating coefficients for the complete hydrostatic bearing	53
3.4 Squeeze film damping effects	55
3.5 Confirmation of the accuracy of the 'mid-land' type of approximation	58

Chapter Four : Relevance of the Required Experimental  
Measurements

4.1	Test Objectives	64
4.2	General equations of motion	64
4.3	Experimental methods for measuring oil film coefficients	68
4.4	Oil film coefficients for the combined hydrodynamic and hydrostatic bearing	71

Chapter Five : Experimental Test Rig

5.1	General description	75
5.2	Test rotor description	79
5.3	Journal bearing	82
5.4	Hydrostatic bearing bush	82
5.5	Static loading	86
5.6	Dynamic loading	88
5.7	Lubricating system	89
5.8	Shaft speed controls	92
5.9	Calibration, instrumentation and data-logging	92
5.10	Aligning the journal and bearing bush	95
5.11	Run-out	95

Chapter Six : Theoretical and Experimental Results

6.1	Static characteristics of the journal bearing	97
6.2	Dynamic oil film coefficients for the journal bearing	97
6.3	Static characteristics of the hydrostatic bearing	102
6.4	Dynamic oil film coefficients for the hydrostatic bearing	
6.4a	theoretical results	114
6.4b	experimental results	123

	<u>Page</u>
6.5 Static characteristics of the combined journal and hydrostatic bearing	130
6.6 Dynamic oil film coefficients for the combined journal and hydrostatic bearing	151
6.7 Theoretical amplitude-frequency response of a typical generator rotor.	162
 <u>Chapter Seven : Accuracy of the Experimental Results</u>	
7.1 Oil viscosity	164
7.2 Journal speed	164
7.3 Specific loading	164
7.4 Bearing clearances	165
7.5 Sommerfeld number	165
7.6 Excitation frequency	165
7.7 Excitation force	166
7.8 Sensitivity of displacement transducers	166
7.9 Phase measurement	167
7.10 Pedestal vibration measurements	167
7.11 Measured oil film force coefficients	168
 <u>Chapter Eight : Discussion of the Theoretical and Experimental Results</u>	
8.1 Static characteristics of the journal bearing	170
8.2 Dynamic oil film coefficients for the journal bearing	171
8.3 Static characteristics of the hydrostatic bearing	172
8.4 Dynamic oil film coefficients for the hydrostatic bearing	
8.4a effect of hydraulic resistance ratio, $R_s/R_a$ , and accumulator operating parameter B	178
8.4b effect of oil inertia	186
8.4c effect of excitation frequency	191

	<u>Page</u>
8.5 Static characteristics of the combined journal and hydrostatic bearing	192
8.6 Dynamic oil film coefficients for the combined journal and hydrostatic bearing	193
8.7 Predicted effect of the hydrostatic bearing on the amplitude-frequency response of a generator rotor	195
 <u>Chapter Nine : Conclusions</u>	
9.1 The current situation	196
9.2 Static characteristics of the journal bearing	197
9.3 Dynamic oil film coefficients for the journal bearing	197
9.4 Static characteristics of the hydrostatic bearing	197
9.5 Dynamic oil film coefficients for the hydrostatic bearing	199
9.6 Static characteristics of the combined journal and hydrostatic bearing	200
9.7 Dynamic oil film coefficients for the combined journal and hydrostatic bearing	201
9.8 Influence of the hydrostatic bearing on rotor amplitude-frequency response	202
 <u>Chapter Ten : Recommendations</u>	
10.1 Further testing of the hydrostatic bearing	203
10.2 Possible improvements in restrictor design	205
10.3 Possible improvements in hydrostatic bearing design	207
10.4 Testing on a full size machine	209
10.5 Possible complications which should be investigated	209



	<u>Page</u>
List of References	212
Bibliography	219
<u>Appendix A : Design procedure for a combined hydrostatic and journal bearing</u>	221
<u>Appendix B : Computer Programs</u>	
I Hydrostatic bearing design program	230
II Two-oil-film bearing program	253
III Finite difference program	267
IV Bearing dynamic oil film coefficient program	281

- viii -  
LIST OF FIGURES

	<u>Page</u>
<u>Chapter One : Introduction</u>	
Fig 1.1 Trend of generator unit power output for machines ordered in Britain, 1950 - 1980	2
1.2 Critical speed curves for a typical 660 MW rotor	4
1.3 A typical large journal bearing bush (photograph)	6
1.4 A typical large turbine generator rotor (photograph)	7
1.5 Schematic of the proposed bearing design	10
 <u>Chapter Three : Theoretical Analysis of Hydrostatic Bearing</u>	
Fig 3.1 Diagram of a hydrostatic bearing pad	42
3.2 Diagram of the hydrostatic bearing oil way connections	46
3.3 General position of a hydrostatic bearing pad	54
3.4 Squeeze film at a bearing land	57
3.5 Plan of one hydrostatic pad	60
3.6 Plan of a hydrostatic pad corner	60
3.7 Comparison of bearing loads determined using analytical and numerical methods	61
3.8 Meshes used for the finite difference work	62
 <u>Chapter Four : Relevance of Required Experimental Measurements</u>	
Fig 4.1 Diagram of the bearing-pedestal system	66
4.2 Diagram of the two-oil-film bearing-pedestal system	72
 <u>Chapter Five : Experimental Test Rig</u>	
Fig 5.1 Diagram of the test rig	76
5.2 The assembled test rig (photograph)	77
5.3 The test rig control panel (photograph)	78
5.4 The main rotor assembly (photograph)	80
5.5 Half of the journal bearing bush (photograph)	83

	<u>Page</u>
5.6 Half of the hydrostatic bearing bush (photograph)	84
5.7 The assembled hydrostatic bearing bush (photograph)	87
5.8 The unbalanced mass assembly (photograph)	90
5.9 The oil supply power pack (photograph)	91
5.10 The data logging equipment (photograph)	94
 <u>Chapter Six : Theoretical and Experimental Results</u>	
Fig 6.1 Shaft Locus - Sommerfeld number relationship	98
6.2 Polar plot of the shaft locus (journal bearing only)	99
6.3 Nyquist diagram for the journal bearing, forward excitation	100
6.4 Nyquist diagram for the journal bearing, reverse excitation	101
6.5 Variation of journal bearing stiffness coefficient $K_{xx}$ with excitation frequency	103
6.6 Variation of journal bearing stiffness coefficient $K_{xy}$ with excitation frequency	104
6.7 Variation of journal bearing stiffness coefficient $K_{yx}$ with excitation frequency	105
6.8 Variation of journal bearing stiffness coefficient $K_{yy}$ with excitation frequency	106
6.9 Variation of journal bearing damping stiffness $\omega C_{xx}$ with excitation frequency	107
6.10 Variation of journal bearing damping stiffness $\omega C_{xy}$ with excitation frequency	108
6.11 Variation of journal bearing damping stiffness $\omega C_{yx}$ with excitation frequency	109

	<u>Page</u>
6.12 Variation of journal bearing damping stiffness $\omega C_{yy}$ with excitation frequency	110
6.13 Theoretical static vertical load - displacement relationship for the hydrostatic bearing bush	111
6.14 Experimental static vertical load - displacement relationship for the hydrostatic bearing bush	112
6.15 Theoretical vertical displacement - oil flow relationship for the hydrostatic bearing bush	113
6.16 Experimental vertical displacement - oil flow relationship for the hydrostatic bearing bush	115
6.17 Theoretical vertical displacement - oil pumping power relationship for the hydrostatic bearing bush	116
6.18 Theoretical influence of the accumulator on the hydrostatic bearing bush stiffness coefficient $K_{yy}$	117
6.19 Theoretical influence of the accumulator on the hydrostatic bearing bush stiffness coefficient $K_{xx}$	118
6.20 Theoretical influence of the accumulator on the hydrostatic bearing bush damping coefficient $C_{yy}$	119
6.21 Theoretical influence of the accumulator on the hydrostatic bearing bush damping coefficient $C_{xx}$	120
6.22 Theoretical variation of hydrostatic bearing bush stiffness coefficient with excitation frequency	121
6.23 Theoretical variation of hydrostatic bearing bush damping stiffness with excitation frequency	122
6.24 Theoretical variation of hydrostatic bearing bush stiffness coefficient $K_{yy}$ with oil inertia	124
6.25 Theoretical variation of hydrostatic bearing bush stiffness coefficient $K_{xx}$ with oil inertia	125

	Page
6.26 Theoretical variation of hydrostatic bearing bush damping coefficient $C_{yy}$ with oil inertia	126
6.27 Theoretical variation of hydrostatic bearing bush damping coefficient $C_{xx}$ with oil inertia	127
6.28 Theoretical effect of displacement and oil inertia on the hydrostatic bearing bush stiffness coefficient $K_{yy}$	128
6.29 Theoretical effect of displacement and oil inertia on the hydrostatic bearing bush damping coefficient $C_{yy}$	129
6.30 Nyquist diagram for the hydrostatic bearing, without accumulators, forward excitation	131
6.31 Nyquist diagram for the hydrostatic bearing, without accumulators, reverse excitation	132
6.32 Variation of hydrostatic bearing bush stiffness coefficient $K_{xx}$ with excitation frequency, (no accumulators)	133
6.33 Variation of hydrostatic bearing bush stiffness coefficient $K_{xy}$ with excitation frequency, (no accumulators)	134
6.34 Variation of hydrostatic bearing bush stiffness coefficient $K_{yx}$ with excitation frequency, (no accumulators)	135
6.35 Variation of hydrostatic bearing bush stiffness coefficient $K_{yy}$ with excitation frequency, (no accumulators)	136
6.36 Variation of hydrostatic bearing bush damping stiffness $\omega C_{xx}$ with excitation frequency, (no accumulators)	137

	<u>Page</u>
6.37 Variation of hydrostatic bearing bush damping stiffness $\omega C_{xy}$ with excitation frequency, (no accumulators)	138
6.38 Variation of hydrostatic bearing bush damping stiffness $\omega C_{yx}$ with excitation frequency, (no accumulators)	139
6.39 Variation of hydrostatic bearing bush damping stiffness $\omega C_{yy}$ with excitation frequency, (no accumulators)	140
6.40 Nyquist diagram for the hydrostatic bearing with accumulators, forward excitation	141
6.41 Nyquist diagram for the hydrostatic bearing with accumulators, reverse excitation	142
6.42 Variation of hydrostatic bearing bush stiffness coefficient $K_{xx}$ with excitation frequency, (with accumulators)	143
6.43 Variation of hydrostatic bearing bush stiffness coefficient $K_{xy}$ with excitation frequency, (with accumulators)	144
6.44 Variation of hydrostatic bearing bush stiffness coefficient $K_{yx}$ with excitation frequency, (with accumulators)	145
6.45 Variation of hydrostatic bearing bush stiffness coefficient $K_{yy}$ with excitation frequency, (with accumulators)	146
6.46 Variation of hydrostatic bearing bush damping stiffness $\omega C_{xx}$ with excitation frequency, (with accumulators)	147

6.47	Variation of hydrostatic bearing bush damping stiffness $\omega C_{xy}$ with excitation frequency, (with accumulators)	148
6.48	Variation of hydrostatic bearing bush damping stiffness $\omega C_{yx}$ with excitation frequency, (with accumulators)	149
6.49	Variation of hydrostatic bearing damping stiffness $\omega C_{yy}$ with excitation frequency, (with accumulators)	150
6.50	Nyquist diagram for the combined bearing, forward excitation	152
6.51	Nyquist diagram for the combined bearing, reverse excitation	153
6.52	Variation of combined bearing stiffness coefficient $K_{xx}$ with excitation frequency	154
6.53	Variation of combined bearing stiffness coefficient $K_{xy}$ with excitation frequency	155
6.54	Variation of combined bearing stiffness coefficient $K_{yx}$ with excitation frequency	156
6.55	Variation of combined bearing stiffness coefficient $K_{yy}$ with excitation frequency	157
6.56	Variation of combined bearing damping stiffness $\omega C_{xx}$ with excitation frequency	158
6.57	Variation of combined bearing damping stiffness $\omega C_{xy}$ with excitation frequency	159
6.58	Variation of combined bearing damping stiffness $\omega C_{yx}$ with excitation frequency	160
6.59	Variation of combined bearing damping stiffness $\omega C_{yy}$ with excitation frequency	161

6.60	Theoretical effect of the hydrostatic bearing on the response of a generator rotor	163
------	---	-----

Chapter Eight : Discussion of Theoretical and Experimental

Results

Fig 8.1	Acceleration, velocity, and displacement phase relationships for an oscillating body	182
---------	---	-----

8.2	Effect of oil inertia on the pressure rise vector in a hydrostatic pocket	189
-----	--	-----

Appendix A : Design Procedure for the Hydrostatic Bearing

Fig A-1	Diagram of a hydrostatic bearing bush	225
---------	---------------------------------------	-----

A-2	Output from the two-oil-film bearing program	228
-----	--	-----



NOTATION

A	Effective area of one hydrostatic bearing pad.
a	Cross-sectional area of a capillary tube.
B	Accumulator operating parameter denoting the increase in accumulator pressure per unit volume of fluid flowing into the accumulator.
C	Damping coefficient, generally.
$C_{ij}$	Dynamic damping coefficient denoting the force in the i direction per unit velocity in the j direction.
c	Film clearance.
$c_o$	Design film clearance.
D	Damping.
e	Eccentricity of the shaft (ie either the journal or the floating ring) relative to its bearing bush.
F	Force
$F_x$	Force in the x direction (horizontal)
$F_{x\ell}$	Force in the local x direction.
$F_{xo}$	Force amplitude in the horizontal direction.
$F_{x1}$	Real force amplitude in the horizontal direction.
$F_{x2}$	Imaginary force amplitude in the horizontal direction.
$F_y$	Force in the y direction (vertical)
$F_{y\ell}$	Force in the local y direction.
$F_{yo}$	Force amplitude in the vertical direction.
$F_{y1}$	Imaginary force amplitude in the vertical direction.

$F_{y2}$	Real force amplitude in the vertical direction.
$[ F ]$	Force matrix.
$I_a$	Inertia coefficient for oil in the accumulator line.
$I_s$	Inertia coefficient for oil in the supply line.
$K_a$	Inverse viscous flow resistance in the accumulator oil line.
$K_s$	Inverse viscous flow resistance in the supply oil line.
$K_{ij}$	Dynamic stiffness coefficient denoting the force in the $i$ direction per unit displacement in the $j$ direction.
$[ K_e ]$	Equivalent single bearing oil film stiffness matrix.
$[ K_h ]$	Hydrostatic bearing oil film stiffness matrix.
$[ K_j ]$	Journal bearing oil film stiffness matrix.
$L$	Length of a hydrostatic pocket from land centre-line to land centre-line.
$l$	Length of land subjected to a squeeze film.
$l'$	Length of capillary in which oil inertia is significant.
$M$	Journal effective mass.
$m$	Mass of oil in a capillary
$N$	Journal rotational frequency.
$P$	Oil pumping power.
$p$	Pressure.
$p'$	Bearing load per unit projected area.
$p_a$	Pressure of oil in the accumulator.
$p_\alpha$	Hydrostatic bearing drain oil pressure.
$p_p$	Hydrostatic bearing pocket oil pressure.

$p_s$	Hydrostatic bearing supply oil pressure.
$p_{po}$	Hydrostatic bearing pocket steady (mean) oil pressure.
$Q$	Oil volume flow rate.
$Q_a$	Oil flow out of the hydrostatic bearing pocket into the accumulator.
$Q_x$	Oil flow out of the hydrostatic bearing pocket over the lands.
$Q_s$	Oil flow into the hydrostatic bearing pocket from the supply.
$Q_v$	Oil flow into the volume swept out by one hydrostatic bearing surface as it moves away from its opposing surface.
$Q_{ao}$	Steady (mean) oil flow out of the hydrostatic bearing pocket into the accumulator.
$Q_{so}$	Steady (mean) oil flow into the hydrostatic bearing pocket from the supply.
$R$	Bearing radius of curvature.
$R_a$	Viscous flow resistance in the accumulator oil line.
$R_s$	Viscous flow resistance in the supply oil line.
$r$	Journal radius.
$S$	Stiffness
$S'$	Sommerfeld number.
$t$	Time interval.
$[u]$	Journal bearing displacement matrix.
$[v]$	Hydrostatic bearing displacement matrix.
$[w]$	Equivalent single bearing displacement matrix.
$x$	Horizontal amplitude of vibration relative to the pedestal.
$x_p$	Pedestal vibration amplitude in the horizontal direction relative to space.

$X_1$	Horizontal vibration amplitude of the shaft relative to the pedestal, component in phase with the horizontal force.
$X_2$	Horizontal vibration amplitude of the shaft relative to the pedestal, component out of phase with the horizontal force.
$X_{1y}$	Component of vibration in the horizontal direction which is in phase with Y.
$X_{2y}$	Component of vibration in the horizontal direction which is out of phase with Y.
$x$	Displacement in the x direction (horizontally) relative to the pedestal.
$x_\ell$	Displacement in the local x direction relative to the pedestal.
$x_p$	Horizontal displacement of the pedestal relative to space.
$Y$	Vertical amplitude of vibration relative to the pedestal.
$Y_p$	Pedestal vibration amplitude in the vertical direction relative to space.
$Y_1$	Vertical vibration amplitude of the shaft relative to the pedestal, component out of phase with the horizontal force.
$Y_2$	Vertical vibration amplitude of the shaft relative to the pedestal, component in phase with the horizontal force.
$y$	Displacement in the y direction (vertically) relative to the pedestal.
$y_\ell$	Displacement in the local y direction relative to the pedestal.
$y_p$	Vertical displacement of the pedestal relative to space.
$\alpha$	Half angle of a hydrostatic pocket between the pocket centre-line and the land centre-line.

- $\alpha_1$  Phase lag of the shaft horizontal displacement relative to the pedestal behind the horizontal force.
- $\alpha_2$  Phase lag of the shaft vertical displacement relative to the pedestal behind the vertical force.
- $\beta$  Ratio  $p_{po}/p_s$  when the floating ring (journal bearing bush) is in its design operating position.
- $\gamma_{a1}$  Component of accumulator pressure amplitude in phase with Y.
- $\gamma_{a2}$  Component of accumulator pressure amplitude out of phase with Y.
- $\gamma_1$  Phase lag of the pedestal horizontal displacement relative to space behind the horizontal force.
- $\gamma_2$  Phase lag of the pedestal vertical displacement relative to space behind the vertical force.
- $\Delta$ - Denoting a change or difference of the following parameter.
- $\delta$  Angle of inclination of one hydrostatic bearing pad.
- $\epsilon$  Ratio of shaft eccentricity to bearing radial clearance.
- $\epsilon_1$  Component of hydrostatic pocket pressure amplitude in phase with Y.
- $\epsilon_2$  Component of hydrostatic pocket pressure amplitude out of phase with Y.
- $\theta$  General position of an element of one hydrostatic bearing pad.
- $\theta'$  Phase of force in the vertical direction relative to displacement in the vertical direction.
- $d\theta$  Element of one hydrostatic bearing pad.
- $\theta_{1,2,3}$  Phase lead of the hydrostatic bearing pocket pressure over the displacement of the journal bearing bush.

- $\mu$  Oil dynamic viscosity.
  - $\rho$  Mass density of the oil.
  - $\Psi_1$  Component of oil flow in the supply line in phase with Y.
  - $\Psi_2$  Component of oil flow in the supply line out of phase with Y.
  - $\phi$  Attitude angle of the shaft relative to its bearing bush.
  - $\phi'$  Phase lag of the horizontal displacement relative to the vertical displacement.
  - $\Psi_1$  Component of oil flow in the accumulator line in phase with Y.
  - $\Psi_2$  Component of oil flow in the accumulator line out of phase with Y.
  - $\omega$  Angular frequency.
  - $\dot{\phantom{x}}$  Denotes derivative with respect to time.
  - $\ddot{\phantom{x}}$  Denotes double derivative with respect to time.
- 

Note: Amplitudes are always 'centre-to-peak' values.

## CHAPTER ONE

### INTRODUCTION

1.1 Background to the Problem

The first high speed ac generator was developed in 1888 by C A Parsons. Its success resulted in the first 'alternators' being put into production the following year, having a rating of 75 KW, single phase at 1000 V. Only 23 years later, in 1912, the possible output from one of Parsons' machines had risen to 25 MW, representing an increase in output of well over 300 times. In the following years the demand for electricity continued to rise, albeit at a slower rate, and by 1930 the output of the largest generator in England, running at 3000 rpm, was 50 MW.

The rise in output demanded from a machine is reflected in the basic design of the rotor. The easier construction of salient pole machines may be utilised for machines of low power rating and low speed because low stress levels are encountered. For machines having a higher power output, however, the limitations of size, weight, and economics may determine that rotors should have two poles, and hence run at 3000 rpm to give a 50 Hz supply. Because of the higher operating speeds of two pole machines, the normal running speed for the machine is nearly always above the first 'critical speed' of the rotor.

The increase in generator output per unit from 1950 onwards is shown in fig 1.1. With the steady increase in size of generators, the rotor length/diameter ratio also necessarily increased even for four pole machines, with the result that many machines now operate with their second, and sometimes third, criticals below running speed. It should be understood at this stage that it is of the utmost importance that the normal running speed of a generator rotor should be away from any of its critical speeds. If this is not the case then high vibration levels are encountered with corresponding high noise levels, rapid wear of



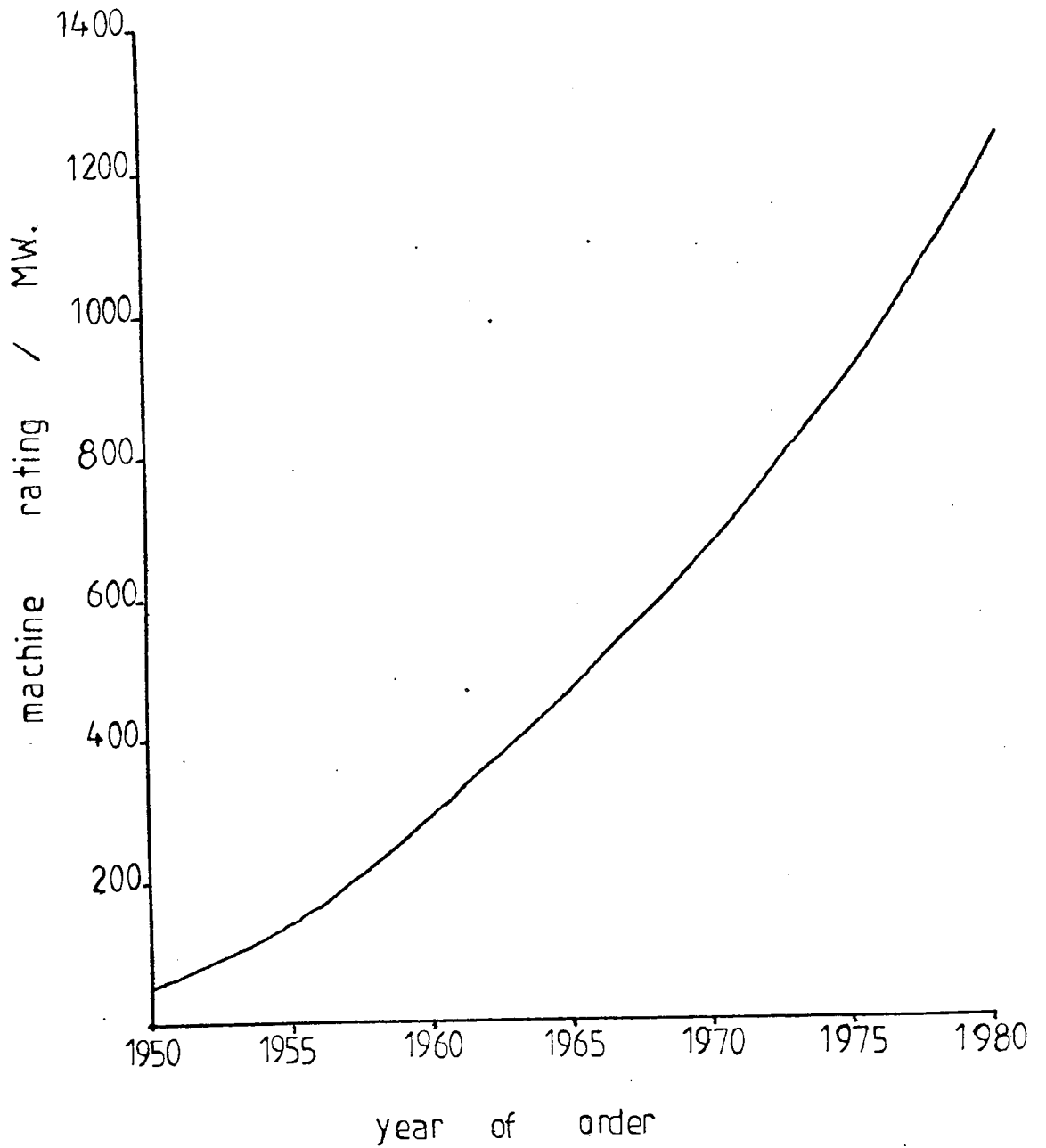


FIG. 1.1 TREND OF GENERATOR UNIT POWER  
OUTPUT FOR MACHINES ORDERED IN  
BRITAIN , 1950 - 1980.

bearings, and higher stress levels in the rotor.

Against the above background it can be understood that extreme accuracy of critical speed calculation and of balancing are vital if vibration free running is to be ensured, both as an isolated rotor during testing, and as a coupled unit with the turbine and exciter on their respective foundations in service. As bearing spans and rotor length/diameter ratios have increased it has become essential to allow for the effects of flexibility of the bearings, of their support structure and of the oil film in order to correctly estimate a rotor's critical speeds. While numerical calculations of sets of eight coefficients describing the behaviour of the oil film under various running conditions are becoming commonplace, there is often inadequate knowledge of values of the all important variables representing bearing pedestal and foundation stiffness and damping. Fig 1.2 shows, for one rotor, how significant the rotor support stiffness is in the determination of a rotor's critical speeds; these curves are presented for excitation frequencies to over 6000 rpm since forcing at twice running speed can occur due to unequal moments of inertia across different diameters.

The present alternatives for dealing with the problem of a rotor critical speed occurring near to normal running speed are not satisfactory. They may include, (i) accepting the excessive vibration near to running speed with the resultant shortening of bearing life and increase of noise level, (ii) rebalancing of the rotor in an attempt to cut down exciting force; this is expensive, time consuming, and not always successful, (iii) deliberately misaligning the bearing bush relative to the rotor so as to alter the effective bearing coefficients and hence change the rotor critical speed; this would result in considerable and uneven wear on both bearing surfaces, and (iv) changing the lubricating oil to one having different properties. This, however, undermines the

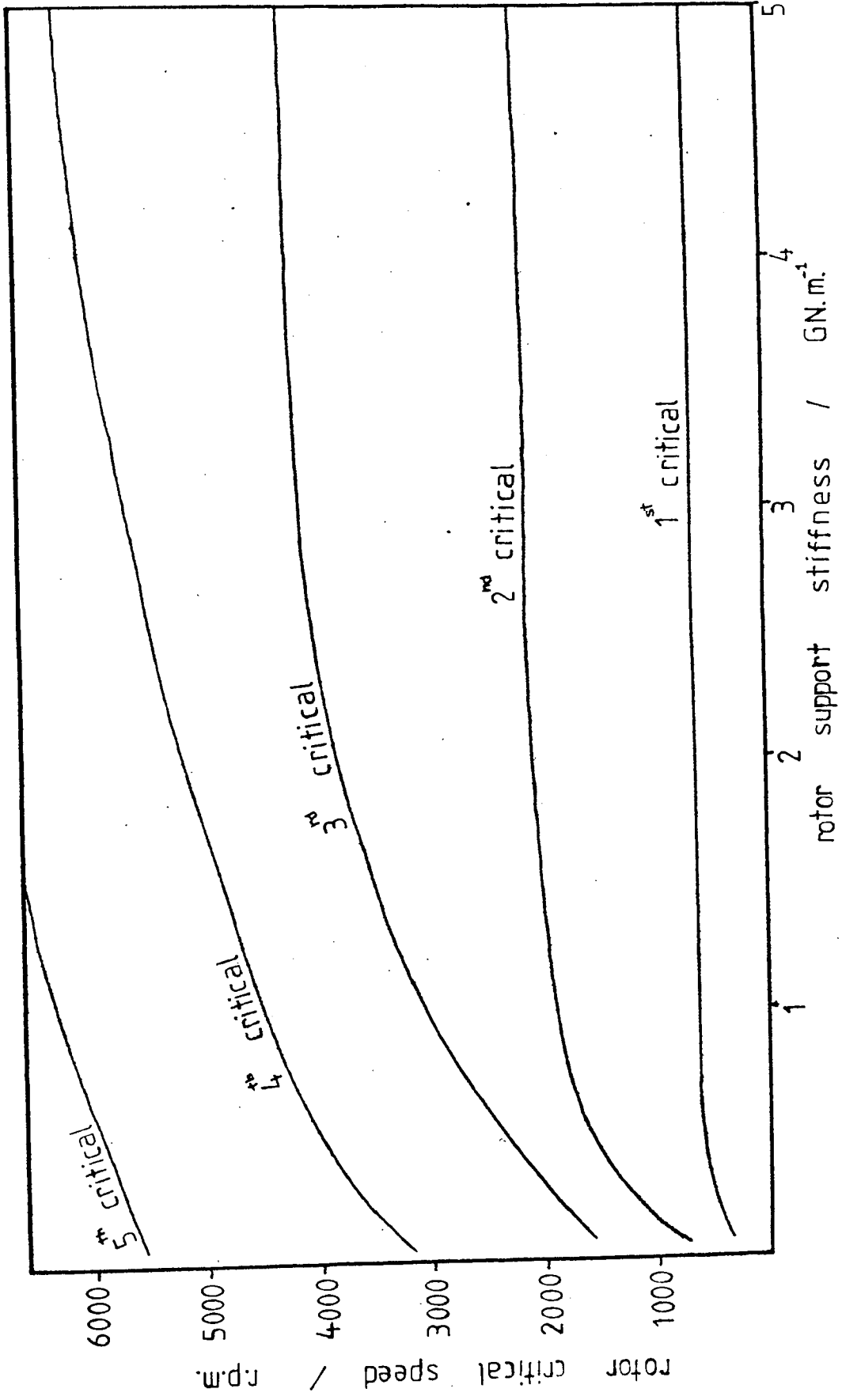


FIG 1.2 CRITICAL SPEED CURVES FOR A TYPICAL 660 MW ROTOR

reasons for selecting the oil in the first instance (ie, heat transfer, resistance to oxidation, viscosity high enough to provide a lubricating film, viscosity low enough to ensure moderate bearing losses, etc).

Changing the bearing (v) to one giving a different performance is another alternative, but again this is expensive and time consuming.

The investigation described in this thesis is an attempt to overcome the problems associated with inadequate knowledge of pedestal and foundation behaviour. The study involved the design and testing of a rotor support whose impedance might easily be altered should it be found, during commissioning of a generator set or during works testing, that the rotor behaviour is somewhat different from that predicted and desired.

At this stage a description of a typical generator rotor bearing, shown in figure 1.3, is appropriate. For a standard bearing the active part of the bush consists of an arc, usually of  $120^{\circ}$  subtended angle. The further  $240^{\circ}$  of the bearing bush is relieved in order to reduce losses in the bearing. Oil normally enters the bearing at one or two ports at either end of the bearing arc at low pressure, typically about 0.15 MPa (20 lb f/in<sup>2</sup>). At the oil port there is an axial distribution groove into which the oil flows before being 'dragged' by the rotating journal into the bearing arc itself. Once inside the bearing arc, the oil pressure is built up to support the journal by hydrodynamic action of the rotating journal itself. From here, the oil may then flow further around the bearing arc and exit through an outlet port, or flow axially out of the bearing bush to be caught in a drain area. Note that there are a series of oil wipers mounted at either end of the bearing bush which act with throwers on the journal to restrict oil flow out of the bearing pedestal assembly. From the drain area the oil is pumped, via coolers, back to a supply tank. Figure 1.4 shows a

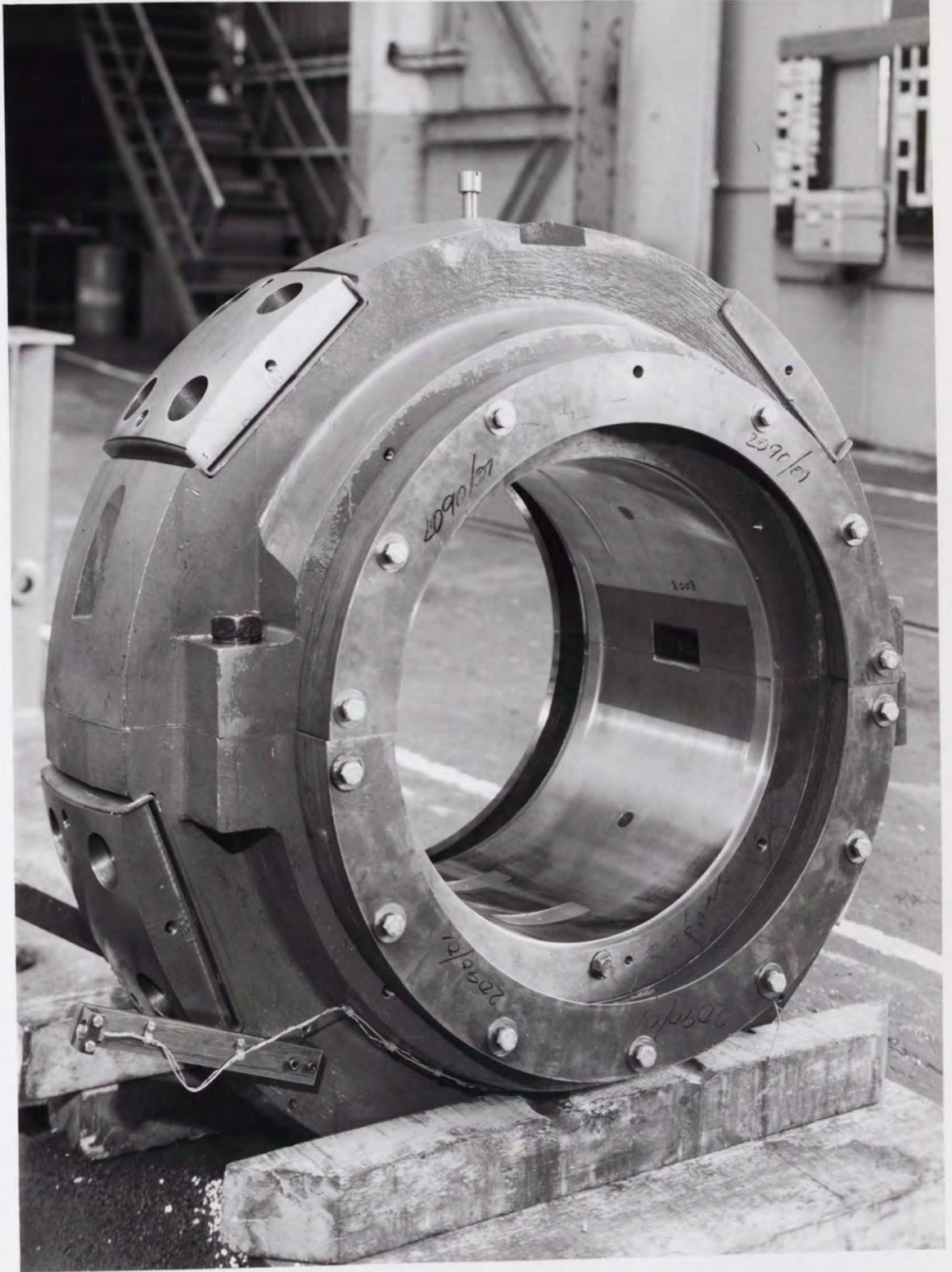


FIG 1.3 A TYPICAL LARGE JOURNAL BEARING BUSH



FIG 1.4 A TYPICAL LARGE TURBINE GENERATOR ROTOR

generator rotor, typical of the design supported by the bearing shown in figure 1.3.

## 1.2 The Proposed New Design of Rotor Support

The object of the investigation is to develop a procedure which may be followed by engineers wishing to design a bearing with an in-built facility to alter the operating characteristics of the bearing at will, in an easy and controlled manner. A bearing with such a feature would help to remove the problems associated with critical speed vibrations occurring at rotor running speed since the critical speed could effectively be shifted to occur at some other frequency, remote from the running speed.

Methods of changing the operating characteristics of a rotor support which were considered are, (i) changing the mechanical fixing of the bearing bush pedestal to earth, ie effectively introducing a very stiff spring between the pedestal and earth, (ii) modifying the oil film operating characteristics by providing high pressure oil inlet at various positions around the circumference of the bearing bush, ie using a form of hybrid bearing, and (iii) introducing a second, hydrostatic, oil film around the conventional hydrodynamic oil film, the two films being separated by a non-rotating steel separating ring.\*

The first alternative considered was dismissed, however, because of its inherent disadvantage of changing support stiffness only in one sense (ie the vertical sense, if the pedestal was connected to earth by feet on its top or bottom surface). The choice between the second and third alternatives was a more difficult decision since their relative advantages and disadvantages are not obvious.

---

\* The proposed combination of a journal and hydrostatic bearing may, in subsequent chapters, be referred to as the "combined bearing", or the "two oil film bearing" (ie the hydrodynamic and the hydrostatic oil film).

It was ultimately decided that work should continue with alternative (iii) since this was more likely to enable operating characteristics (ie bearing stiffness and damping coefficients) to be altered without undesired side-effects such as changing oil flow rate, altering effective eccentricity ratio etc. Furthermore, it was felt that this design held more promise to alter horizontal and vertical bearing coefficients independently, if separate hydrostatic pockets\* were utilised at the top, bottom, and sides of the hydrostatic oil film.

Figure 1.5 shows a schematic section of the bearing design proposed. The conventional hydrodynamic oil film is separated from the hydrostatic bearing oil film by the non-rotating steel ring<sup>‡</sup>. Oil enters and leaves the hydrodynamic bearing in the normal way discussed in section 1.1. The drain oil from the hydrodynamic film may or may not mix with oil draining from the hydrostatic bearing. For the model built for the project, separate drains were utilised, showing that the use of different oils and temperatures for the two bearings is not unrealistic. Oil enters the hydrostatic bearing pockets, at the top, bottom and on each side of the hydrostatic bearing bush, from a constant pressure supply of 2.8 MPa (about 400 lb f/in<sup>2</sup>) via restrictors. Oil then flows from the hydrostatic pockets over the lands surrounding the pocket and out to a drain area, from which it is pumped back to a supply tank.

---

\* The term 'hydrostatic pocket' refers to the active bearing area contained within a length of land, the land forming a closed boundary around the pocket. The term 'hydrostatic pad' refers to the hydrostatic pocket plus its surrounding land, both being load bearing areas.

‡ For a combined journal and hydrostatic bearing the journal bearing bush effectively floats between the hydrodynamic and hydrostatic oil films. For this reason it may subsequently be referred to as the 'floating ring' or 'separating ring'.



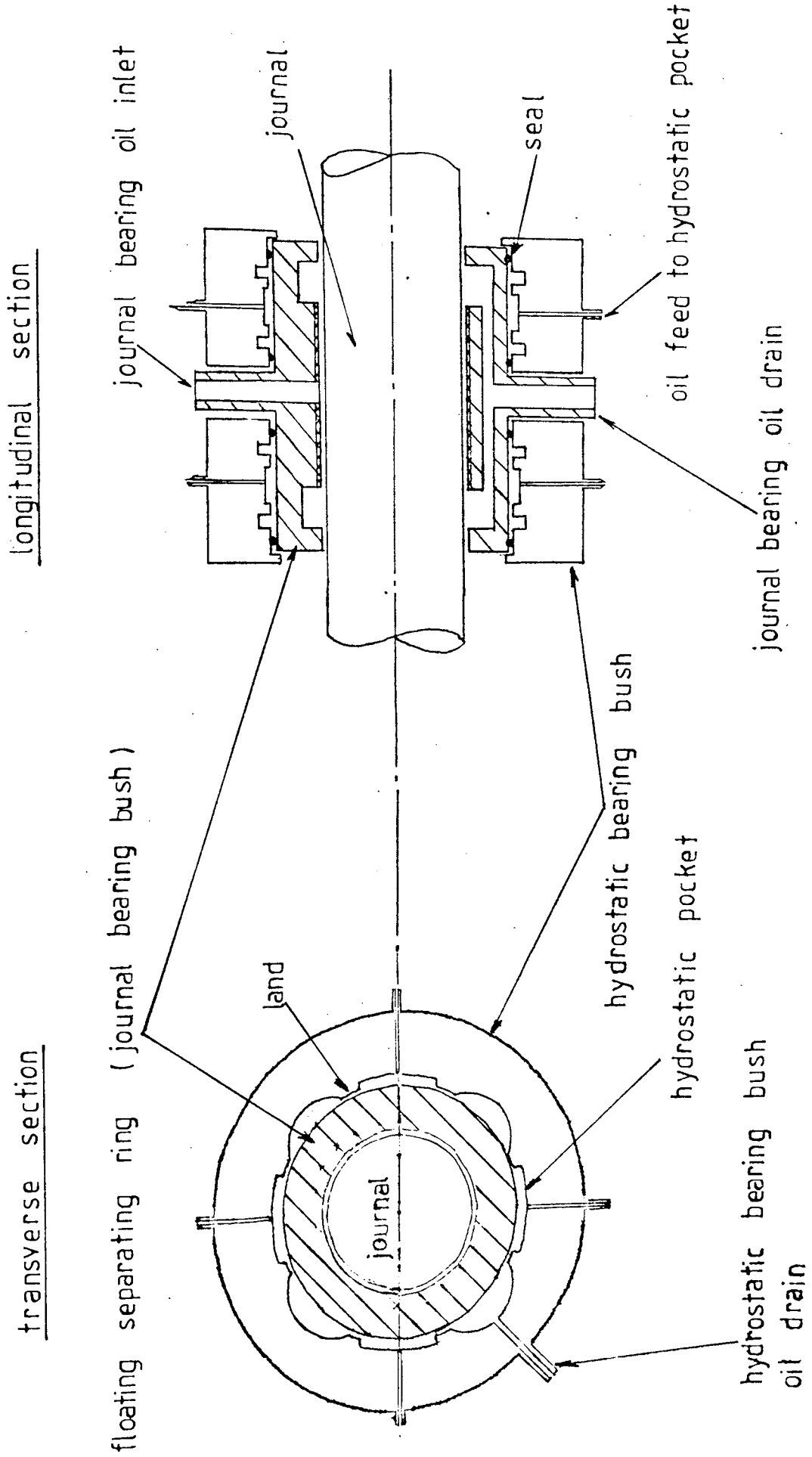


FIG 1.5 SCHEMATIC OF THE PROPOSED BEARING DESIGN

The misalignment of the steel separating ring with the hydrostatic bearing bush and the rotor journal is restricted because there is one set of four hydrostatic pockets (spaced circumferentially) at each end of the bush. This means that should the ring become displaced more at one end of the hydrostatic bush than the other, then the appropriate pressure changes occur in only the set of hydrostatic pockets at that end of the bush, and hence a resisting moment is applied to the ring by forces acting at that set of hydrostatic pockets.

Under normal circumstances, where no critical speed problems are evident, the oil supply to the hydrostatic bearing would be turned off, and the steel separating ring clamped rigidly to the hydrostatic bearing bush. This would allow the rotor support to behave as normal, and only the hydrodynamic oil film would be active. If it was desired that the rotor support characteristics be changed, however, for example in order to move a critical speed away from running speed, then the steel separating ring would be released and the hydrostatic bearing would also be used. This would effectively reduce the support impedance of the generator rotor in both the horizontal and vertical directions. Note also that accumulators may be connected, via hydraulic resistances, to each hydrostatic pocket. The purpose of these accumulators would be to allow manipulation of the dynamic operating characteristics of the rotor support without affecting the static characteristics. That is, the stiffness and damping of the hydrostatic bearing could be altered by reducing the hydrostatic bearing supply pressure for example, but this would also mean that the static pocket pressures would also be lower and the eccentricity of the separating ring would increase. With the accumulators in the system however, and maintaining the same supply pressure, pulsations of pocket pressures are partly eliminated since instead of considerably changing its

pressure in the pocket, the oil flows to and from the accumulator. Designing an accumulator into the system, then, allows a change in dynamic stiffness and damping coefficients without affecting the hydrostatic bearing oil supply and hence the static characteristics of the bearing. Furthermore, the hydraulic resistances and the accumulator operating parameter are two important parameters which can be used to control the amount by which the dynamic operating characteristics of the rotor are changed when the hydrostatic bearing is introduced to the system.

It should also be noted, that the suggested bearing design does have its limitations and disadvantages. The design is of little help to the problem where the rotor critical speed occurs such that the rotor 'free-free' mode shape\* exhibits nodes at the rotor supports. If this is the case then altering the support stiffness and damping will have little effect on the rotor vibration amplitudes away from the nodes since the rotor journal will not be tending to vibrate relative to the pedestal anyway. Other disadvantages are that it involves the manufacture and maintenance of two bearings (hydrodynamic and hydrostatic) at each rotor support, which will be more time consuming and more expensive, and that the presence of the hydrostatic bearing and separating ring introduces more unreliability to the rotor support system.

### 1.3 Project Specification and Objectives

The project specification is very much linked to the design specification given that the development of the bearing design outlined in section 1.2 is the basis of the work.

---

\* The rotor 'free-free' mode shape refers to harmonic modes of vibration of the rotor when it is not held by any supporting mechanism.

Procedures and guidelines for the design of hydrodynamic journal bearings are already commonplace, and so the main body of the project was concerned with the development of the theory relating to the hydrostatic bearing and a method by which calculated oil film coefficients of the hydrostatic bearing could be 'added' to oil film coefficients describing the journal bearing behaviour, thus giving an indication of the net bearing characteristics. The design and manufacture of a test-rig used to verify the theory was also of paramount importance.

The initial specification of the hydrostatic bearing was that it should have dynamic stiffness and damping coefficients such that a critical speed shift of about 400 rpm would be possible. The order of magnitude of support stiffness change to be effected by the introduction of the hydrostatic bearing is indicated by figure 1.2 where it can be seen that, for the rotor considered, a support stiffness change of about  $0.6 \text{ GN.m}^{-1}$  ( $3 \text{ lb f/in}$ ) may shift the critical speed by 400 rpm. It will be shown in subsequent chapters, however, that provided the hydrostatic bearing has a nominally high impedance, then the required reduction in oil film stiffness and damping can be obtained by manipulating the accumulator operating parameter, and accumulator hydraulic resistance, leaving the basic hydrostatic bearing design to be governed by static operating conditions.

To summarise, the project aims were (a) to establish a method for designing a bearing support that could be used to optimise the dynamic behaviour of a turbine generator rotor. (b) To substantiate the theory by experimental evidence. (c) To show how such a bearing could improve the dynamic characteristics of a large rotor. (d) To suggest further experimental work and further developments of the bearing.

CHAPTER TWO

LITERATURE SURVEY

CHAPTER TWO

LITERATURE SURVEY

2.1 Journal Bearings, Their Foundation and Rotor Response

The functioning of journal bearings began to be understood in 1886 when Reynolds (1) explained the presence of a pressurised oil film between a journal and its bearing bush, discovered three years earlier by Towers (2). Prior to 1883, surface to surface contact had been thought to exist as part of the normal operating conditions.

Interest in the modelling of the oil film under dynamic excitation has grown considerably since the 1920's when Stodola (3) was able to show that under such circumstances the oil film behaved elastically and that such elasticity was significant enough to reduce rotor critical speeds below those calculated on the basis of rigid rotor supports.

The complexity of such models increased steadily. In 1956, Hagg and Sankey (4) modelled the oil film with two spring coefficients, but introduced also two damping coefficients. These were the first elastic and damping properties of oil films to be published, but could only be applied to rotors having similar operating conditions to those investigated by Hagg and Sankey, that is synchronous vibration and no cross-coupling.

The work of Hagg and Sankey may be contrasted with later attempts by many authors (5-8) being some, using eight coefficients. The results of these investigations are generally inconclusive, however, since they are often based on unqualified simplifying assumptions, are valid for only one bearing geometry, or contradict other similar papers. These papers usually assume complete linearity of the oil film over the working range and neglect journal misalignments.

In 1976, Bannister (9) published the results of his work on the

measurement of the dynamic oil film force coefficients for a 5" diameter journal bearing, giving both theoretical and experimental results indicating the effects of non-linearity and misalignment. He concluded that the eight linearised oil film force coefficients may be used to predict journal whirl trajectory to an accuracy of 6% provided that the major vibration amplitude is less than 15% of the bearing radial clearance and that the frequency of excitation is less than 50% of the journal rotational frequency. Otherwise, twenty-eight coefficients, taking non-linearity into account, were recommended. Bannister's results also show a significant decrease in rotor whirl amplitude when the journal is misaligned in the bearing bush. Bannister's work shows very good agreement of his experimental results with his theory and his recommendations may therefore be taken as important guidelines when measuring the eight linearised oil film force coefficients experimentally.

Design guidelines covering the static characteristics of journal bearings are well recorded. Raimondi and Boyd (10) in 1958, presented design curves for a range of bearing arcs. Their paper is well complemented by that of Martin (11) whose 1974 paper considers plain bearings in particular but also takes into account journal misalignment.

Accurate modelling of journal bearing dynamic operation is not the only consideration necessary to predict the dynamic response of a flexible rotor, however. It is important to recognise how the rotor support characteristics interact with the flexibility of the rotor to determine the rotor critical speeds.

In 1962, Lund and Sternlicht (5) presented a theoretical analysis of the response of a symmetrical rotor with a central point mass supported in two plain journal bearings. A finite difference technique was used to solve Reynold's equation and determine the eight bearing coefficients.

These were then taken into account with the rotor flexibility and mass to determine the force transmitted at the bearing pedestal for a range of exciting frequencies. Results showed an attenuation of force transmitted to the bearing pedestal by the presence of the oil film, as compared to rigid rotor mountings. The paper concludes that for maximum force attenuation it is desirable to run the bearings operating at a low eccentricity ratio, low stiffness and high damping. It is also stated, however, that these conditions imply a low critical speed and a tendency for resonant whip.

Lund's paper reaffirms the fact already widely known by engineers, that oil film type journal bearings lower the critical speeds of a rotor system and maintain vibration at criticals to a low and usually safe level. The usefulness of the work presented is limited, however, by the assumptions of plain bearings, symmetrical rotor and point mass. Plain bearings are not common in the turbine generator industry, whilst generator rotors are only nominally symmetrical, furthermore the high length/diameter ratio of many rotors makes the point mass assumption invalid.

In 1972, Kirk and Gunter (12) carried out a theoretical analysis of the effects of using a flexible bearing foundation on rotor resonant frequencies. Results were again presented for a single mass flexible rotor for various values of foundation impedance, and showed that with correct tuning of the foundation characteristics, the rotor resonant frequencies could be moved and/or the vibration amplitudes considerably reduced. Furthermore, Kirk argued that for low values of support mass, the required value of optimum damping is not critical and can vary by a factor of ten without appreciably affecting rotor performance.

Kirk's work is a significant step towards recognising the importance of the dynamic operation of the foundations on which the bearing is mounted.



Unfortunately, Kirk's model assumes rigid bearings which is obviously inapplicable to generator rotor bearings. Furthermore, the work would need to be extended to take into account a multimass rotor and confirmed experimentally before it can be used seriously as a design basis for the turbine generator industry.

A further paper indicating the significance of generator rotor bearing foundation impedance was published by Gasch (13) in 1976. Gasch presents a finite element method of modelling the rotor, enabling a realistic mass distribution to be used to predict its dynamic response. In his analysis, Gasch considered the receptances of the oil film and foundation to be acting as connected in series and added them accordingly to produce a single receptance for the complete shaft support. This is in accordance with the method used by the author in his analysis. Gasch deduced from his work that the foundation dynamics are particularly important when the foundation natural frequency is in close proximity to that of the shaft. To support this conclusion he presented two sets of response curves for a vertical water turbine generator, with generator foundation natural frequencies of 40 Hz and 20 Hz. The curves show a decrease in generator first resonant frequency of about 500 rpm with the decrease in foundation natural frequency, while the actual amplitudes of vibration remain reasonably constant.

Although presenting a thorough mathematical analysis of the system, Gasch fails to put forward a physical explanation of why the generator resonant frequency is altered but response amplitude away from the critical is not altered. Furthermore, it is not clear exactly how much changes in support stiffness and damping independently alter dynamic response.

It is clear from the papers discussed above that confusion still exists

surrounding accurate modelling of a journal bearing under dynamic excitation. It is apparent, however, that the dynamic operation of the bearing and the foundation of that bearing plays an important part in the dynamic response of the rotor itself. It is also apparent that an ability to alter the impedance of the support foundation effectively alters the impedance of the supports as felt by the rotor, thus enabling control over the rotor dynamic response. It is this evidence, then, that provides part of the background to the work contained in this thesis.

## 2.2 Oil Lubricated Hydrostatic Bearings

In view of the fact that the proposed bearing design with which the project is concerned incorporates a number of hydrostatic bearings, it is pertinent to discuss here recent developments in hydrostatic bearing design.

The static characteristics of hydrostatic bearings have been well-documented since the late 1950's, some of the more notable authors being Raimondi and Boyd (14) and Rippel (15). These investigations cover a wide range of pad geometries and include calculations of bearing static load, oil flow, static stiffness and pumping power, for bearings which normally have either orifice or capillary restrictors. Methods of assessing oil pressure at various positions in the hydrostatic film ( and hence assess load carried by the bearing) include exact (15) and approximate (14) analytical, finite difference (16) and electrical analogue (17) methods. Raimondi and Boyd's approximation, assuming constant pocket pressure and an effective bearing area defined by the centre line of the land surrounding the pocket, is now generally accepted as giving reasonable accuracy for most applications. This approximation does not completely take into account flow irregularities

over lands at the corners of rectangular pocket bearings and depends on the magnitude of the land width as compared with the pocket dimensions for its accuracy. It is used by the author in his theoretical analysis, and the accuracy confirmed by a finite difference technique.

Other authors have attempted to modify bearing characteristics by using special restrictors for the oil to flow through before entering the hydrostatic pocket, rather than the simple orifice or capillary. Such restrictors include constant flow valves and pressure sensing valves all aimed at increasing the load-carrying ability and static stiffness. Some of these special valves are discussed in O'Donoghue and Rowe's paper (18) which also gives design procedures, on the basis of static characteristics, for hydrostatic bearings of various geometries.

More recent attempts to design special restrictors include those by Davies (19), Bassani (20) and Singh (21). Davies in 1973, examined experimentally and theoretically the possibility of using an all-metallic flexible plate as one surface of the hydrostatic bearing, thus eliminating the need for any entrance restrictor. The bearing was intended to derive its stiffness from the fact that when the bearing load is increased, the increase in oil pressure on the pocket causes the flexible surface to move further away from the other bearing surface, particularly near the centre of the pocket, thus providing less resistance to oil flow. This enabled the high pocket pressure region of the bearing to increase in area as the effective land width decreased, and hence the bearing could support the increased load. Davies presented experimental results for load carrying capacity only, which agree to within 10% of his theoretical values. More important curves of stiffness variable are not presented, however. In any instance, the argument that the design eliminates the need for compensation is unconvincing since the design itself is only a special form of compensated hydrostatic bearing.

Bassani's (20) 1975 paper gives details of hydrostatic bearings consisting of two discs mounted on a shaft supporting an axial load, the lands being active between both surfaces of each disc and its corresponding casing surface, with inlet supply between the discs. Again, no additional capillary or orifice compensation is deemed necessary. Bassani claims that the bearing has stiffness characteristics comparable with those obtained when opposed pads (each side of the discs) are supplied by two separate pumps and motors, and uses the same pumping power. The cost saving obtained by using the Bassani valve, instead of using two pumps of half the power rating each, is not clear however.

In 1976 Singh and Singh (21) discussed a method of stiffness optimisation of a variable restrictor compensated hydrostatic bearing system. The restrictor consisted of a spring loaded piston and cylinder where oil entered the cylinder against the spring loaded piston face, flowing through the small clearance between piston face and the end of the cylinder and exiting to the bearing pocket from a side port in the cylinder. Singh's paper, whilst providing a useful example of how to optimise some of the design parameters, such as spring pre-load, cylinder diameter, etc to give maximum bearing stiffness, does not give details of the restrictor performance and no comparison is made with other forms of compensation. This being the case, Singh's restrictor cannot yet be seriously considered as a useful entity to industry.

Thus far, papers dealing with only the static characteristics of hydrostatic bearings have been discussed, when it is really the performance under dynamic loading which will be the most important consideration, as far as the bearing design investigated in this thesis is concerned. Any improvement in static characteristics could be regarded as being a convenience rather than a necessity. Unfortunately, the papers dealing with dynamic characteristics of hydrostatic bearings

are relatively scarce, and to this end the author's work may be a pertinent contribution. Five papers which deal with hydrostatic bearing dynamic characteristics have been noted by the author however, and these are worthy of some attention.

Brown's (22) paper in 1961 contained a theoretical approach to the dynamics of a hydrostatic bearing. His analysis assumes that the static stiffness of the bearing acts in parallel with, and completely independent of the stiffness and damping due to compressibility and squeeze effects which are themselves shown to be represented by a series spring and damper. This argument is difficult to prove or disprove. He makes the unqualified assumption, however, that oil inertia is negligible. Furthermore, no mention is made of squeeze film damping as distinct from damping brought about by the general outflow of oil from the pocket over the lands.

Brown backs up his theoretical work with experimental results for an annular thrust bearing excited by an electro-magnetic vibrator. His experimental results agree with his theory over only the frequency range 5-20 Hz, however. Outside this range, errors of up to 40% are apparent, although the general trends of stiffness and damping are confirmed. He concludes that a hydrostatic bearing dynamic stiffness is at all times greater than the static stiffness, and that there is always considerable damping.

The approach adopted by Brown to his work may be considered as a useful starting point, since, at the time of publishing, other authors had not attempted a dynamic analysis. The theory probably needs revising, however, and confirmed experimentally for some different pad geometries.

In 1964, Licht and Cooley (23) published a theoretical analysis of the dynamic response of a hydrostatic slider bearing. In this paper, no results are actually published except in the form of equations, only

trends are described as a function of squeeze number (defined as the ratio of volume flow rate of oil through the land clearance due to vibration to the steady flow rate of oil).

The conclusions reached are that for large squeeze numbers, if flow is incompressible, then damping is considerable. (This seems to be logical since a large volume of oil will have to be squeezed through the land clearance on each vibration cycle.) For compressible flow, however, the effect is described as being 'like that of a pneumatic cylinder' where fluid is compressed instead of being driven out over lands, thus providing high stiffness but little damping. For small squeeze numbers, Licht states that the compressible and incompressible fluids provide similar results, ie little damping and no change from the static stiffness (this would again appear logical since the low squeeze number implies that for the incompressible fluid case, the flow fluctuations are insignificant and for the compressible case the fluid may tend to flow rather than be compressed).

Licht's paper provides an interesting way of considering the functioning of a bearing but the lack of any results, theoretical or experimental, means that ultimately nothing useful has been proved or disproved.

A further criticism is that it is not clear exactly how Licht considers stiffness and damping to vary between squeeze numbers of zero and infinity, a consideration which could well have been portrayed with a graph.

Ingers (24) in 1973, used Laplace transforms to determine the characteristic equation for a hydrostatic bearing and from the roots of the equation finds the limits of stability. Equations are also determined which describe the amplitude-frequency relationship. Ingers concludes that for realistic values of bearing geometry parameters, instability is

unlikely and that increases in oil viscosity, bearing area, and pocket pressure together with decreases in the bearing clearance and oil compressibility, lead to reductions in vibration amplitude, (this is probably obvious since it effectively increases the stiffness of the bearing). It is also concluded that the presence of air bubbles in the fluid (high fluid compressibility) leads to excessive vibration levels. This seems logical since it effectively removes most of the stiffness of the bearing.

Inger's paper is a useful example of how Laplace transforms may be used to determine vibration amplitudes and stability limits for a hydrostatic bearing. It does, however, reach some conclusions which were probably already apparent. Furthermore, the paper must be criticised from the viewpoint that results are only presented in the form of equations and no distinction is made between the stiffness and damping of the bearing and how these vary with other parameters.

In 1974, Newton and Howarth (25) published a theoretical approach to predicting the changes in operating variables for hydrostatic thrust pads as a result of tilt and dynamic action. He used perturbation theory to examine the effects of sliding movement of one bearing surface relative to the other, and of squeeze action. Newton concludes that stiffness and damping are a maximum under no tilt conditions.

In this paper no results are presented which describe the actual values of stiffness and damping, only parameters which describe the change from the initial condition as a result of tilting and sliding. For the parameters which are given, corresponding experimental values are also presented which differed from theoretical values by between 10 and 25%. Although Newton's work sheds useful light on the effects of tilt and sliding on a hydrostatic bearing, it is not useful from a vibration

point of view since the stiffness referred to in the paper is a static stiffness, and the damping refers to a force as a result of constant steady velocity. This means that the effects of oil inertia and compressibility are not encountered in the experimental work and do not enter the theory. These factors may not always be ignored under vibrational excitation, however.

In 1977, Tully (26) discussed the static and dynamic performance of an infinite stiffness hydrostatic thrust bearing. In Tulley's bearing, the restrictor is formed between the bearing body and a spring-mounted conical plug. Decrease in film clearance due to an increase in load leads initially to a higher pocket pressure, this increase in pressure pushes the plug against its spring resulting in a decrease in restrictor hydraulic resistance and a consequent further increase in pocket pressure and corresponding increase in clearance.

Steady state performance curves of clearance and flow versus load are presented for various cone angles and the dynamic response to forced sinusoidal vibrations is examined using the conventional perturbation technique. Frequency response curves for various plugs and damping are presented. Tully concludes that a high static stiffness over a substantial load range may be obtained and that stiffness is substantially independent of load, which may be matched to requirements by selection of bearing area and pressure; furthermore, the variable flow restrictor serves to obtain maximum economy of lubricant supply under varying load conditions (the supply automatically almost switching off under no load conditions). The vibration analysis shows that the restrictor may be designed to act as a vibration absorber.

Tulley's work is novel in that it provides another interesting way of modifying hydrostatic bearing characteristics to obtain higher stiffnesses than might otherwise have been obtained using conventional



orifices or capillaries. The frequency response curves are informative, showing the magnitude of change in response that can be achieved with different cones and different lubricant (the change of viscosity being used to change the damping). The results are incomplete, however, in that although response curves are presented, the variation in dynamic stiffness and damping with frequency is not shown. Also, the influences of fluid inertia and compressibility are ignored, no mention of them being made. The theoretical results might be more convincing if they were confirmed experimentally.

Of the five papers discussed above, dealing with hydrostatic bearing dynamics only one, that of Brown (22), is of any interest as far as hydrostatic bearing design for operation under dynamic excitation is concerned. Those of Licht and Cooley (25) and of Ingerter (24) provide little information as to how stiffness and damping vary with frequency, and Newton's (25) work is not really applicable since it deals with steady loads and velocities. Tulley's work (26) is slightly more relevant but he is more concerned with the dynamic response as a result of using his restrictor design rather than a general assessment of dynamic stiffness and damping.

The author concludes that his work may offer a contribution towards the calculation of operating parameters in the design of hydrostatic bearings subjected to dynamic excitation. The use of hydrostatic bearings by the author is original in that a) it is a special application - to provide flexible supports for a journal bearing (although the idea has been suggested by Heathcote (27)) and b) the author proposes the use of accumulators to control the dynamic characteristics of the bearing. The originality of the work stems from the fact that while most authors of papers dealing with hydrostatic bearings attempt to exhibit high stiffnesses, typically for use in the machine tool industry, this work

is concerned with maintaining a reasonably high static stiffness but a dynamic stiffness which can be considerably reduced in a controlled manner.

At this stage it is appropriate to mention hydrostatic bearings that are gas lubricated, sometimes referred to as aerostatic bearings. These are occasionally fed not from a capillary or orifice at a single point but through the entire working area of one of the surfaces, made to be porous. A dynamic analysis of such bearings has been carried out by several authors, (28, 29, 30) being some, to determine either the bearing stiffness and damping characteristics or the stability. The results obtained from such analyses, however, are not directly applicable to oil lubricated hydrostatic bearings because of the compressibility of the fluid film that is assumed; generally, this results in a much more flexible fluid film than would be obtained with oil lubrication. A relationship between pressure and volume as described by the gas laws is normally used but this relationship is not applicable to oil. It is pertinent, however, to mention that the method used in these analyses, namely a perturbation method assuming a linear relationship between displacement and pressure for small amplitudes, is the one that is used by the author in his analysis of oil lubricated hydrostatic bearings (see section 3.2). The method has also been used to analyse oil lubricated hydrostatic journal bearings, for example reference (47). These are discussed in more detail in section 2.3.

### 2.3 Modifications to Bearing Characteristics

It is recognised that the project is primarily concerned with taking an existing bearing and designing it such that a secondary bearing exists around it, the secondary bearing in this particular case being a hydrostatic bearing system. The purpose of the secondary bearing is

effectively to add flexibility to the primary bearing foundations and thereby influence the response of the rotor to a forced vibration. This being the case, it is relevant to discuss previous attempts by other authors to change bearing characteristics by putting a secondary bearing into the system. These attempts have included the use of hydrodynamic oil films, hydrostatic damping films, spring and oil film damper combinations, electro-magnetic fields and hybrid bearings.

Shaw and Nussdorfer (30), researching into aircraft engine bearing performance in 1947, were among the first to develop a full-floating journal bearing. Their bearing consisted of a double journal bearing system, the two oil films being separated by a rotating, separating ring and the loading being applied by means of a weight via a lever and fulcrum. The purpose of the research carried out by Shaw was not to alter the dynamic characteristics of the bearing but to provide more oil to the bearing, allowing it to run cooler without increasing the bearing power loss unduly, as might result from merely pumping more oil through the clearance. Whilst succeeding in reducing steady operating temperatures of the bearing, Shaw frequently encountered instability of the bearing, sometimes of the inner film and sometimes of the outer, and particularly under lightly loaded operation. It was also found that under loaded start-up, the outer oil film frequently remained in a seized condition.

Shaw's work is significant in that it opened the path to further research into second bearings around a conventional design of primary bearing. Because of the problems of instability and seizing at loaded start, however, it was hardly successful. The work also left a gap in the area of dynamic operation of the bearing, no mention being made of changes in bearing stiffness and damping or of shaft resonant frequency as a result of introducing the second oil film.

In 1954, Kettleborough (32) also carried out an investigation of a full-floating journal bearing similar to that used by Shaw (31). Again, the advantages being sought were a lower running temperature and reduced frictional losses. Kettleborough's test rig consisted of a 3 inch diameter shaft supported by two slave rolling bearings, the test bearing between the two consisting again of one hydrodynamic bearing within another, the separating ring being rotating. Kettleborough was able to show improvements in bearing running temperature and frictional losses similar to those of Shaw (31) but also encountered the same problems of bearing seizure at loaded start. Kettleborough also noted that the specific loading that could be applied to the full floating bearing, as compared to a simple journal bearing operating at the same shaft speed, is less because the relative speed of journal to bush for each film is lower, and hence the thickness of the oil film is smaller than in the conventional journal bearing. Kettleborough's model, unlike Shaw's, did not exhibit any instability.

Again, Kettleborough's work leaves a gap where operating of the bearing under forced vibration is concerned. Unfortunately, the validity of some of Kettleborough's results could be called into question since he used dial test indicators to monitor shaft vibration amplitudes, a method which would be considered inaccurate by today's standards, but even more important, used hydraulic cylinders to provide a static load. The hydraulic cylinders would undoubtedly have an inherent stiffness and would therefore affect the dynamic operation of the test bearing; this brings into question the stability that Kettleborough observed on his model.

In 1968, Orcutt and Ng (33) also published a theoretical analysis of a full-floating bearing similar to those used by Shaw and by Kettleborough. This paper did indicate the variation of the net effective stiffness and

damping coefficients with the inner film eccentricity ratio, however, but did not go so far as to show how these varied with clearance ratio of the two films. The object of the work was to demonstrate improvements in friction losses and to provide detailed data on load capacity and stability characteristics.

Orcutt attempted to confirm his theoretical results with work on a 4 inch diameter shaft supported in the test bearing at one end, and a ball-bearing at the other. Static load was applied via a ball-bearing-mounted puller, on a shaft section overhung from the test bearing. The puller was connected to a low spring-rate coil spring. Dynamic excitation was applied by shaft unbalance applied at the overhung section.

Orcutt concludes that theory relating to static operation is confirmed experimentally but again, the problem of ring seizure during a loaded start occurs. The case for confirming the theoretical values of bearing coefficients rests on a comparison of whirl amplitudes; unfortunately only experimental orbits are shown and the graph of whirl-major semi-axis amplitude versus speed for theory and experiment, whilst showing agreement to about 6%, does not allow for phase differences which could exist and are not mentioned. As far as stability is concerned, Orcutt suggests in his introduction that the full floating bearing should offer improved stability because of the presence of extra damping due to the presence of two oil films; this statement is not substantiated with the appropriate theory, however. Indeed, the results of the experimental work suggest that the opposite could be true since the number of meaningful results taken was severely limited by many cases of instability. It is also suggested here that the validity of the experimental work for static and dynamic characteristics could be jeopardised by the loading of the shaft on one overhang, thus presenting the possibility of significant shaft distortion and misalignment at the journal.

The 1970's saw more attention focussed on the influence of rotor dynamic characteristics that could be achieved by the presence of an oil film around a conventional bearing. Most of the research conducted on this subject was for the aircraft engine industries, however, where compressor shafts running in rolling bearings frequently exhibited large amplitude whirling. The squeeze film dampers investigated were usually positioned outside the outer race of a rolling bearing, the damper oil film being continuous around the circumference of the bearing. Because of the continuity of the oil film, these dampers have no stiffness for purely radial motion of the inner bearing surface, and hence of the rotor. This means that if purely radial motion is present, or alternatively, a static load, they are usually supplemented by a spring of some description.

In 1974 Thomsen and Andersen (34) published results of experimental measurement of the damping coefficient relating to a squeeze film around the outer race of a rolling bearing mounted on a vertical shaft (no static load). Thomsen's damper ring outer diameter measured 7 cm and had an effective length of 3.5 cm. The damper ring was positioned by means of four axial flex bars. Tests were conducted at speeds of up to 10,000 rpm with damper bearing radial clearances of 300, 180 and 118  $\mu\text{m}$  and with oil viscosities of 0.006 and 0.020 Pa s.

Thomsen's experimental results compare reasonably well with theoretical damping coefficients for which he puts forward a formula for only two combinations of radial clearance and oil viscosity examined. Errors of the order of 25% are apparent for most of the other results published; Thomsen suggests that the reason for the discrepancy in the results could be the employed method of feeding the oil which could affect the boundary conditions for the film.

Thomsen gives no explanation of the origin of the equation put forward for calculating damping coefficient but he concludes that it gives an

agreement with practice that is acceptable. Certainly the calculated values are of the right order of magnitude for the damper investigated, but experimental work with larger bearing dampers is yet to be carried out.

Another paper presented by Mohan and Hahn (35) in 1974 gives design data for squeeze film dampers supporting a rigid rotor. The paper contains theory for calculating bearing force transmissibility for various excitation frequencies. The paper describes a number of stable synchronous circular modes of operation including the inverted (where rotor displacement and exciting force are out of phase by about  $180^\circ$ ) and uninverted (no phase difference), stating that the inverted mode should be the design objective since this mode gives lower transmissibilities. Data is also presented concerning a 'critical unbalance' above which the squeeze film bearing mount behaves worse than a rigid support.

Mohan's paper does not present calculated and experimental values of bearing damping coefficient which would have been useful for comparison with Thomsen's results. The paper is nevertheless a good starting point for potential designers of squeeze film bearings, and a useful design example is included. Mohan's results are not backed up by any experimental work, however, and this must leave a question-mark over his theory.

In 1976 two further papers dealing with the subject of squeeze films around rolling bearings were published. That by Botman (36) describes the results of experiments on a pressure-fed damper for a vertical shaft at speeds up to 60,000 rpm. Experimental results are shown for the variation of response amplitude, force transmissibility and oil film limiting pressure for cavitation against speed. Theory relating to the behaviour of the damper is also shown and theoretical curves presented for the variation of bearing effective damping and stiffness.

Whilst results showing increase of response amplitude and of limiting

pressure for cavitation for increase in speed exhibit good agreement between theory and experiment, the curve showing the variation of force transmissibility with frequency shows good agreement for less than half of the frequency range examined, the best agreement being at the lower frequencies. Botman concludes that experiment and theory agree reasonably well for speeds below that at which cavitation of the oil film occurs and that the limiting speed of operation of the bearing in high speed applications, must be set by the onset of cavitation.

Botman's equations describing speed for onset of cavitation for a given oil pressure and effective bearing stiffness and damping offer a useful contribution to the subject. Although his theory develops an equation for damper coefficient which bears some resemblance to that used by Thomsen (31), his predictions of force transmissibility leave something to be desired. The experimental transmissibility measurements show a trend not unlike that predicted by Mohan (35) although, unlike Mohan's paper, Botman's work assumes a flexibility of damper bearing support systems also.

Hahn followed up his work with Mohan by presenting another paper in 1976 as co-author with Simandiri (37) on the effects of pressurisation on the vibration isolation capability of squeeze film bearings. In his 1974 paper (35), Hahn spoke of possible bistable operation of the damper bearing in inverted or uninverted modes (the inverted mode providing lower transmissibilities), depending on the bearing design and operating conditions. The 1976 paper shows that pressurisation of the oil film tends to increase the 'jump free region' where no sudden change from one mode of operation to another is likely. Simandiri and Hahn also deduced that pressurisation reduces the possibility of fluid film cavitation resulting in full film lubrication and hence smaller whirl orbit amplitudes; transmissibility, however, increases slightly with pressurisation.



The variation of system resonant frequency with damper bearing design parameter is also shown.

Whilst providing adequate data to design such a squeeze film damper, the phenomenon of bistable operation is not fully explained and it is not clear what exactly decides which mode of operation the damper will run at. The theoretical work presented by Simandiri and Hahn was, again, not backed up with experimental results.

In 1977, Hahn produced another paper with Rabinowitz (38) which summarised the findings of his previous papers (35,37). The emphasis of this paper was on the stability of the bearing, and it was concluded that for maximum stability the bearing should be operated with a pressurised oil supply and at low eccentricity orbits. Again no experimental results were evident to back up the theory.

Another paper was published by Gunter, Barrett and Allaire (39) which provided guidelines for the design of squeeze film dampers. This study investigates the transient response of the dampers in addition to the steady state response. The steady state equations for the hydrodynamic bearing forces were used to determine the damper equivalent stiffness and damping coefficients, and thus to determine the damper configuration which would provide optimum support characteristics from a stability point of view.

Gunter's results show the variation of bearing effective stiffness and damping and of limiting pressure for cavitation, all with eccentricity. Also shown are 'stability maps', indicating the variation of the real part-root of the characteristic equation with support damping. Also presented in this paper are whirl orbit traces of compressor shafts with and without the presence of squeeze film dampers, designed using the method outlined.

Gunter concludes that for optimum stability and low force transmissibility, the squeeze film bearing should operate at an eccentricity ratio of about 0.4. He also suggests that for a given damper design there is a limit to the level of self-excitation that it can stabilise. It is shown that excessive squeeze film stiffness or damping will reduce the effectiveness of the damper.

Whilst the experimental traces of compressor whirl orbits presented are encouraging, there are no corresponding theoretical results with which to compare them. This means that Gunter's theory may also be called into question.

Further papers, dealing with squeeze film dampers, published in 1980, include that by Taylor and Kumar (40) and that by Cookson and Kossa (41).

In the paper by Taylor (40) the stability of the squeeze film damper is analysed and the non-linearity of the oil film is taken into account. The analysis involved the determination of the steady-state operating position and then, assuming the shaft to be displaced from this position, calculating the fluid film forces on the bearing using the integration of Reynolds equation as a starting point, and examining the resulting motion in a given time interval. At the end of that time interval a new operating position would have been reached and new film forces were calculated. The criterion for stability was that the bearing would return to its original steady-state operating position if sufficient time steps were investigated. A forced vibration frequency response for the bearing system was also presented.

Taylor examined the cases for an oil film around the full circumference of the bearing ( $2\pi$  film) and for an oil film around only half of the circumference ( $\pi$  film), and concluded that the  $2\pi$  film behaved almost linearly. The transient responses were different for the  $\pi$  and  $2\pi$  films,

with a number of possible steady-state operating positions being possible for the  $\pi$  film for given conditions.

Whilst providing a further insight into how squeeze film dampers can be analysed for their steady-state and dynamic response, Taylor's results are not compared with any experimental data and so the accuracy of his method is not confirmed.

In the paper by Cookson and Kossa (41) the effect of a squeeze film damper without a centralising spring on the frequency response of a flexible rotor was examined. The short bearing approximation of Reynolds equation was used as the starting point to determine the fluid film forces for a  $\pi$  film model. Amplitude and force transmissibility response for various excitation frequencies were presented and the effect of different rotor and bearing masses, different static loads, and different bearing geometries was examined. Responses were compared to that of the rigid system (no squeeze film damper).

Cookson concluded that the best response would be obtained with a low static load and with the rotor mass positioned towards the rotor mid-span. It was also shown that for un-optimised running conditions the response could be significantly worse than would be obtained without squeeze film dampers.

Cookson's paper shows a method of analysis similar to that used by other authors, but experimental results are again not included for comparison. The disadvantage of his analysis is that it assumes a linear oil film when in fact the  $\pi$  film is very non-linear. This means that the analysis is only applicable to the case where vibration amplitudes are small.

A substantial amount of work has been done to establish the relations between loads, deflection and velocity for oil film dampers and

experimental data has been obtained on a number of rigs in attempts to determine oil film dynamic coefficients. In general, however, results show considerable scatter and it must be concluded that the theoretical solutions are based on assumptions which do not hold in practice. It is probably true that the oil film behaviour is very sensitive to geometrical dimensions and physical oil properties that are not sufficiently controlled in the tests. Although the use of such dampers is well established for lightweight turbomachinery in aerospace applications, their use on heavy machinery such as a turbine generator rotor is yet to be seen. Such an application is not beyond possibility, however.

There are also two other novel ways of modifying shaft dynamic behaviour that have been investigated. These methods include the use of springs and dampers to provide foundation flexibility at a rotor shaft bearing and the use of electro-magnetic devices to provide shaft damping.

In 1979, Nikolajsen and Holmes (42) conducted an experiment on a 2 inch diameter shaft supported in journal bearings which were surrounded by a squeeze film damper similar to that whose use with rolling bearings was discussed earlier (31-36). The ring separating hydrodynamic and damper films was supported by three guide rods of Belleville washers, positioned circumferentially around the separating ring, with the guide rods' axes pointing towards the centre of the bearing. Whereas other authors (31-36) had relied on retainer springs only to centralise the shaft in the damper film, Nikolajsen was now able to use the stiffness of his retainer springs to actively modify the bearing characteristics. Support stiffness was varied by changing the number of Belleville washers used to locate the separate ring whilst support damping was altered by using different oil viscosities and damper film clearances. Nikolajsen's theoretical and experimental results on the variation of

rotor vibration amplitude with rotational speed, for various values of support damping agree well, showing a significant decrease in response amplitude with decrease in support damping, for the range of damping investigated. The theoretical approach to variation of rotor amplitude with support stiffness shows some decrease of critical speed and corresponding resonant amplitude with decrease in support stiffness. The corresponding experimental results, however, show little variation of critical speeds or response amplitudes for the range of stiffness investigated, a discrepancy which is not explained. A considerable improvement in rotor stability was observed theoretically and experimentally when suitable external damping is employed, although some non-linear subharmonic steady-state vibrations or orders up to four could not be eliminated.

Nikolajsen's work clearly demonstrates how effectively shaft vibration can be controlled by varying bearing foundation stiffness and damping. It should not be concluded from the work, however, that further decrease in support damping beyond those values chosen for experimental investigation will necessarily result in a decrease in rotor response amplitude. This trend is only true for the particular values used by Nikolajsen. Some correlation, then, might be found with the work of Kirk and Gunter (12) whose work indicates that there is an optimum value of support damping which gives minimum rotor response amplitude. It is difficult to compare the two papers directly, however, because of the different parameters used by the different authors. Whilst Nikolajsen's work remains of interest to the turbo-generator industry, it cannot be claimed that it answers all questions relating to flexible damped supports for generator rotors; indeed it is difficult to imagine scaled-up giant Belleville washers on a 1200 MW generating set!

Nikolajsen produced a further paper in 1979 as co-author with Holmes and Gondhalekar (43) concerning a theoretical and experimental investigation of an electromagnetic damper for the control of vibrations in a transmission shaft. The damper consisted of four electromagnets positioned circumferentially around the shaft; probes measuring shaft vibrational velocity were used to transmit their output signals to power amplifiers supplying the electromagnets, the particular electromagnets energised depending upon the instantaneous velocity of the shaft.

The results presented for a rotor bearing system consisting of 52 mm diameter shafts totalling 3.2 m long and running in four journal bearings show good agreement with theory for response amplitude local to the first critical speed, results for higher criticals not being presented. Response at the first critical speed was reduced in both cases as damping capacity of the electromagnets was increased. In addition, it was found that the damper was effective in suppressing system instability associated with fluid film bearings and the second order vibrations associated with shaft stiffness asymmetry. For the cases examined the instability was not completely eliminated, however.

Whilst this paper offers an alternative to mechanical methods of rotor vibration damping, the work has yet to be extended to a shaft of the size used in a turbine generator. The damper used by Nikolajsen was used in conjunction with standard journal bearings and is not a new design of bearing in its own right. This means that the disadvantage of the need for additional mounting space around the shaft is necessary. A pertinent point not discussed in the report is the possible power consumption of such a damper (including power amplifiers) and how this compares with frictional losses in the journal bearings.

There is another alternative method which could be used for modifying

journal bearing operating characteristics which has not yet been discussed. That is by way of applying external pressurisation to one or several inlet ports around the bearing bush. Such hydrostatic journal bearings (or hybrid bearings as they are often termed) are well documented in the literature for both their static characteristics (14,15,16,18,44-46) and dynamic characteristics (47-49). It has been shown in these papers that both static and dynamic characteristics can be altered by changing flow restrictor design, operating eccentricity, bearing geometry and other design parameters.

The design of such hybrid bearings primarily depends on the angular variation of the applied load. When the load angle does not change a single hydrostatic pad is normally used. However, multipad hydrostatic journal bearings may be used to increase bearing stiffness and/or provide lateral stiffness. For rotating loads a number of pads are distributed around the bearing circumference.

The use of such hybrid bearings in place of journal bearings to modify dynamic behaviour of generator rotor shafts, by altering one of the bearing operating parameters, is apparently a possibility. It does, however, suffer from a number of disadvantages. The optimised design of hybrid bearing for stiffness and load carrying capacity, and minimum pumping power, results in a bearing whose bush surface area is largely occupied by hydrostatic pocket rather than land. Only when the bearing operates at high eccentricities is the hydrodynamic load appreciable, and under these circumstances frictional losses are considerably higher than pumping losses; the latter results in high temperature rises while high eccentricities mean that there is a danger of shaft to bearing contact.

It can be seen then that the operation of such a bearing without the hydrostatic supply, ie under purely hydrodynamic action, is not feasible.

This means that the pumping losses attributable to the hydrostatic bearing would have to be endured even if no change in dynamic characteristics was desired. A further disadvantage of the use of the hybrid bearing for control of dynamic characteristics is that altering one characteristic, eg damping, by modifying, say, the flow restrictor, would automatically influence other operating parameters, eg load and stiffness.

To summarise the present position concerning bearings with special design features for modifying their characteristics, a number of types have been studied. The full floating ring bearing (31,32,33) has not been researched into recently, apparently being dropped for the time being due to the problems of ring instability and seizure during loaded start. Damping films usually in conjunction with some form of centralising spring have been investigated by many authors (34-42) but experimental results still show frequent departure from theory. Experimental work with this type of bearing has yet to be carried out for bearings of the size used in the turbine generator industry. An electromagnetic damper has also been studied (43) but only for use on a transmission shaft and this would be required in addition to a normal bearing. Operating characteristics of hybrid bearings are well documented (44-49) and although such a bearing has certain control parameters which might be used to alter rotor response characteristics, other disadvantages, ie inefficient hydrodynamic action and the dependency of several operating characteristics on each control parameter, mean that this is not an obvious solution to the problem.

As far as the author is aware, the use of a combined hydrostatic and hydrodynamic bearing similar to that investigated in this thesis has not yet been studied by any other author. The work contained in this thesis is original in this respect.



CHAPTER THREE

THEORETICAL ANALYSIS OF THE HYDROSTATIC BEARING

CHAPTER THREE

THEORETICAL ANALYSIS OF THE HYDROSTATIC BEARING

3.1 Static Characteristics of one Hydrostatic Bearing

This section develops the equation for flow out of one hydrostatic pocket, considering only static operation. This equation is then used to determine the other static characteristics of that hydrostatic pocket, namely supported load and required pumping power.

Consider the diagram in fig 3.1 showing a general operating position of a single hydrostatic bearing pad of part cylindrical form. The displacement of the floating ring from a position concentric with the hydrostatic bush is described by  $x$  and  $y$  displacements (or alternatively by  $e$ , the eccentricity and  $\phi$ , the attitude angle). The nominal (design) film clearance of the hydrostatic bearing is  $c_0$ . Movement of the floating ring from the concentric position is:

$$\text{from left to right } x = e \sin \phi \quad . . . \quad 3.1$$

$$\text{upwards } y = - e \cos \phi \quad . . . \quad 3.2$$

The film clearance at any angle  $\theta$  is:

$$c = c_0 - x \sin \theta + y \cos \theta \quad . . . \quad 3.3$$

At this stage a 'mid-land' type approximation is used, similar to that used by Raimondi and Boyd (14) which assumes that oil flows over the bearing lands only in a direction perpendicular to the land centre line and that the pocket pressure is active over an area defined by the land centre-lines. The accuracy of this approximation is discussed in section 3.5.

If the bearing bush radius of curvature is  $R$ , the oil pocket pressure  $P$ , oil dynamic viscosity  $\mu$ , and hydrostatic pocket land width  $W$ , the oil flow through an element  $d\theta$ , as shown in fig 3.1, over one of the curved lands (not shown on fig 3.1) ie, out through the plane of the page, is:

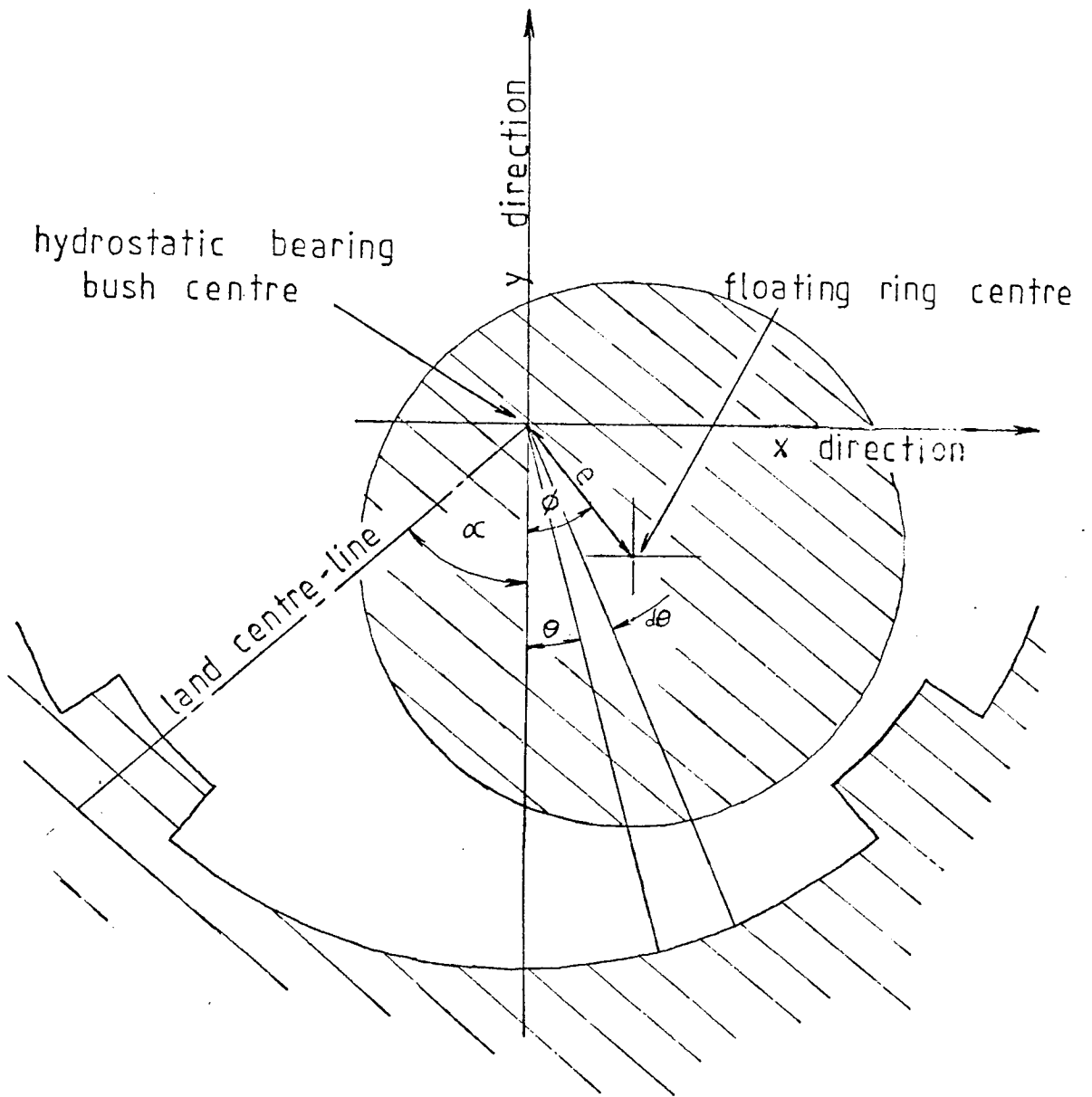


FIG 3.1      DIAGRAM OF A HYDROSTATIC  
BEARING PAD.

$$dQ = \frac{c^3 R d\theta P_p}{12 \mu W}$$

and substituting the value of c from equation 3.3 gives:

$$dQ = \frac{P_p R}{12 \mu W} [c_o + y \cos \theta - x \sin \theta]^3 d\theta \quad \dots \quad 3.4$$

Integrating this, the total oil flow through both curved lands is determined as:

$$Q = \frac{P_p R c_o^3}{12 \mu W} \left[ 4 \alpha + \frac{1}{c_o} 12 y \sin \alpha + \frac{1}{c_o^2} (6 \alpha (y^2 + x^2) + 3 \sin 2 \alpha (y^2 - x^2)) + \frac{1}{c_o^3} (4 y^3 (\sin \alpha - \frac{\sin^3 \alpha}{3}) + 12 x^2 y \frac{\sin^3 \alpha}{3}) \right] \quad \dots \quad 3.5$$

If the length of the hydrostatic pocket from land centre-line to land centre-line is L, then the total oil flow through the two non-curved lands at  $\alpha$  and  $-\alpha$  shown in fig 3.1 is:

$$Q = \frac{P_p L}{12 \mu W} [c_o + y \cos \alpha - x \sin \alpha]^3 + \frac{P_p L}{12 \mu W} [c_o + y \cos (-\alpha) - x \sin (-\alpha)]^3$$

which on re-arranging gives:

$$Q = \frac{P_p L c_o^3}{12 \mu W} \left[ 2 + \frac{1}{c_o} 6 y \cos \alpha + \frac{1}{c_o^2} (6 y^2 \cos^2 \alpha + 6 x^2 \sin^2 \alpha) + \frac{1}{c_o^3} (2 y^3 \cos^3 \alpha + 6 x^2 y \sin^2 \alpha \cos \alpha) \right] \quad \dots \quad 3.6$$

Then the total oil flow out of the hydrostatic pocket is given by summing the two flows of equations 3.5 and 3.6 as below:

$$Q_{\ell} = \frac{P_p c_o^2}{12 \mu W} f(x, y) \quad \dots \quad 3.7$$

where  $f(x, y) = [(2 L + 4 R \alpha) + \frac{1}{c_o} (12 R y \sin \alpha + 6 L y \cos \alpha)$

$$+ \frac{1}{c_o^2} (6 R \alpha (y^2 + x^2) + 3 R \sin 2 \alpha (y^2 - x^2)$$

$$+ 6 y^2 L \cos^2 \alpha + 6 x^2 L \sin^2 \alpha)$$

$$+ \frac{1}{c_o^3} (4 R y^3 (\sin \alpha - \frac{\sin^3 \alpha}{3}) + 12 R x^2 y \frac{\sin^3 \alpha}{3}$$

$$+ 2 L y^3 \cos^3 \alpha + 6 L x^2 y \sin^2 \alpha \cos \alpha)] \quad \dots \quad 3.8$$

For small displacements  $\delta x$  and  $\delta y$  of the floating ring about the steady operating position described by  $x$  and  $y$ , the change in total oil flow out of the pocket will be given by:

$$\Delta Q_{\ell} = \frac{P_p c_o^3}{12 \mu W} f_x \delta x + f_y \delta y \quad \dots \quad 3.9$$

where  $f_x$  is the differential of  $f(x, y)$  with respect to  $x$  and  $f_y$  is the differential of  $f(x, y)$  with respect to  $y$ . These are given by:

$$f_x = \left[ \frac{1}{c_o^2} (12 R \alpha x - 6 R x \sin 2 \alpha + 12 x L \sin^2 \alpha) + \frac{1}{c_o^3} (24 R x y \frac{\sin^3 \alpha}{3} + 12 L x y \sin^2 \alpha \cos \alpha) \right] \dots \quad 3.10$$

and

$$f_y = \left[ \frac{1}{c_o} (12 R \sin \alpha + 6 L \cos \alpha) + \frac{1}{c_o^2} (12 R \alpha y + 6 R y \sin 2 \alpha + 12 y L \cos^2 \alpha) + \frac{1}{c_o^3} (12 R y^2 (\sin \alpha - \frac{\sin^3 \alpha}{3}) + 12 R x^2 \frac{\sin^3 \alpha}{3} + 6 L y^2 \cos^3 \alpha + 6 L x^2 \sin^2 \alpha \cos \alpha) \right] \dots \quad 3.11$$

Equations 3.9 to 3.11 are not used to determine the hydrostatic bearing static characteristics but have been developed at this stage for convenience. The flow into the hydrostatic pocket through the capillary from the supply is given by:

$$Q = K_s (P_s - P_p) \quad \dots \quad 3.12$$

where  $K_s$  is a constant, the value of which is determined by the geometry of the feed capillary, and  $P_s$  is the supply oil pressure. This in flow must balance the flow out of the hydrostatic pocket across the lands, hence:

$$K_s (P_s - P_p) = \frac{P_p c_o^3}{12 \mu W} f(x, y) \quad \dots \quad 3.13$$

It is convenient to define the capillary coefficient  $K_s$  in terms of the ratio of pocket supply pressure at the design position, ie with the floating ring concentric with the hydrostatic bush. Defining pressure

ratio in this position as  $\beta$ , and equating flows in and out of the pocket gives:

$$K_s = \frac{\beta}{1 - \beta} \frac{c_0^3}{12 \mu W} (4 R \alpha + 2 L) \quad \dots \quad 3.14$$

Equation 3.14 defines the value of flow resistance required for a given hydrostatic pocket to operate at any selected  $\beta$  ratio operating parameter. Substituting 3.14 into 3.13 gives:

$$P_p = \frac{P_s \frac{\beta}{1 - \beta} (4 R \alpha + 2 L)}{\frac{\beta}{1 - \beta} (4 R \alpha + 2 L) + f(x, y)} \quad \dots \quad 3.15$$

Equation 3.15 gives the steady value of pocket pressure for the hydrostatic bearing, then the load on the bearing is:

$$F_y = P_p A \quad \dots \quad 3.16$$

where  $A$  is the projected effective area of the hydrostatic bearing (defined by the centre-line of each of the hydrostatic bearing lands).

The total pumping power required by one hydrostatic bearing pad is defined by:

$$P = Q_p P_s \quad \dots \quad 3.17$$

### 3.2 Dynamic Characteristics of one Hydrostatic Bearing Pad

In this section the hydrostatic bearing is assumed to be operating under forced dynamic excitation, and is assumed to have an accumulator connected to the bearing pocket thus influencing its operation.

Equations determining the various instantaneous oil flows into and out of the bearing pocket are determined, and developed to give the bearing dynamic operating coefficients.

Consider the oil flow equations for the system shown in figure 3.2.

For flow from the oil supply into the pocket:

$$P_s - P_p = \frac{1}{K_s} Q_s + I_s \frac{dQ_s}{dt} \quad \dots \quad 3.18$$

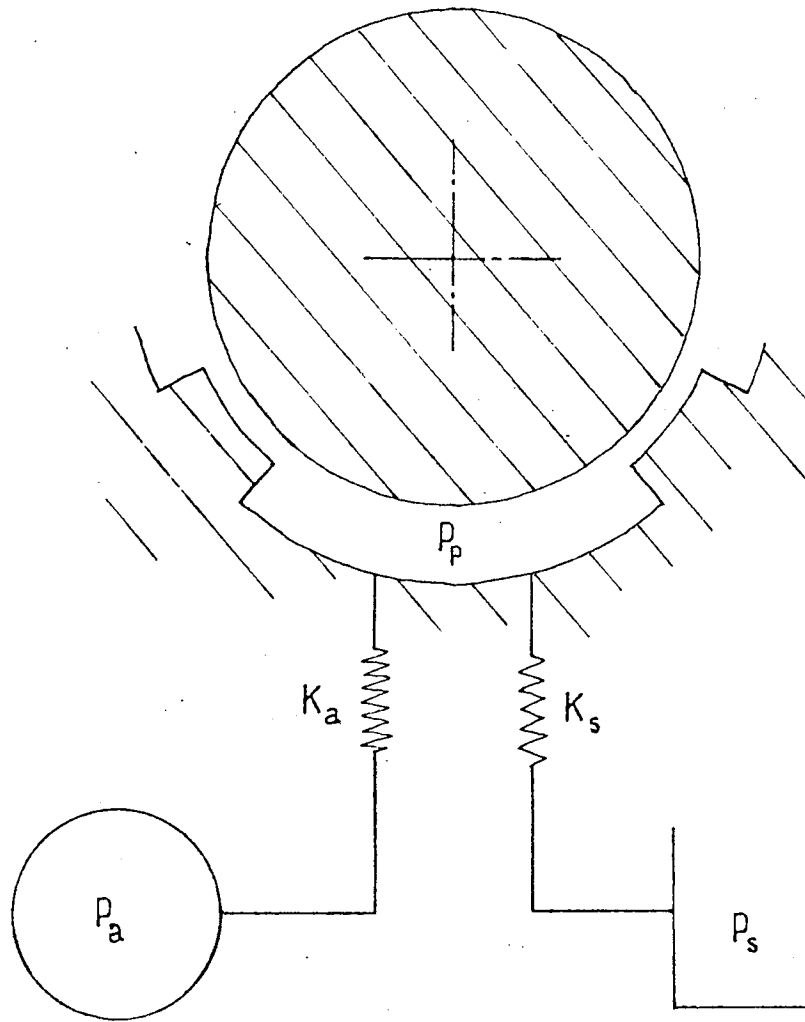


FIG 3.2 DIAGRAM OF THE HYDROSTATIC  
BEARING OIL WAY CONNECTIONS

where  $Q_s$  is the oil volume flow rate,  $K_s$  is the inverse of flow resistance provided by the feed capillary and  $I_s$  is an inertia coefficient which allows for the fact that we are considering unsteady flow and that the net pressure has to first accelerate the fluid as well as overcome viscous resistance to flow. Normally, the inertia term will be small, but for long capillaries it may become more significant than the viscous term as the mass of fluid in the capillary becomes large.

Similarly for flow in the accumulator oil line

$$P_p - P_a = \frac{1}{K_a} Q_a + I_a \frac{dQ_a}{dt} \quad \dots \quad 3.19$$

where  $Q_a$  is the oil flow from the hydrostatic pocket into the accumulator,  $K_a$  is the inverse flow resistance, and  $I_a$  is the appropriate inertia coefficient.

As the two bearing surfaces shown in fig 3.2 move away from each other (due to part of a vibration cycle) then the volume of oil contained between them is increased at a rate given by:

$$Q_v = A \frac{dy}{dt} \quad \dots \quad 3.20$$

where  $Q_v$  is the volume flow rate of oil to fill the available space,  $A$  is the effective area of the bearing defined by the land centre lines, and  $dy/dt$  the velocity at which the upper bearing surface moves away from the pocket surface. This extension of the 'mid land' approximation to define effective bearing area assumes that as the bearing surfaces approach each other at the lands, half of the oil on the land flows back into the pocket and half out to the drain area. These flows are, of course, superimposed on the steady oil flow out of the pocket.

The pressure changes in the accumulator are described by the accumulator operating characteristic B as:

$$\frac{dP_a}{dt} = B Q_a \quad \dots \quad 3.21$$



The three flow equations 3.18 to 3.20 are related by the fact that a flow balance exists, ie oil does not appear from nowhere and does not disappear. If  $Q_L$  is defined as in equations 3.7 to 3.11, and if the oil is assumed to be incompressible then we may write the flow balance equation

$$Q_s - Q_v - Q_a = Q_L$$

$$= \frac{P_p c_o^3}{12 \mu W} f(x, y) + \frac{P_p c_o^3}{12 \mu W} f_x \delta x + \frac{P_p c_o^3}{12 \mu W} f_y \delta y \quad 3.22$$

If oil compressibility was taken into account then equation 3.22 would have to be modified accordingly. In practice, however, the additional flow term to be included is small compared with the other flows.

Assuming that the floating ring vibrates sinusoidally in its hydrostatic bush and that the vibration amplitudes are small enough to cause oil pressure and flow to vary linearly with floating ring displacement, then these parameters also vary sinusoidally. Then:

$$\delta y = Y_0 \sin \omega t \quad . . . \quad 3.23$$

$$\delta x = X_1 \sin \omega t + X_2 \cos \omega t \quad . . . \quad 3.24$$

$$P_p = P_{p0} + \epsilon_1 \sin \omega t + \epsilon_2 \cos \omega t \quad . . . \quad 3.25$$

$$P_a = P_{p0} + \gamma_1 \sin \omega t + \gamma_2 \cos \omega t \quad . . . \quad 3.26$$

$$Q_s = Q_{s0} + \tau_1 \sin \omega t + \tau_2 \cos \omega t \quad . . . \quad 3.27$$

$$Q_a = Q_{a0} + \psi_1 \sin \omega t + \psi_2 \cos \omega t \quad . . . \quad 3.28$$

Where Y is the amplitude of vertical vibration of the hydrostatic bearing surface relative to the pocket surface,  $X_1$  and  $X_2$  are the in phase and out of phase horizontal vibration amplitudes,  $\epsilon_1$  and  $\epsilon_2$  the in phase and out of phase pressure fluctuations in the hydrostatic pocket,  $\gamma_1$  and  $\gamma_2$  the in phase and out of phase pressure fluctuations in the accumulator,  $\tau_1$  and  $\tau_2$  the flow amplitudes in phase and out of phase for the supply oil line, and  $\psi_1$  and  $\psi_2$  the in phase and out of phase flow amplitudes for the accumulator oil line.

Substituting equations 3.23 to 3.28 into equations 3.18 to 3.22 gives

$$\begin{aligned}
 -\epsilon_1 \sin \omega t - \epsilon_2 \cos \omega t &= \frac{1}{Ks} (\tau_1 \sin \omega t + \tau_2 \cos \omega t) \\
 &+ I_s \omega (\tau_1 \cos \omega t - \tau_2 \sin \omega t) \quad \dots \quad 3.29
 \end{aligned}$$

$$\begin{aligned}
 \epsilon_1 \sin \omega t + \epsilon_2 \cos \omega t - \gamma_1 \sin \omega t - \gamma_2 \cos \omega t \\
 &= \frac{1}{Ka} (\psi_1 \sin \omega t + \psi_2 \cos \omega t) + I_a \omega (\psi_1 \cos \omega t - \psi_2 \sin \omega t) \\
 &\dots \quad 3.30
 \end{aligned}$$

$$Q_v = A \omega Y \cos \omega t \quad \dots \quad 3.31$$

$$\gamma_1 \omega \cos \omega t - \gamma_2 \omega \sin \omega t = B(\psi_1 \sin \omega t + \psi_2 \cos \omega t) \dots \quad 3.32$$

$$\begin{aligned}
 Q_{s_o} + \tau_1 \sin \omega t + \tau_2 \cos \omega t - A \omega Y \cos \omega t - Q_{a_o} - \psi_1 \sin \omega t \\
 - \psi_2 \cos \omega t &= P_{po} f(x,y) + f(x,y) (\epsilon_1 \sin \omega t + \epsilon_2 \cos \omega t) \\
 &+ P_{po} f_x (X_1 \sin \omega t + X_2 \cos \omega t) + (\epsilon_1 \sin \omega t + \epsilon_2 \cos \omega t) \\
 &f_x (X_1 \sin \omega t + X_2 \cos \omega t) + P_{po} f_y Y \sin \omega t + (\epsilon_1 \sin \omega t \\
 &+ \epsilon_2 \cos \omega t) f_y Y \sin \omega t \quad \dots \quad 3.33
 \end{aligned}$$

Considering equation 3.33 it may be seen that some of the terms cancel each other out since  $Q_{s_o} = P_{po} c_o^3 f(x,y)/12 \mu W$ . Furthermore, the steady flow in the accumulator line,  $Q_{a_o}$  has to be zero since it forms a closed part of the system. Further simplifications may be made if we consider that products of small terms may be ignored since these will be insignificantly small, namely the products  $f(\epsilon_1, \epsilon_2)$ ,  $f(X_1, X_2)$  and  $f(\epsilon_1, \epsilon_2) \cdot Y$ . Equation 3.33 may then be rewritten:

$$\begin{aligned}
 \tau_1 \sin \omega t + \tau_2 \cos \omega t - A \omega Y \cos \omega t - \psi_1 \sin \omega t - \psi_2 \cos \omega t \\
 &= f(x,y) (\epsilon_1 \sin \omega t + \epsilon_2 \cos \omega t) + P_{po} f_x (X_1 \sin \omega t \\
 &+ X_2 \cos \omega t) + P_{po} f_y Y \sin \omega t \quad \dots \quad 3.34
 \end{aligned}$$

Comparing terms of  $\sin \omega t$  and  $\cos \omega t$  in equations 3.29, 3.30, 3.32 and 3.34 yields eight further equations which are written below in matrix form.

$$\begin{bmatrix} -1 & 0 & -1/Ks & I_s\omega & 0 & 0 & 0 & 0 \\ 0 & -1 & -I_s\omega & -1/Ks & 0 & 0 & 0 & 0 \\ 1 & 0 & 0 & 0 & -1 & 0 & -1/Ka & I_a\omega \\ 0 & 1 & 0 & 0 & 0 & -1 & -I_a\omega & -1/Ka \\ 0 & 0 & 0 & 0 & 0 & -\omega & -B & 0 \\ 0 & 0 & 0 & 0 & \omega & 0 & 0 & -B \\ -f(x,y) & 0 & 1 & 0 & 0 & 0 & -1 & 0 \\ 0 & -f(x,y) & 0 & 1 & 0 & 0 & 0 & -1 \end{bmatrix} \begin{bmatrix} \epsilon_1 \\ \epsilon_2 \\ \tau_1 \\ \tau_2 \\ \gamma_1 \\ \gamma_2 \\ \psi_1 \\ \psi_2 \end{bmatrix} = \begin{bmatrix} 0 \\ 0 \\ 0 \\ 0 \\ 0 \\ 0 \\ P_{po} f_x X_1 \\ +P_{po} f_y Y \\ A\omega Y + P_{po} f_x X_2 \end{bmatrix} \dots 3.35$$

The inertia terms  $I_s$  and  $I_a$  may be evaluated by considering the force to accelerate a column of fluid. Note that this will be only a fraction of the total force available, the rest of the force being used to overcome viscous resistance. Applying Newton's second law gives:

$$\Delta P a = m \dot{v} \dots 3.36$$

where  $\Delta P$  is the pressure difference across the column of oil,  $a$  is the cross-sectional area of the tube,  $m$  the mass of fluid contained in the tube and  $\dot{v}$  the acceleration of the column of fluid. Then

$$\Delta P = \frac{V\rho}{a} \dot{Q} \dots 3.37$$

where  $V$  is the volume of oil in the pipe and  $\rho$  the oil density.

Comparing equations 3.37 and 3.20 and 3.21 it can be seen that the inertia coefficients are given by

$$\begin{aligned} I &= \frac{V\rho}{a^2} \\ &= \frac{\ell'\rho}{a} \dots 3.38 \end{aligned}$$

where  $\ell'$  is the length of the tube connecting the pressure supply to the hydrostatic pocket ( $I_s$ ), or connecting the hydrostatic pocket and accumulator ( $I_a$ ). Note that a corresponding inertia coefficient for oil at the hydrostatic bearing lands would be insignificantly small compared with the other inertia terms and can thus be neglected.

Equation 3.35 was solved on a HP9845A desktop computer to determine values under various operating conditions of  $\epsilon_1$ ,  $\epsilon_2$ , etc. It is the values of  $\epsilon_1$  and  $\epsilon_2$ , ie, the pressure fluctuations in the hydrostatic pocket which lead to the determination of the stiffness and damping for the bearing. The force-displacement relationship for the top bearing surface of fig 3.2 may be written

$$F_y = yK_{yy} + xK_{yx} + yC_{yy} + xC_{yx} \quad \dots \quad 3.39$$

where  $F_y$  is the force in the y direction,  $K_{yy}$  and  $C_{yy}$  the direct stiffness and damping in the y direction and  $K_{yx}$  and  $C_{yx}$  the stiffness and damping in the y direction corresponding to displacement and velocity respectively in the x direction (the cross-coupling terms). Equation 3.39 neglects the force arising due to squeeze film damping at the bearing lands. This action would result in an additional parabolic pressure distribution at the bearing land over and above the linear distribution assumed by the mid-land approximation. The force due to squeeze film damping is discussed in more detail in section 3.4 where it is shown to be insignificantly small.

If the motion of the top bearing surface relative to the bottom bearing surface is:

$$y = Y \sin \omega t \quad \dots \quad 3.40$$

$$\text{and } x = X \sin (\omega t + \phi') \quad \dots \quad 3.41$$

then

$$\dot{y} = \omega Y \cos \omega t \quad \dots \quad 3.42$$

$$\dot{x} = \omega X (\cos \omega t + \phi') \quad \dots \quad 3.43$$

and the corresponding force is

$$F_y = F_0 \sin (\omega t + \theta') \quad \dots \quad 3.44$$

where Y and X are the vibration amplitudes in the y and x directions respectively,  $F_0$  is the force amplitude in the y direction and  $\phi'$  and  $\theta'$  indicate phase angles of the x displacement and y direction force respectively, relative to the y displacement. Note that there is no

force in the x direction because it is assumed that the pressure in the hydrostatic pocket is uniformly distributed over the pocket area, and the pocket extends an equal amount in the positive and negative x directions. Substituting equations 3.40 to 3.44 into equation 3.39, and comparing coefficients of  $\sin \omega t$  and  $\cos \omega t$  gives

$$F_0 \cos \theta' = Y K_{yy} + X K_{yx} \cos \phi' - \omega X C_{yx} \sin \phi' \quad \dots \quad 3.45$$

$$F_0 \sin \theta' = X K_{yx} \sin \phi' + \omega Y C_{yy} + \omega X C_{yx} \cos \phi' \quad \dots \quad 3.46$$

If  $X = 0$  then

$$K_{yy} = \frac{F_0 \cos \theta'}{Y} \quad \dots \quad 3.47$$

$$C_{yy} = \frac{F_0 \sin \theta'}{\omega Y} \quad \dots \quad 3.48$$

and if  $Y = 0$  then

$$K_{yx} = \frac{F_0}{X} (\sin^2 \phi' + \cos \phi' \cos \theta') \quad \dots \quad 3.49$$

$$C_{yx} = \frac{F_0}{\omega X} \sin (\theta' - \phi') \quad \dots \quad 3.50$$

The pressure fluctuations in the hydrostatic pocket are described by

$$\begin{aligned} P_p &= \epsilon \sin (\omega t + \theta') \\ &= \epsilon (\sin \omega t \cos \theta' + \cos \omega t \sin \theta') \\ &= \epsilon_1 \sin \omega t + \epsilon_2 \cos \omega t \quad \dots \quad 3.51 \end{aligned}$$

then the force amplitude  $F_0$  is given by

$$F_0 = A \sqrt{\epsilon_1^2 + \epsilon_2^2} \quad \dots \quad 3.52$$

and the phase angle  $\theta'$  by

$$\theta' = \tan^{-1} [\epsilon_2 / \epsilon_1] \quad \dots \quad 3.53$$

Hence all four stiffness and damping coefficients for the hydrostatic pocket are determined.

### 3.3 Operating Coefficients for the Complete Hydrostatic Bearing

The theory developed so far refers to a single hydrostatic bearing pad. A complete hydrostatic bearing bush may have several such pads positioned at various localities around its circumference, however. For example, the bearing discussed in section 6.4 has hydrostatic pockets at four different angular positions. This section discusses how the operating coefficients for each individual pad may be used to determine operating coefficients for the complete hydrostatic bush. Consider the hydrostatic bearing shown inclined at an angle  $\delta$  in fig 3.3. Motions in the local x and y direction for the bearing, ie in the  $x_\ell$  and  $y_\ell$  directions are

$$dx_\ell = dx \cos \delta + dy \sin \delta \quad \dots \quad 3.54$$

$$dy_\ell = dy \cos \delta - dx \sin \delta \quad \dots \quad 3.55$$

The forces in the global x and y directions are

$$F_x = F_{x_\ell} \cos \delta - F_{y_\ell} \sin \delta \quad \dots \quad 3.56$$

$$F_y = F_{x_\ell} \sin \delta + F_{y_\ell} \cos \delta \quad \dots \quad 3.57$$

The individual bearing force in the  $x_\ell$  direction,  $F_{x_\ell}$ , is always zero and the force in the y direction,  $F_{y_\ell}$ , depends on the stiffness and damping coefficients for the bearing, hence using equations 3.54 and 3.55, equation 3.56 becomes

$$F_x = - \sin \delta [K_{y_\ell y_\ell} (dy \cos \delta - dx \sin \delta) + K_{y_\ell x_\ell} (dx \cos \delta + dy \sin \delta) + C_{y_\ell y_\ell} (\dot{dy} \cos \delta - \dot{dx} \sin \delta) + C_{y_\ell x_\ell} (\dot{dx} \cos \delta + \dot{dy} \sin \delta)] \quad \dots \quad 3.58$$

$$\text{But } F_x = K_{xx} dx + K_{xy} dy + C_{xx} \dot{dx} + C_{xy} \dot{dy} \quad \dots \quad 3.59$$

by definition. Hence, comparing coefficients of dx, dy,  $\dot{dx}$  and  $\dot{dy}$  in equations 3.58 and 3.59 gives

$$K_{xx} = K_{y_\ell y_\ell} \sin^2 \delta - K_{y_\ell x_\ell} \sin \delta \cos \delta \quad \dots \quad 3.60$$

$$K_{xy} = - K_{y_\ell y_\ell} \sin \delta \cos \delta - K_{y_\ell x_\ell} \sin^2 \delta \quad \dots \quad 3.61$$

$$C_{xx} = C_{y_\ell y_\ell} \sin^2 \delta - C_{y_\ell x_\ell} \sin \delta \cos \delta \quad \dots \quad 3.62$$

$$C_{xy} = - C_{y_\ell y_\ell} \sin \delta \cos \delta - C_{y_\ell x_\ell} \sin^2 \delta \quad \dots \quad 3.63$$

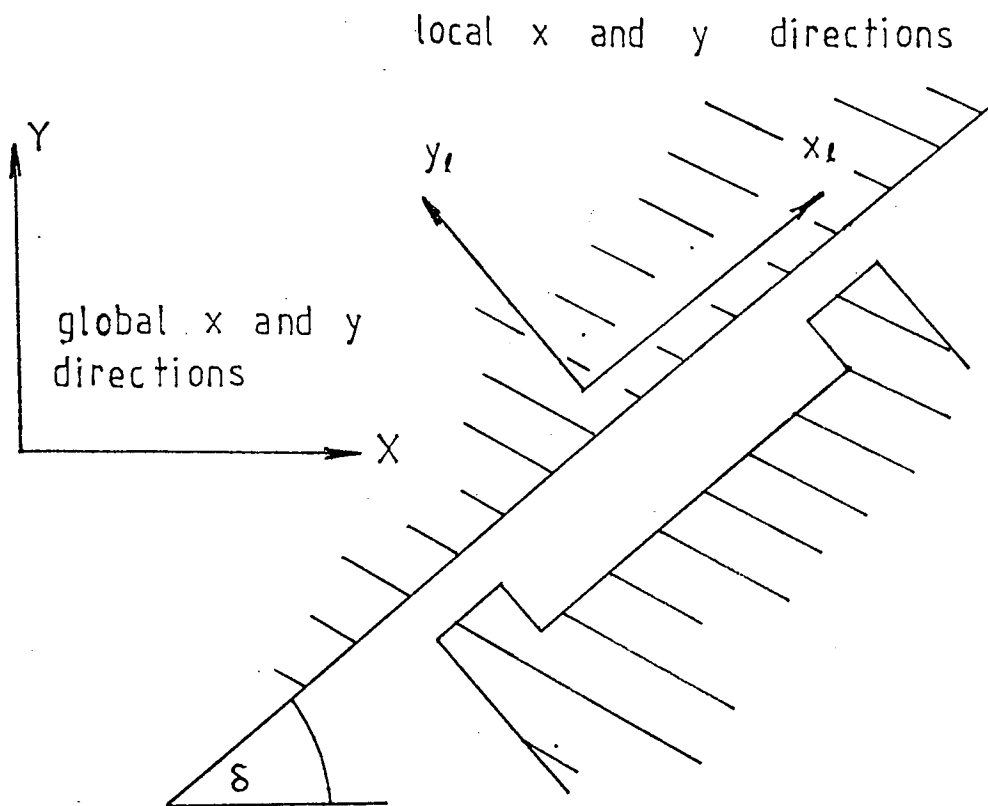


FIG 3.3 GENERAL POSITION OF A HYDROSTATIC BEARING PAD

Similarly, equation 3.57 may be developed to give

$$K_{yy} = K_{ylyl} \cos^2 \delta + K_{ylxl} \sin \delta \cos \delta \quad \dots \quad 3.64$$

$$K_{yx} = - K_{ylyl} \sin \delta \cos \delta + K_{ylxl} \cos^2 \delta \quad \dots \quad 3.65$$

$$C_{yy} = C_{ylyl} \cos^2 \delta + C_{ylxl} \sin \delta \cos \delta \quad \dots \quad 3.66$$

$$C_{yx} = - C_{ylyl} \sin \delta \cos \delta + C_{ylxl} \cos^2 \delta \quad \dots \quad 3.67$$

Since hydrostatic bearings are positioned in the hydrostatic bush at four different angles  $\delta = 0, \pi/2, \pi, 3\pi/2$  then to determine the coefficients for the complete hydrostatic bush we must add the appropriate values, ie

$$\begin{aligned} K_{yy} \text{ bush} &= K_{yy}_{\delta=0} + K_{yy}_{\delta=\pi/2} + K_{yy}_{\delta=\pi} + K_{yy}_{\delta=3\pi/2} \\ &= K_{ylyl} + 0 + K_{ylyl} + 0 \\ &= 2 K_{ylyl} \quad \dots \quad 3.68 \end{aligned}$$

Similarly

$$K_{yx} \text{ bush} = 2 K_{ylxl} \quad \dots \quad 3.69$$

$$K_{xx} \text{ bush} = 2 K_{ylyl} \quad \dots \quad 3.70$$

$$K_{xy} \text{ bush} = - 2 K_{ylxl} \quad \dots \quad 3.71$$

$$C_{yy} \text{ bush} = 2 C_{ylyl} \quad \dots \quad 3.72$$

$$C_{yx} \text{ bush} = 2 C_{ylxl} \quad \dots \quad 3.73$$

$$C_{xx} \text{ bush} = 2 C_{ylyl} \quad \dots \quad 3.74$$

$$C_{xy} \text{ bush} = 2 C_{ylxl} \quad \dots \quad 3.75$$

Hence operating characteristics for the complete hydrostatic bearing are determined. The theory described above, and in sections 3.1 and 3.2 was transformed into a computer program (see section B-I) which could be used by the designer of such a hydrostatic bearing bush.

### 3.4 Squeeze Film Damping Effects

One additional source of damping which has not been considered thus far is squeeze film damping at the lands of the hydrostatic bearing pads. During vibration oscillations of the bearing surface against the lands, the oil in the clearance must move accordingly to allow the clearance to decrease or to fill the gap as the clearance increases. Reaction to this fluid motion is provided by viscous shear forces against both



bearing surfaces and gives rise to squeeze film damping. An estimation of the magnitude of squeeze film damping is shown below. Considering the land shown in fig 3.4 the flow equation for the oil in the clearance may be obtained from Reynolds equation

$$\frac{d}{dx} \left( \frac{c^3}{12 \mu} \frac{dp}{dx} \right) = \frac{dc}{dt} \quad \dots \quad 3.76$$

Integrating twice with respect to x, assuming dc/dt constant, and applying the boundary conditions  $p = 0$  at  $x = \pm W/2$  yields values for the constants of integration. Hence, the equation 3.77 describing the pressure distribution over the lands is obtained.

$$p = \frac{12 \mu}{c^3} \left[ \left( \frac{dc}{dt} \right) \frac{x^2}{2} - \left( \frac{dc}{dt} \right) \frac{W^2}{8} \right] \quad \dots \quad 3.77$$

The force opposing motion of the bearing surfaces relative to each other is given by integrating p over the land area.

Then, if the length of the land is  $\ell$ , the total force offered by the squeeze film action is

$$F = - \frac{dc}{dt} \frac{W^3 \mu}{c^3} \ell \quad \dots \quad 3.78$$

But the damping coefficient is related to damping force by

$$F = - C \left( \frac{dc}{dt} \right) \quad \dots \quad 3.79$$

then by comparing equations 3.78 and 3.79 the value of the damping coefficient due to squeeze film action is

$$C = \mu \frac{W^3}{c^3} \ell \quad \dots \quad 3.80$$

Substituting values of  $\mu$ ,  $W$ ,  $c$  and  $\ell$  into equation 3.80 applicable to the hydrostatic bearing used in the experimental work described in this thesis, it was found that the squeeze film damping was insignificantly small when compared with that due to oil flow in the hydrostatic bearing system.

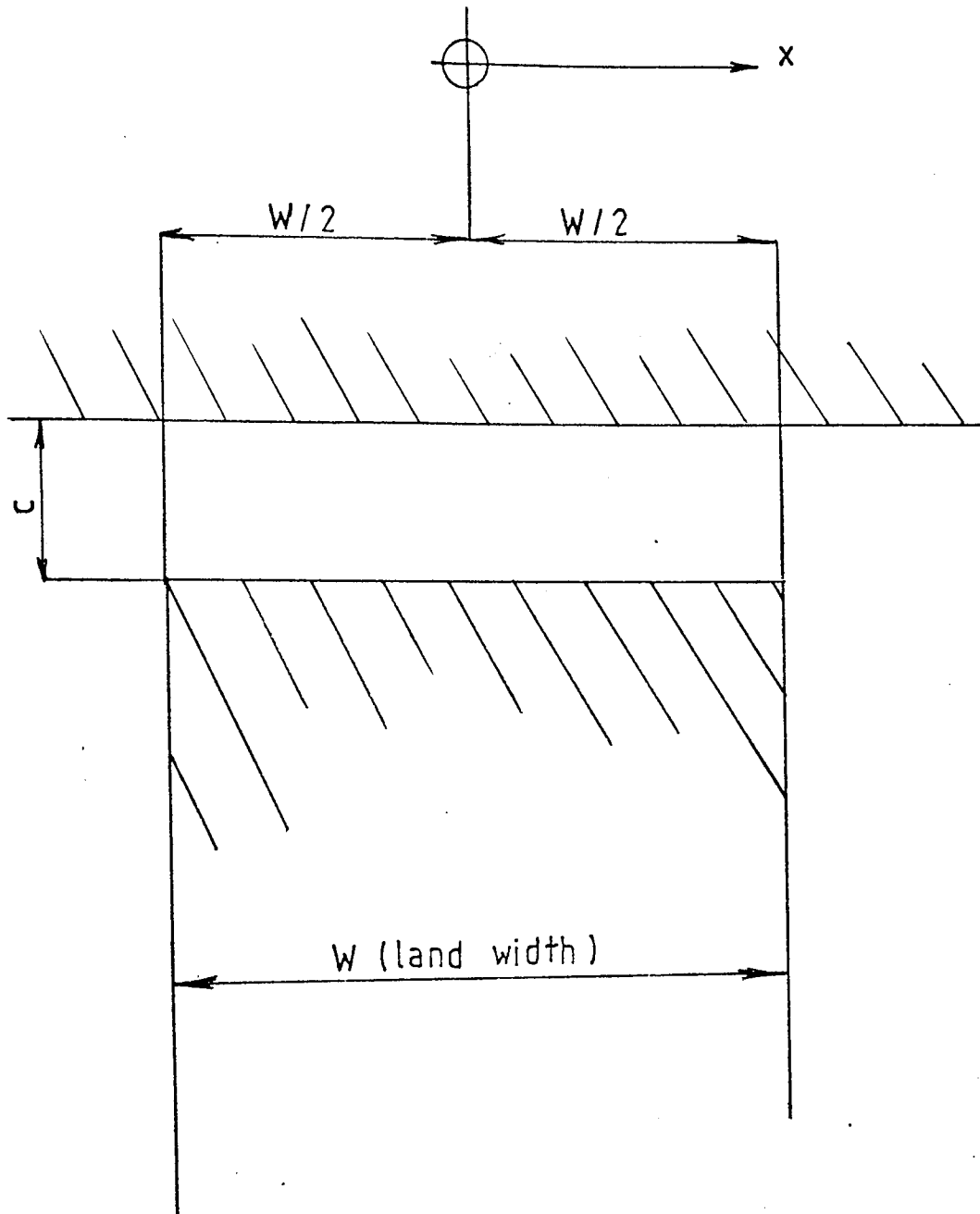


FIG 3.4 SQUEEZE FILM AT A BEARING LAND

### 3.5 Confirmation of the Accuracy of the 'mid-land' type of Approximation

The flow equations developed for the hydrostatic bearing in sections 3.1 and 3.2 utilise a mid-land approximation for effective bearing area as far as calculation of load on the bearing is concerned. This approximation assumes that the effective bearing pressure is equal to the pocket pressure and acts over an effective bearing area defined by the centre-line of the land surrounding the pocket (see figure 3.5). For the straight sections of land this is the same as assuming a linear pressure drop across the lands, which is normal. For the land sections local to the corners of the hydrostatic pockets it is difficult to say, intuitively, exactly what the pressure distribution is, however. The corner sections of land offer a bigger flow area for the oil leaving the corner of the pocket, as the oil flows further away from the pocket, and so the oil pressure is likely to decrease more rapidly (see figure 3.6). Obviously, then the accuracy of the approximation is dependent on the magnitude of the land width compared to other pocket dimensions (the larger the land width, the greater the inaccuracy).

It is necessary then to estimate the accuracy of the mid-land approximation when used for the hydrostatic bearing details appropriate to the test rig. To do this a finite difference computer program (see appendix BIII) was written which calculated the oil pressures at various positions on the bearing land, and thus determined more accurately the bearing load. Because of the symmetry of the hydrostatic bearing it was only necessary to examine a quarter section of the land surrounding the pocket. The mesh was made more and more fine until the load apparently converged to a constant value as indicated by the graph of figure 3.7. The meshes used are shown in figure 3.8. Since the error percentage is what was required, the pocket pressure was assumed to be 10 Pa, and the drain pressure zero, for ease of calculation. Bearing dimensions used were length = 7 cm, width = 4 cm, land width = 1 cm.

It can be seen from fig 3.7 that the bearing load, as suggested by finite difference methods is  $17.7 \times 10^{-3}$  N. This compares with a load calculated using the mid-land approximation of  $18.0 \times 10^{-3}$  N. Thus the error introduced by using the mid-land approximation is 1.7% which is low enough to be acceptable. Note this analysis could yield an appropriate correction factor to be used if deemed necessary.

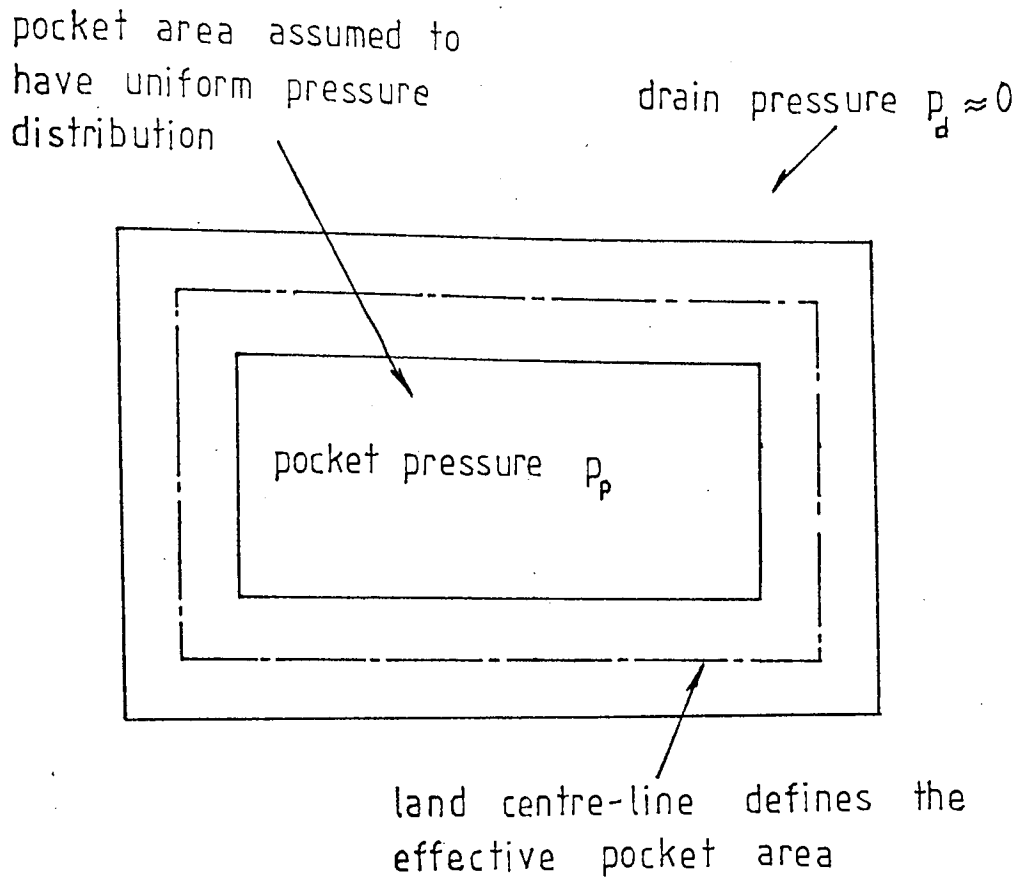


FIG 3.5 PLAN OF ONE HYDROSTATIC PAD

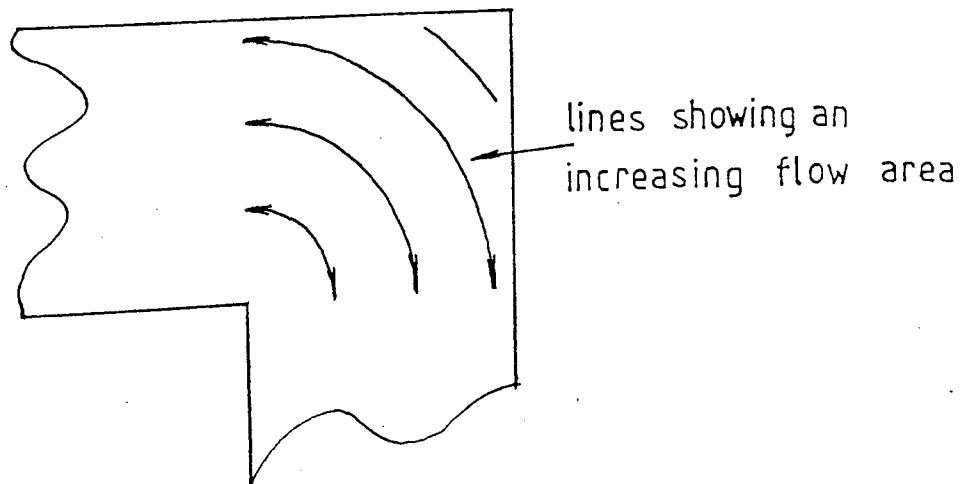


FIG 3.6 PLAN OF A HYDROSTATIC PAD CORNER

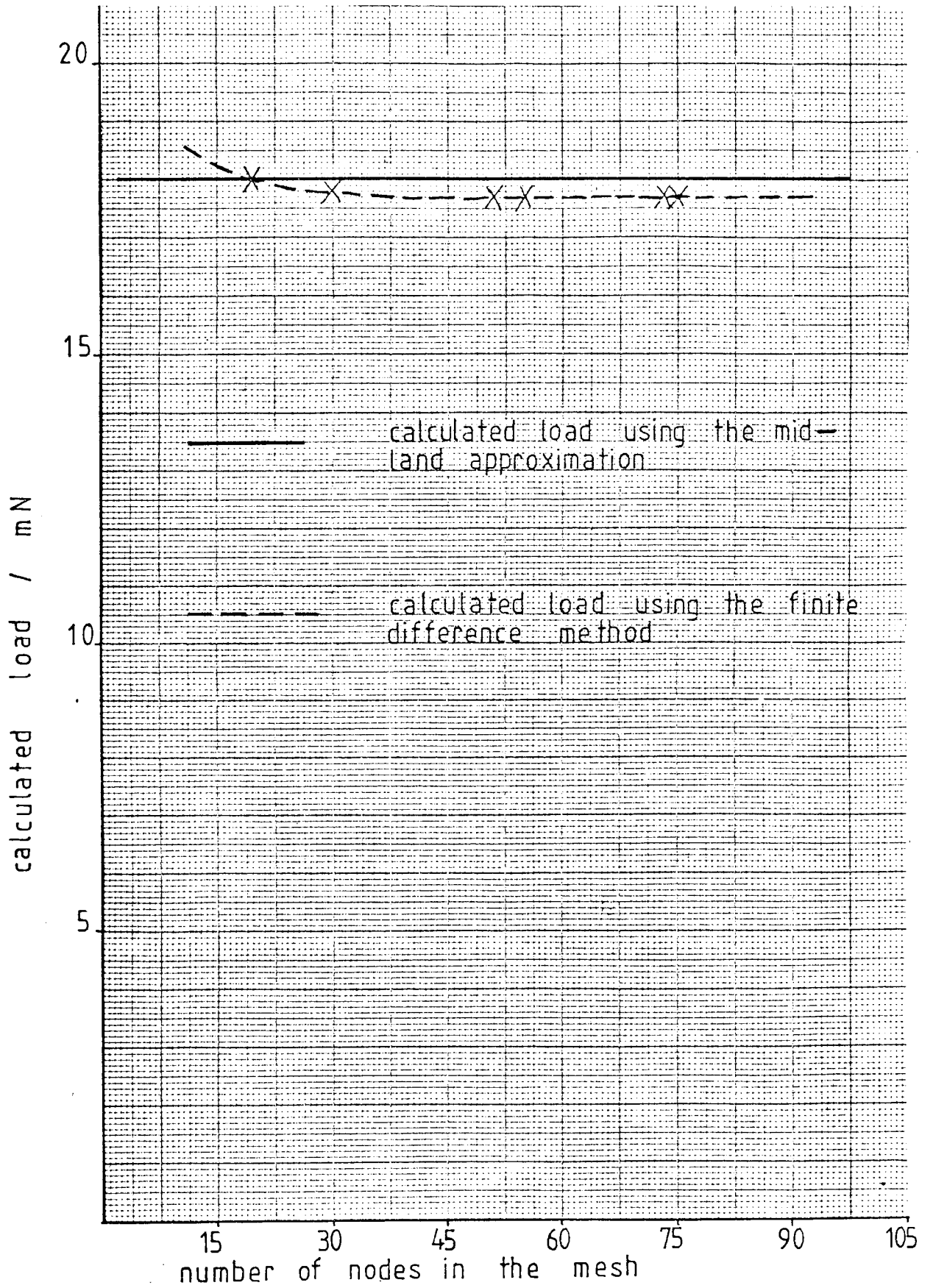
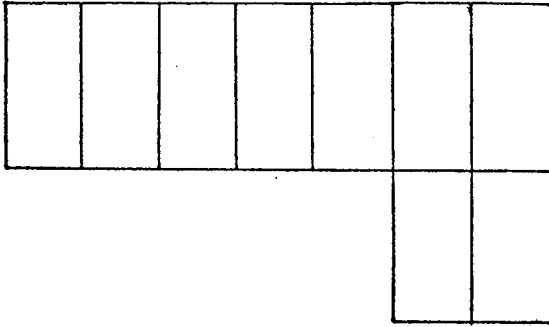
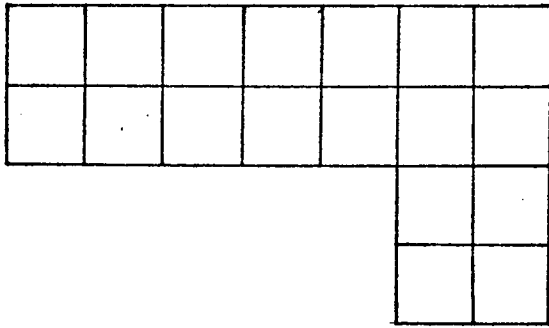


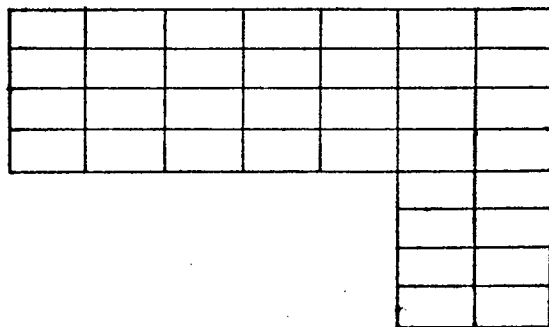
FIG 3.7 COMPARISON OF BEARING LOADS DETERMINED  
USING ANALYTICAL AND NUMERICAL METHODS



mesh 1, 19 nodes, load = 18.0 mN

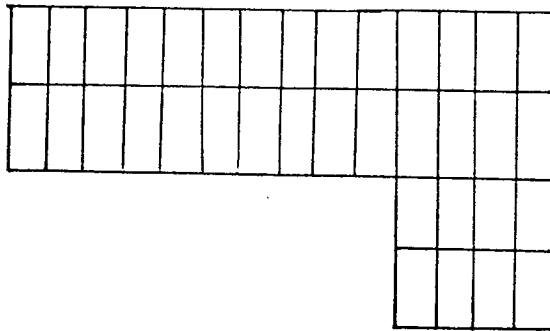


mesh 2, 30 nodes, load = 17.8 mN

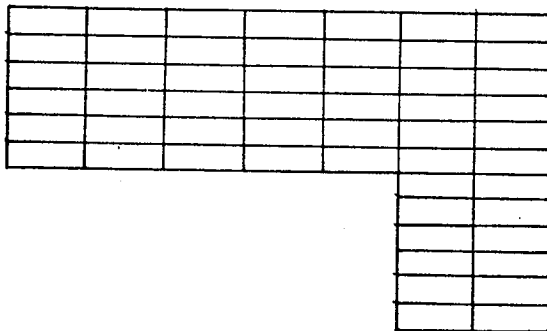


mesh 3, 52 nodes, load = 17.7 mN

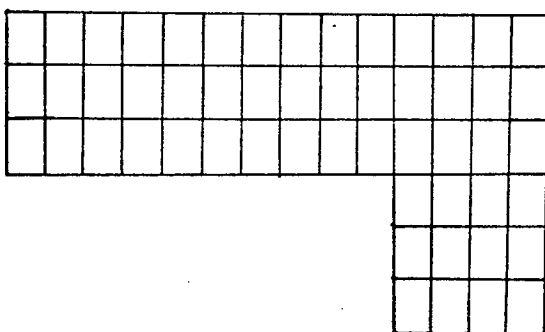
FIG 3.8a MESHES USED FOR THE FINITE DIFFERENCE WORK



mesh 4, 55 nodes, load=17.7 mN



mesh 5, 74 nodes, load=17.7 mN



mesh 6, 75 nodes, load=17.7 mN

FIG 3.8 b MESHES USED FOR THE FINITE DIFFERENCE  
WORK



## CHAPTER FOUR

### RELEVANCE OF THE REQUIRED EXPERIMENTAL MEASUREMENTS

## CHAPTER FOUR

### RELEVANCE OF THE REQUIRED EXPERIMENTAL MEASUREMENTS

#### 4.1 Test Objectives

Designing a bearing of the proposed two-oil-film type for installation on a machine requires two basic pre-conditions. These are 1) that one is able to predict the static and dynamic performance of the hydrostatic bearing and 2) that one is able to predict how the hydrostatic bearing interacts with the journal bearing, under both static and dynamic operating conditions, to provide bearing characteristics that may be completely different to the original journal bearing characteristics. (Knowledge of the journal bearing characteristics is assumed. Theory has been presented in several papers, references (6), (7) and (9) being some, and further development of it is not part of the specification of the work contained in this thesis). The objectives of the testing, then, were to prove the hydrostatic bearing theory and that of how the hydrostatic bearing interacts with the journal bearing. In order to do this it was necessary to measure the static characteristics and the dynamic stiffness and damping coefficients of both bearings independently, and of the combined two oil film bearing. The next two sections discuss methods of measuring the dynamic oil film coefficients, and the theory to determine the performance characteristics of the two oil film bearing, knowing those of the two bearings independently.

#### 4.2 General Equations of Motion

In this section the equations of motion for the shaft-bearing system are developed to a form from which the bearing dynamic oil film coefficients may be derived. It is assumed that the test journal, bearing bush and pedestal structures are rigid, that the journal is aligned in the bearing such that motion can be considered in one plane only as

described by fig 4.1, and that the oil film forces vary linearly with instantaneous displacement and velocity such that eight bearing coefficients can be used to describe its behaviour.

The journal is subjected to a harmonic forcing in the horizontal and vertical directions by forces  $F_x$  and  $F_y$  respectively, where

$$F_x = F_{x0} \sin \omega t \quad \dots \quad 4.1$$

$$F_y = F_{y0} \cos \omega t \quad \dots \quad 4.2$$

such that the horizontal force lags the vertical force by  $90^\circ$  phase difference. These forces accelerate the journal and are acted against by the oil film stiffness and damping as described below by the equations of motion for the journal.

$$F_x = M(\ddot{x} + \ddot{x}_p) + K_{xx}.x + K_{xy}.y + C_{xx}.\dot{x} + C_{xy}.\dot{y} \quad \dots \quad 4.3$$

$$F_y = M(\ddot{y} + \ddot{y}_p) + K_{yy}.y + K_{yx}.x + C_{yy}.\dot{y} + C_{yx}.\dot{x} \quad \dots \quad 4.4$$

where  $M$  is the journal mass and  $x$  and  $y$  are the displacements of the journal relative to the bearing bush in the horizontal and vertical directions respectively.  $K_{ii}$  and  $C_{ii}$  are the direct stiffness and damping coefficients for the oil film where  $K_{ij}$  and  $C_{ij}$  indicate force in the  $i$  direction per unit displacement or velocity respectively in the  $j$  direction (the cross coupling terms).  $x_p$  and  $y_p$  are the respective horizontal and vertical displacements of the pedestal holding the bearing bush relative to space. Since the forcing is harmonic, the motion of the shaft and pedestal will also be harmonic. The journal motion will be assumed to lag the exciting force by phase angles  $\alpha_1$  and  $\alpha_2$  in the horizontal and vertical directions respectively. Similarly, the pedestal phase lags will be  $\gamma_1$  and  $\gamma_2$ . Then

$$x = X \sin(\omega t - \alpha_1) \quad \dots \quad 4.5$$

$$y = Y \cos(\omega t - \alpha_2) \quad \dots \quad 4.6$$

where  $X$  and  $Y$  are the horizontal and vertical vibration amplitudes respectively of the journal relative to the bearing bush, and

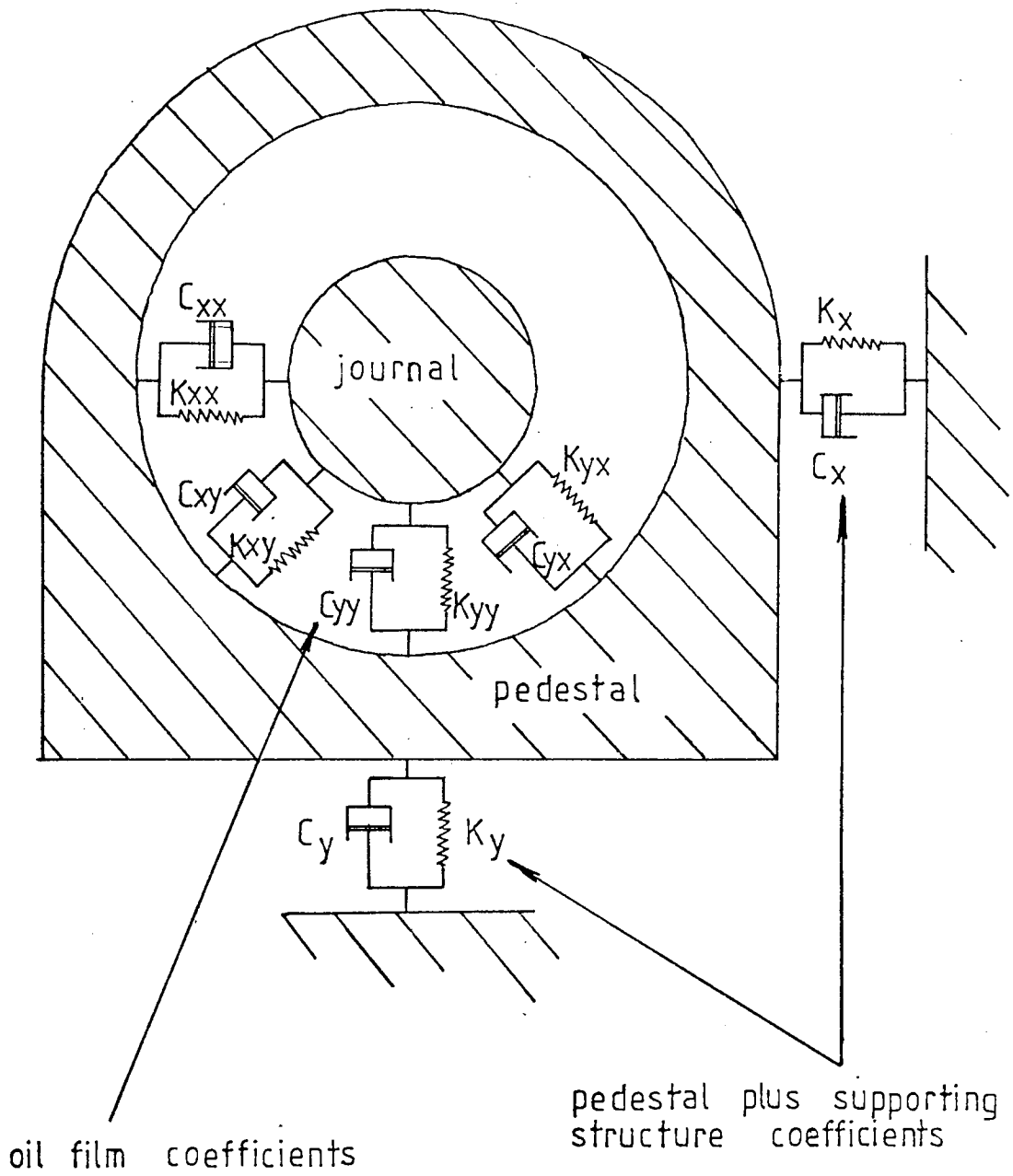


FIG 4.1    DIAGRAM OF THE BEARING-PEDESTAL SYSTEM

$$x_p = X_p \text{ Sin } (\omega t - \gamma_1) \quad \dots \quad 4.7$$

$$y_p = Y_p \text{ Cos } (\omega t - \gamma_2) \quad \dots \quad 4.8$$

where  $X_p$  and  $Y_p$  are the horizontal and vertical vibration amplitudes respectively of the pedestal relative to space. Substituting equations 4.1 and 4.2, together with equations 4.5 to 4.8 and their differentials with respect to time, into equations 4.3 and 4.4 gives

$$\begin{aligned} F_{x0} \text{ Sin } \omega t = & M[- X \omega^2 \text{ Sin}(\omega t - \alpha_1) - X_p \omega^2 \text{ Sin}(\omega t - \gamma_1)] \\ & + K_{xx} X \text{ Sin}(\omega t - \alpha_1) + K_{xy} Y \text{ Cos}(\omega t - \alpha_2) \\ & + C_{xx} X \omega \text{ Cos}(\omega t - \alpha_1) - C_{xy} Y \omega \text{ Sin}(\omega t - \alpha_2). \end{aligned} \quad 4.9$$

and

$$\begin{aligned} F_{y0} \text{ Cos } \omega t = & M[- Y \omega^2 \text{ Cos}(\omega t - \alpha_2) - Y_p \omega^2 \text{ Cos}(\omega t - \gamma_2)] \\ & + K_{yy} Y \text{ Cos}(\omega t - \alpha_2) + K_{yx} X \text{ Sin}(\omega t - \alpha_1) \\ & - C_{yy} Y \omega \text{ Sin}(\omega t - \alpha_2) + C_{yx} X \omega \text{ Cos}(\omega t - \alpha_1). \end{aligned} \quad 4.10$$

Setting  $\omega t$  to zero, in equations 4.9 and 4.10 gives

$$\begin{aligned} 0 = & M[- X \omega^2 \text{ Sin}(-\alpha_1) - X_p \omega^2 \text{ Sin}(-\gamma_1)] \\ & + K_{xx} X \text{ Sin}(-\alpha_1) + K_{xy} Y \text{ Cos}(-\alpha_2) \\ & + C_{xx} X \omega \text{ Cos}(-\alpha_1) - C_{xy} Y \omega \text{ Sin}(-\alpha_2) \end{aligned} \quad \dots \quad 4.11$$

and

$$\begin{aligned} F_{y0} = & M[- Y \omega^2 \text{ Cos}(-\alpha_2) - Y_p \omega^2 \text{ Cos}(-\gamma_2)] \\ & + K_{yy} Y \text{ Cos}(-\alpha_2) + K_{yx} X \text{ Sin}(-\alpha_1) \\ & - C_{yy} Y \omega \text{ Sin}(-\alpha_2) + C_{yx} X \omega \text{ Cos}(-\alpha_1) \end{aligned} \quad \dots \quad 4.12$$

and setting  $\omega t$  to  $\pi/2$  gives

$$\begin{aligned} F_{x0} = & M[- X \omega^2 \text{ Cos}(\alpha_1) - X_p \omega^2 \text{ Cos}(\gamma_1)] \\ & + K_{xx} X \text{ Cos}(\alpha_1) + K_{xy} Y \text{ Sin}(\alpha_2) \\ & + C_{xx} X \omega \text{ Sin}(\alpha_1) - C_{xy} Y \omega \text{ Cos}(\alpha_2) \end{aligned} \quad \dots \quad 4.13$$

and

$$\begin{aligned} 0 = & M[- Y \omega^2 \text{ Sin}(\alpha_2) - Y_p \omega^2 \text{ Sin}(\gamma_2)] \\ & + K_{yy} Y \text{ Sin}(\alpha_2) + K_{yx} X \text{ Cos}(\alpha_1) \\ & - C_{yy} Y \omega \text{ Cos}(\alpha_2) + C_{yx} X \omega \text{ Sin}(\alpha_1) \end{aligned} \quad \dots \quad 4.14$$



Equations 4.11 to 4.14 may be re-arranged and expressed in matrix form as

$$\begin{bmatrix} M\omega^2 - K_{xx} & K_{xy} & \omega C_{xx} & \omega C_{xy} \\ -K_{yx} & K_{yy} - M\omega^2 & \omega C_{yx} & \omega C_{yy} \\ \omega C_{xx} & -\omega C_{xy} & K_{xx} - M\omega^2 & K_{xy} \\ \omega C_{yx} & -\omega C_{yy} & K_{yx} & K_{yy} - M\omega^2 \end{bmatrix} \begin{bmatrix} X \sin \alpha_1 \\ Y \cos \alpha_2 \\ X \cos \alpha_1 \\ Y \sin \alpha_2 \end{bmatrix} = \begin{bmatrix} -M\omega^2 X_p \sin \gamma_1 \\ F_{y0} + M\omega^2 Y_p \cos \gamma_2 \\ F_{x0} + M\omega^2 X_p \cos \gamma_1 \\ M\omega^2 Y_p \sin \gamma_2 \end{bmatrix} \quad \dots \quad 4.15$$

Equation 4.15 contains four simultaneous expressions in eight variables (the eight oil film coefficients). To solve for the eight coefficients requires knowledge of journal and pedestal vibration amplitudes and phases, of the journal mass, of the force amplitudes and of the exciting frequency. All of these variables can be measured. Ways in which equation 4.15 can be used to solve for the eight bearing coefficients are discussed in section 4.3.

The BASIC computer program in appendix B (section IV) is based on equation 4.15 and was used to determine effective dynamic oil film coefficients necessarily implied by experimentally measured shaft vibrations.

### 4.3 Experimental Methods for Measuring Oil Film Coefficients

In this section some of the practical implications of using equation 4.15 to determine the eight oil film coefficients are discussed. A number of alternative methods of measuring bearing coefficients are compared.

A problem with using equation 4.15 to determine the bearing coefficients was that it is itself composed of four simultaneous equations whereas to solve for eight variables, eight such equations would be required. Thus another four equations were required. These were developed as equation 4.15 but with a different value for one of the measured

variables. Alternatives considered were to change a) the exciting force magnitude, b) the journal mass, c) pedestal stiffness or d) exciting frequency.

Change of exciting force was not considered to be the best solution because this was chosen to give small vibration amplitudes initially, such that errors in the measured oil film coefficients resulting from non-linearity of the bearing oil film were kept small. (The oil film forces were approximated to being proportional to instantaneous displacement and velocity of the journal, for small amplitudes, whereas a more accurate model would also have forces proportional to powers of displacement and velocity). Increasing the magnitude of the exciting force would have increased the vibration amplitudes and thus would have increased these errors.

An increase in the journal mass, large enough to significantly alter the force required to give a certain vibration amplitude could have resulted in the addition of very large weights which would have been impractical. A corresponding change would also have had to be made of the externally applied static load in order to keep the Sommerfeld number the same, and of exciting force to maintain the original vibration amplitude.

A change of pedestal stiffness (or mass) could have been used to change the pedestal vibration amplitudes. Such a facility, which would have ensured a large enough stiffness change to significantly affect vibration amplitudes, would have complicated the design of the test rig however.

A change of exciting frequency was another alternative. A corresponding change in force amplitude to maintain the original vibration amplitudes might also have been necessary here, depending on the rig design. This is the alternative which was chosen, and its use was made simple by designing the test rig to be excited by rotating unbalance weights

around the same axis as that which the journal rotated about, but which were mounted on a separate independently driven shaft inside the test journal (see Chapter 5). By changing the direction of rotation of the unbalanced shaft, but maintaining the same speed, it was possible to effect a change of exciting frequency and maintain the same exciting force amplitude (and hence similar vibration amplitudes) without having to alter the unbalance.

Other means of applying the exciting force considered were a) the use of vibrators acting on the rotor (or bearing bush) and b) the use of an unbalance attached to the test journal.

The advantage offered by the shakers was the ease with which force and frequency could have been varied independently. Disadvantages were the cost of the equipment and the complication of having to correctly phase horizontal and vertical shakers to accurately stimulate a rotating unbalance (for an accurate model it would have been necessary to simulate the pressure wedge that builds up in front of a shaft as it whirls).

The use of an unbalanced test journal, despite its simplicity, would have limited the exciting frequency to that of the journal. This would have meant that a reversal of direction of rotation of the unbalance, as discussed above, would not have been possible as it would have changed the Sommerfeld Number. Exciting at journal rotational frequency would also have permitted the possibility of runout\* affecting the measured vibrations (see also section 5.11). If this method of exciting the journal had been used, another method would still have had to be found for testing the hydrostatic bearing.

---

\* For a definition of the term 'runout' see section 5.11.



Another method of measuring bearing coefficients which was considered was the transient technique whereby the shaft is displaced by a known force and then suddenly released. The resulting transient vibrations are then used to determine the oil film coefficients. Disadvantages of this method are that the transient vibrations last only for a short time which could make measuring difficult, and that the pressure wedge effect discussed earlier is not simulated. For these reasons the method was rejected.

#### 4.4 Oil Film Coefficients for the Combined Hydrodynamic and Hydrostatic Bearing

If a bearing designer is to be able to predict the dynamic operation of the proposed two oil film bearing then an understanding of the way in which the hydrodynamic and hydrostatic oil films interact is necessary. The equations developed below show how the two independent sets of bearing coefficients can be used to determine a set of coefficients for the combined bearing. It then becomes clear that the coefficients for the combined bearing can be measured in the same way as those for one of the individual bearings.

The system being considered is that of figure 4.2 where alignment and rigidity of the components is assumed and the journal bearing bush has negligible mass. The journal is subjected to a harmonic forcing in the horizontal and vertical directions as stated in section 4.2. Then the equations 4.1 and 4.2 describing the force may be re-written as below.

$$F_x = F_{x0} \sin \omega t = F_{x1} \sin \omega t + F_{x2} \cos \omega t \quad \dots \quad 4.16$$

$$F_y = F_{y0} \cos \omega t = F_{y1} \sin \omega t + F_{y2} \cos \omega t \quad \dots \quad 4.17$$

where  $F_x$  is the force in the horizontal direction and  $F_y$  the force in the vertical direction.  $F_{x1}$  and  $F_{x2}$  are the real and imaginary force amplitudes respectively in the horizontal direction and  $F_{y2}$  and  $F_{y1}$  the

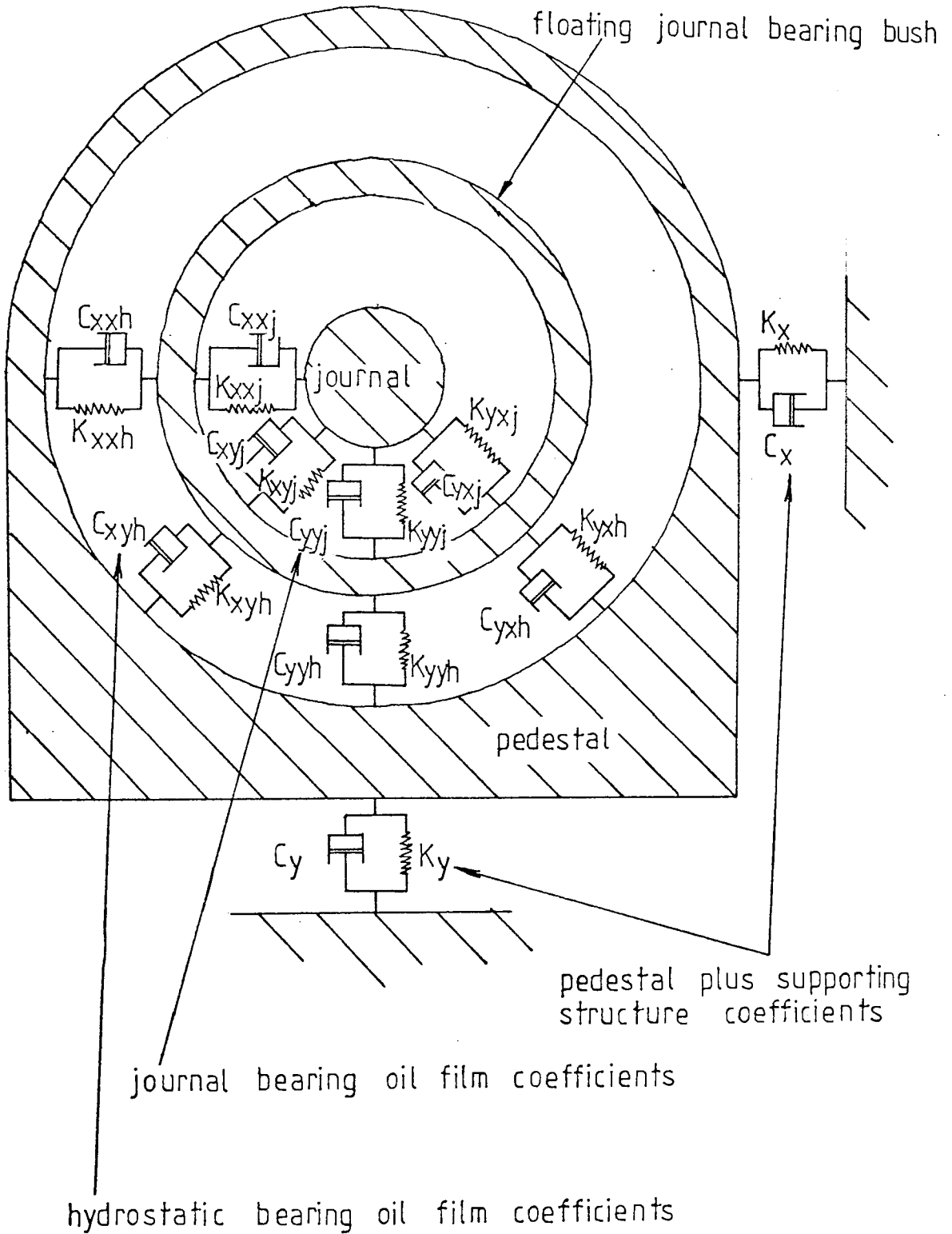


FIG 4.2 DIAGRAM OF THE TWO-OIL-FILM BEARING-  
PEDESTAL SYSTEM

real and imaginary force amplitudes respectively in the vertical direction. Let the corresponding deflections of the journal relative to the journal bearing bush be  $x$  and  $y$  where

$$x = X_1 \sin \omega t + X_2 \cos \omega t \quad \dots \quad 4.18$$

$$y = Y_1 \sin \omega t + Y_2 \cos \omega t \quad \dots \quad 4.19$$

where  $X_1$  and  $X_2$  are the displacement component amplitudes in phase and out of phase respectively, with the horizontal force. Similarly  $Y_2$  and  $Y_1$  are the in phase and out of phase component amplitudes respectively, of displacement in the vertical direction, relative to the force in the vertical direction. Then the velocities, in the horizontal and vertical directions, of the journal relative to the journal bearing bush are

$$\dot{x} = \omega X_1 \cos \omega t - \omega X_2 \sin \omega t \quad \dots \quad 4.20$$

$$\dot{y} = \omega Y_1 \cos \omega t - \omega Y_2 \sin \omega t \quad \dots \quad 4.21$$

The force-displacement relationships for movement of the journal relative to its bush are

$$F_x = K_{xx} x + K_{xy} y + C_{xx} \dot{x} + C_{xy} \dot{y} \quad \dots \quad 4.22$$

$$F_y = K_{yx} x + K_{yy} y + C_{yx} \dot{x} + C_{yy} \dot{y} \quad \dots \quad 4.23$$

Substituting equations 4.16 to 4.21 into equations 4.22 and 4.23, and comparing coefficients of  $\sin \omega t$  and  $\cos \omega t$  gives, in matrix form

$$\begin{bmatrix} F_{x1} \\ F_{x2} \\ F_{y1} \\ F_{y2} \end{bmatrix} = \begin{bmatrix} K_{xx} & K_{xy} & -\omega C_{xx} & -\omega C_{xy} \\ \omega C_{xx} & \omega C_{xy} & K_{xx} & K_{xy} \\ K_{yx} & K_{yy} & -\omega C_{yx} & -\omega C_{yy} \\ \omega C_{yx} & \omega C_{yy} & K_{yx} & K_{yy} \end{bmatrix} \begin{bmatrix} X_1 \\ Y_1 \\ X_2 \\ Y_2 \end{bmatrix} \quad \dots \quad 4.24$$

which may be simplified and rewritten as

$$[F] = [K_j] [u] \quad \dots \quad 4.25$$

where the suffix 'j' indicates that the stiffness matrix refers to the

journal bearing. Similarly, equation 4.26 may be developed describing the hydrostatic bearing operation

$$[F] = [K_h] [v] \quad \dots \quad 4.26$$

where the suffix 'h' indicates that the stiffness matrix refers to the hydrostatic bearing bush, and the v matrix describes motion of the journal bearing bush relative to the hydrostatic bearing bush. But the total deflection of the journal relative to the hydrostatic bearing bush is  $w = u + v$ , ie the vector sum of the two deflections u and v, where

$$[w] = \left[ [K_j]^{-1} + [K_h]^{-1} \right] [F] \quad \dots \quad 4.27$$

which may be re-arranged to give

$$[F] = [K_e] [w] \quad \dots \quad 4.28$$

where

$$[K_e] = \left[ [K_j]^{-1} + [K_h]^{-1} \right]^{-1} \quad \dots \quad 4.29$$

$K_e$  is the stiffness matrix of an equivalent single bearing having the same performance characteristics as the combined hydrodynamic and hydrostatic bearings. Since  $K_e$  is of the same form as  $K_j$  and  $K_h$ , the equivalent bearing coefficients may be measured in the same way as those of the journal and hydrostatic bearings.

The above theory was transformed into a BASIC computer program (see section B-II) used to determine theoretical operating characteristics for a combined hydrostatic and hydrodynamic bearing arrangement.

CHAPTER FIVE

EXPERIMENTAL TEST RIG

CHAPTER FIVE

EXPERIMENTAL TEST RIG

5.1 General Description

General considerations influencing the design were that the rig was to be used to study operating characteristics of the journal bearing alone, the hydrostatic bearing alone, and the combined journal and hydrostatic bearing. These factors were facilitated by enabling the journal bearing bush to be clamped rigidly to the hydrostatic bush (for journal bearing testing), or to the test journal (for hydrostatic bearing testing) when necessary. The size of the rig was fixed by the necessity for it to be realistically large whilst not being too expensive. A diagram of the test rig is shown in figure 5.1. It consisted of a main rotor assembly (containing the unbalanced excitation shaft), two bearing bushes, and three fabricated pedestals.

The main rotor assembly was 'pinned' at one end by mounting it in a self-aligning rolling bearing whilst the other end was supported by the test bearing. A journal, representing the journal of a generator rotor, was machined on the test rotor at the site of the test bearing. This was held in a bearing bush similar in design to bearing bushes normally used to hold generator rotors. The difference in this case, was that instead of always being rigidly clamped to the pedestal, this bush could be held by the eight hydrostatic pads surrounding it. The hydrostatic bearing bush was, in turn, clamped between the cap and main structure of a fabricated pedestal.

Static loads could be applied to the rotor assembly via pneumatic cylinders, one at each end of the test pedestal, whilst dynamic excitation could be applied by means of a rotating unbalanced shaft, mounted inside the main rotor assembly. The test journal and excitation shaft were both

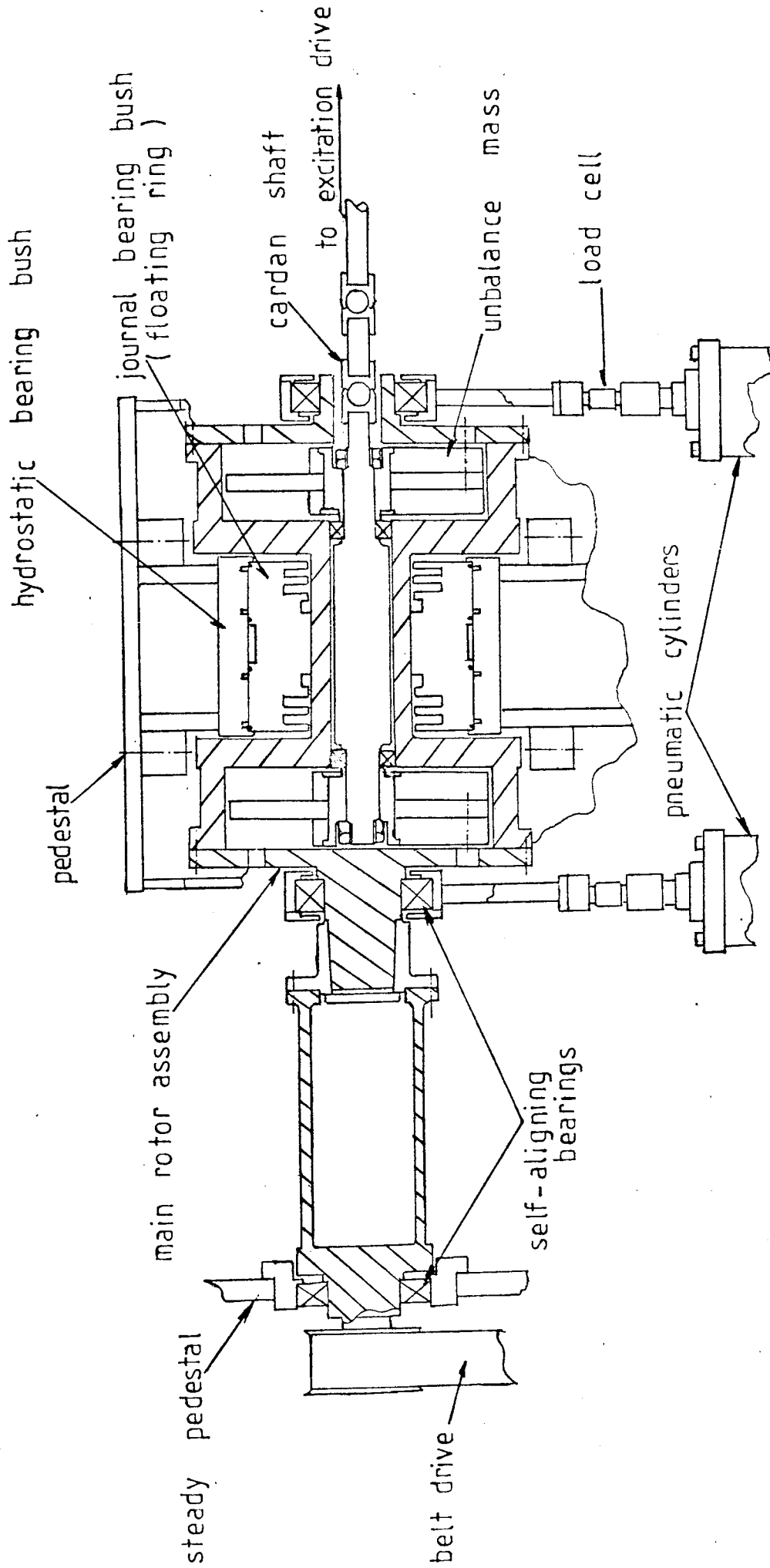


FIG 5.1 DIAGRAM OF THE TEST RIG.

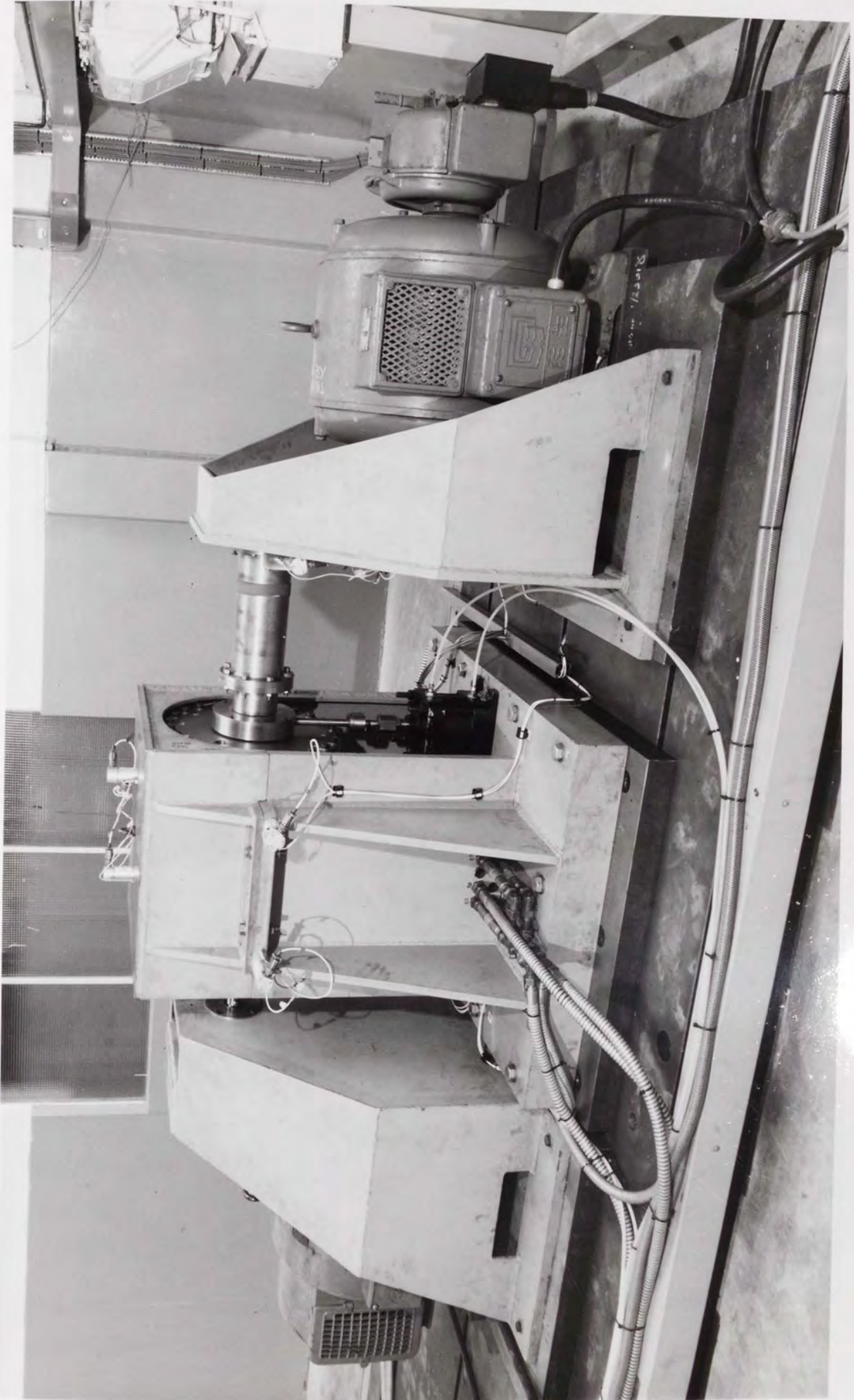


FIG 5.2 THE ASSEMBLED TEST RIG



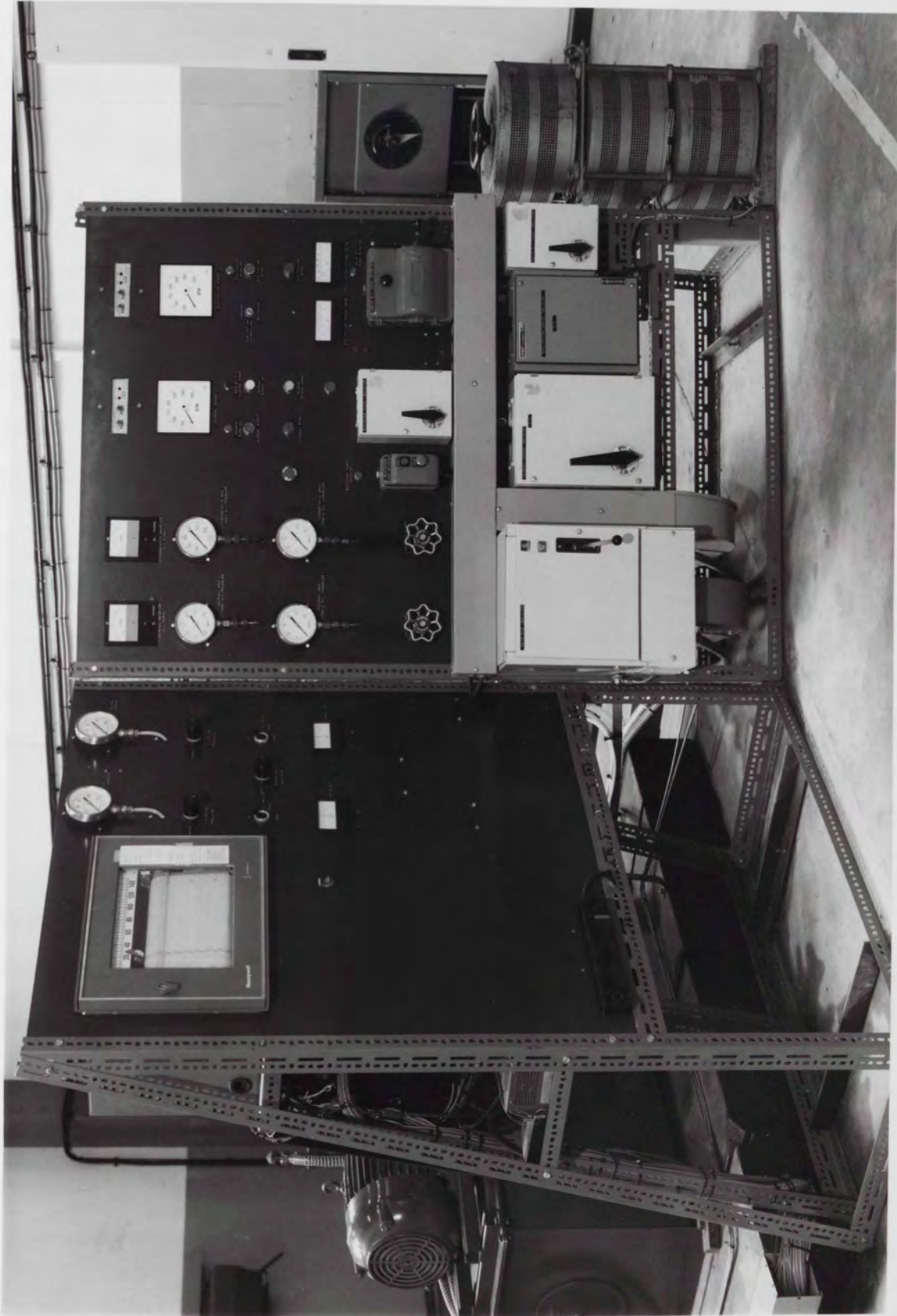


FIG 5.3 THE TEST RIG CONTROL PANEL

belt driven from opposite ends of the test rig.

The assembled test rig can be seen in figure 5.2 while figure 5.3 shows the control panel housing some of the instrumentation. Individual components of the test rig are discussed in more detail in the following sections of this chapter.

## 5.2 Test Rotor Description

The test rotor, shown in figure 5.4, was manufactured from a typical generator rotor steel and consisted of four basic parts. The test journal was 125 mm in diameter and at each end of the test journal the rotor opened out to 420 mm diameter. These two large diameter sections of the rotor were bored out to house unbalance masses used to excite the journal dynamically. The entire section of rotor that included the journal was bored to house a second shaft on which the unbalance masses were mounted. This was the main part of the test rotor, and it was complemented by two end-covers held in position by fitted bolts, which concealed the unbalance masses once they had been mounted.

The fourth part of the test rotor was a hollow extension shaft which was bolted to a flanged hub mounted on one of the end covers, and which had a self-aligning rolling bearing mounted on its other end. The self-aligning bearing was ultimately located in a second pedestal remote from the test bearing pedestal. The purpose of the extension shaft was twofold. Primarily it resulted in a test rotor that was pinned at one end considerably raising the 'rocking' stiffness of the rotor support mechanism. The extension shaft was hollow in order to keep down the corresponding diametral moment of inertia of the rotor and hence promote a high corresponding natural frequency that was above running speed. Secondly, the extension shaft served to maintain the alignment of the test journal in its bearing once this had been established. The

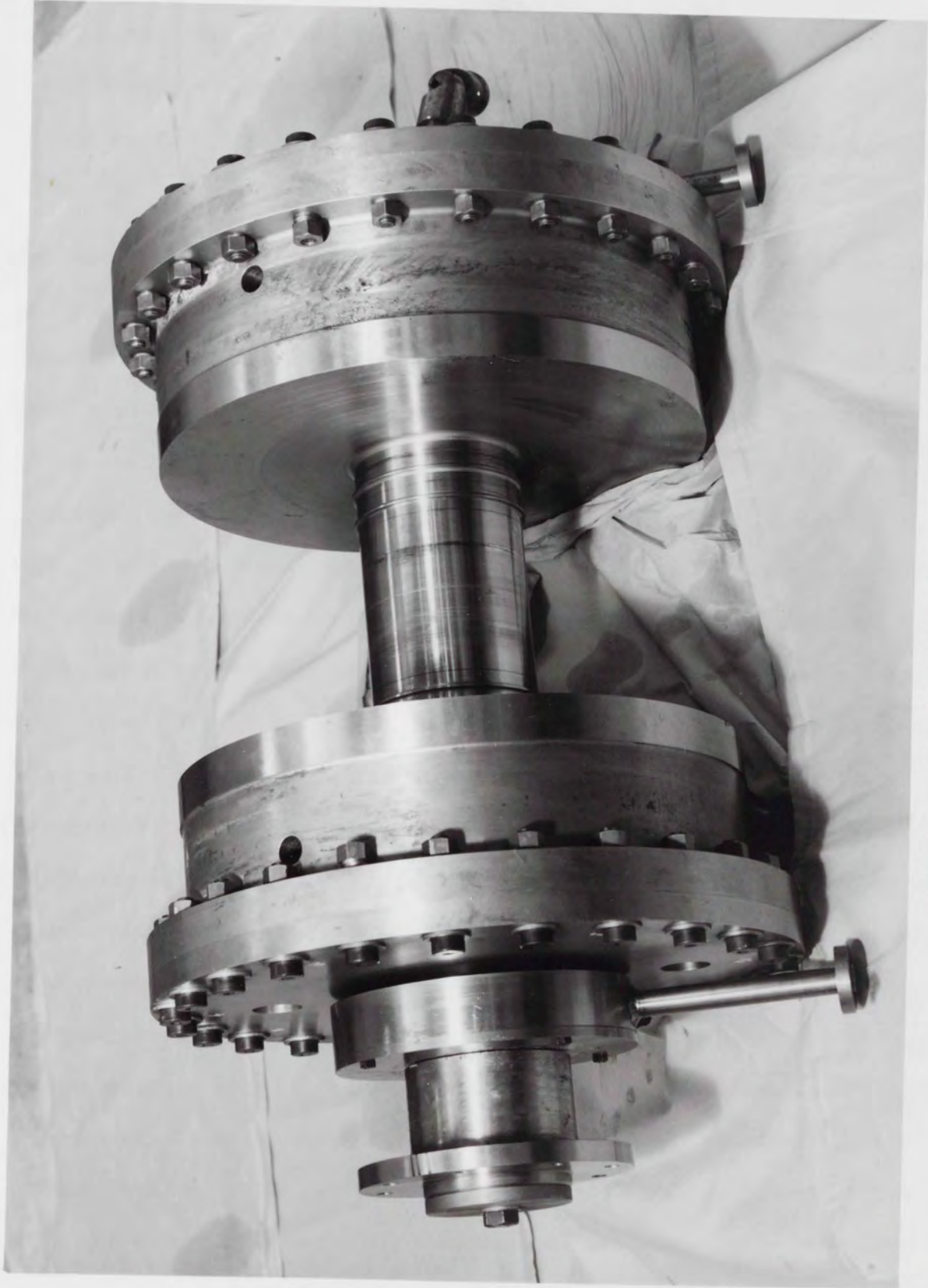


FIG 5.4 THE MAIN ROTOR ASSEMBLY

distance between the centres of the test bearing and the self-aligning bearing was made large enough to ensure that any displacement of the test journal in its bearing did not result in a forced misalignment of the journal (due to the other end of the shaft being pinned) large enough to significantly influence the test bearing performance. The misalignment resulting from a tilt ratio of about 0.1 was assumed to be tolerable, its effect on the bearing performance being minimal (see reference (9)).

Movement of the test journal was detected by means of inductive proximity probes mounted on the pedestal and 'looking at' the section of rotor housing the unbalance masses, immediately adjacent to the test journal. Four probes were mounted at each end of the test pedestal to observe rotor movement. A push-pull arrangement was adopted with two probes observing vertical movement, and two observing horizontal movement in each instance. Each probe also had a velocity probe mounted next to it to measure pedestal vibration so that ultimately the shaft movement in space could be deduced. The surfaces which the proximity probes observed were ground to  $0.4 \mu\text{m}$ , as was the test journal, and were machined concentric with the test journal to within  $6 \mu\text{m}$ . These tolerances reduced the possibility of the proximity probes measuring a signal that was caused mostly by mechanical runout\* rather than journal vibration during experiments which were performed using synchronous excitation. With asynchronous excitation the filtering network in the response analyser eliminated signals due to runout. The surfaces on which the proximity probes registered were checked for electrical runout before testing was carried out to ensure that this was small enough not to significantly affect results. This was done by rotating the rotor at 100 rpm, such that the rotor experienced an insignificant unbalance force, and comparing the amplitude indicated by the proximity probes to the known mechanical runout.

---

\* For a definition of the term 'runout' see section 5.11.

### 5.3 Journal Bearing

The test journal bearing was 125 mm (4.92") in diameter, had a length/diameter ratio of 0.6 and a 120° partial arc. The bearing radial clearance of 0.127 mm (0.005") was large enough to ensure that vibration amplitudes, whilst being large enough to measure, were not large enough compared with the radial clearance to result in non-linearity effects of the oil film affecting the results.

An oil inlet was provided midway along the length of the bush and an outlet at the corresponding position on the other side of the bush. This enabled additional cooling oil to be passed over the test journal as required. The remainder of the drain oil was collected by wipers after flowing axially out of the ends of the bearing. All oil inlets and outlets to the journal bearing bush were made ultimately at special fittings midway along the length of the bush, which enabled oil to be supplied to the journal bearing without affecting its movement and function as a part of the hydrostatic bearing. One journal bearing half bush is shown in figure 5.5.

The running temperature of the journal bearing bush was monitored by means of six thermocouples, mounted in holes drilled in the bush, with their hot junctions just touching the underside of the bearing bush white-metal. Oil inlet and outlet temperature was also monitored by means of thermocouples suitably positioned in the appropriate oil lines. Such temperature monitoring served to confirm normal operating conditions for the journal bearing and correct alignment.

### 5.4 Hydrostatic Bearing Bush

The hydrostatic bearing bush contained one group of hydrostatic bearing pads at each end, thus restricting tilt misalignment of the journal bearing bush. Each group consisted of one top, one bottom, one left

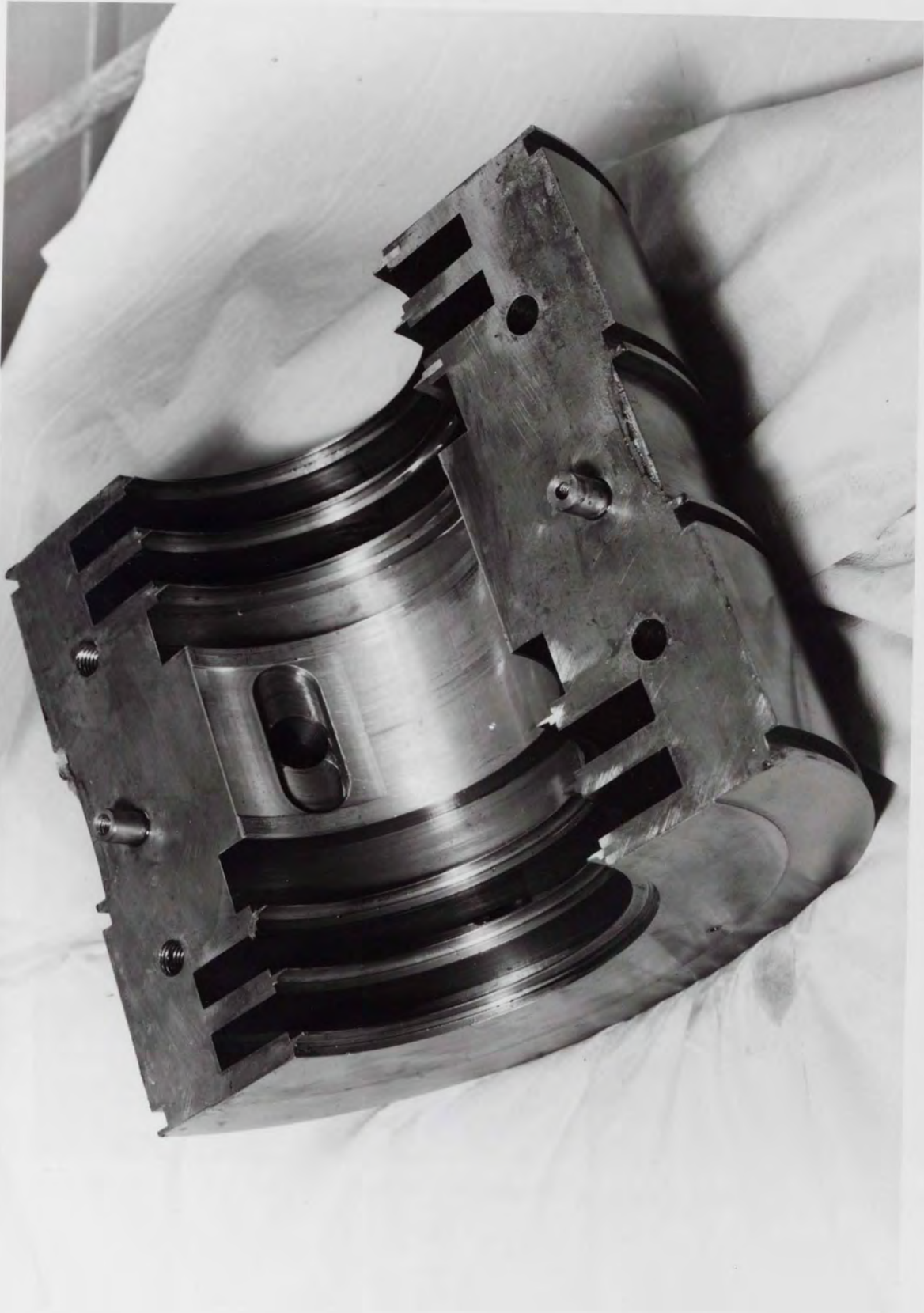


FIG 5.5 HALF OF THE JOURNAL BEARING BUSH

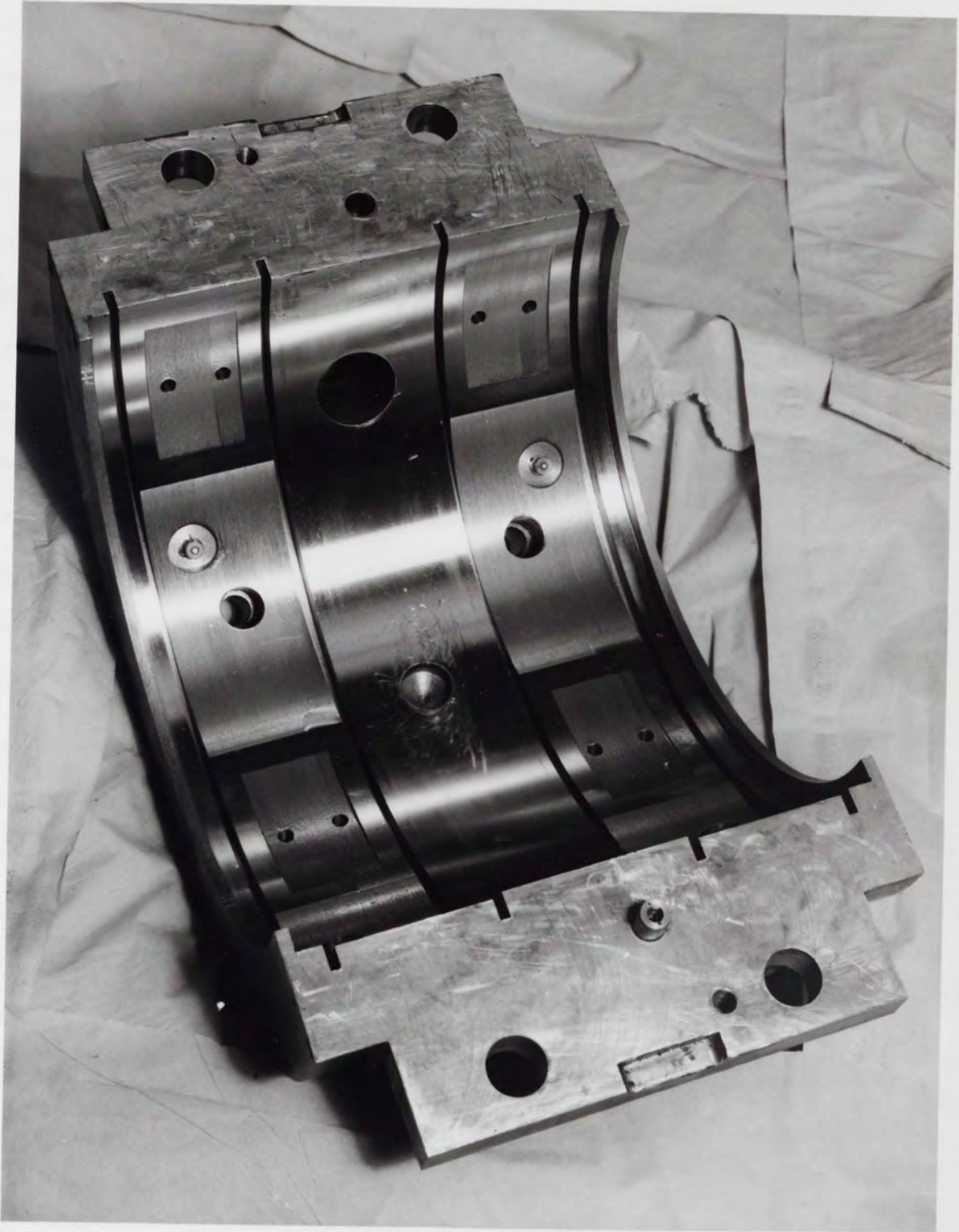


FIG 5.6 HALF OF THE HYDROSTATIC BEARING BUSH

and one right hydrostatic pad, each 4 cm x 7 cm projected dimensions, including 1 cm land width, ie there were four bearings in all controlling the vertical movement of the journal bearing bush and four controlling the horizontal movement. Because of the presence of horizontal hydrostatic pads, the bush was split at an angle to the horizontal into two half bushes, one of which is shown in figure 5.6 (this split line also matched the split line on the journal bearing bush). 'O' ring seals\* on each side of each group of hydrostatic pads ensured that the drain oil flowed into the specially machined drain grooves between the seals and hydrostatic pads, and from there into drain manifolds. Oil inlet to each pocket was via a capillary restrictor. Rotation of the journal bearing bush relative to the hydrostatic bearing was resisted by a pin which screwed into the journal bearing bush and registered in a blind hole in the bore of the hydrostatic bush.

Towards each end of the hydrostatic bush was mounted a group of four inductive proximity probes, equispaced circumferentially, monitoring journal bearing bush movement relative to the hydrostatic bush. Because of spatial limitations these probes were mounted at 33° to the vertical and horizontal. These probes could be used to confirm readings taken from the pedestal mounted inductive probes and to observe any instability of the journal bearing bush. The presence of two axial groups of proximity probes here enables any conical mode of instability of the journal bearing bush to be detected.

---

\* The impedance of the 'O' rings had to be taken into account when measuring the hydrostatic bearing oil film impedance since these were acting in parallel with the oil film. Their stiffness was measured at only lower excitation frequencies (because for a given unbalance moment, higher excitation frequencies would have resulted in an unacceptably large vibration amplitude) and found to be 25 MN m<sup>-1</sup>, whilst damping and cross-coupling were insignificantly small. Work carried out by Stambaugh (50) confirms that for the type of rubber used, there is little change in the dynamic characteristics as frequency is increased.



Also mounted in the hydrostatic bush were two pressure transducers, one in each of one vertical hydrostatic pocket and one horizontal hydrostatic pocket. These transducers were used to confirm the operating parameters  $\beta$  for the hydrostatic bush and to monitor dynamic pressure fluctuations in the hydrostatic bearing.

Between the two groups of hydrostatic pads oil inlets and drains to the journal bearing bush passed through holes in the hydrostatic bearing bush. There existed a clearance between these holes and the fittings which passed through them to the journal bearing bush which ensured that they did not affect the hydrostatic bearing performance. The hoses connected to these fittings were judged to have small stiffnesses compared to the hydrostatic bearing oil film stiffness.

Each hydrostatic bearing pad was fed via a 2 mm bore capillary of a length which gave a bearing operating parameter  $\beta = 0.175$ . For the tests with accumulators connected to the hydrostatic bush, standard gas bag accumulators were used, which would give a dynamic performance corresponding to those of an accumulator operating parameter  $B = 0$ . When the accumulators were connected a resistance ratio  $R_S/R_A = 10$  was used. The inertia coefficients for the capillaries was of the order of  $3 \times 10^7 \text{ kg m}^{-4}$  for the supply line and  $3 \times 10^6 \text{ kg m}^{-4}$  for the accumulator line.

In figure 5.7, the assembled hydrostatic bush is shown, together with the rotor assembly. In this figure can be seen the connections to the oil feed capillaries, accumulators and some of the displacement and velocity transducers.

### 5.5 Static Loading

Static loading could be applied to the bearing by means of pneumatic cylinders, one positioned at each end of the test pedestal. The pistons

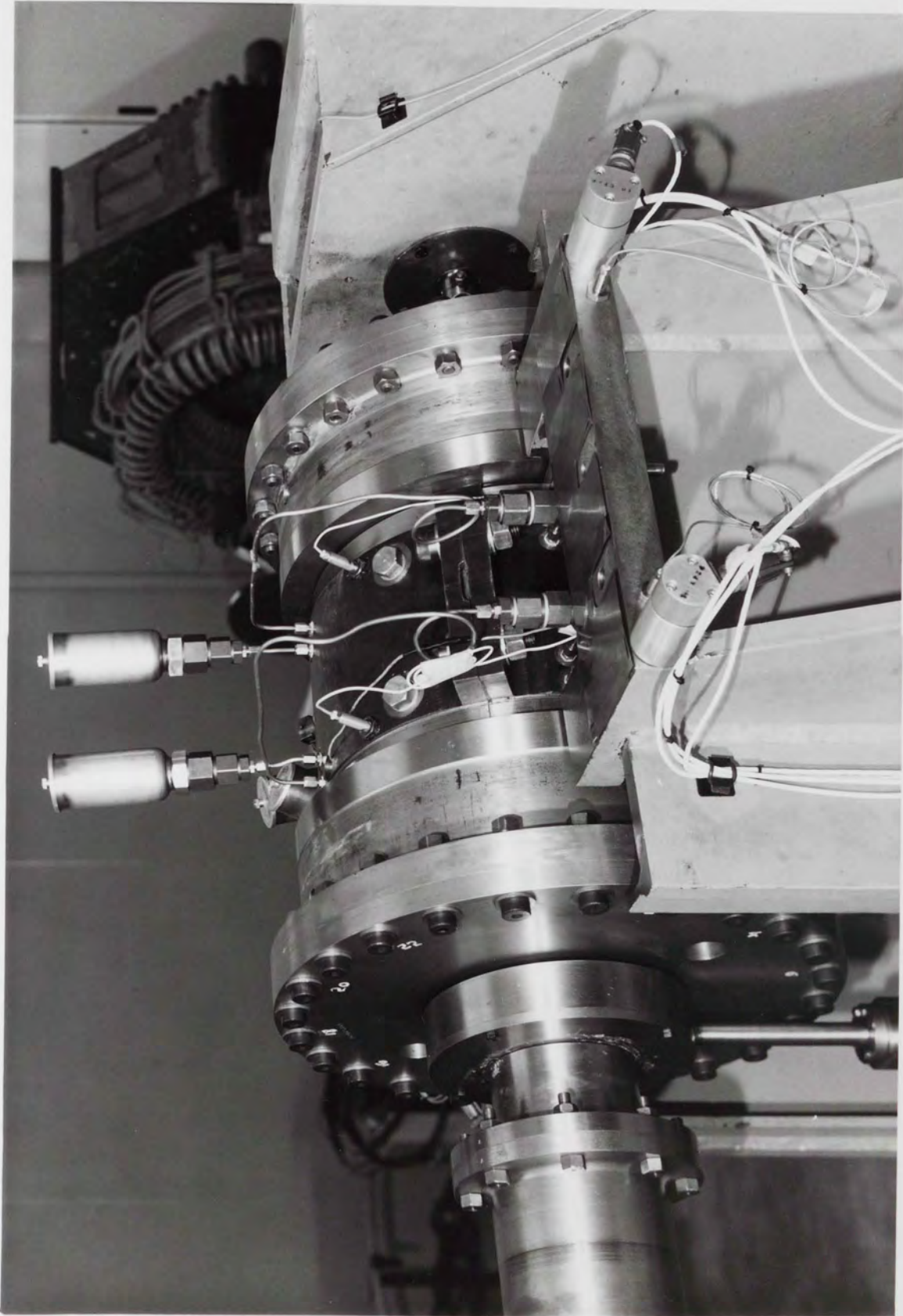


FIG 5.7 THE ASSEMBLED HYDROSTATIC BEARING BUSH

REFORMATION SERVICE

of each cylinder were connected, via a force transducer, to a housing containing the outer race of a rolling bearing, the inner races being mounted on the end covers of the rotor. Thus the rotor remained free to rotate.

In determining the actual static load applied to the bearing under test one had to take into account the weight of the test rotor and any reactions arising from high belt tension acting on the drive pulley of the rotor. These forces were determined by measuring the force required to just raise the rotor inside the test bearing bush. For journal bearing testing this was straight forward but for hydrostatic bearing testing, when the journal bearing was clamped it was the force required to position the journal bearing concentric with the hydrostatic bearing since there was a nominal '0' ring stiffness which had to be taken into account. These measurements were all taken with zero oil flow.

Air supply to the pneumatic cylinders was via a regulator for each cylinder, and via a master regulator, so that the force at each cylinder could be adjusted independently were it ever deemed necessary, or both cylinders could be supplied with exactly the same pressure thus maintaining alignment of the test rotor.

It should be noted that the use of pneumatic cylinders ensured that the static loading system did not affect dynamic measurements, since the fluid in the cylinder was compressible, having an insignificant stiffness compared to the bearing oil film stiffnesses.

#### 5.6 Dynamic Loading

This was applied by an unbalanced shaft, which was mounted on rolling bearings inside the test journal (see figure 5.1) and which was driven through a hole in one of the end covers via a cardan shaft. On each end of the unbalanced shaft were one concentrically mounted steel disc and

two smaller steel discs not mounted concentrically with the shaft. One of the smaller discs was free to rotate relative to the other discs thus enabling adjustment of the nett unbalance at that end of the shaft. A suitable excitation force amplitude was selected by positioning the 'free' disc at the appropriate phase relative to the other small disc and fixing to the large disc by means of a screw. Several available holes were drilled and tapped on the large disc at different angular positions. Adjustment could be made without removing the main rotor end covers since access holes were machined in them. Figure 5.8 shows the unbalance mass assembly at one end of the rotor.

Force amplitude was obviously dependent on unbalance moment and exciting frequency. Exciting frequency was adjusted by controlling the speed of the excitation shaft. Adjustment of the unbalance moment also adjusted its nett phase relative to a key phasor (pulse marker) on the excitation shaft; this had to be taken into account when analysing results since it affected the apparent rotor vibration phase relative to the exciting force.

### 5.7 Lubricating System

Oil was supplied from a power pack, figure 5.9, delivering oil at up to 3.5 MPa. This was a self contained unit incorporating oil tank, pump and 7.5 kW a.c. motor. The oil exited from the tank via a pressure regulator and an in-line ten micron filter. The oil temperature, which was maintained at about 30 °C, could be controlled by a water cooler built into the return line. From the tank the oil was split into two flow paths to form supplies for the hydrostatic and journal bearings. The supply pressure and flow to each bearing were controlled by means of handwheel operated valves mounted on the control panel. Temperature and pressure of the oil was monitored at inlet and outlet to each bearing bush, and a flowmeter was installed in each supply line.



FIG 5.8

THE UNBALANCED MASS ASSEMBLY

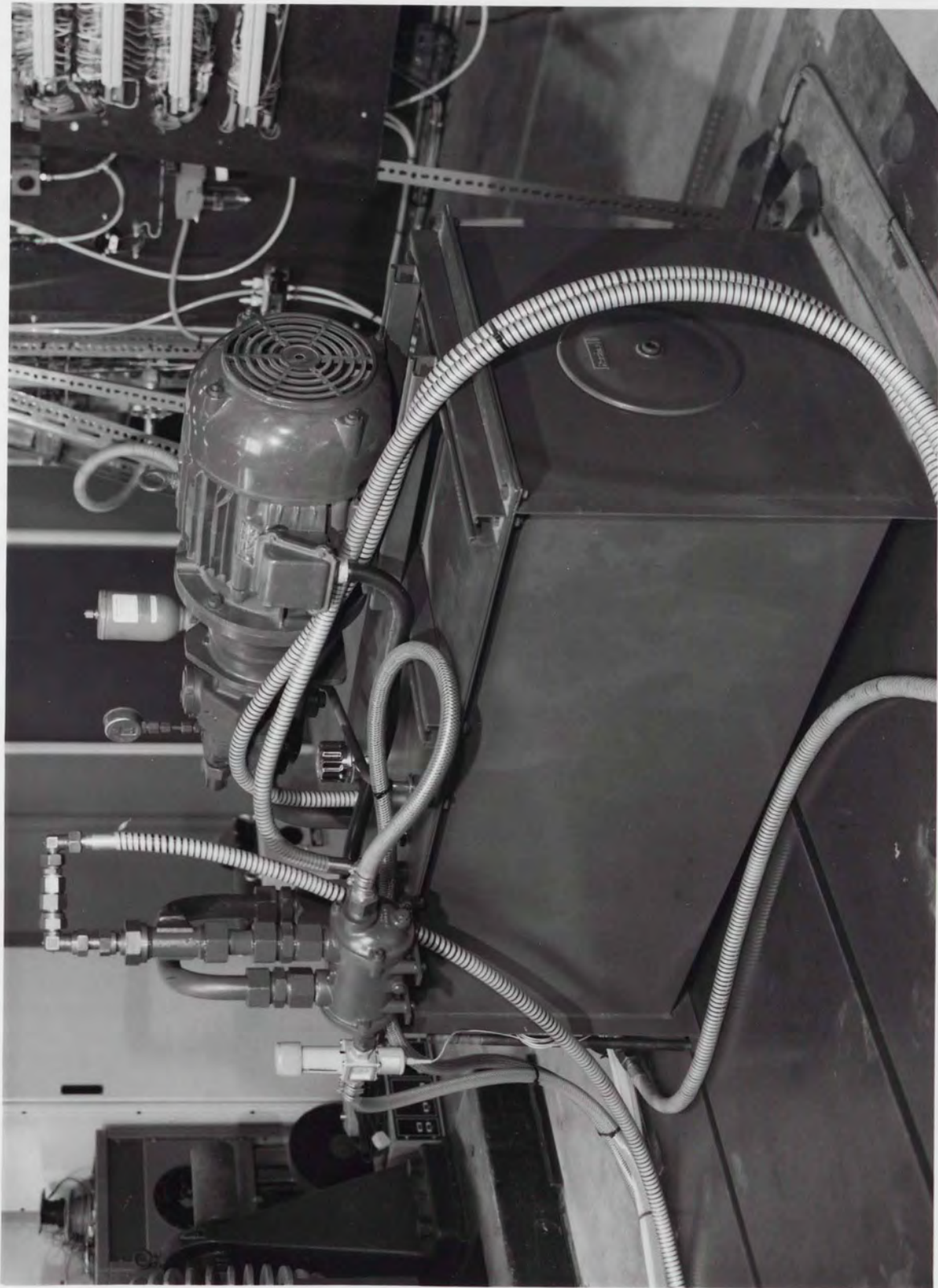


FIG 5.9 THE OIL SUPPLY POWER PACK

REPRODUCTION SERVICES

### 5.8 Shaft Speed Controls

The main rotor was belt driven by a 22 kW 3 phase slip ring induction motor which was speed controlled by a 3 phase variable frequency current supply. The speed of the test rotor was monitored by an inductive sensor detecting the frequency of the passing of a bolt head on the rotor extension shaft at the 'steady' pedestal. The signal from the inductive sensor was transmitted to an rpm meter for rig control purposes.

The excitation shaft was belt driven by an 11 kW d.c. motor, and was speed controlled by a 3 phase rheostat which was in the current supply line before the rotor current was rectified. By reversing the polarity of the motor field current, the direction of rotation of the excitation shaft could be changed. The excitation shaft speed was also monitored by an inductive probe detecting a bolt head on the excitation drive shaft. This signal was transmitted to an rpm meter for rig control purposes and also to the frequency analyser as a datum for phase measurements.

### 5.9 Calibration, Instrumentation and Data-Logging

Calibration of the inductive proximity probes for measuring vibration and displacement was carried out in the laboratory before the probes were assembled on the rig. Each probe was calibrated with its particular driving proximeter. Static calibration against a piece of steel, which was of the same form and composition as the test rotor steel, was performed by moving the steel sample using a barrel micrometer, and noting the probe output voltage. Dynamic calibration was done by using a disc, of the same rotor steel, which was rotated at high speed, the surface of the disc not being at  $90^\circ$  to the axis of its drive shaft. The resulting once per rev high spot was detected by the probe being

calibrated. Each probe was calibrated using the frequency analyser which was to be used to take test results.

Velocity probes, used to measure pedestal vibrations, were calibrated, using the frequency analyser, by mounting them on a vibrating platform whose amplitude and frequency were measured by a proximity probe of known calibration. These probes were calibrated for phase and amplitude.

Calibration of each individual force transducer and pressure transducer on the test rig was carried out by the respective manufacturers and the corresponding calibration certificates were accepted. Supplied calibration data was also accepted for thermocouples, these not being crucial as regards the performance of the test bearings.

Output signals from all of the transducers on the test rig were taken initially to a marshalling board at the rig and from there to a data logging room, remote from the test rig. At the logger room the steady state signals were multiplexed into a digital voltmeter and readings recorded on a magnetic disc. Dynamic signals were multiplexed into a frequency response analyser for measurement of frequency, amplitude and phase relative to the pulse marker on the excitation shaft (this signal also being fed into the analyser). Readings from the analyser were then stored on the magnetic disc. All of these automatic logging operations were controlled via an HPIB (IEEE) bus by a desktop computer which also gave a printed output of results as they were collected.

The data logging equipment is shown in figure 5.10.

In order to decrease the effect of any random errors in result taking due to the resolution of the measuring equipment and instability of operating conditions, experimental readings were taken for each bearing running condition examined, several times. Once result taking was complete the magnetic disc was removed to the office where a second



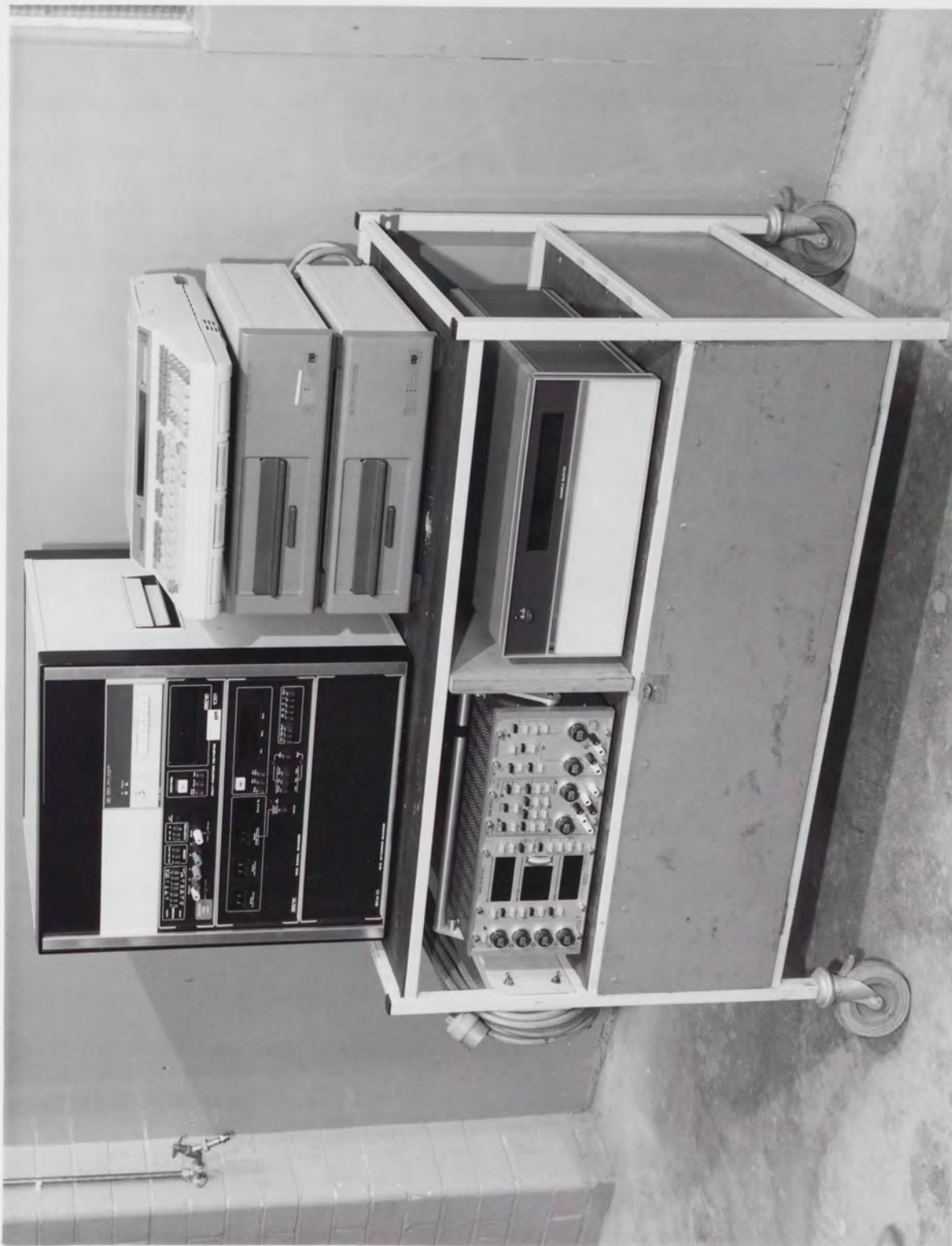


FIG 5.10 THE DATA LOGGING EQUIPMENT

PROPERTY OF THE  
INFORMATION SERVICES

desktop computer was used to give a full print out of results. These results were then used as input data to a computer program which would yield bearing coefficients (see appendix A IV).

#### 5.10 Aligning the Journal and Bearing Bush

Alignment of the test journal in the journal bearing bush was ensured by clamping the bush around the journal with shim material in the clearance space. The rotor and journal bearing bush were then assembled in the hydrostatic bearing lower half bush. The pneumatic cylinders were used to pull the journal bearing bush down onto the hydrostatic bush thus ensuring alignment in the vertical plane. Alignment in the horizontal plane was then adjusted by 'tapping' the steady pedestal end of the rotor extension shaft with a mallet, and checked by sliding feeler gauges in the appropriate clearance spaces at each end of the bearing. When a satisfactory alignment had been achieved, the steady bearing end of the rotor extension was clamped in position using fitted bolts connecting the rolling bearing housing and the pedestal.

#### 5.11 Run-out

Before conducting bearing testing it was necessary to ensure that any vibration signals detected were actually a result of shaft vibration. A shaft surface which has not been machined to a true circular form, or is not concentric with the axis of rotation of the shaft will result in an output signal from a proximity probe that indicates a vibration when in fact the shaft is not vibrating. Such a phenomenon is termed mechanical run-out. A vibration signal can also be apparent, when the true vibration level is zero and there is no mechanical run-out. Inhomogeneity of the shaft material in the form of alloying, or the presence of local residual magnetism or residual stress caused possibly by a machining process, will result in a difference of the materials electrical properties at different points on the shaft circumference; these differences will themselves give rise to an apparent vibration signal. Mechanical runout

can be cured by re-grinding the target area to ensure a concentric circular section whilst various surface treatments are available which remove electrical runout (proximity probe manufacturers will usually advise).

In order to eliminate the possibility that either electrical or mechanical run-out could affect the vibration measurements being taken, a filtering system was used whereby only frequencies within 12 rpm of the excitation frequency were observed in the signals received from transducers mounted on the test rig. Any such signal received as a result of mechanical or electrical run-out would have its frequency determined by the test journal speed, which was not close enough to the excitation frequency to affect the measurements.

CHAPTER SIX

THEORETICAL AND EXPERIMENTAL RESULTS

11  
12  
13  
14  
15  
16  
17  
18  
19  
20  
21  
22  
23  
24  
25  
26  
27  
28  
29  
30  
31  
32  
33  
34  
35  
36  
37  
38  
39  
40  
41  
42  
43  
44  
45  
46  
47  
48  
49  
50  
51  
52  
53  
54  
55  
56  
57  
58  
59  
60  
61  
62  
63  
64  
65  
66  
67  
68  
69  
70  
71  
72  
73  
74  
75  
76  
77  
78  
79  
80  
81  
82  
83  
84  
85  
86  
87  
88  
89  
90  
91  
92  
93  
94  
95  
96  
97  
98  
99  
100

## CHAPTER SIX

### THEORETICAL AND EXPERIMENTAL RESULTS

#### 6.1 Static Characteristics of the Journal Bearing

A check on the locus of the shaft centre as it ran in the journal bearing bush, whilst the Sommerfeld number was changed, was carried out and the results are presented in figure 6.1, showing the variation of eccentricity ratio with Sommerfeld number, and figure 6.2, a polar plot of the journal locus. In each case a line representing the theoretical locus suggested in the text book by Pinkus and Sternlicht (see bibliography) is also shown.

#### 6.2 Dynamic Oil Film Coefficients for the Journal Bearing

Tests were carried out on the journal bearing, with its bush held rigidly inside the hydrostatic bearing bush by two clamping bolts. These tests were to determine the dynamic oil film coefficients of the journal bearing alone so that they could be compared with the measured coefficients of the combined journal and hydrostatic bearing. It was also required that these coefficients be known so that they could be used to determine the theoretical bearing coefficients for the combined journal and hydrostatic bearing.

The journal bearing coefficients were measured with the journal running at 1500 rpm (since this was roughly in the middle of the speed range of interest) and with a specific loading of 350 k Pa (50 lbf/in<sup>2</sup>). Tests were conducted at excitation frequencies ranging from 400 rpm to 1500 rpm.

Measured values of amplitude and phase for forward and reverse directions of excitation are shown in figures 6.3 and 6.4, in the form of polar plots. For each running condition the mean and standard deviation are

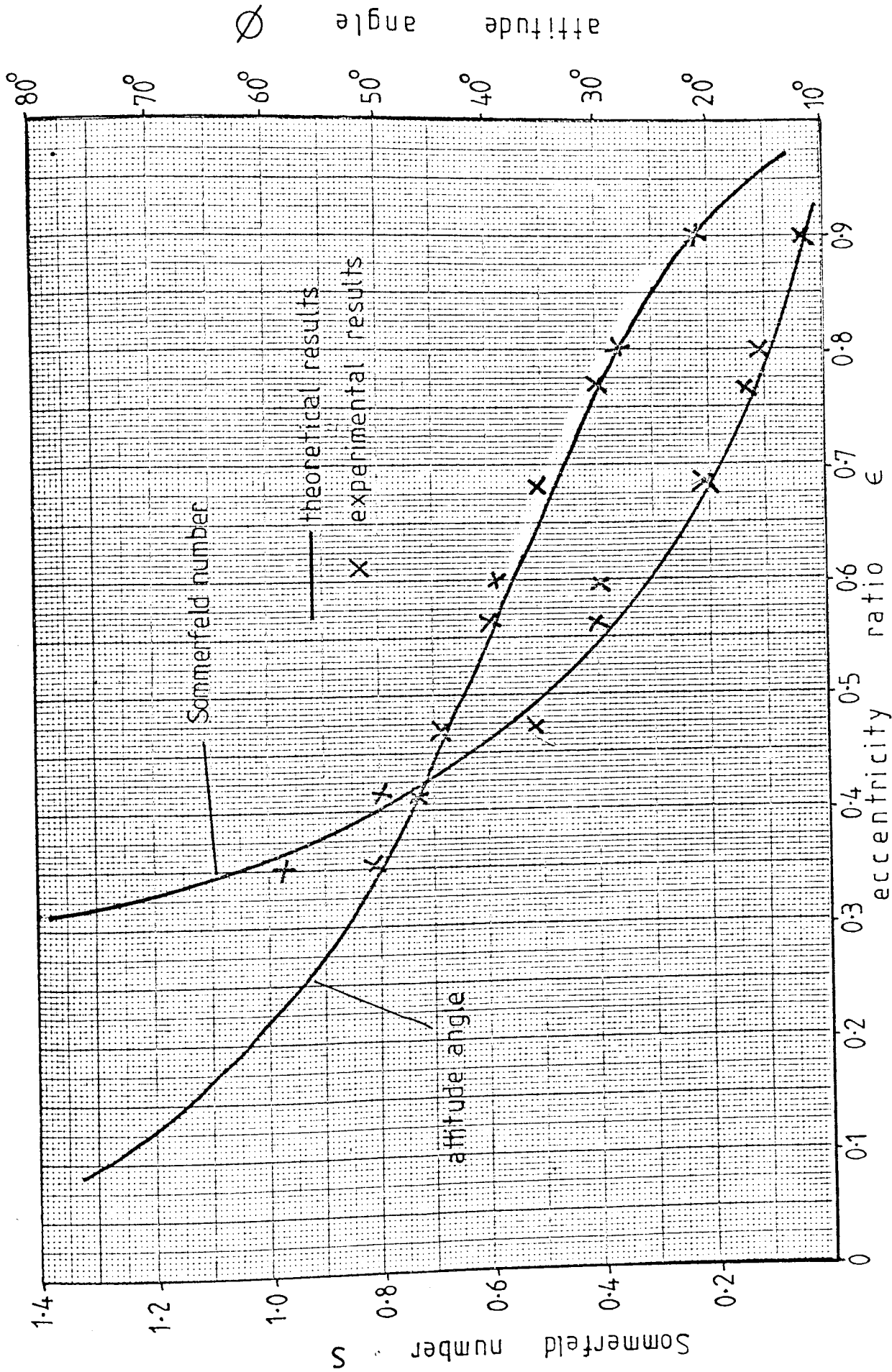
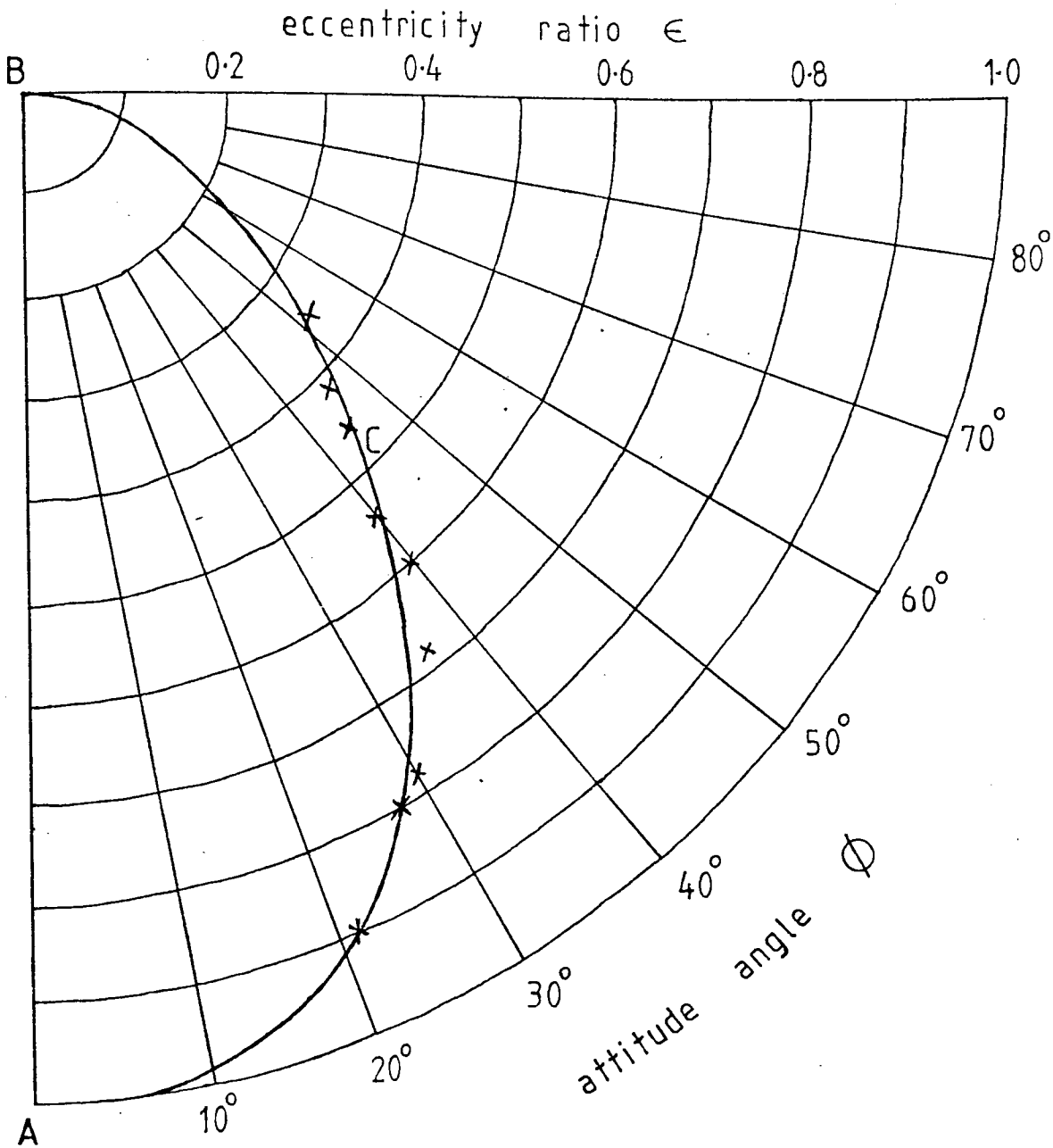
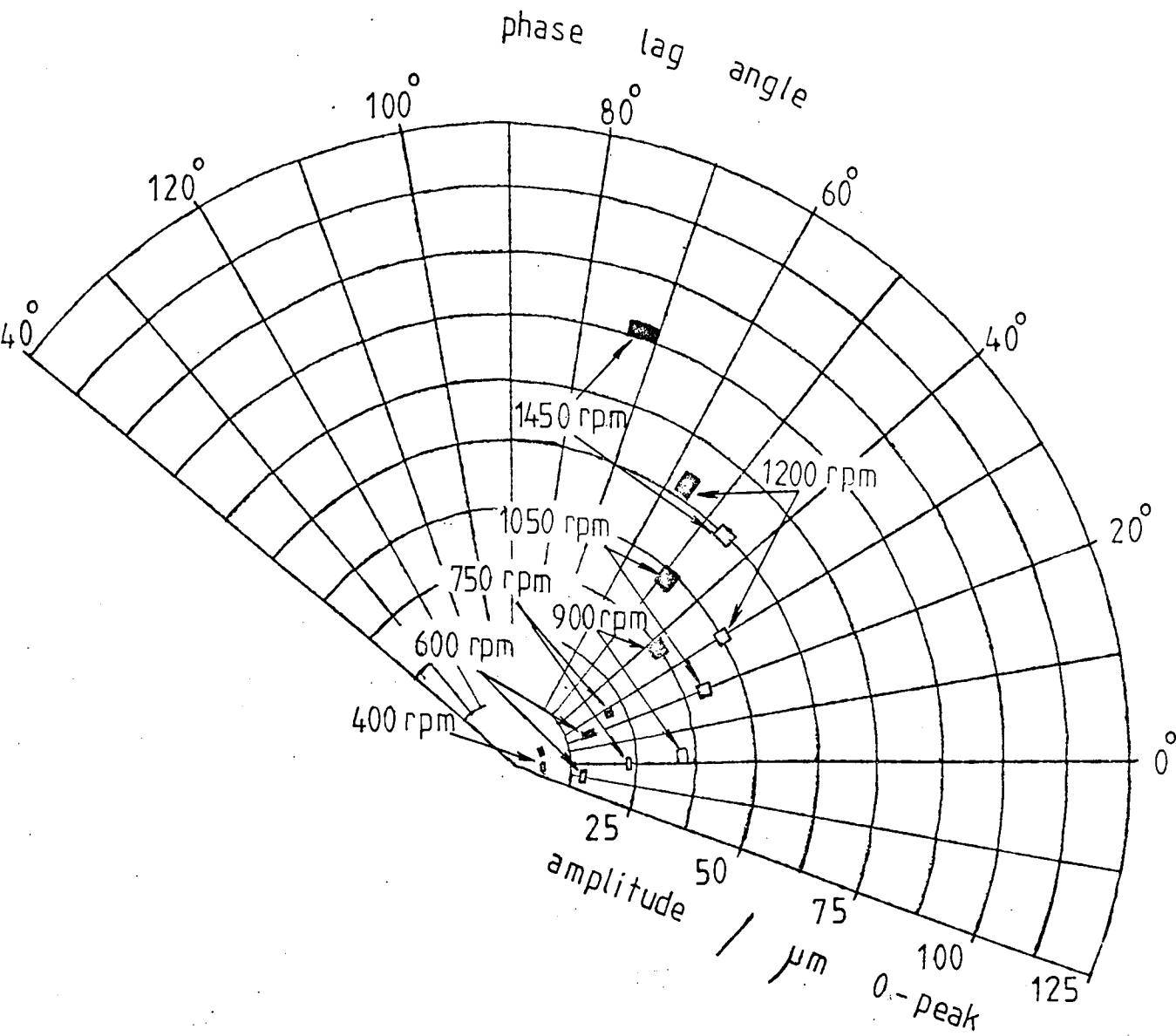


FIG 6.1 SHAFT LOCUS - SOMMERFELD NUMBER RELATIONSHIP



— theoretical results  
x experimental results

FIG 6.2 POLAR PLOT OF THE SHAFT LOCUS  
( JOURNAL BEARING ONLY )



■ horizontal response  
□ vertical response

FIG 6.3 NYQUIST DIAGRAM FOR THE JOURNAL BEARING, FORWARD EXCITATION



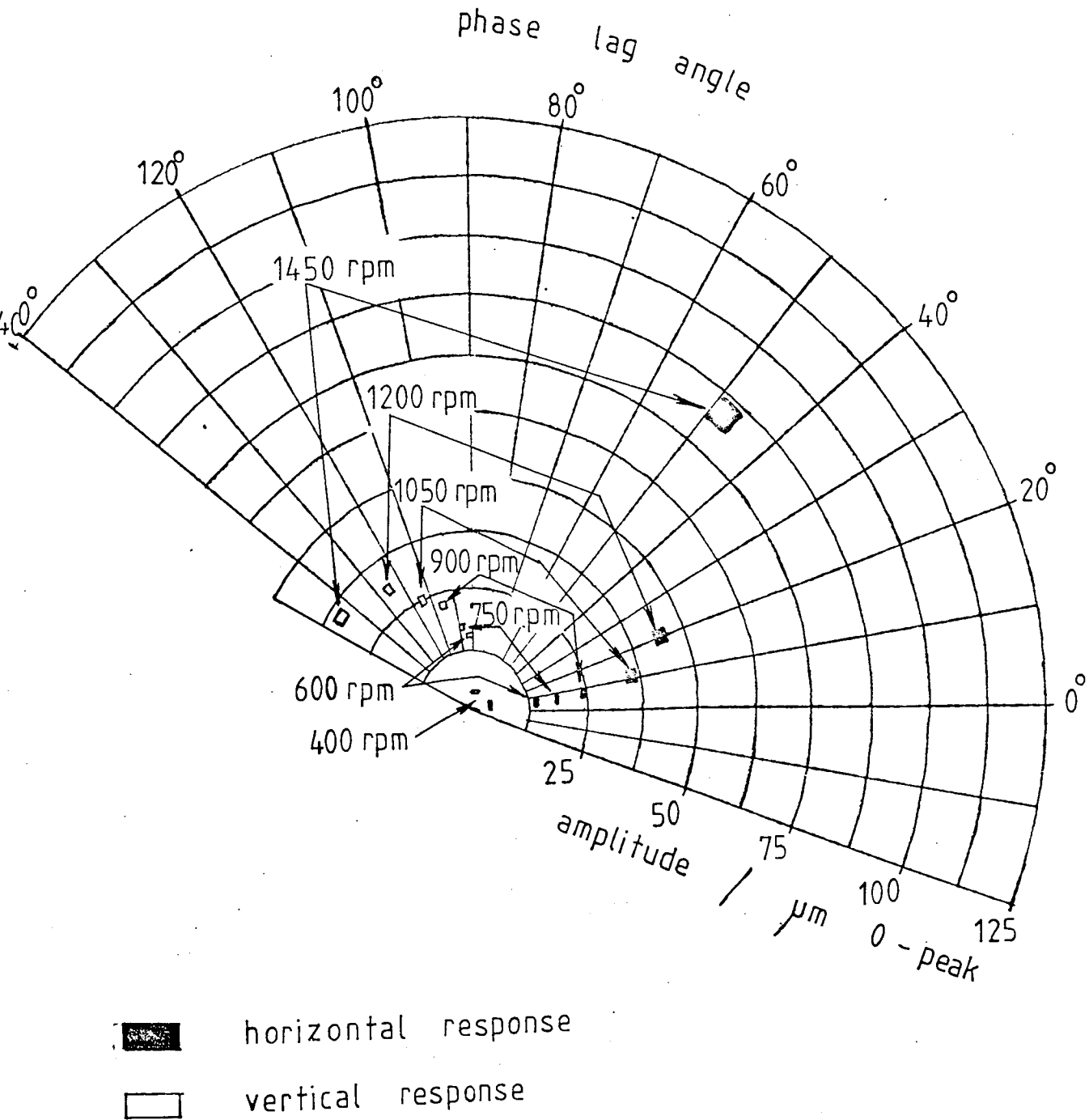


FIG 6.4 NYQUIST DIAGRAM FOR THE JOURNAL BEARING, REVERSE EXCITATION

indicated having been determined from about sixteen measured values. From these results, values for the eight bearing coefficients were computed and are shown in figures 6.5 to 6.12 where they are plotted as bars indicating the mean and standard deviation. (In this instance the standard deviation was estimated from a sample of ten sets of bearing coefficients, since to carry out the full analysis, combining the sixteen forward excitation results with the corresponding sixteen reverse excitation results in all possible combinations and permutations would be a formidable task.)

For the values of bearing coefficients indicated in figures 6.5 to 6.12, a 'smoothed' curve (best fit by eye) was then drawn through the plotted results and values indicated by this line were used with theoretical hydrostatic bearing coefficients to determine theoretical coefficients for the combined bearing.

### 6.3 Static Characteristics of the Hydrostatic Bearing

The steady state performance of the hydrostatic bearing was measured in terms of static load and oil flow vs vertical displacement of the floating ring (ie, journal bearing bush) relative to the hydrostatic bearing bush. These characteristics were compared with theoretical characteristics obtained using a computer program based on the theory described in sections 3.1 to 3.3. The BASIC computer program, suitable for use with a HP9845A desktop computer, is presented in appendix A1.

Figure 6.13 shows the theoretical variation of static vertical load with vertical displacement for the test hydrostatic bearing floating ring, for various values of the operating parameter  $\beta$ . Experimental results were obtained for the case where  $\beta = 0.175$  and are shown in figure 6.14 where the appropriate theoretical curve is reproduced for comparison. Similarly, figure 6.15 shows the theoretical variation of oil flow vs

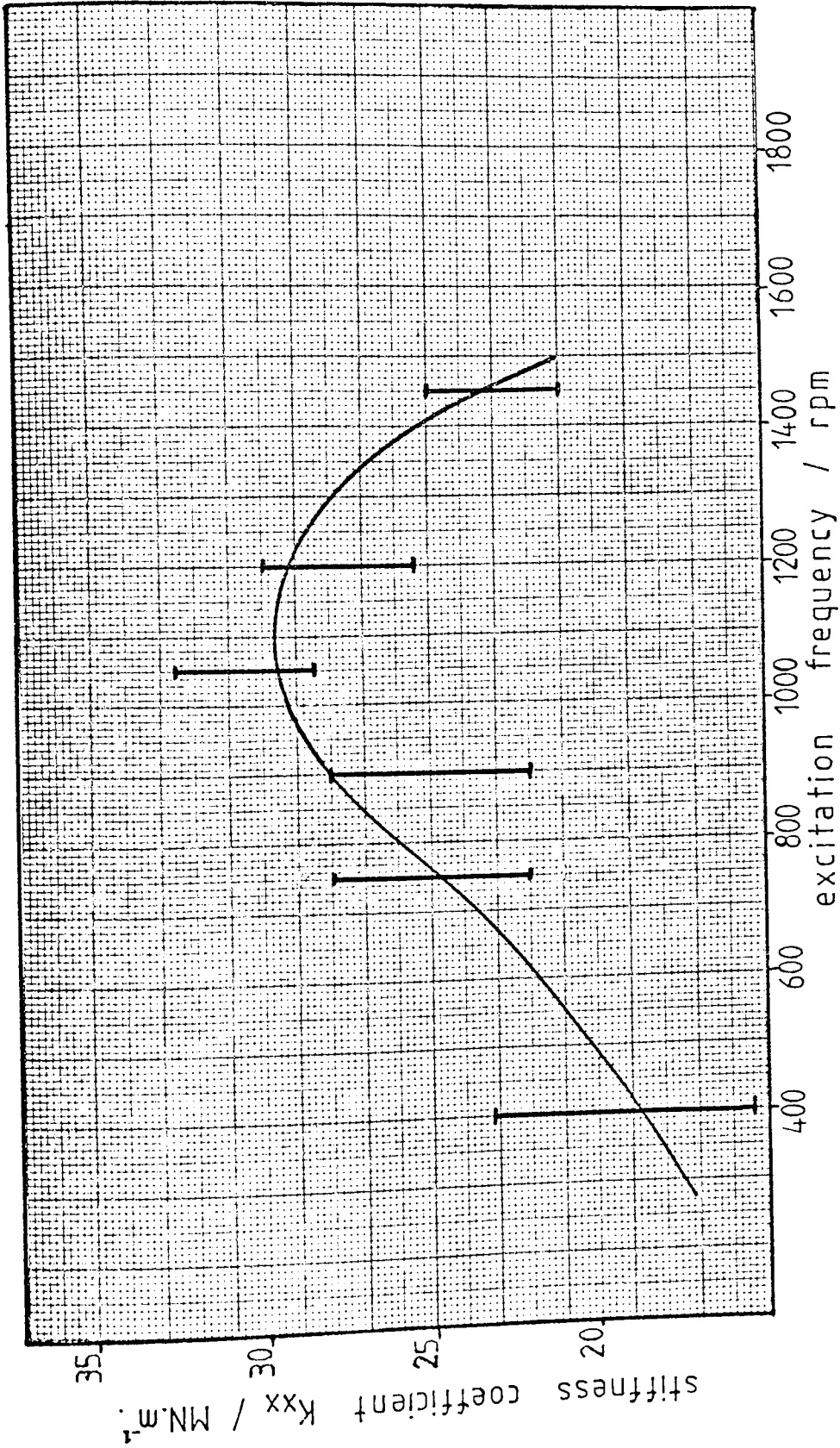


FIG 6.5 VARIATION OF JOURNAL BEARING STIFFNESS COEFFICIENT  $K_{xx}$  WITH EXCITATION FREQUENCY

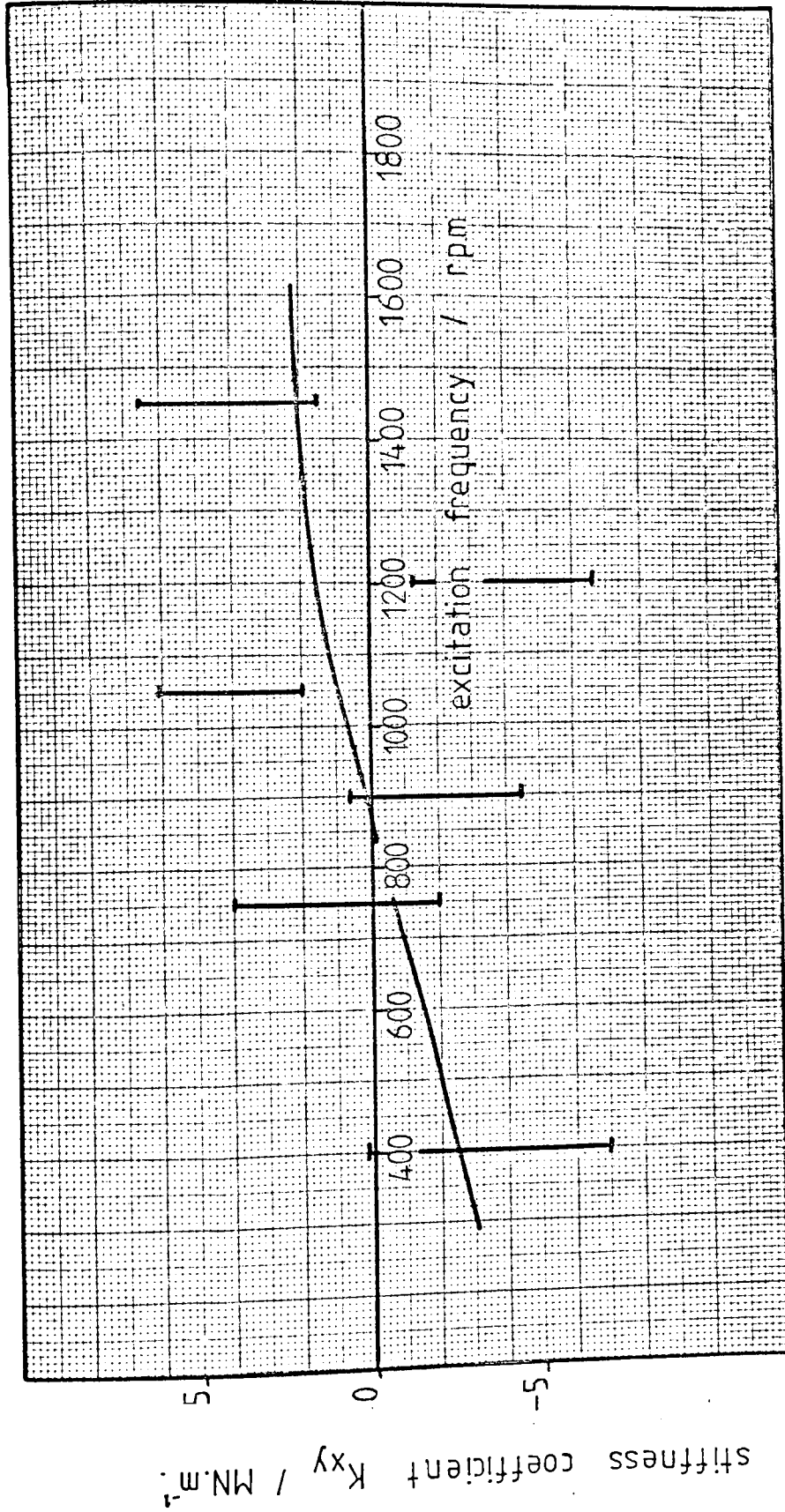


FIG 6.6 VARIATION OF JOURNAL BEARING STIFFNESS COEFFICIENT  $K_{xy}$  WITH EXCITATION FREQUENCY

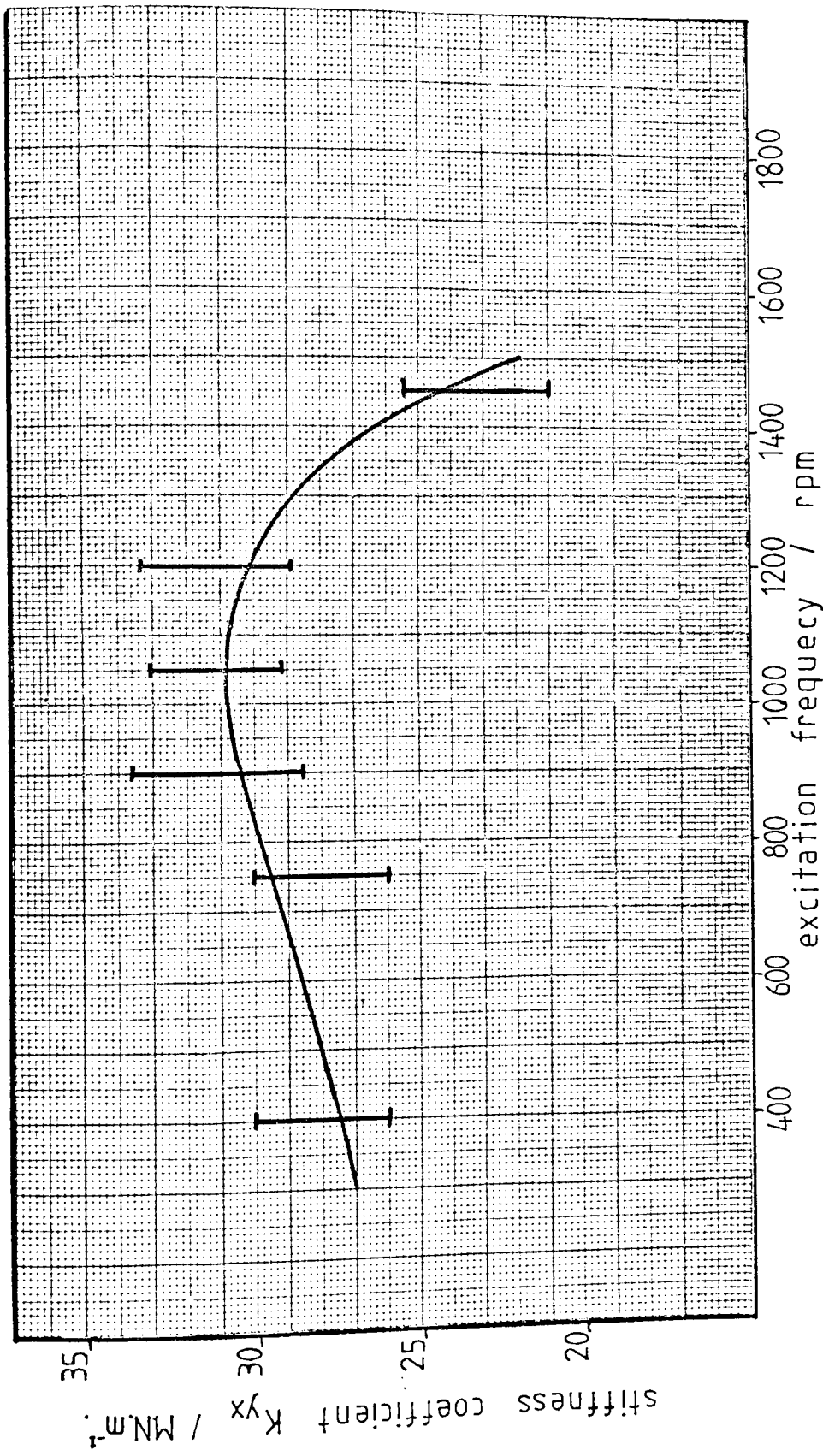


FIG 6.7 VARIATION OF JOURNAL BEARING STIFFNESS COEFFICIENT  $K_{yx}$  WITH EXCITATION FREQUENCY

STEFAN P. ...

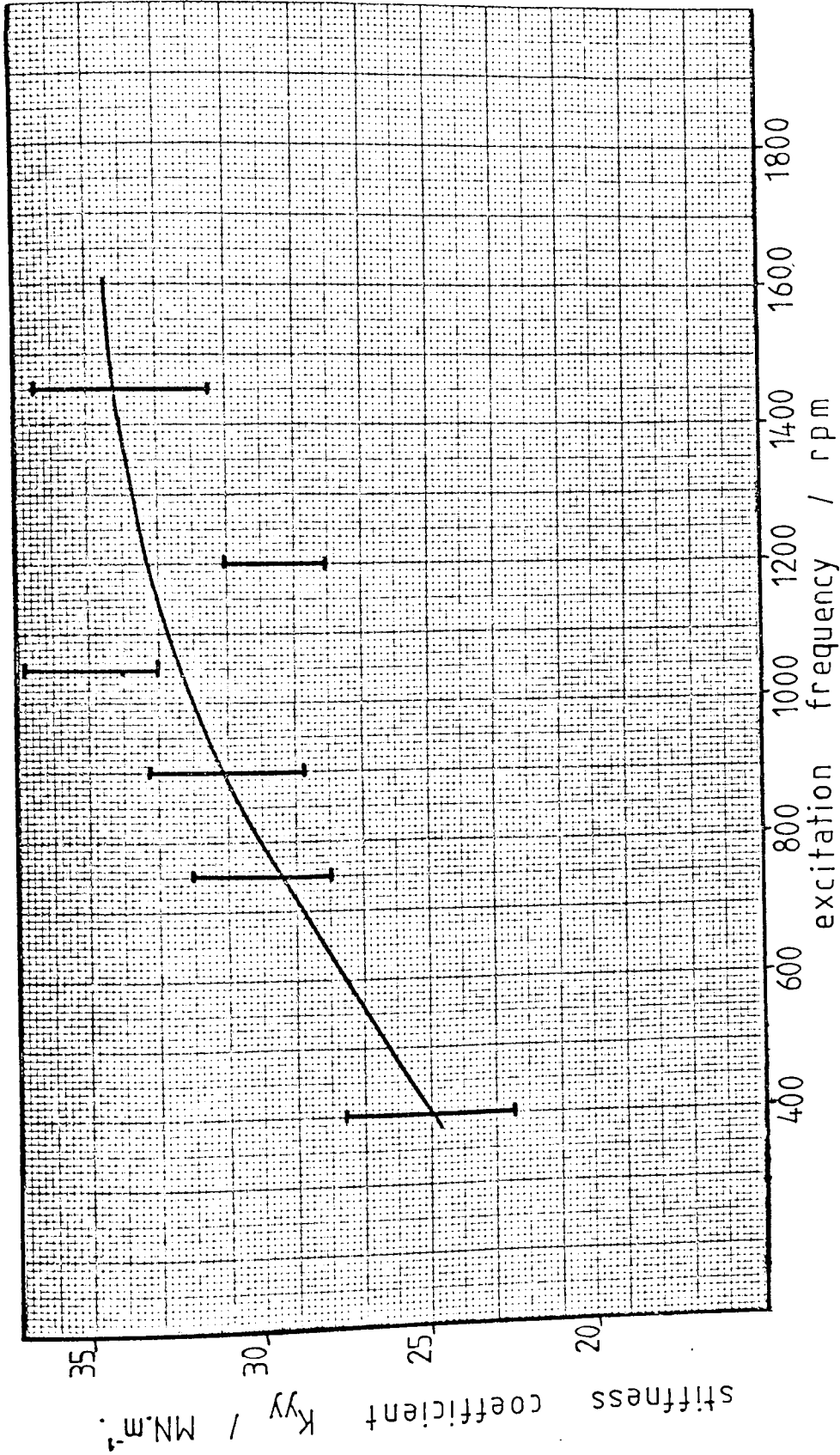


FIG 6.8 VARIATION OF JOURNAL BEARING STIFFNESS COEFFICIENT  $K_{yy}$  WITH EXCITATION FREQUENCY

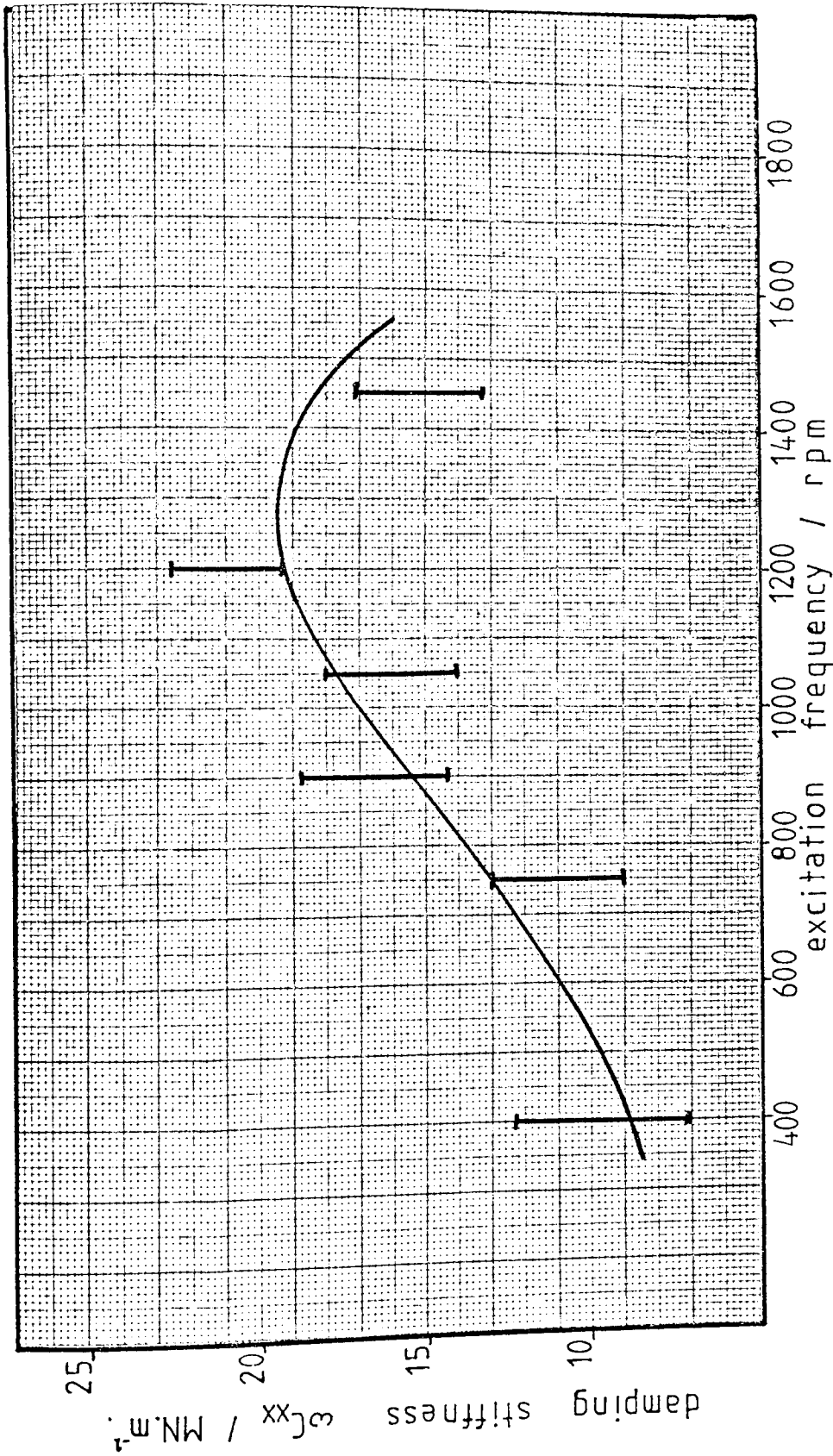


FIG 6.9 VARIATION OF JOURNAL BEARING DAMPING STIFFNESS  $\omega C_{xx}$  WITH EXCITATION FREQUENCY

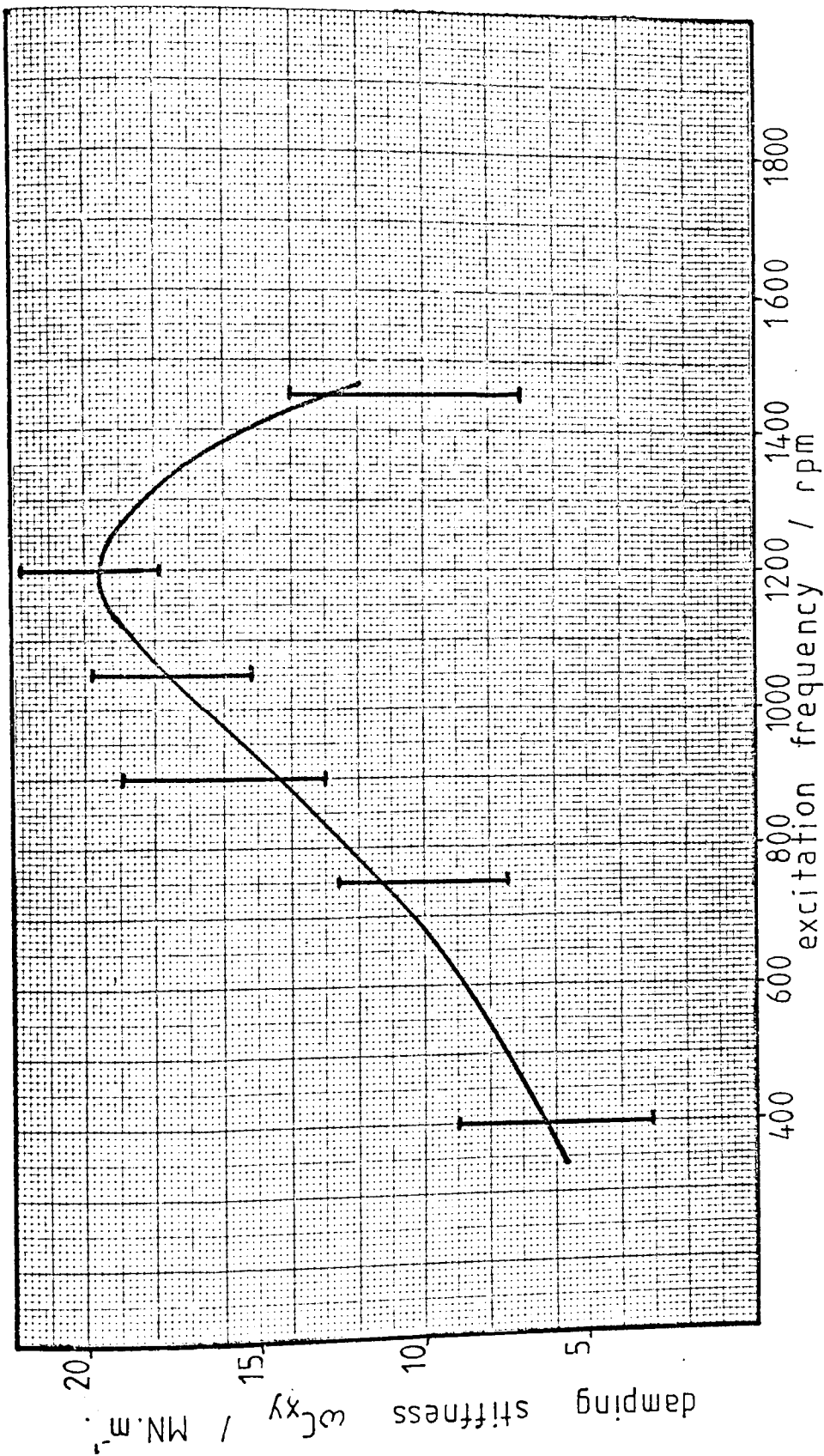


FIG 6.10 VARIATION OF JOURNAL BEARING DAMPING STIFFNESS  $\omega c_{xy}$ —  
WITH EXCITATION FREQUENCY



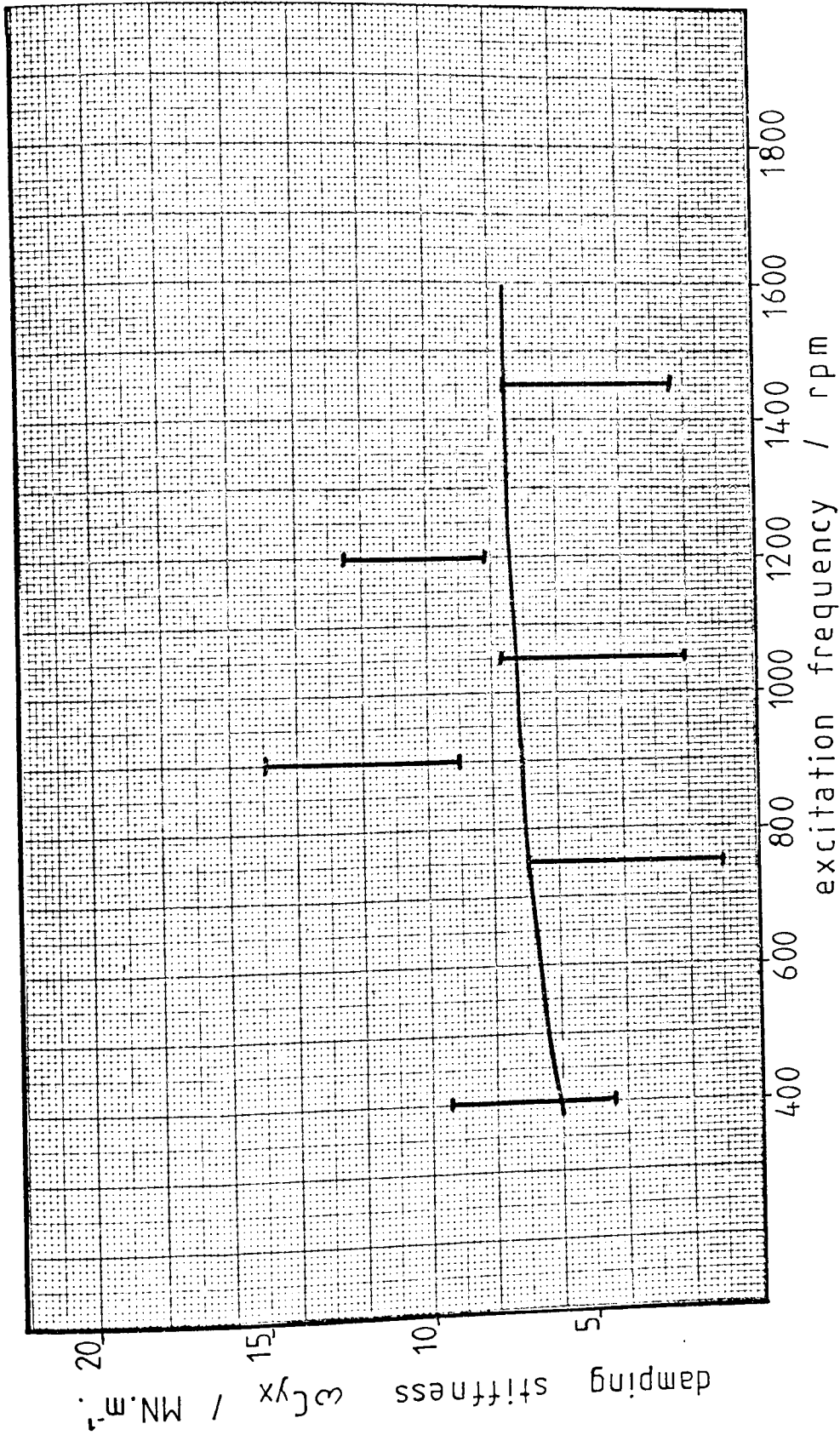


FIG 6.11 VARIATION OF JOURNAL BEARING DAMPING STIFFNESS  $\omega_{cyx}$  WITH EXCITATION FREQUENCY

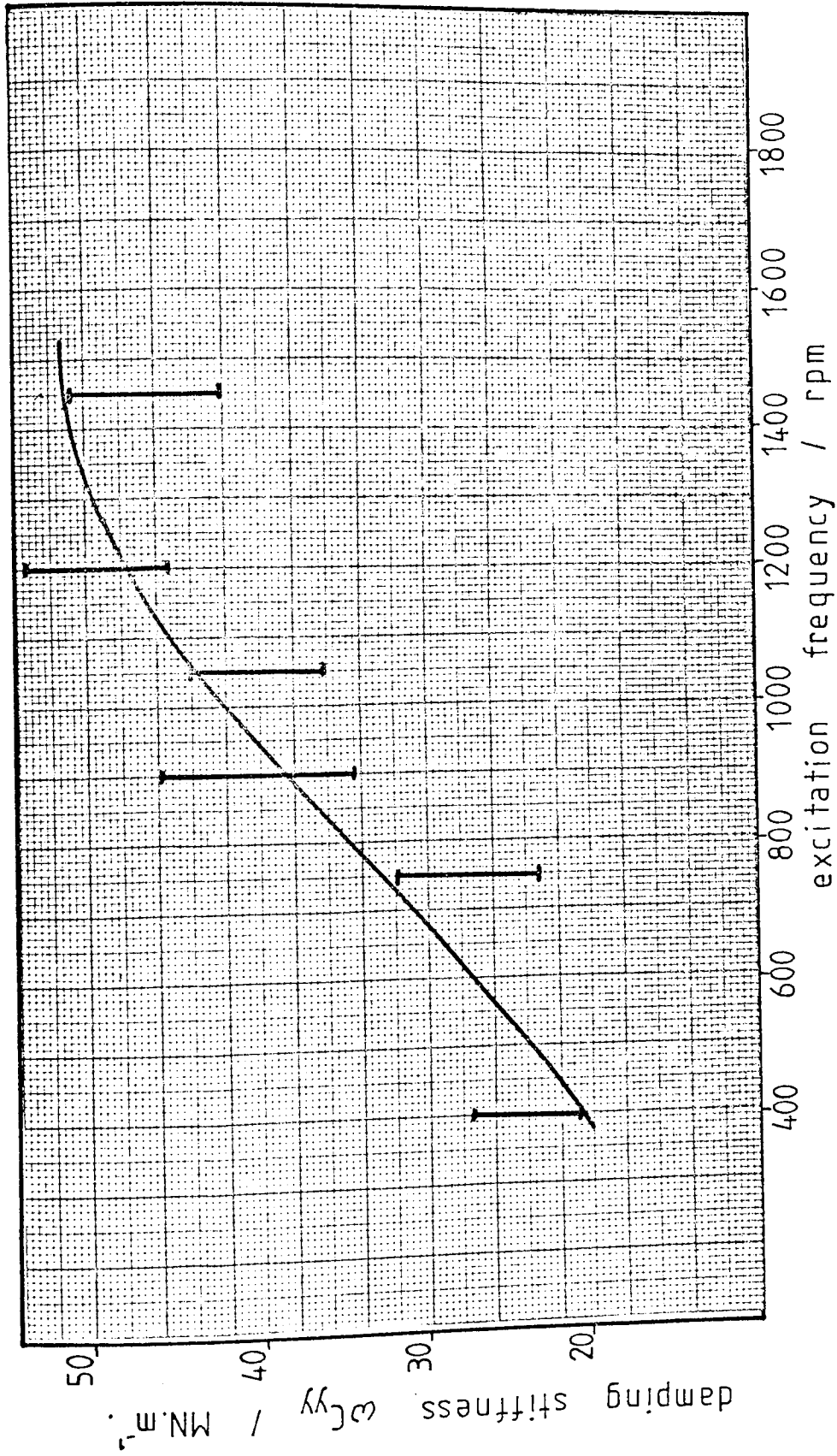


FIG 6.12 VARIATION OF JOURNAL BEARING DAMPING STIFFNESS  $\omega C_{yy}$  WITH EXCITATION FREQUENCY

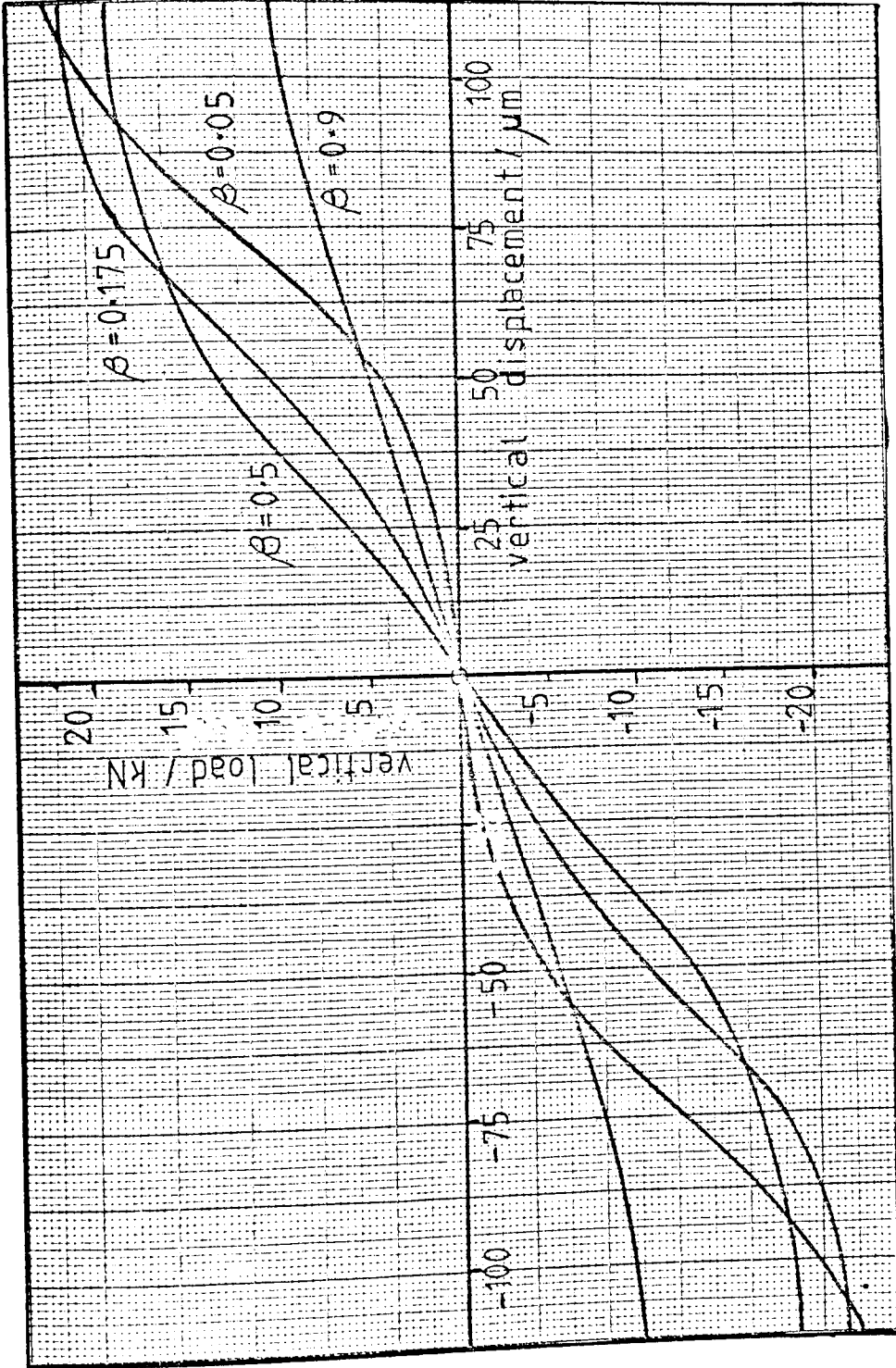


FIG 6.13 THEORETICAL STATIC VERTICAL LOAD -- DISPLACEMENT  
RELATIONSHIP FOR THE HYDROSTATIC BEARING BUSH

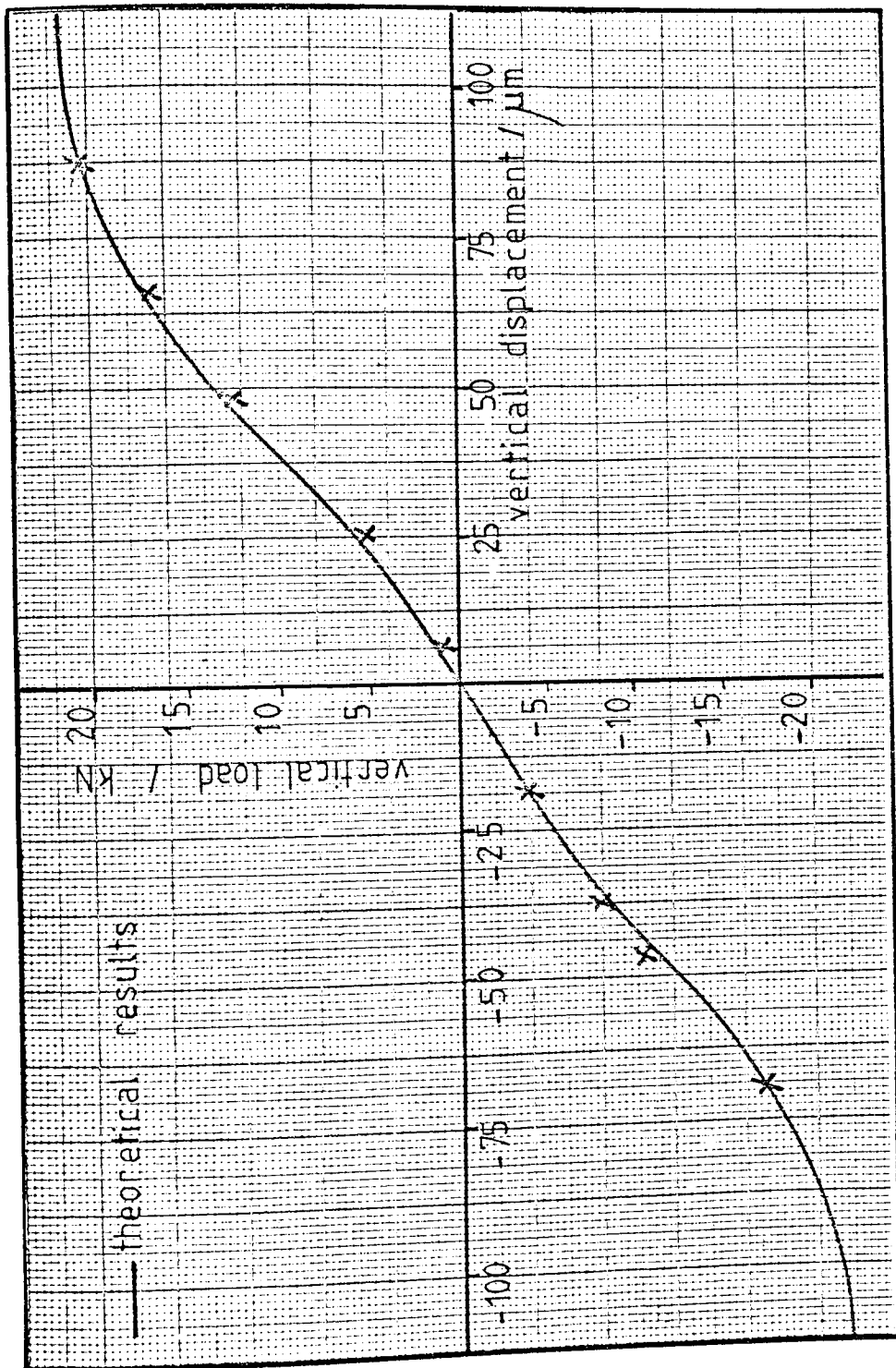


FIG 6.14 EXPERIMENTAL STATIC VERTICAL LOAD - DISPLACEMENT  
RELATIONSHIP FOR THE HYDROSTATIC BEARING BUSH

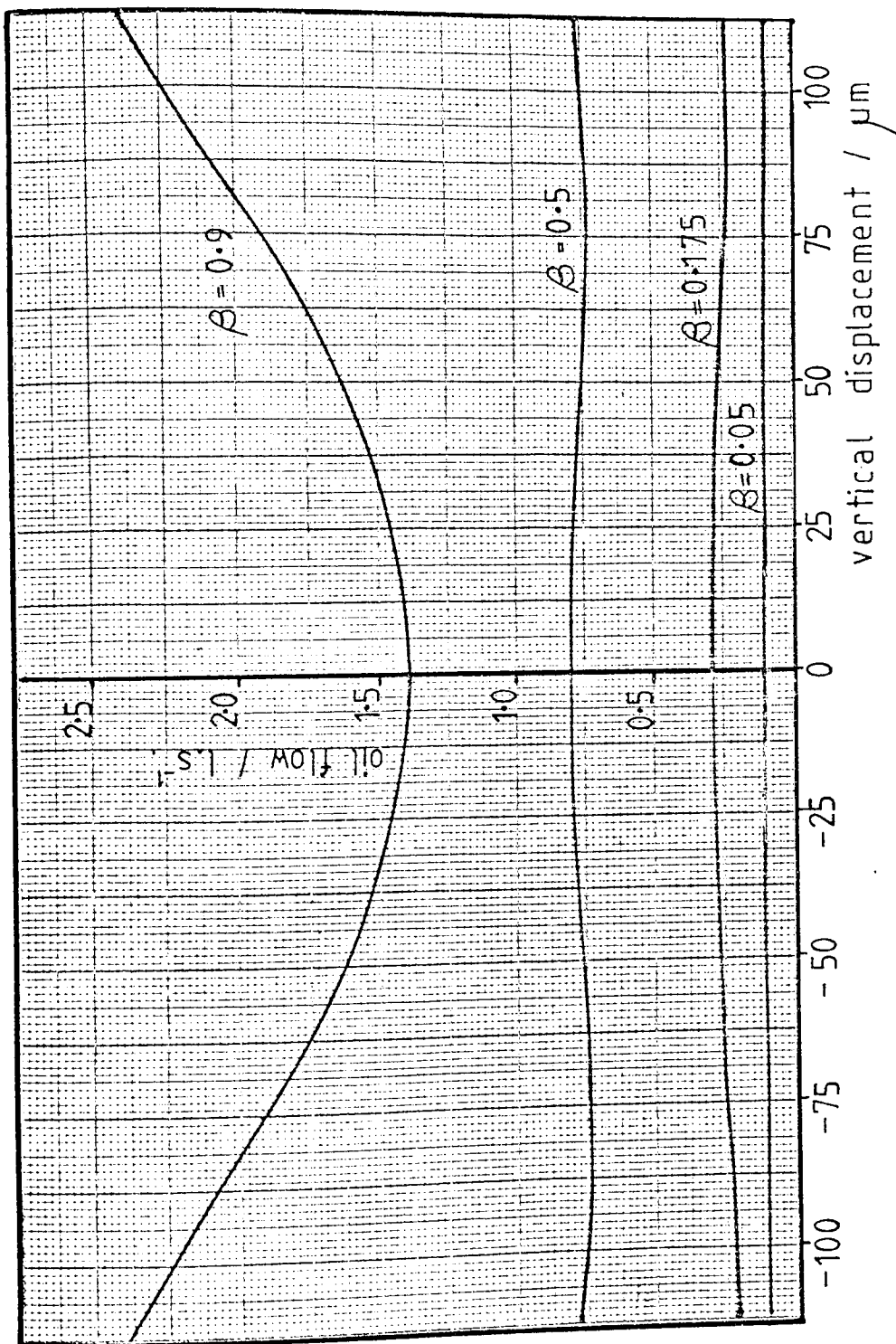


FIG 6.15 THEORETICAL VERTICAL DISPLACEMENT -- OIL FLOW  
RELATIONSHIP FOR THE HYDROSTATIC BEARING BUSH

Engineering Drawing

vertical displacement for the test bearing for various  $\beta$  values whilst figure 6.16 shows the experimental results for  $\beta = 0.175$ . Again the theoretical values are reproduced in figure 6.16 for comparison. The theoretical variation of required oil pumping power, with vertical displacement is shown in figure 6.17 (again for zero horizontal displacement).

#### 6.4 Dynamic Oil Film Coefficients for the Hydrostatic Bearing

##### 6.4a Theoretical results

The theoretical variation of the test hydrostatic bearing bush dynamic oil film coefficients with hydraulic resistance ratio  $R_s/R_a$ , accumulator operating parameter B, and excitation frequency was determined using the theory presented in chapter 3, with the aid of a HP9845A desktop computer. The effect of oil inertia in the capillary restrictors was also examined.

Figures 6.18 to 6.21 show the variation of the horizontal and vertical direct stiffness and damping coefficients with resistance ratio  $R_s/R_a$ , and accumulator operating parameter B, for a constant excitation frequency of 3000 rpm (the cross coupling coefficients all take a zero value, the reason for this being discussed in section 8.4). Figures 6.18 to 6.21 apply for the case where the static load on the hydrostatic bearing bush is 3.6 kN (0.36 tons force), corresponding to a specific loading on the test journal bearing of 350 kPa. (50 lbf/in<sup>2</sup>).

The effect of excitation frequency on the bearing dynamic oil film coefficients is shown in figures 6.22 and 6.23 for the case where hydraulic resistance ratio  $R_s/R_a = 10$  and accumulator operating parameter B = 0, an arrangement which might be typical. Figure 6.22 shows the variation of bearing stiffness coefficients  $K_{xx}$  and  $K_{yy}$  with excitation frequency, and figure 6.23 a similar curve for the 'damping stiffnesses'  $\omega C_{xx}$  and  $\omega C_{yy}$ .

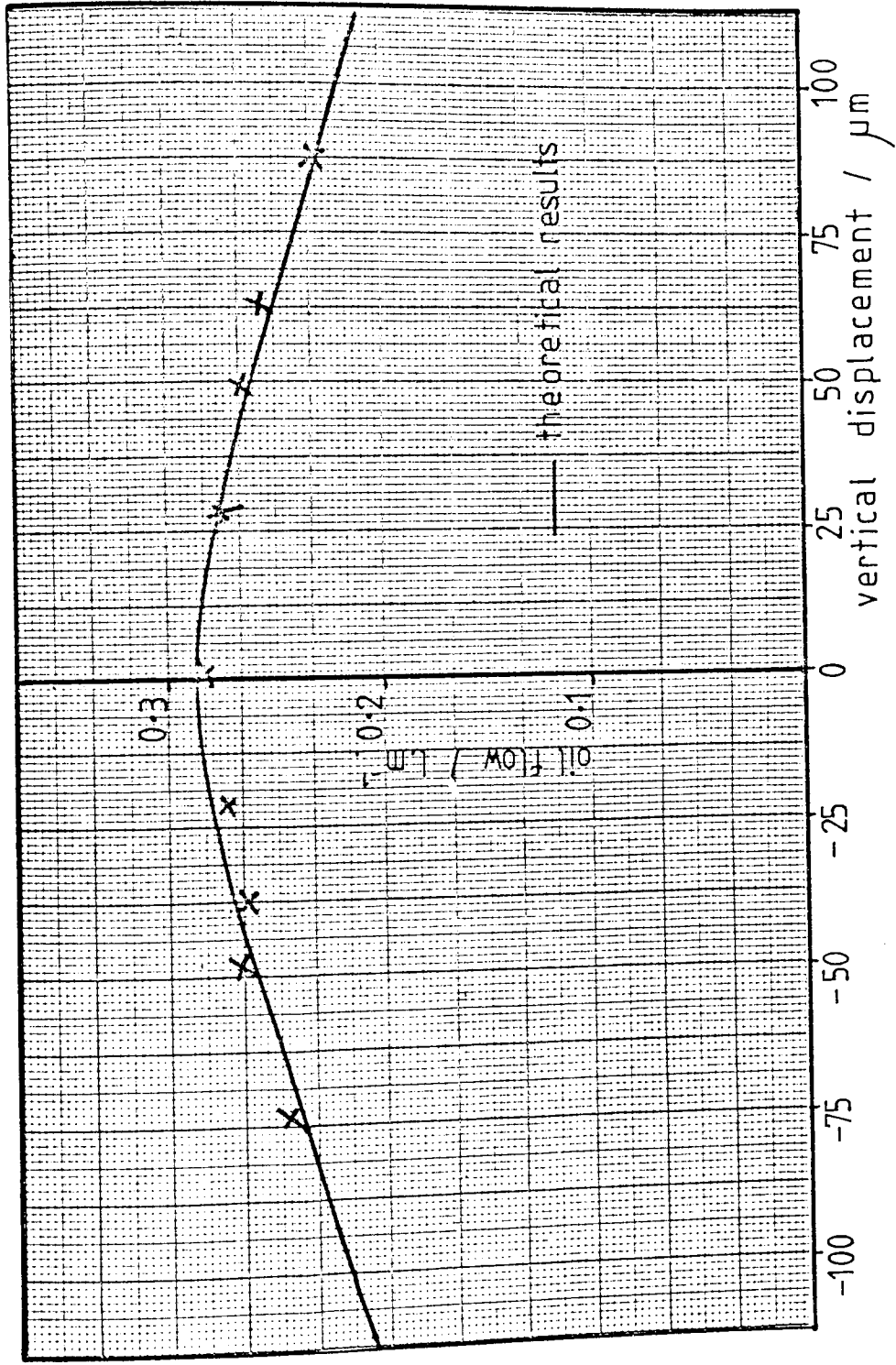


FIG 6.16 EXPERIMENTAL VERTICAL DISPLACEMENT --- OIL FLOW  
RELATIONSHIP FOR THE HYDROSTATIC BEARING BUSH

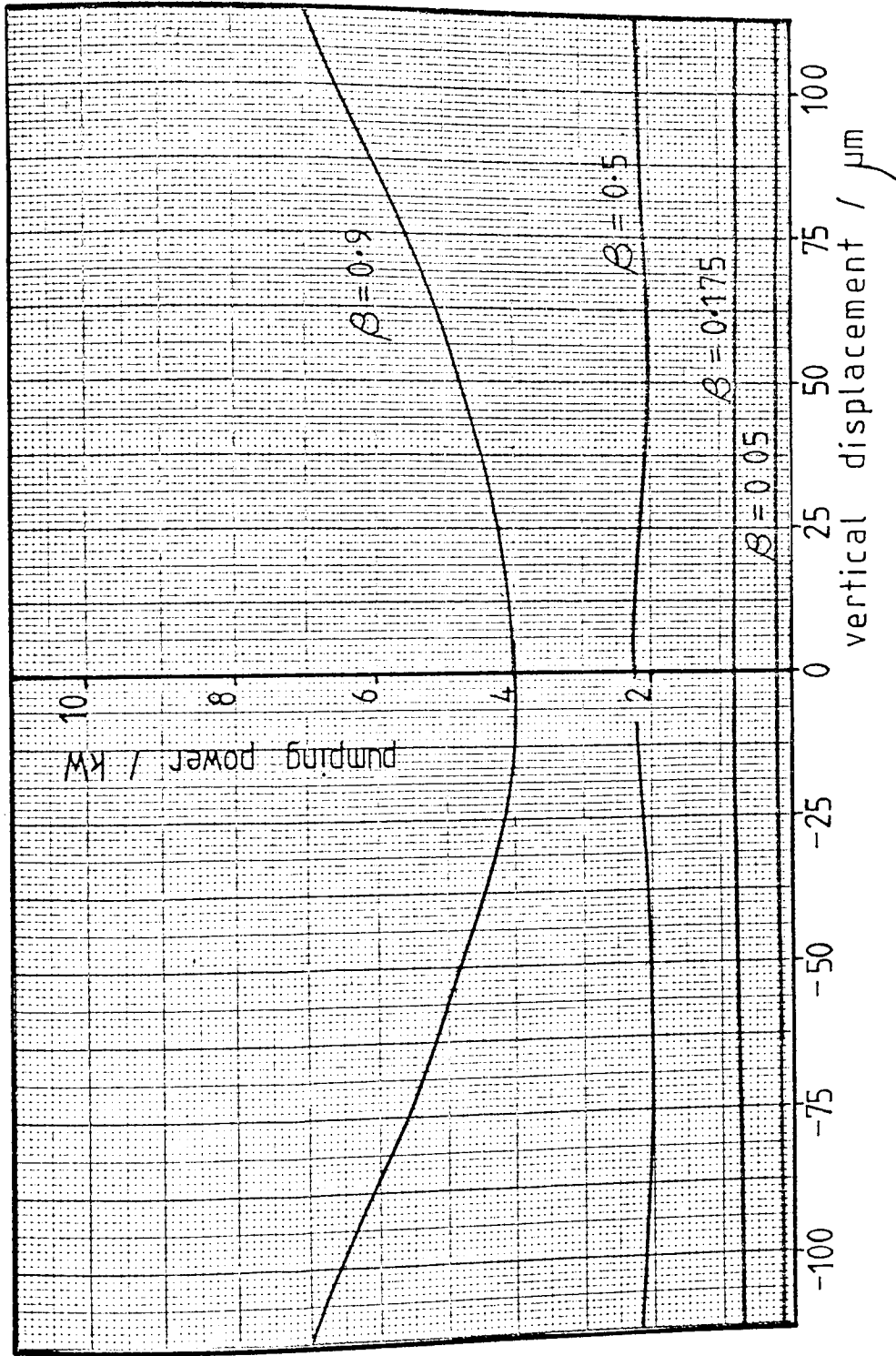


FIG 6.17 THEORETICAL VERTICAL DISPLACEMENT -- OIL PUMPING POWER  
RELATIONSHIP FOR THE HYDROSTATIC BEARING BUSH

Engineering Drawing



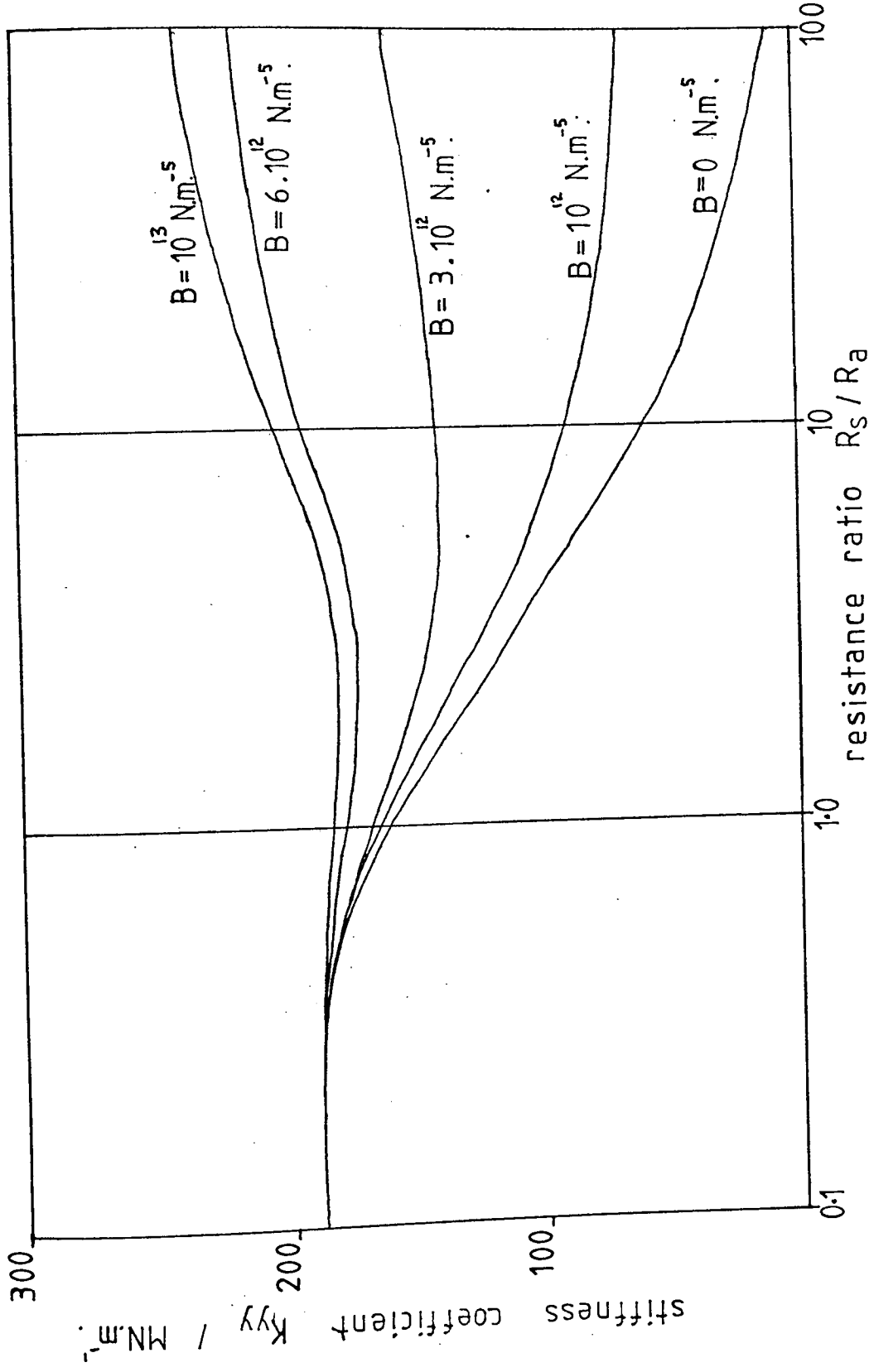


FIG 6.18 THEORETICAL INFLUENCE OF THE ACCUMULATOR ON THE HYDROSTATIC BEARING BUSH STIFFNESS COEFFICIENT  $K_{yy}$ —

Hydrostatic Bearings

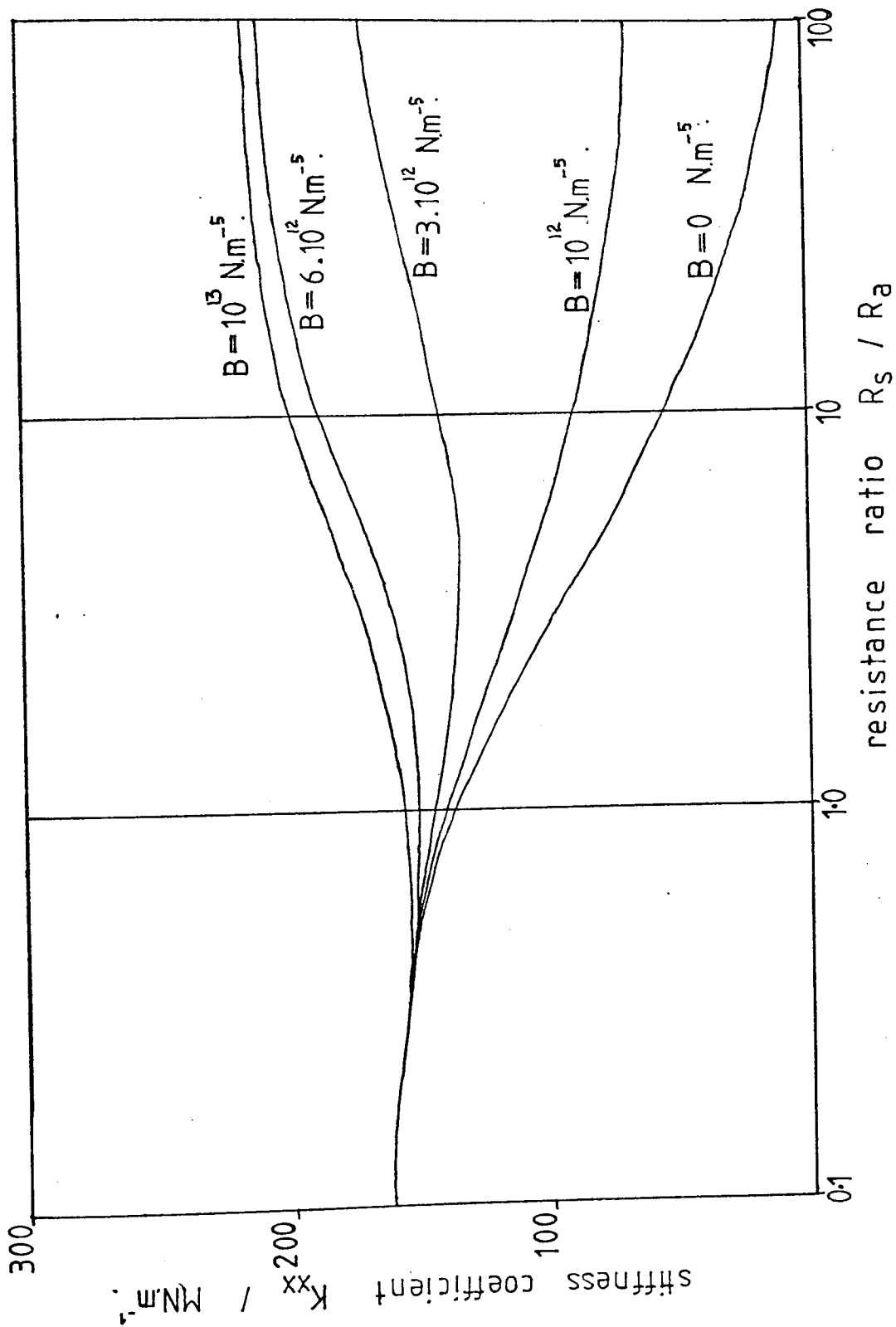


FIG 6.19 THEORETICAL INFLUENCE OF THE ACCUMULATOR ON THE HYDROSTATIC BEARING BUSH STIFFNESS COEFFICIENT  $K_{xx}$ —

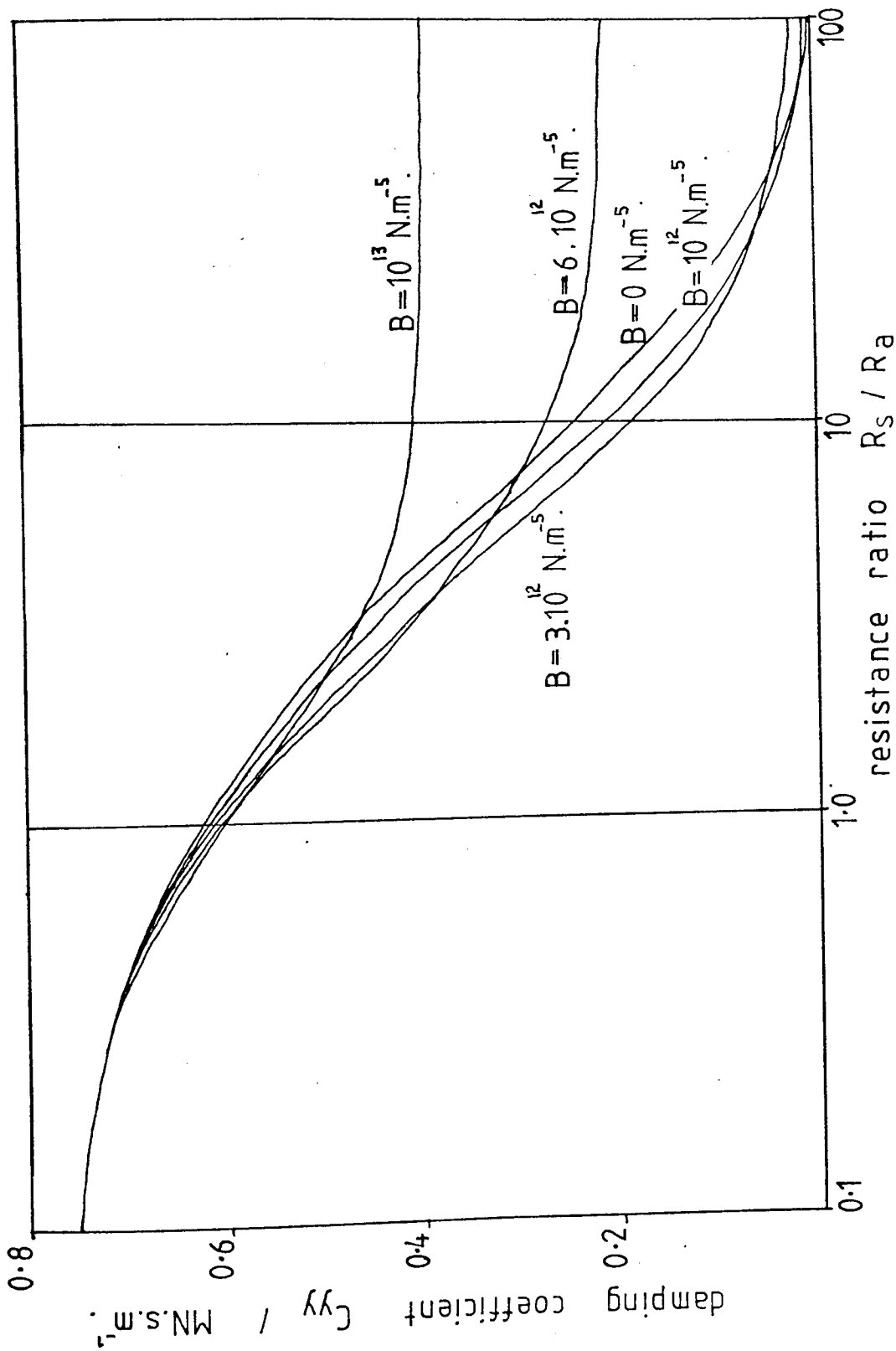


FIG 6.20 THEORETICAL INFLUENCE OF THE ACCUMULATOR ON THE HYDROSTATIC BEARING BUSH DAMPING COEFFICIENT  $C_{yy}$ —

Approved for release by NSA on 05-08-2014 pursuant to E.O. 13526

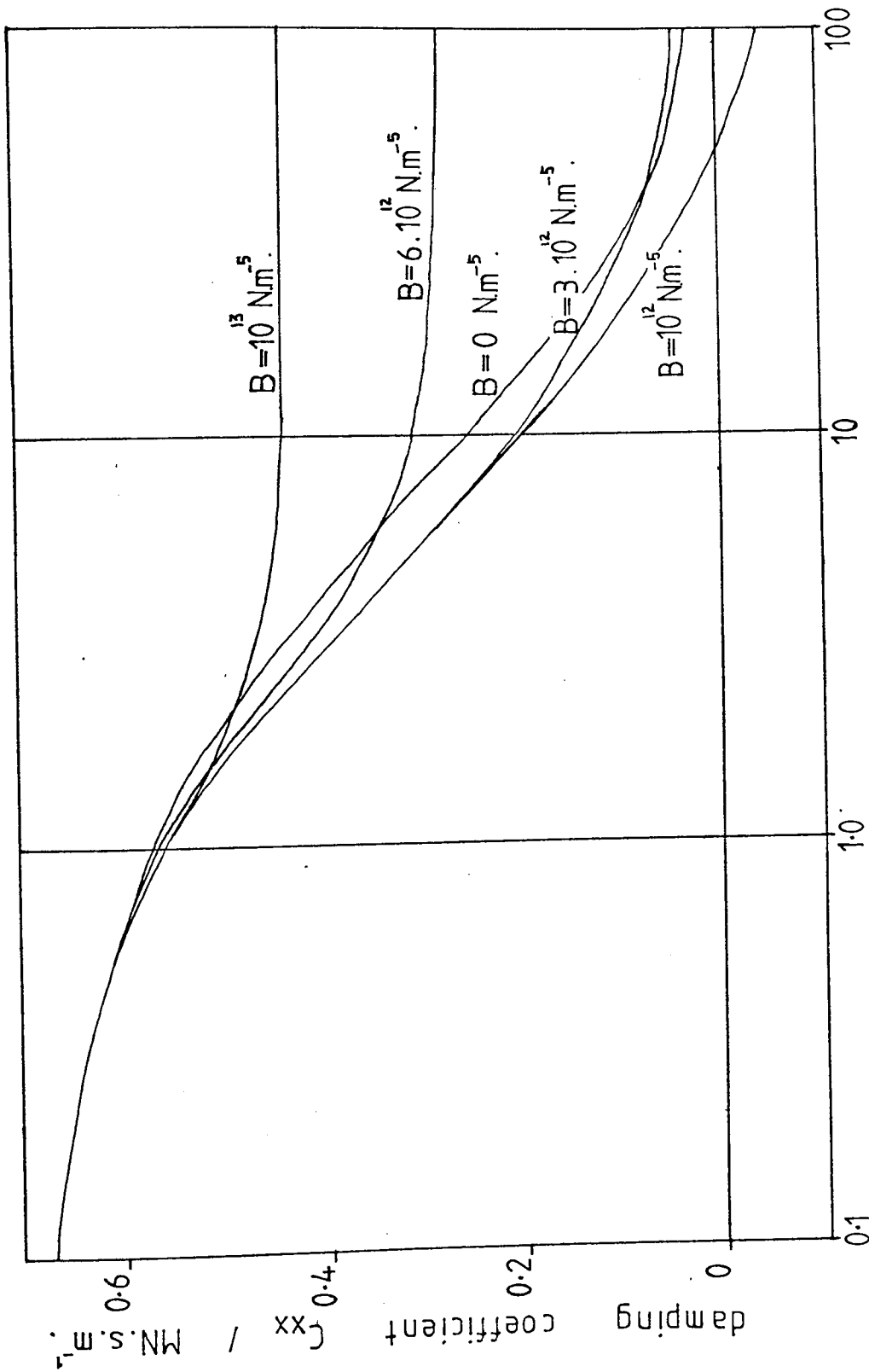


FIG 6.21 THEORETICAL INFLUENCE OF THE ACCUMULATOR ON THE  
HYDROSTATIC BEARING BUSH DAMPING COEFFICIENT  $C_{xx}$

Approved for release

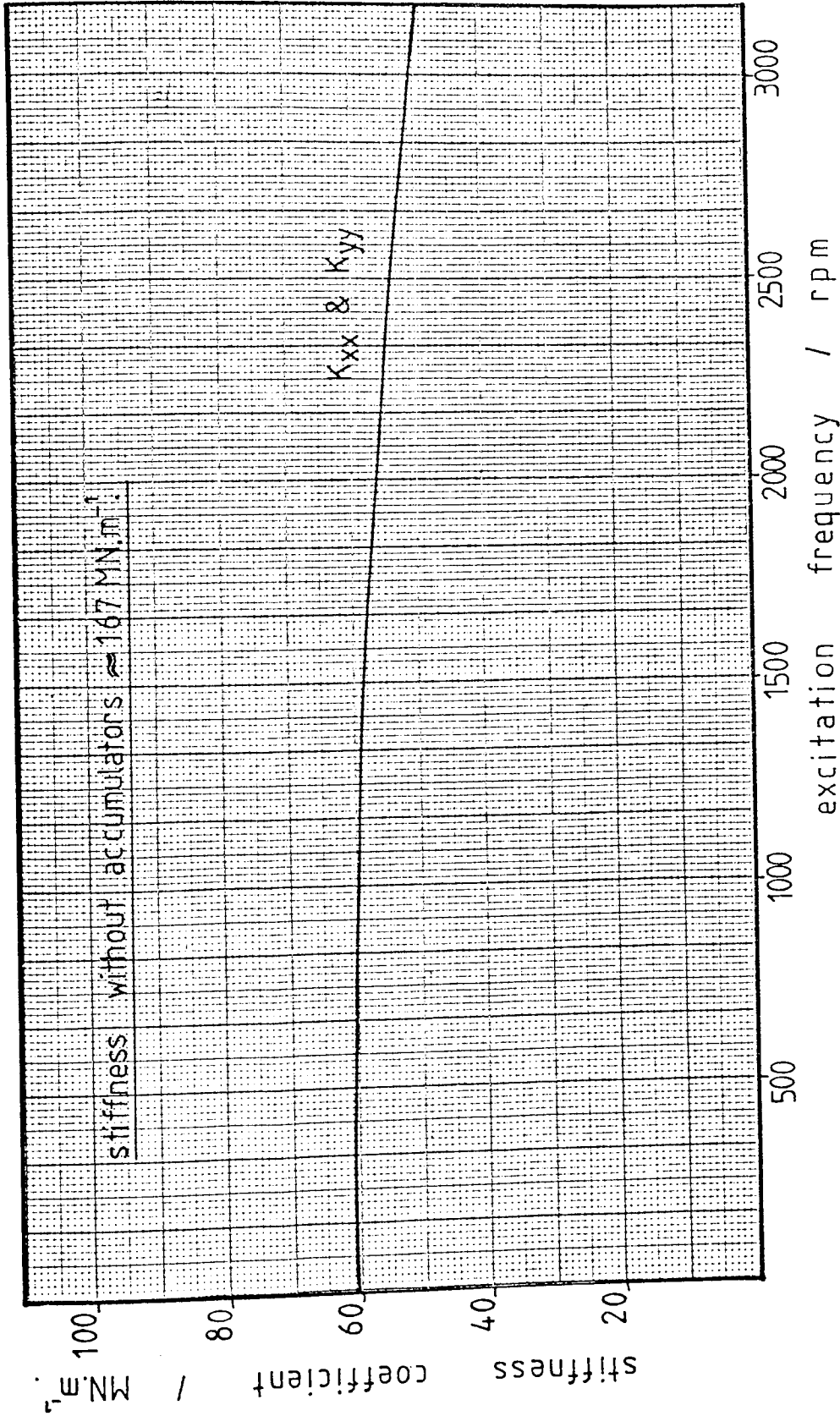


FIG 6.22 THEORETICAL VARIATION OF HYDROSTATIC BEARING BUSH STIFFNESS COEFFICIENT WITH EXCITATION FREQUENCY

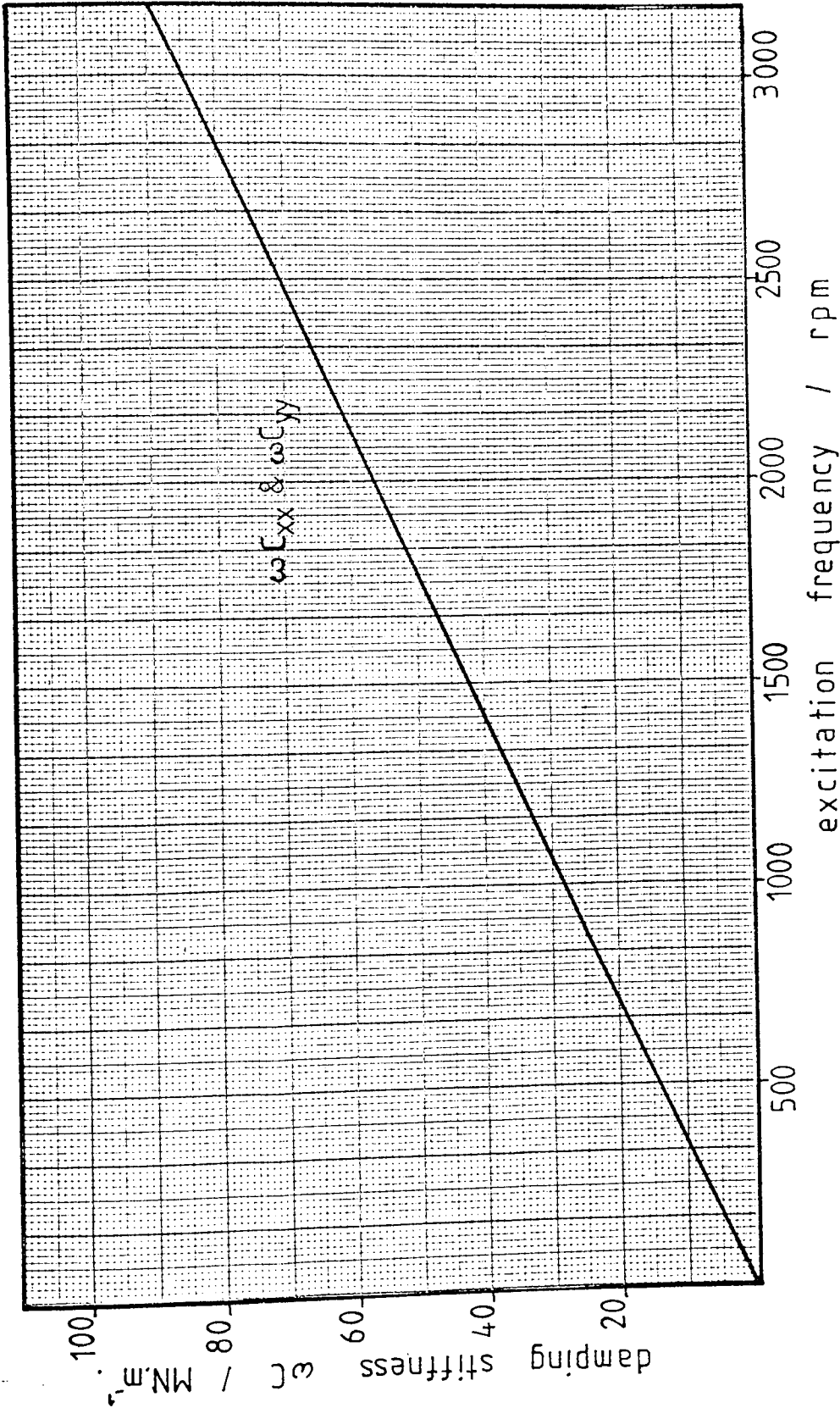


FIG 6.23 THEORETICAL VARIATION OF HYDROSTATIC BEARING BUSH  
DAMPING STIFFNESS WITH EXCITATION FREQUENCY

Theoretical curves for the variation of bearing coefficient with oil inertia in the capillary restrictors are shown in figures 6.24 to 6.27. Again, these are for the case where resistance ratio  $R_S/R_a = 10$ , accumulator operating parameter  $B = 0$  and an excitation frequency of 3000 rpm. Figures 6.28 and 6.29 show theoretical curves for the variation of direct vertical stiffness and damping coefficient with vertical displacement of the floating ring (journal bearing bush) for various amounts of oil inertia in the capillary restrictors but with the amount of inertia proportional to the viscous flow resistance such that  $I_S/I_a = 10$ .

The significance of all of the above theoretical results is discussed in chapter 8.

#### 6.4b Experimental results

If a hydrostatic bearing were to be designed for use with a turbine generator as proposed, then for a given bearing arrangement, the most important variable would be exciting frequency since this would vary in the machines service. It is for this reason that experimental measurements of amplitude and phase to determine the bearing dynamic oil film coefficients have been made for a range of excitation frequencies. Such measurements have been made for the case where no accumulators are connected to the hydrostatic bearing bush, and for the case where accumulators having operating characteristics described by the  $B = 0$  curves of figures 6.18 to 6.21 are connected to the hydrostatic pockets such that resistance ratio  $R_S/R_a = 10$ . These two cases were selected since they represent two of the most likely circumstances under which such a hydrostatic bearing would be used, and because the resulting measured bearing coefficients would clearly indicate the influence of the accumulator on the bearing oil film impedance.

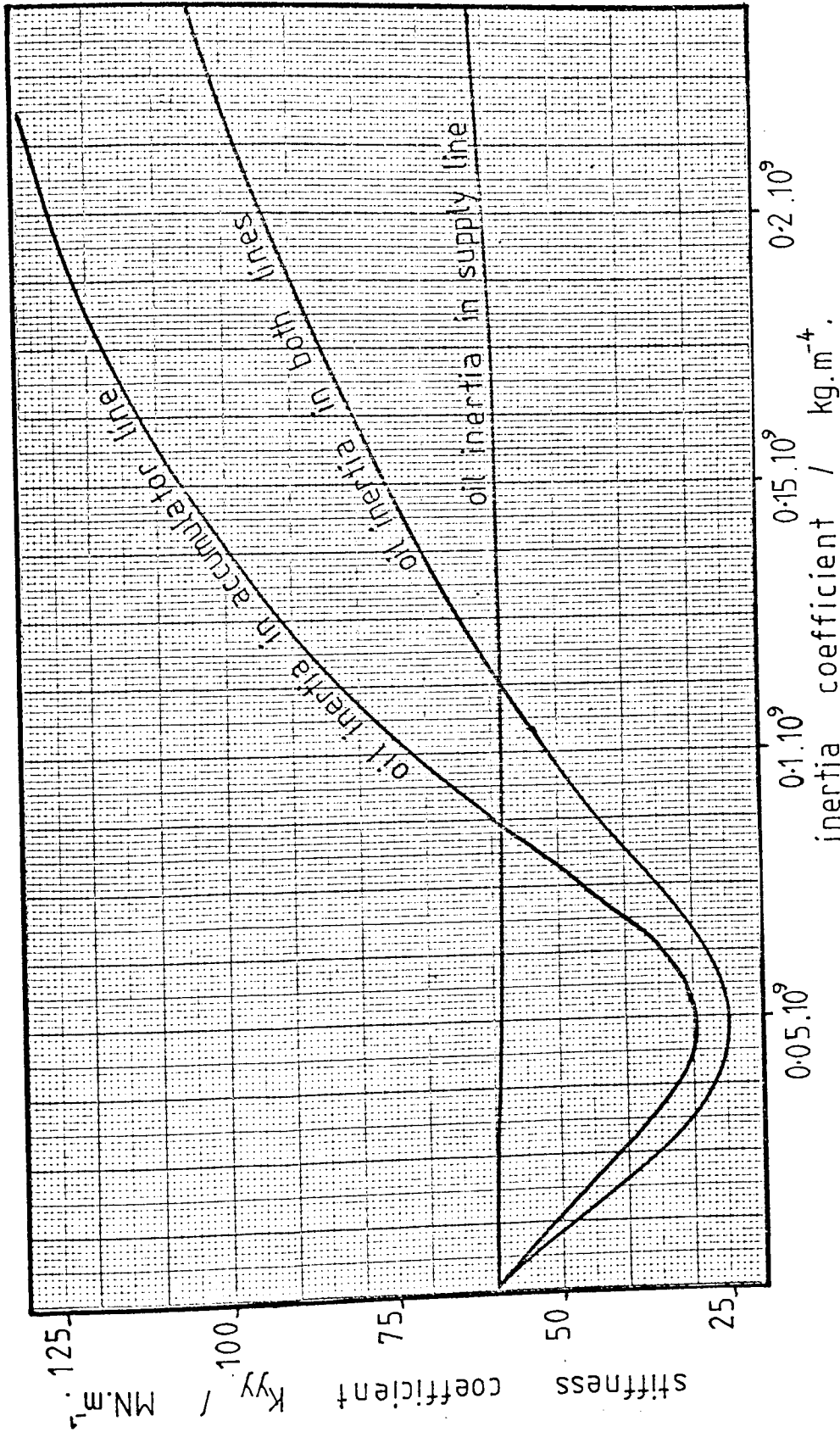


FIG 6.24 THEORETICAL VARIATION OF HYDROSTATIC BEARING BUSH STIFFNESS COEFFICIENT  $K_{yy}$  WITH OIL INERTIA



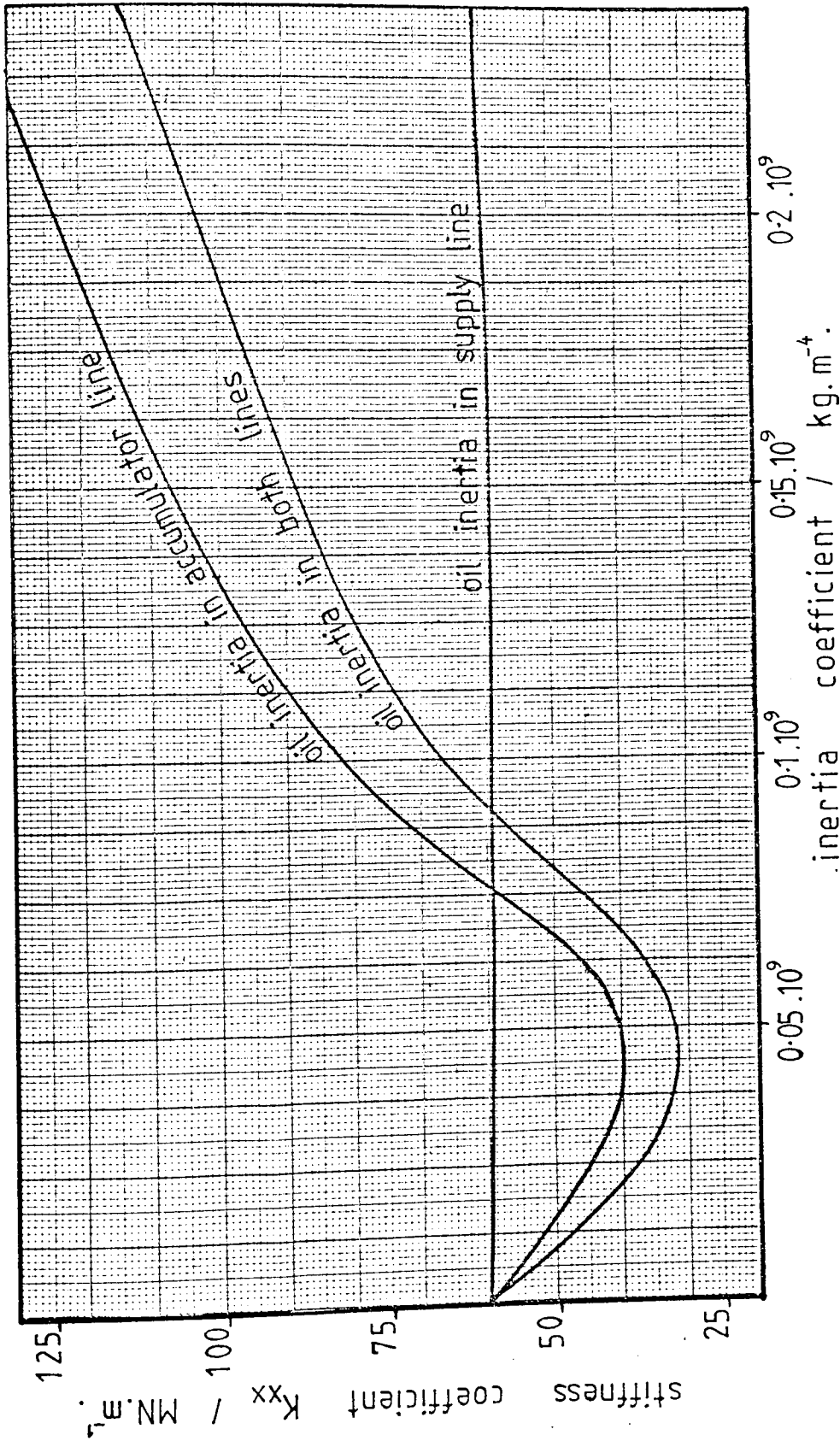


FIG 6.25 THEORETICAL VARIATION OF HYDROSTATIC BEARING BUSH STIFFNESS COEFFICIENT  $K_{xx}$  WITH OIL INERTIA

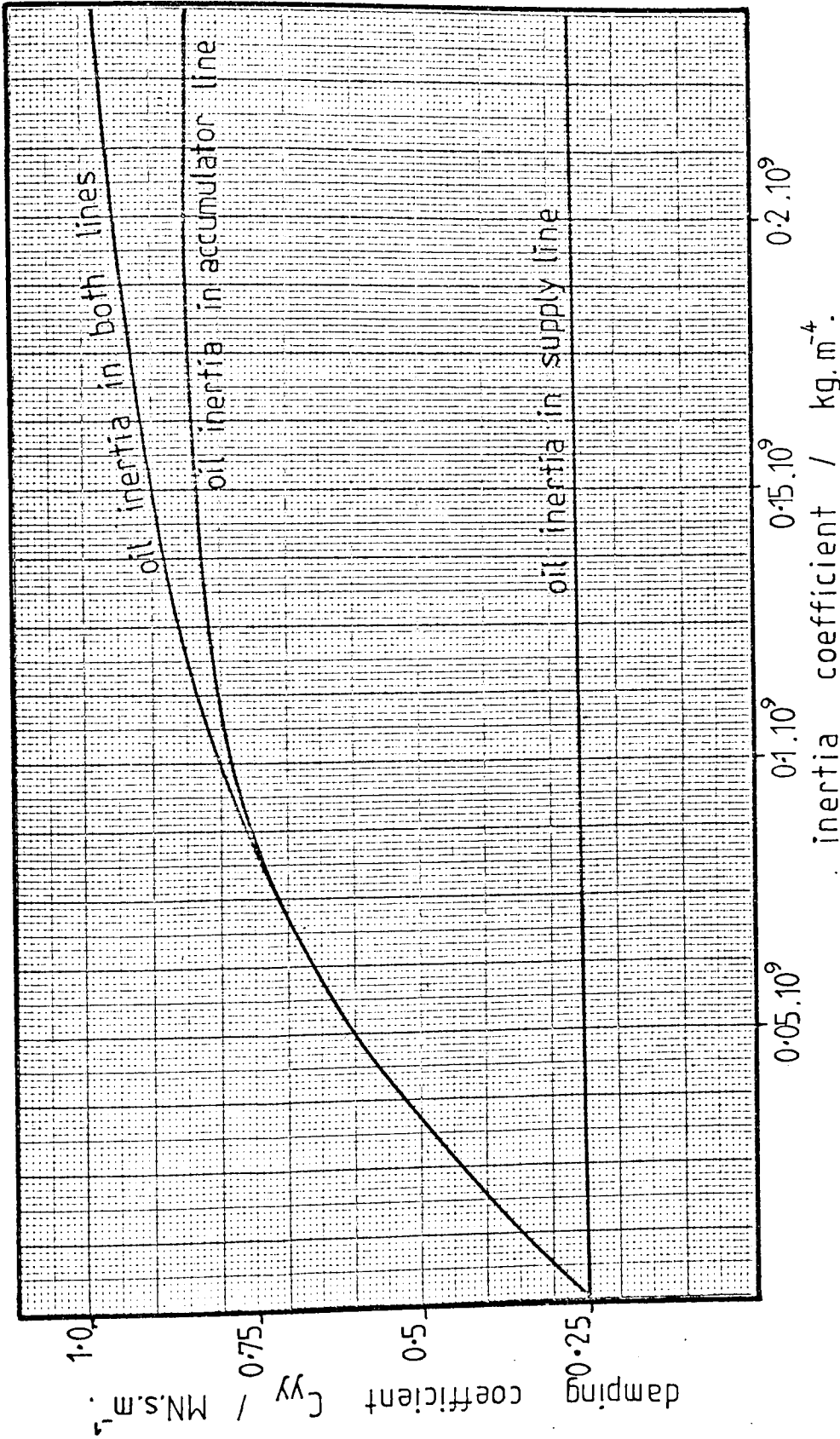


FIG 6.26 THEORETICAL VARIATION OF HYDROSTATIC BEARING BUSH  
DAMPING COEFFICIENT  $C_{yy}$  WITH OIL INERTIA

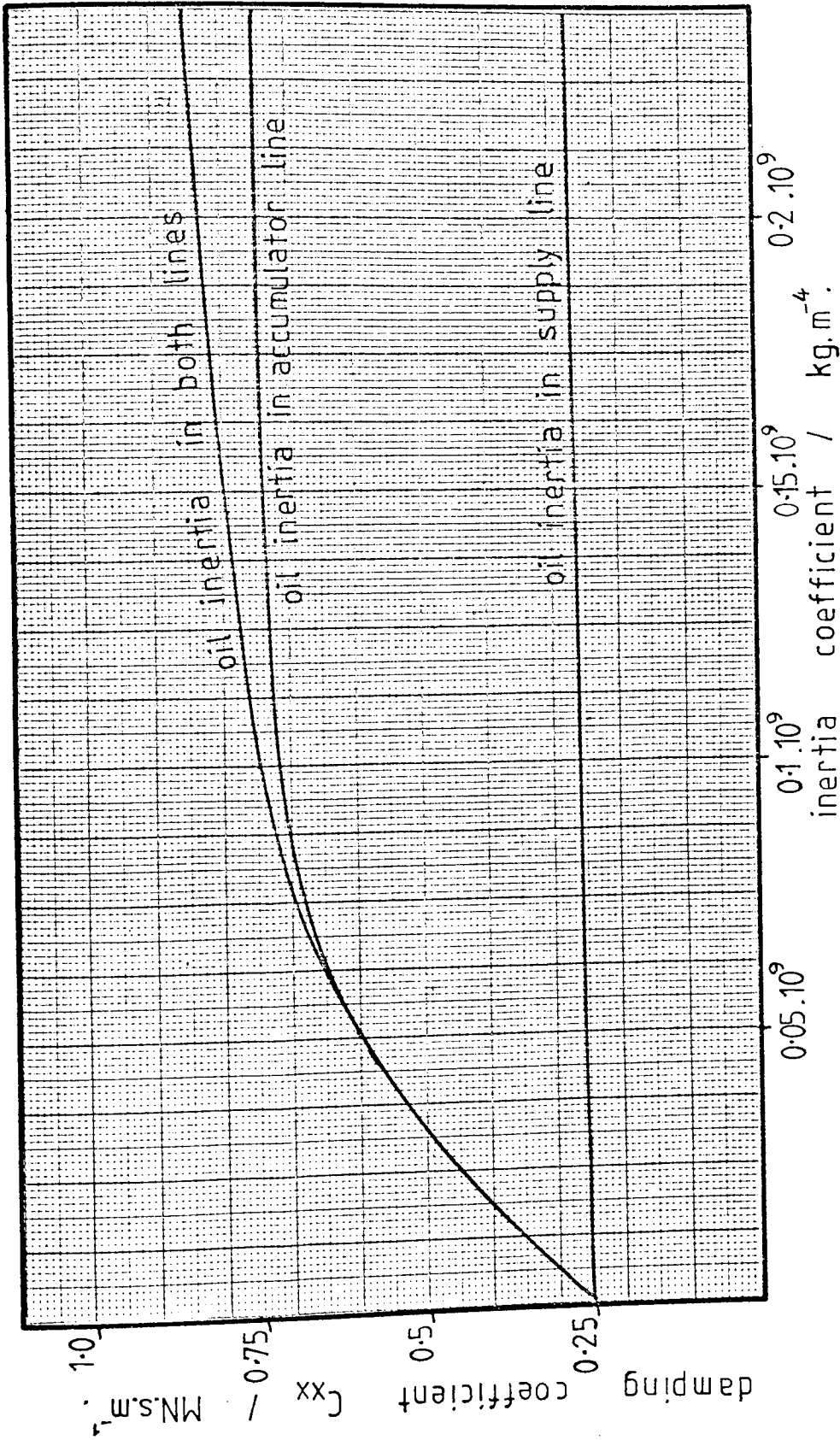


FIG 6.27 THEORETICAL VARIATION OF HYDROSTATIC BEARING BUSH DAMPING COEFFICIENT  $C_{xx}$  WITH OIL INERTIA

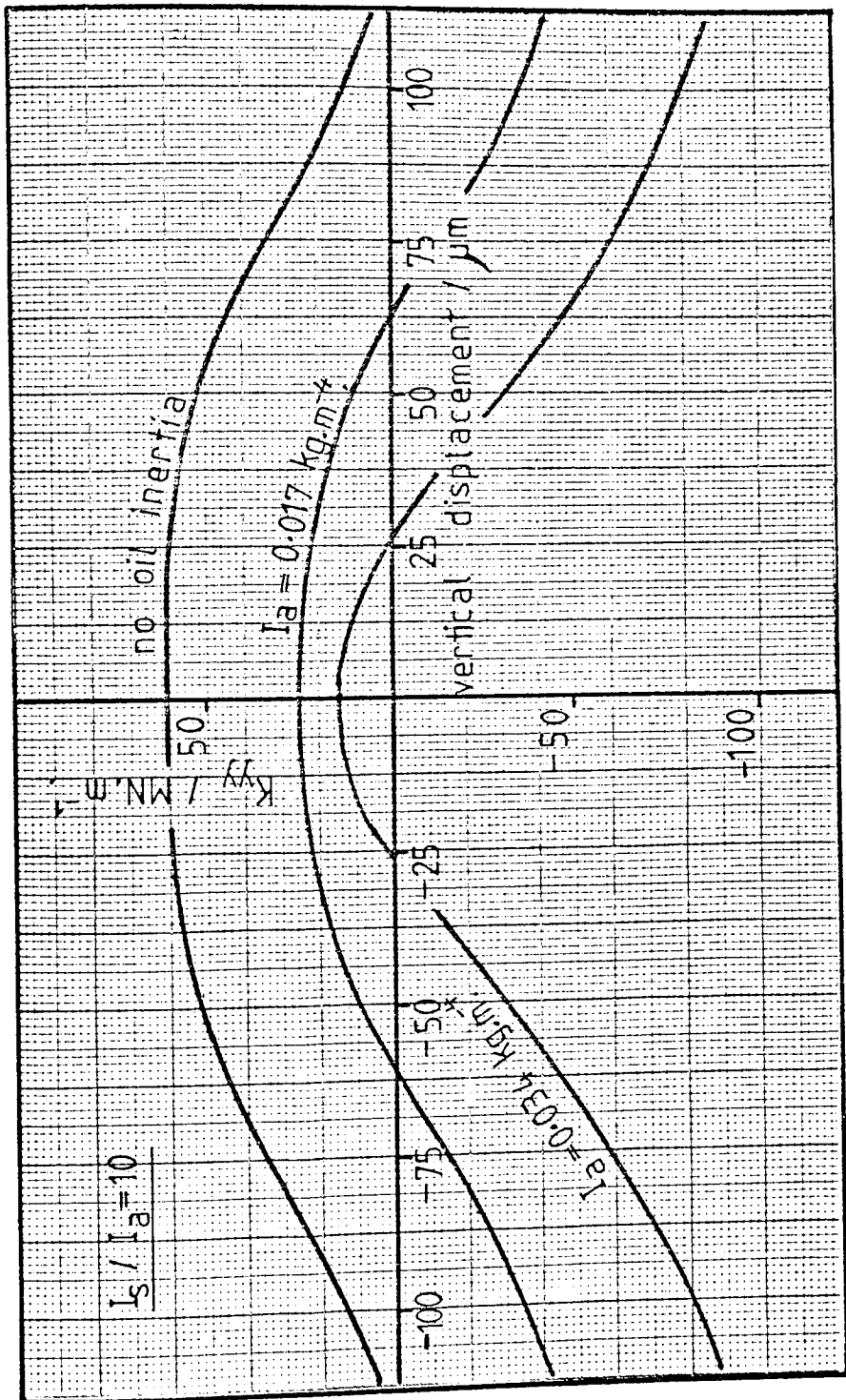


FIG 6.28 THEORETICAL EFFECT OF DISPLACEMENT AND OIL INERTIA ON THE HYDROSTATIC BEARING BUSH STIFFNESS COEFFICIENT  $K_y$

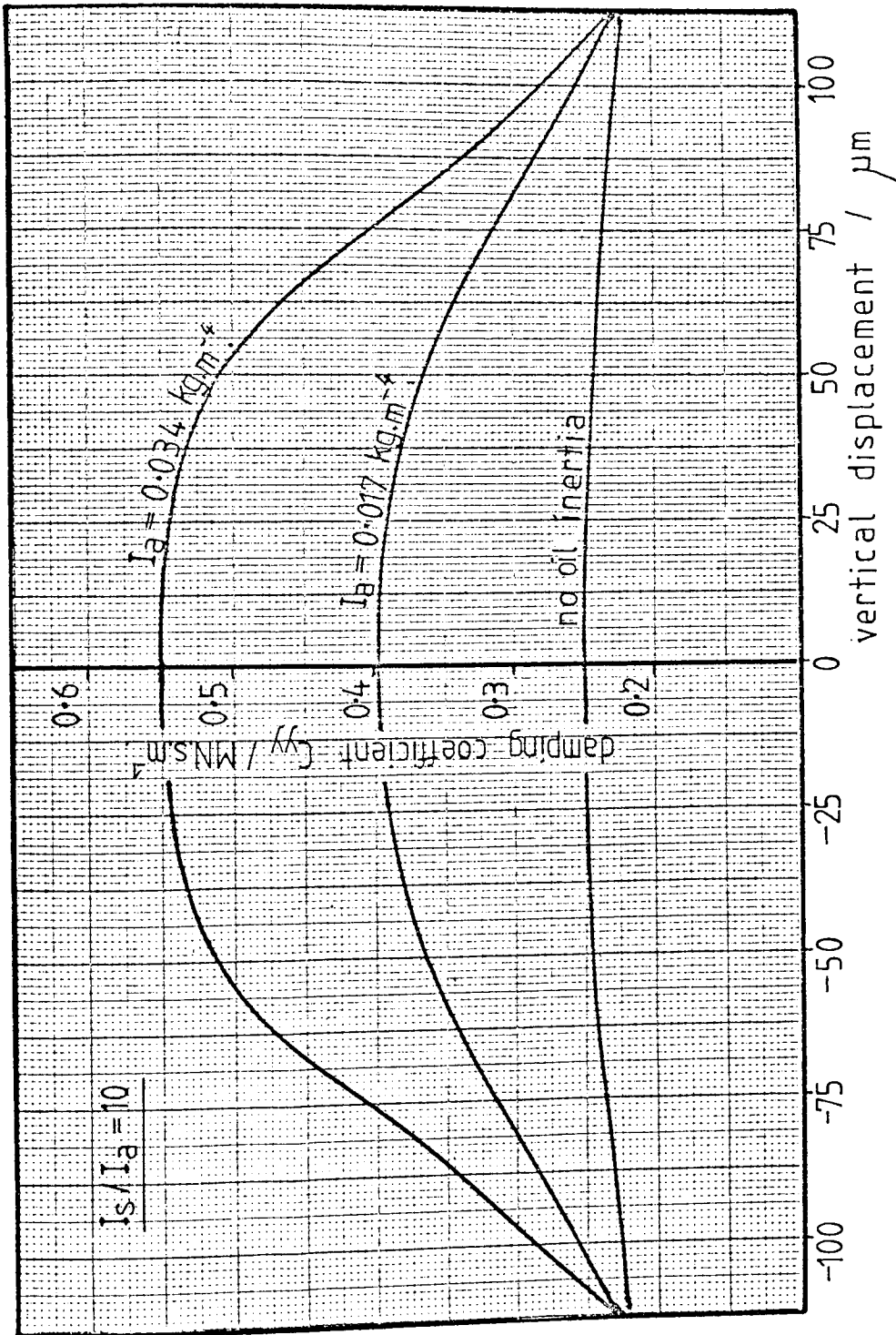


FIG 6.29 THEORETICAL EFFECT OF DISPLACEMENT AND OIL INERTIA ON THE HYDROSTATIC BEARING BUSH DAMPING COEFFICIENT  $C_{yy}$ -

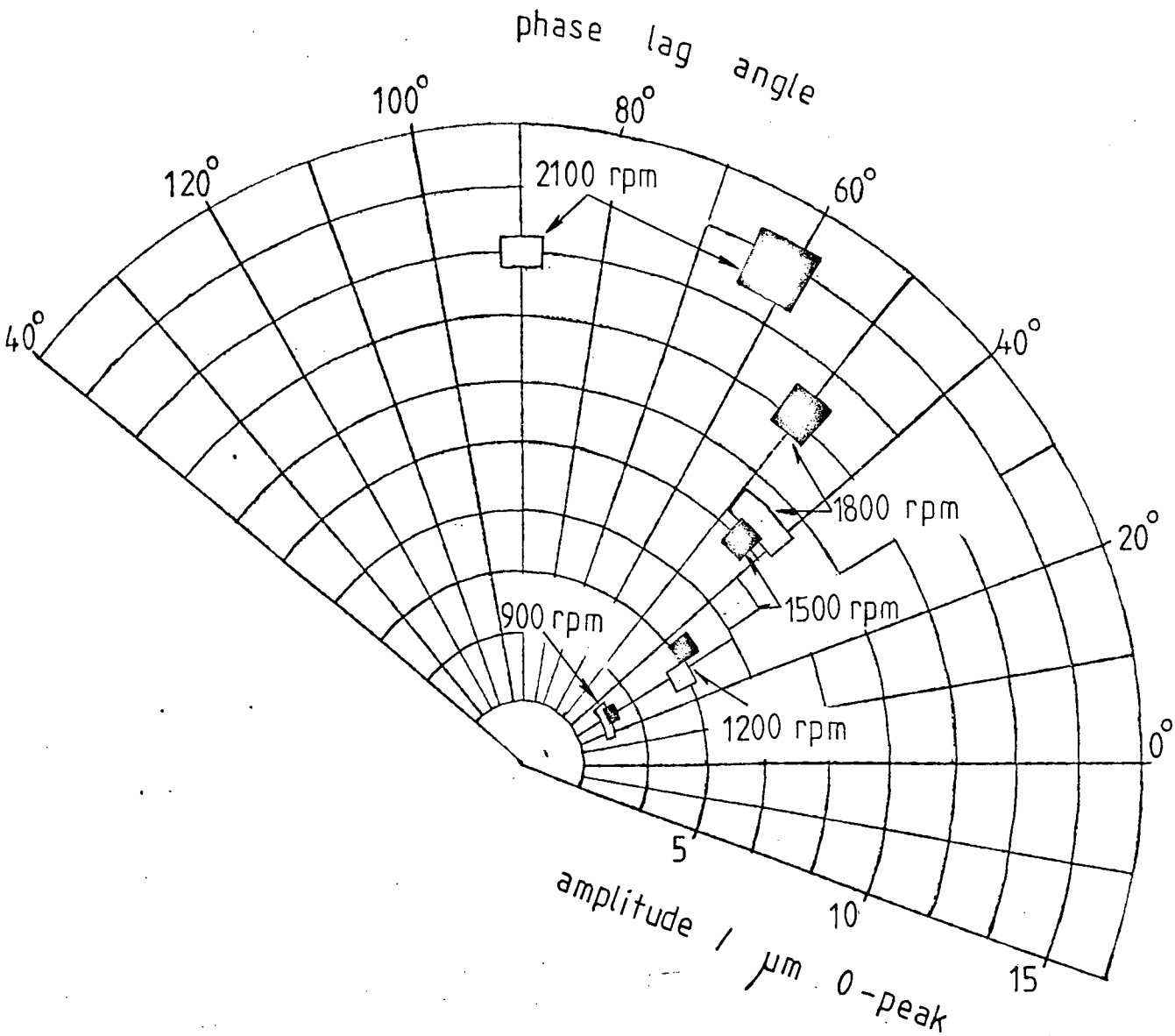
Figures 6.30 and 6.31 show the measured amplitude and phase mean and standard deviation in polar plot form, for the forward and reverse directions of excitation respectively. These figures apply to the hydrostatic bearing only, without accumulators connected to the system, and figures 6.32 to 6.39 show the corresponding computed bearing coefficients for various excitation frequencies together with the corresponding theoretical values for comparison. Again the standard deviations indicated on figures 6.32 to 6.39 have been estimated from a sample of results.

For the case where accumulators are connected to the hydrostatic bearing, figures 6.40 and 6.41 show the measured amplitude and phase means and standard deviations in polar plot form for forward and reverse excitation directions respectively. The corresponding bearing coefficient means, and estimated standard deviations, for the range of excitation frequencies, are shown in figures 6.42 to 6.49 together with theoretical values for comparison.

#### 6.5 Static Characteristics of the Combined Journal and Hydrostatic Bearing

The static characteristics for the combined bearing are determined by a combination of the static characteristics for the two individual bearings. That is, for a given load and speed the vertical and horizontal displacements are the sums of the corresponding displacements for the two individual bearings. To present experimental results here would be to merely repeat those already presented in sections 6.1 and 6.3.

Some very small variation from the relationship described above does occur, due to the fact that the hydrostatic bush exerts a force on the journal bearing bush at the anti-rotation peg, thereby causing an additional small displacement of the journal and its bush. For the test rig this force was insignificantly small compared with the other oil film forces. It is a point to be checked during the design of two-



- horizontal response
- vertical response

FIG 6.30 NYQUIST DIAGRAM FOR THE HYDROSTATIC BEARING WITHOUT ACCUMULATORS, FORWARD EXCITATION

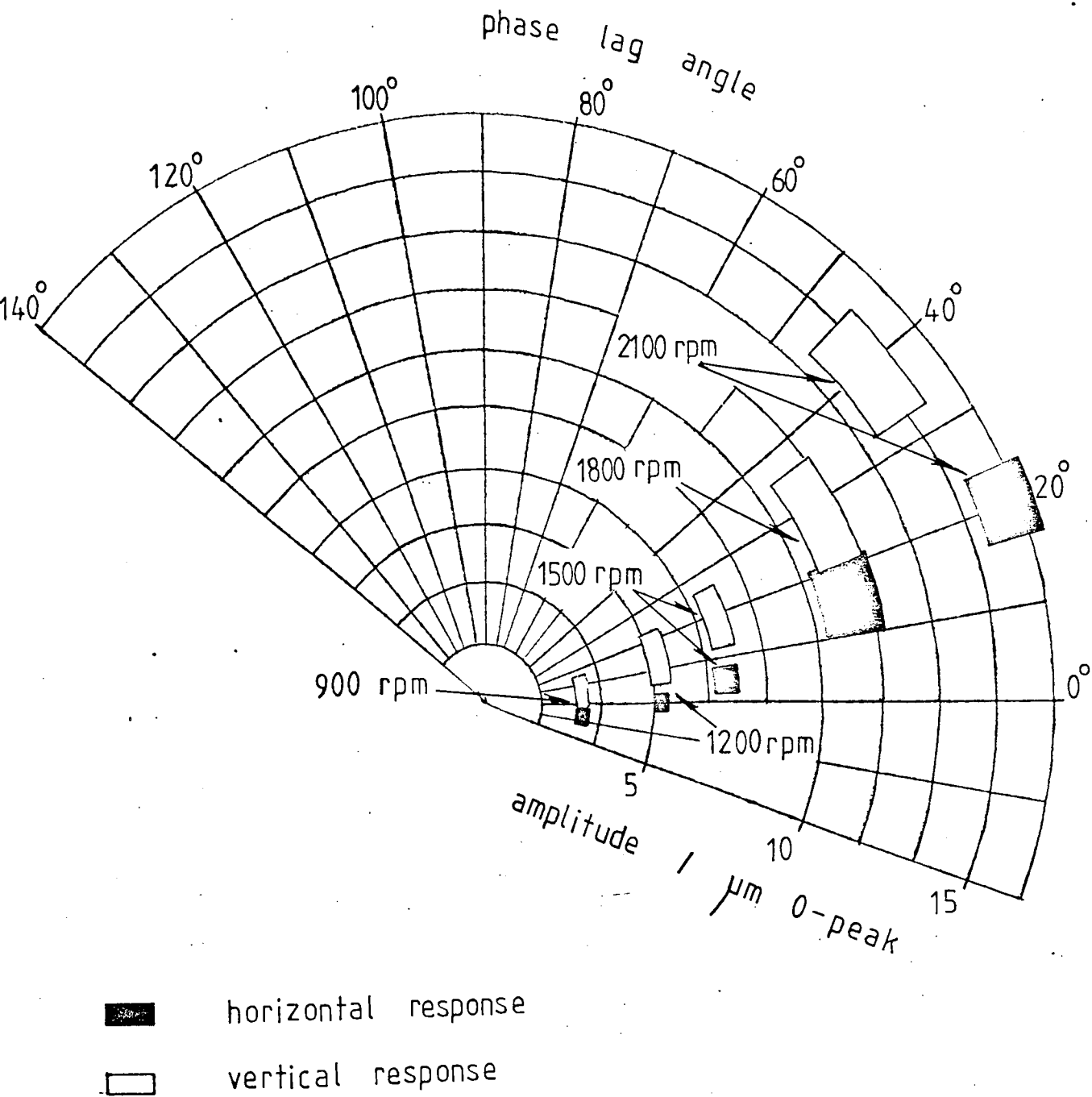


FIG 6.31 NYQUIST DIAGRAM FOR THE HYDROSTATIC BEARING WITHOUT ACCUMULATORS, REVERSE EXCITATION



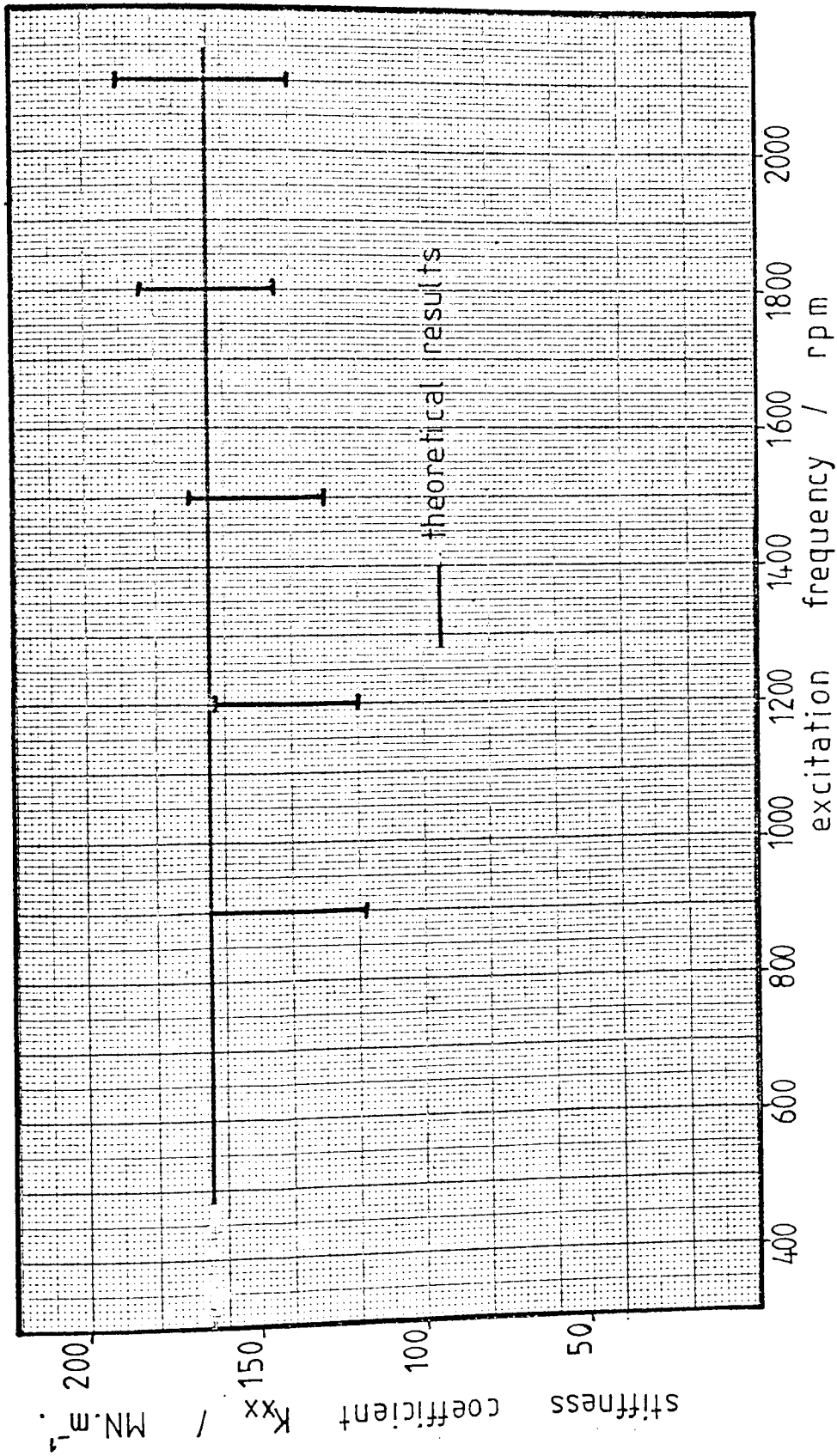


FIG 6.32 VARIATION OF HYDROSTATIC BEARING BUSH STIFFNESS COEFFICIENT  $K_{xx}$  WITH EXCITATION FREQUENCY, ( NO ACCUMULATORS )

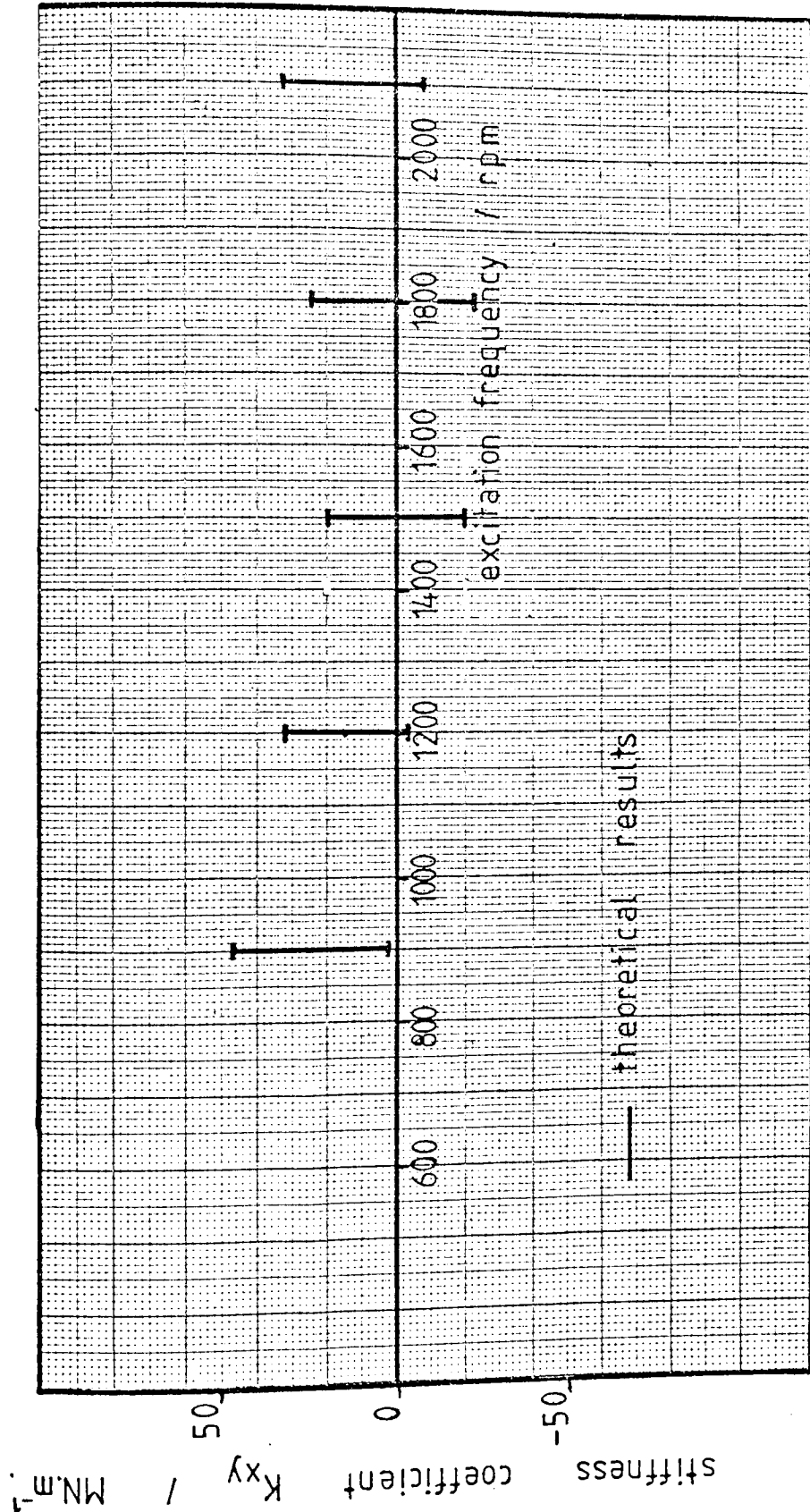


FIG 6.33 VARIATION OF HYDROSTATIC BEARING BUSH STIFFNESS COEFFICIENT  $K_{xy}$  WITH EXCITATION FREQUENCY, (NO ACCUMULATORS)

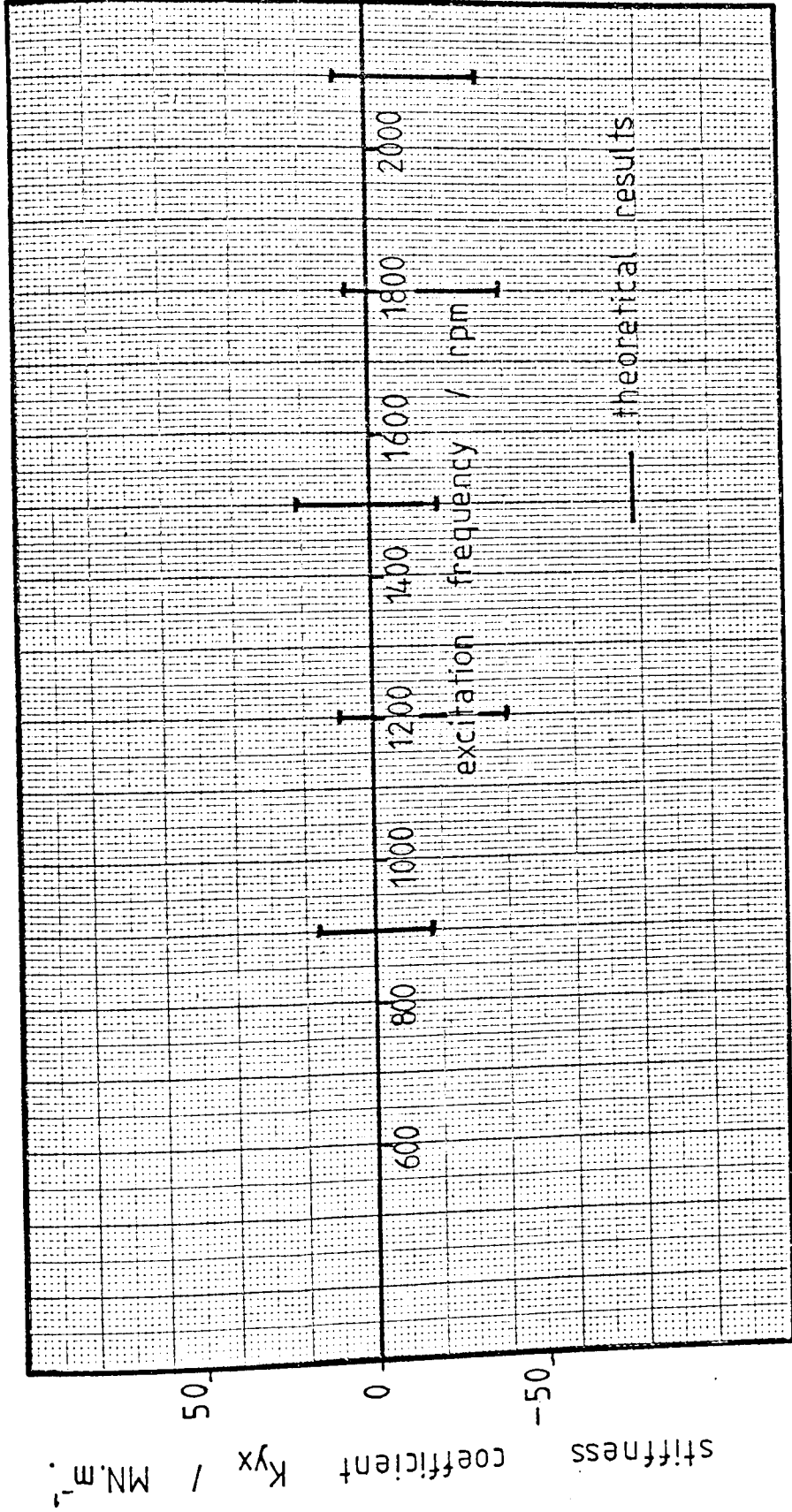


FIG 6.34 VARIATION OF HYDROSTATIC BEARING BUSH STIFFNESS COEFFICIENT  $K_{yx}$  WITH EXCITATION FREQUENCY, (NO ACCUMULATORS)

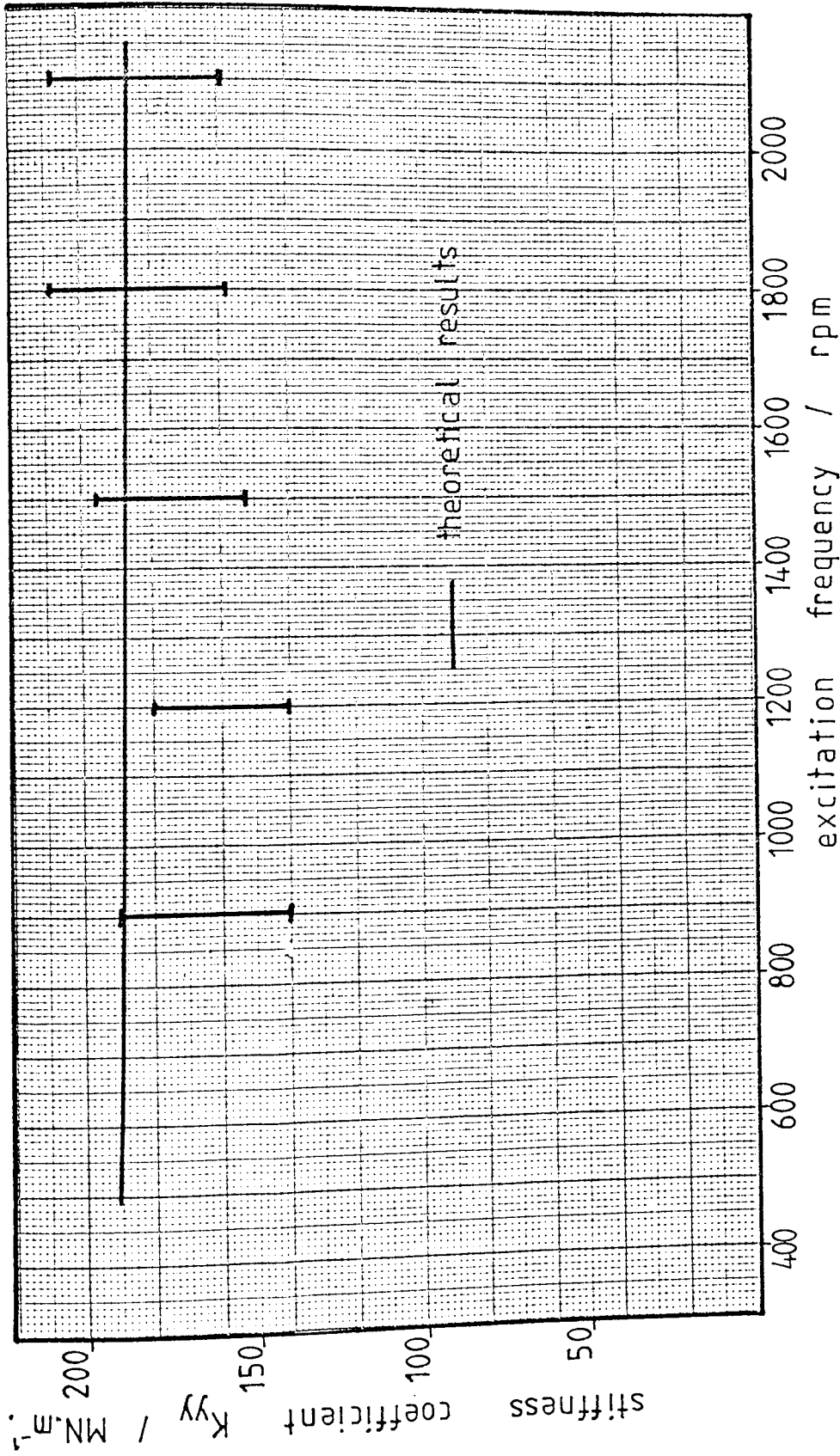


FIG 6.35 VARIATION OF HYDROSTATIC BEARING BUSH STIFFNESS COEFFICIENT  $K_{yy}$  WITH EXCITATION FREQUENCY (NO ACCUMULATORS)

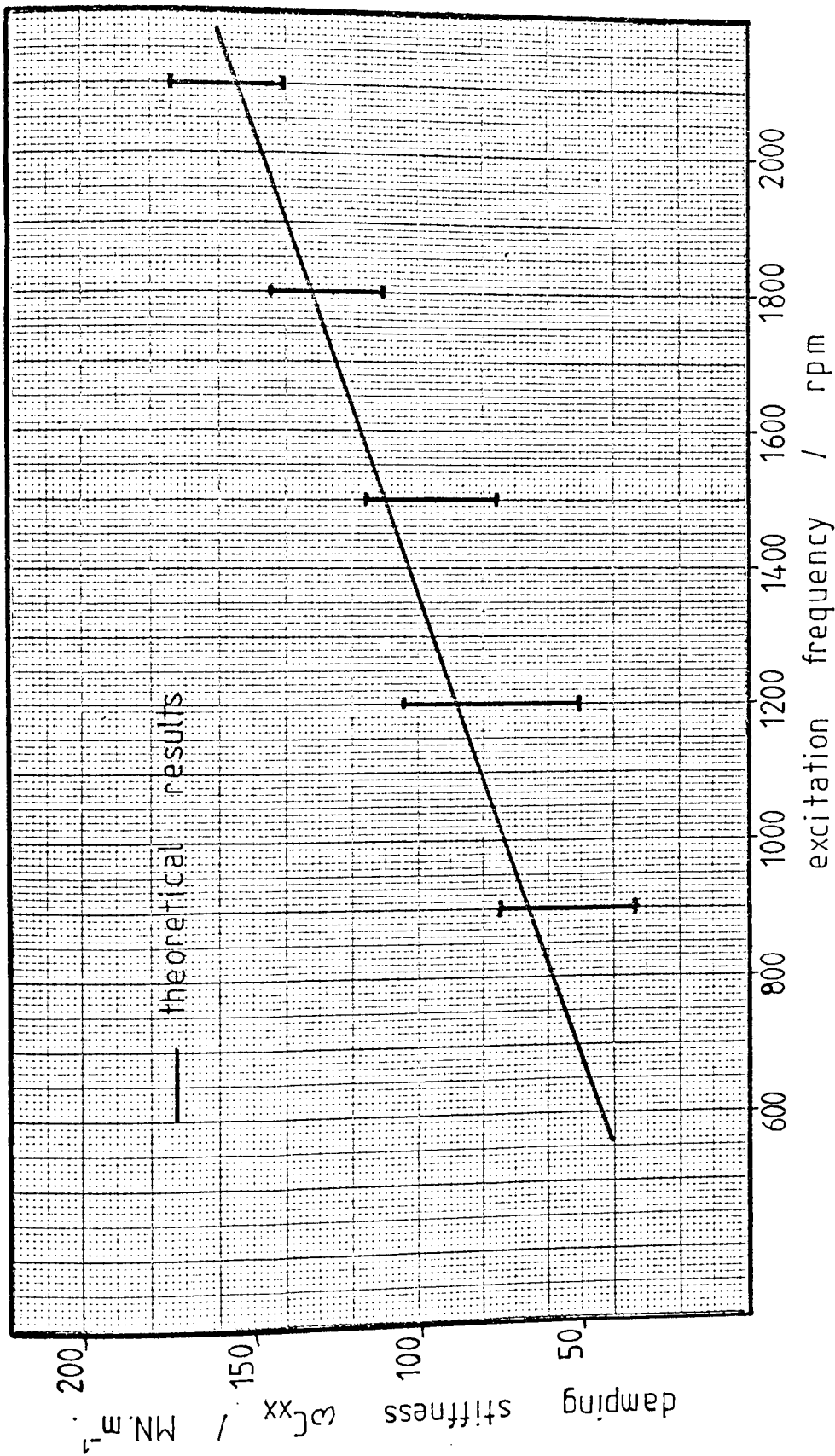


FIG 6.36 VARIATION OF HYDROSTATIC BEARING BUSH DAMPING STIFFNESS  $\omega C_{xx}$  WITH EXCITATION FREQUENCY, ( NO ACCUMULATORS )

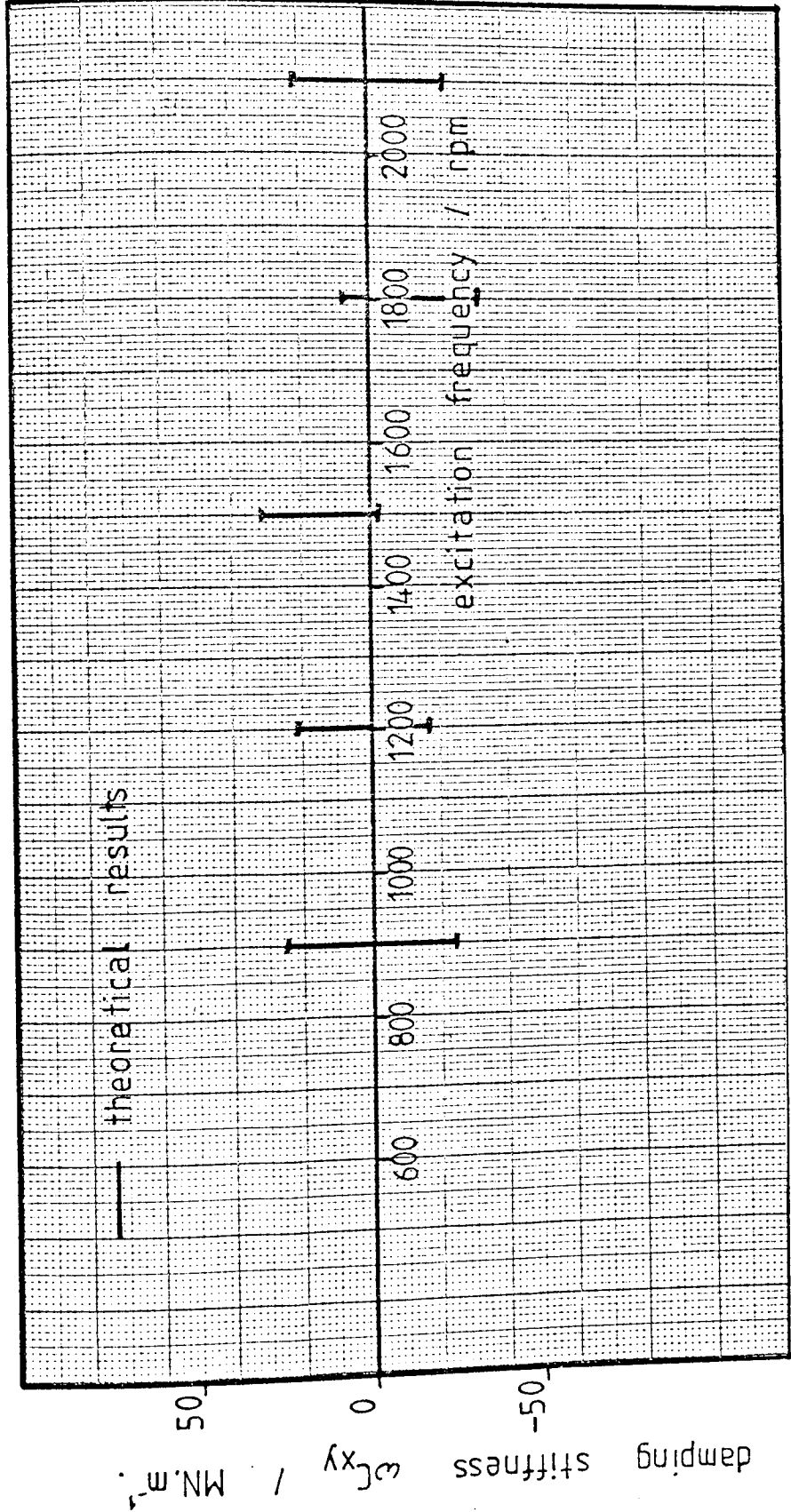


FIG 6.37 VARIATION OF HYDROSTATIC BEARING BUSH DAMPING STIFFNESS  $\omega C_{xy}$  WITH EXCITATION FREQUENCY, ( NO ACCUMULATORS )

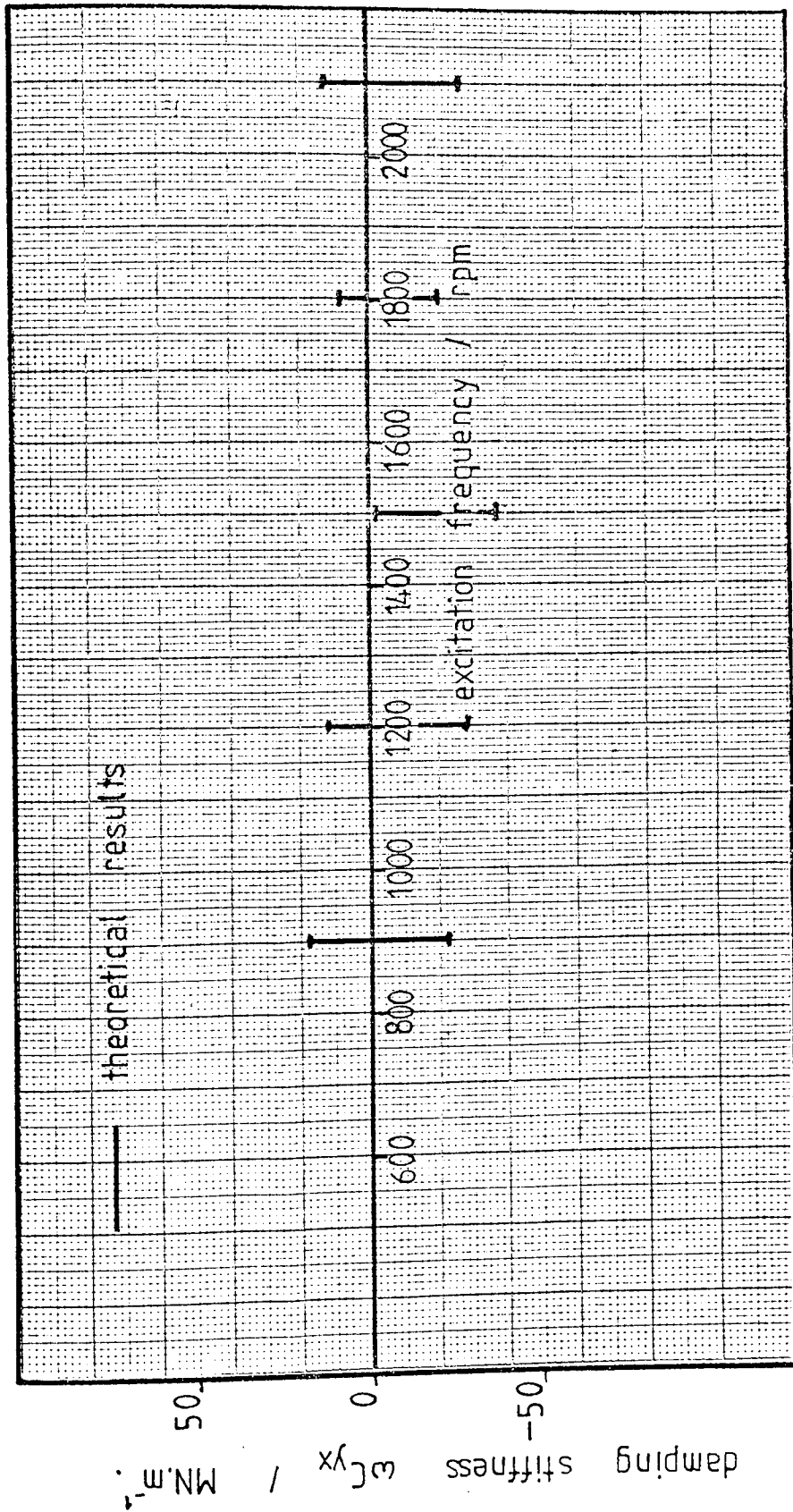


FIG 6.38 VARIATION OF HYDROSTATIC BEARING BUSH DAMPING STIFFNESS  $\omega c_{yx}$  WITH EXCITATION FREQUENCY, (NO ACCUMULATORS)

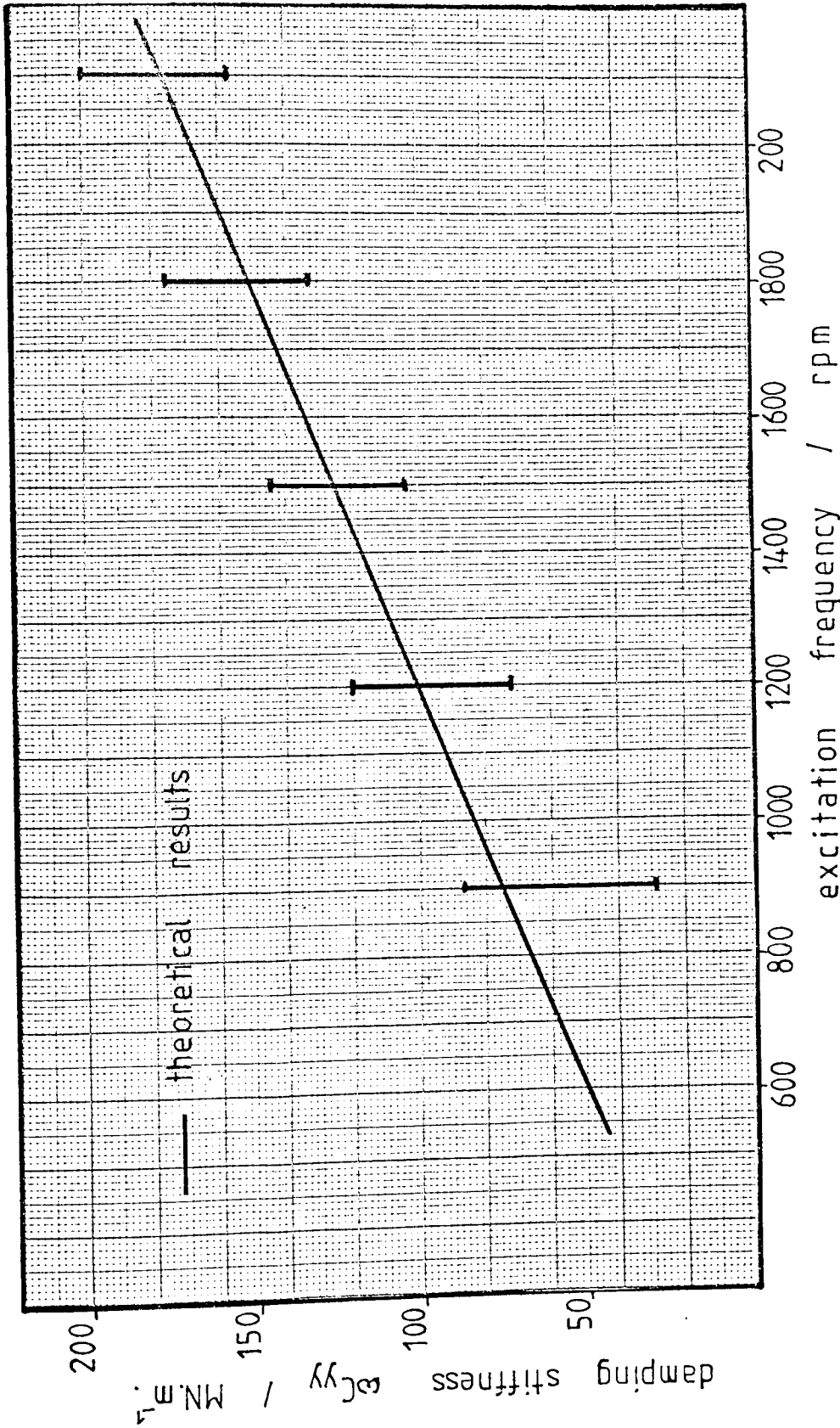


FIG 6.39 VARIATION OF HYDROSTATIC BEARING BUSH DAMPING STIFFNESS  $\omega c_{yy}$  WITH EXCITATION FREQUENCY, ( NO ACCUMULATORS )



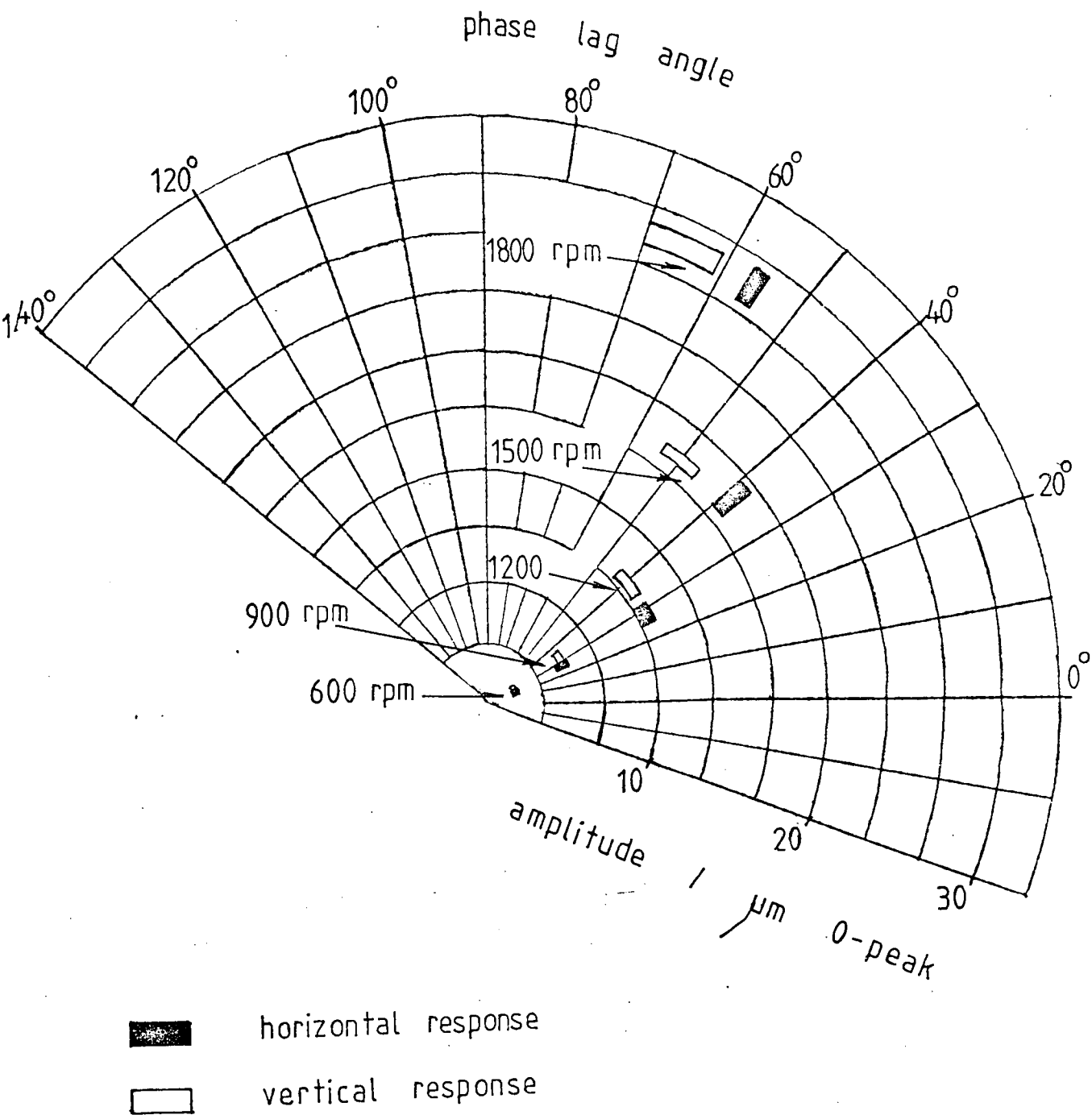
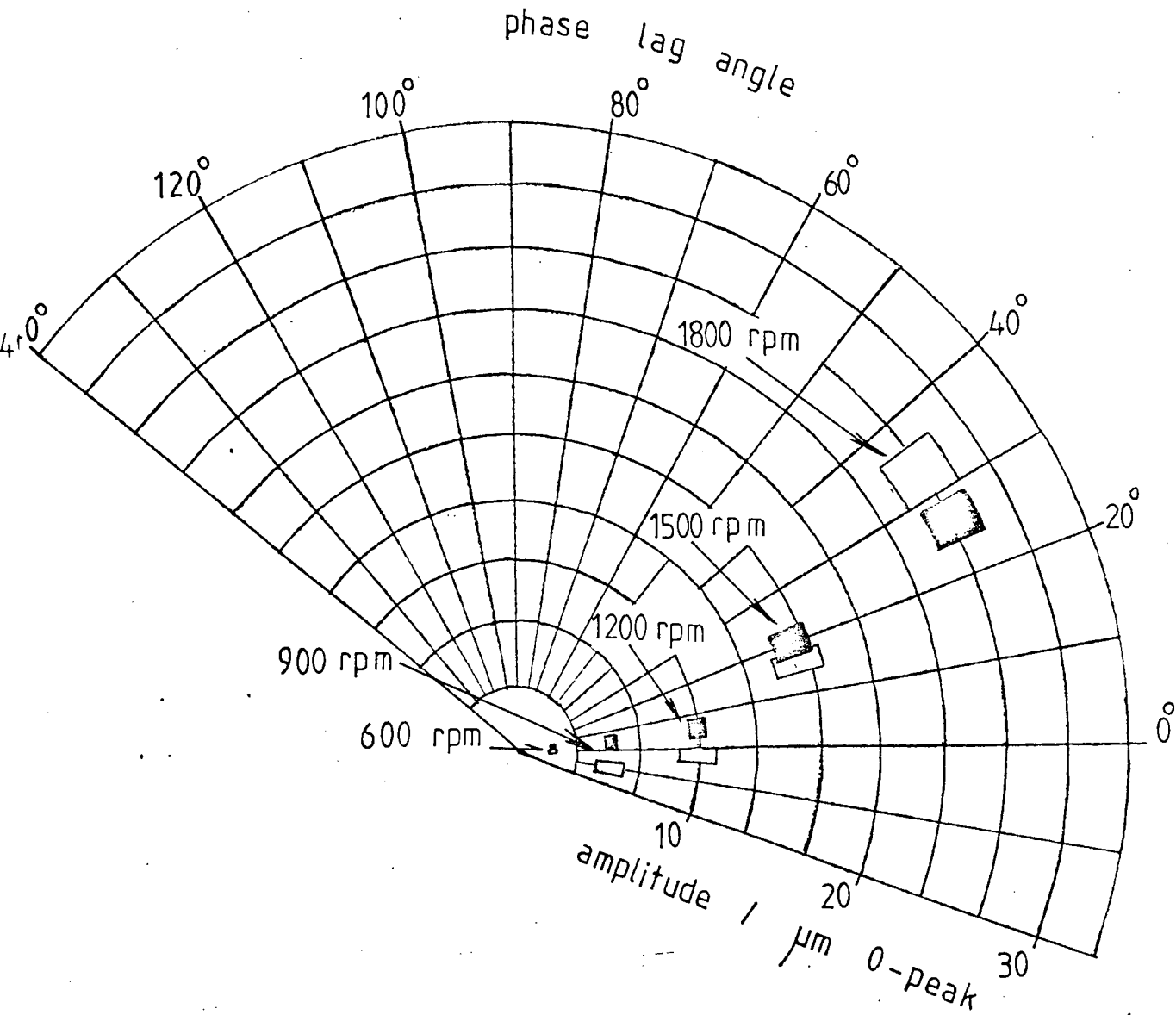


FIG 6.40 NYQUIST DIAGRAM FOR THE HYDROSTATIC BEARING WITH ACCUMULATORS, FORWARD EXCITATION



■ horizontal response  
□ vertical response

FIG 6.41 NYQUIST DIAGRAM FOR THE HYDROSTATIC BEARING WITH ACCUMULATORS, REVERSE EXCITATION

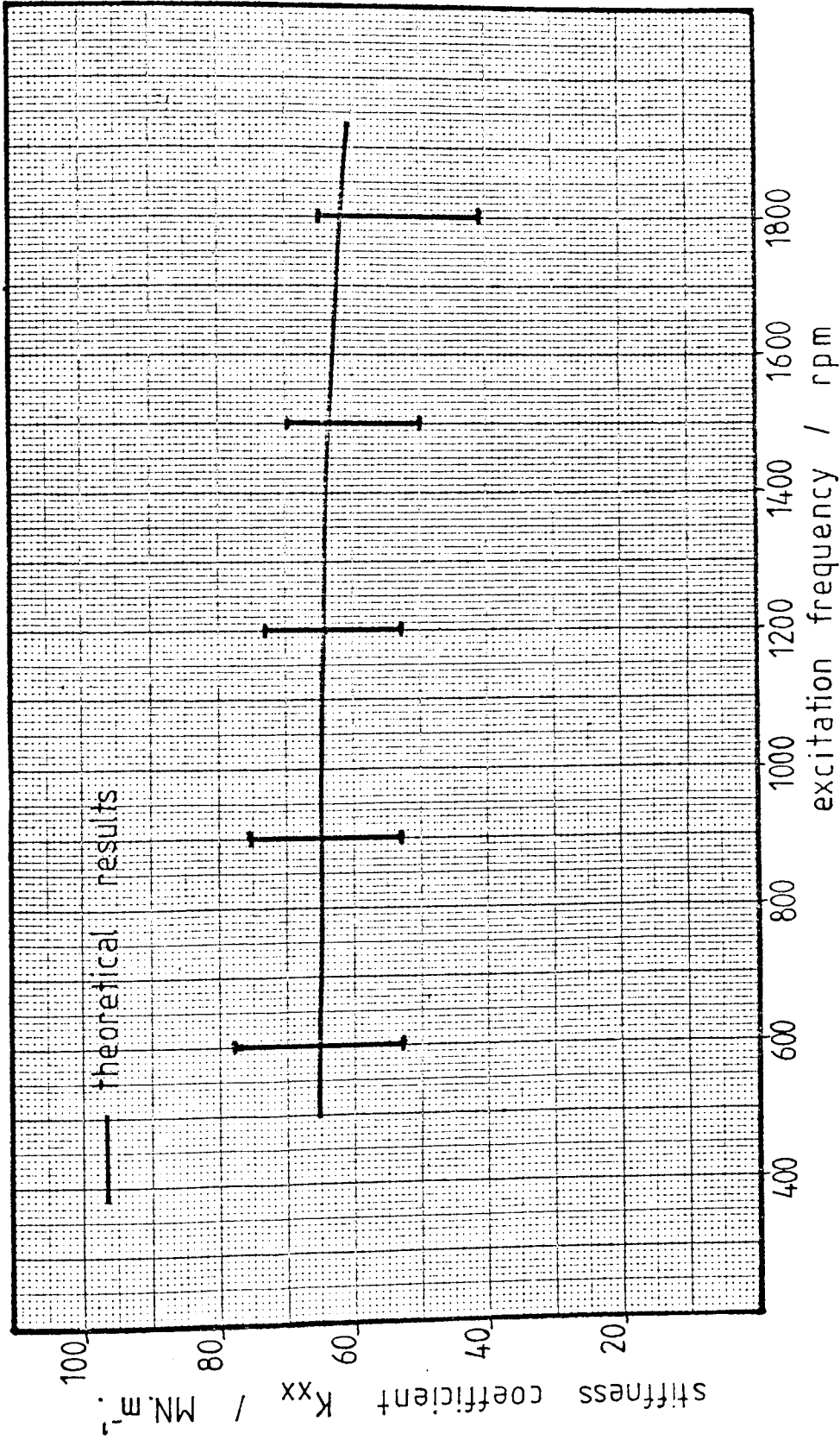


FIG 6.42 VARIATION OF HYDROSTATIC BEARING BUSH STIFFNESS COEFFICIENT  $K_{xx}$  WITH EXCITATION FREQUENCY, ( WITH ACCUMULATORS )

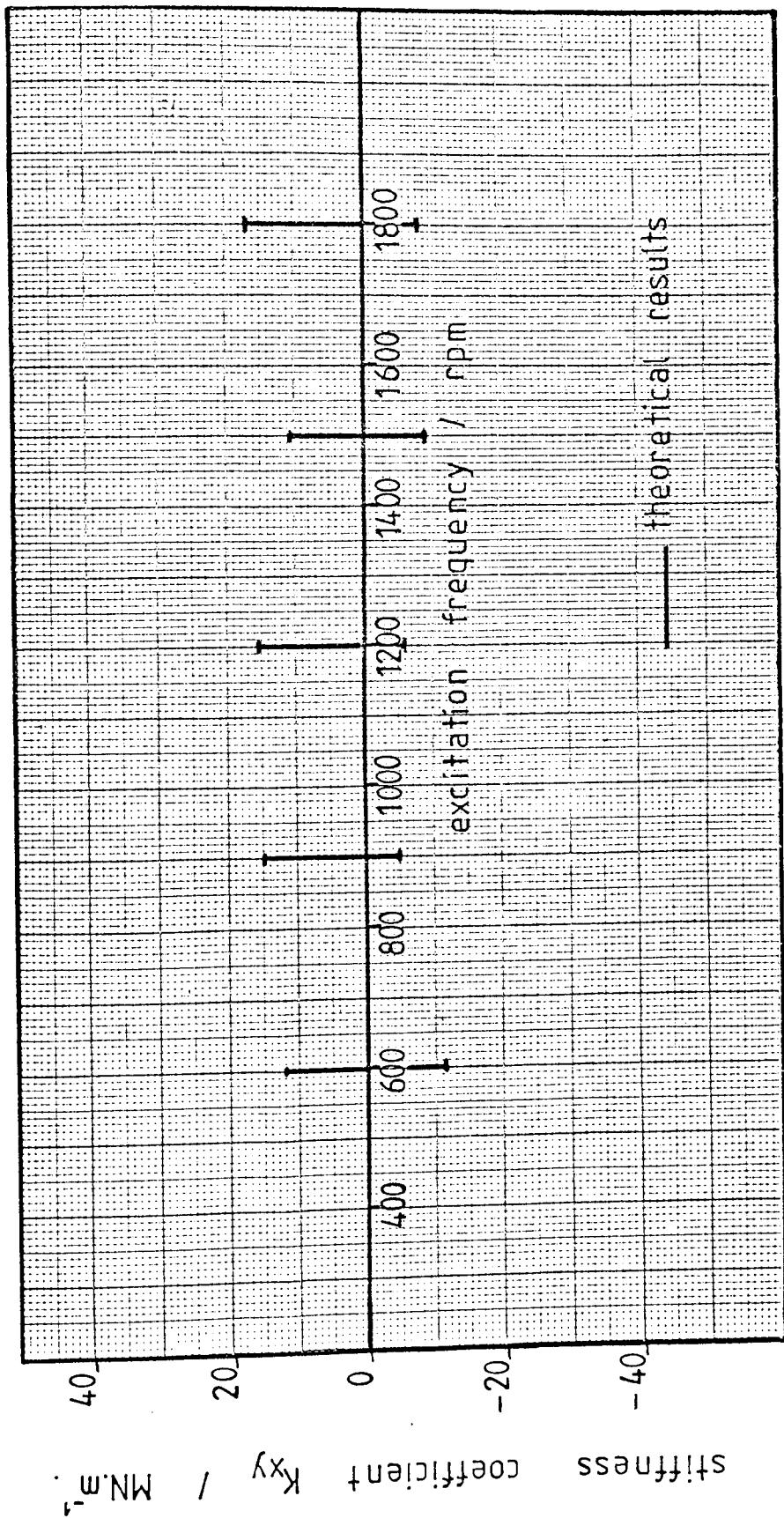


FIG 6.43 VARIATION OF HYDROSTATIC BEARING BUSH STIFFNESS COEFFICIENT  $K_{xy}$  WITH EXCITATION FREQUENCY, ( WITH ACCUMULATORS )

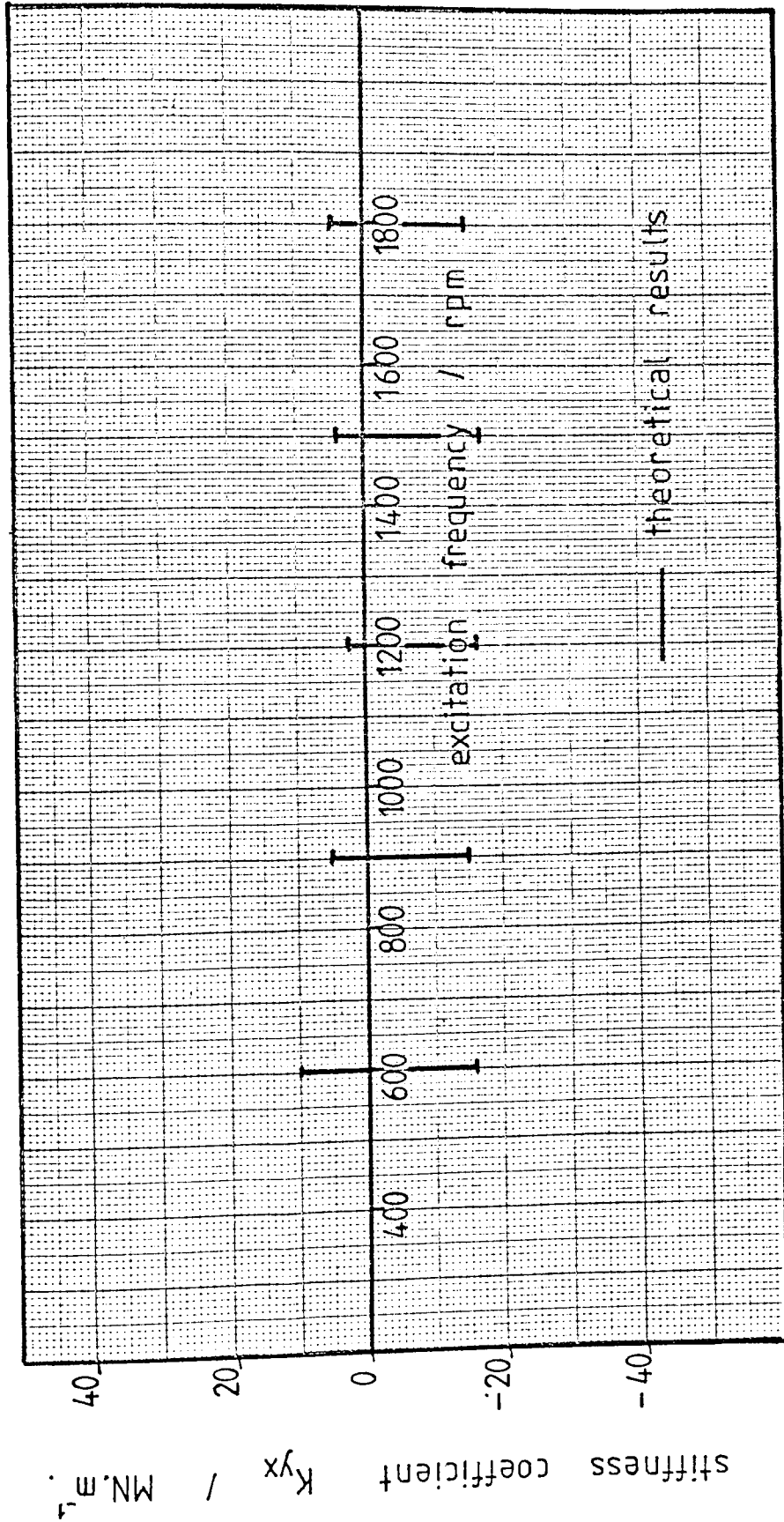


FIG 6.44 VARIATION OF HYDROSTATIC BEARING BUSH STIFFNESS COEFFICIENT  $K_{yx}$  WITH EXCITATION FREQUENCY, ( WITH ACCUMULATORS )

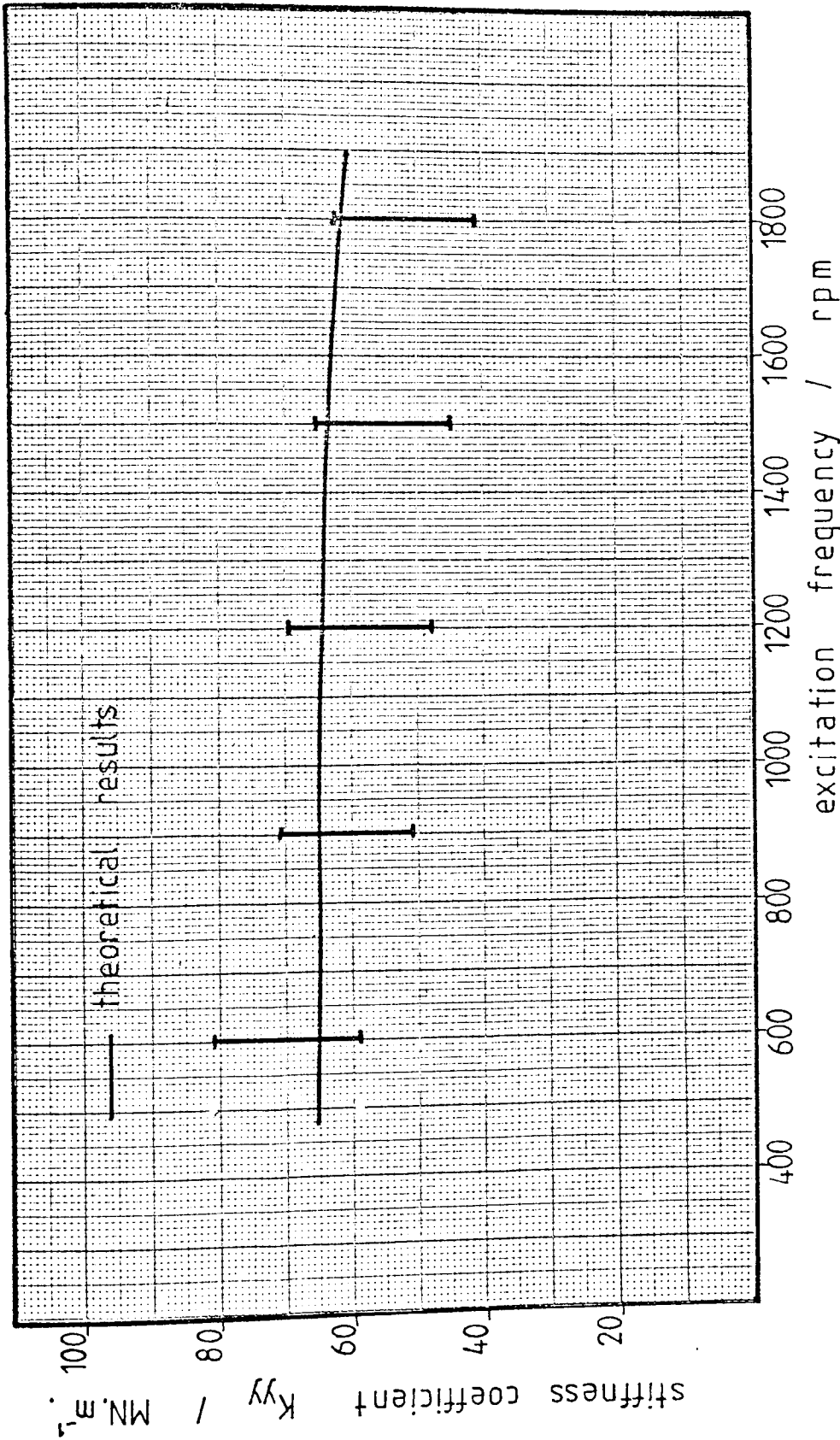


FIG 6.45 VARIATION OF HYDROSTATIC BEARING BUSH STIFFNESS COEFFICIENT  $K_{yy}$  WITH EXCITATION FREQUENCY, ( WITH ACCUMULATORS )

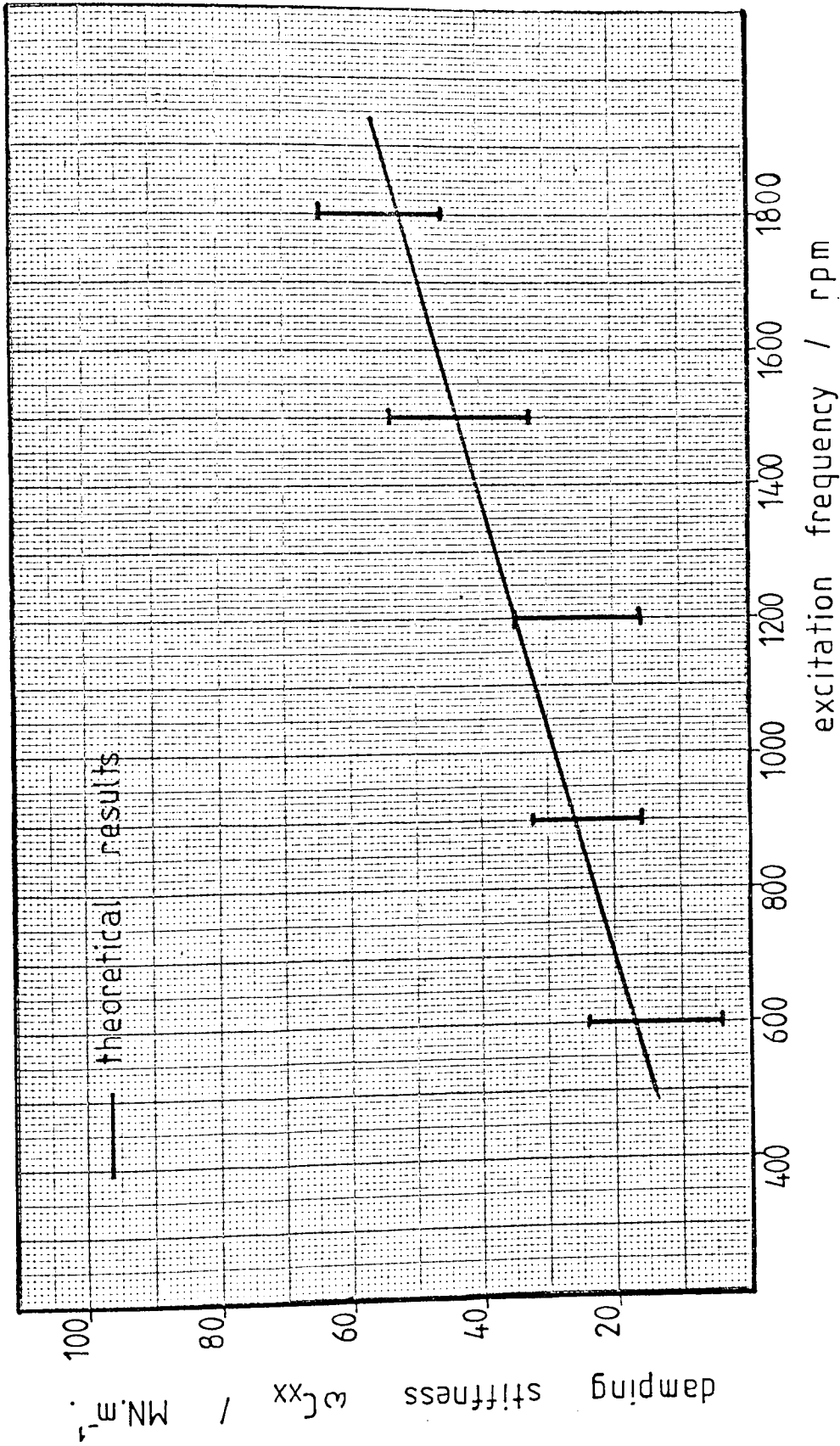


FIG 6.46 VARIATION OF HYDROSTATIC BEARING BUSH DAMPING STIFFNESS  $\omega_c^{xx}$  WITH EXCITATION FREQUENCY, ( WITH ACCUMULATORS )

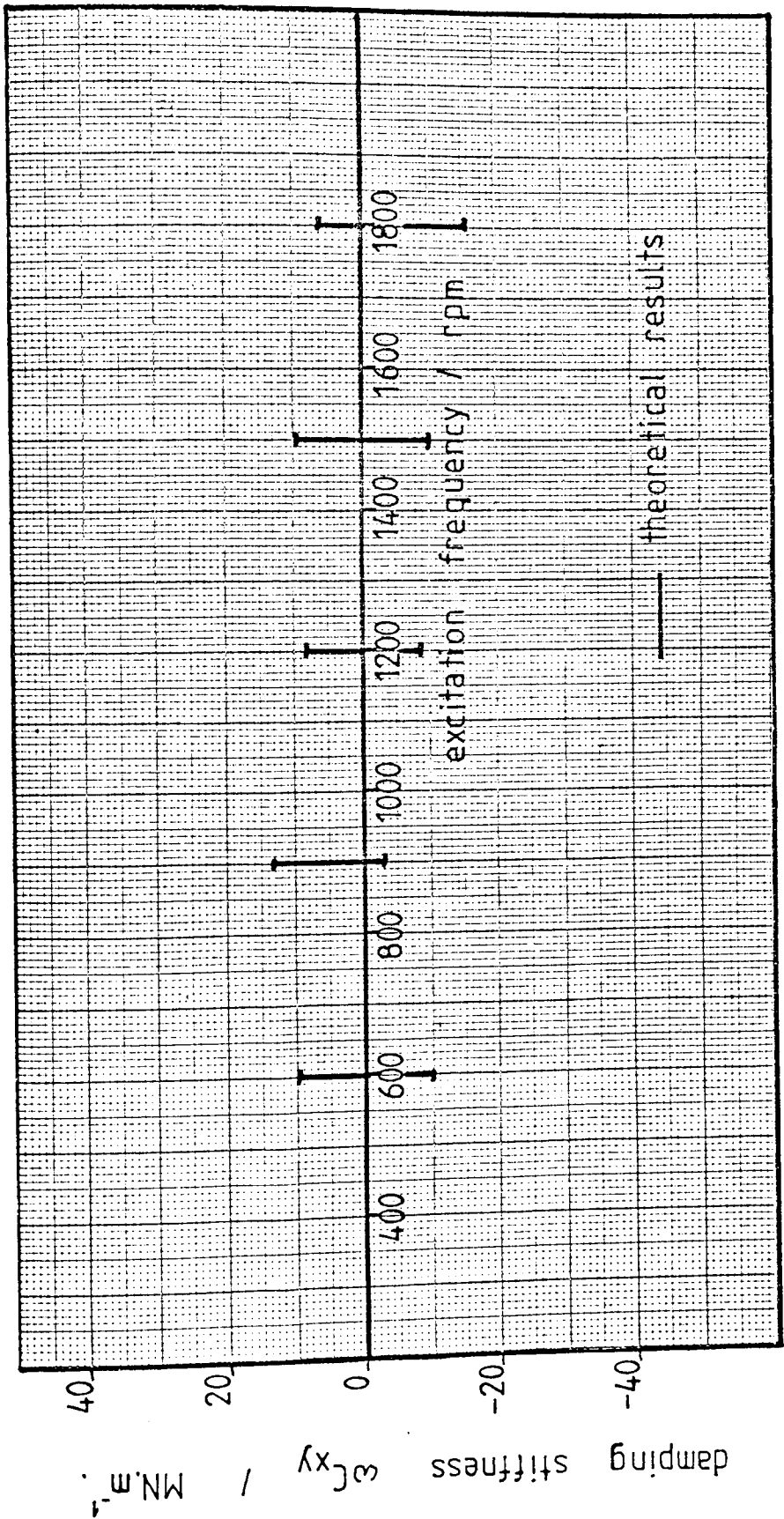


FIG 6.47 VARIATION OF HYDROSTATIC BEARING BUSH DAMPING STIFFNESS

$\omega c_{xy}$  WITH EXCITATION FREQUENCY, ( WITH ACCUMULATORS )



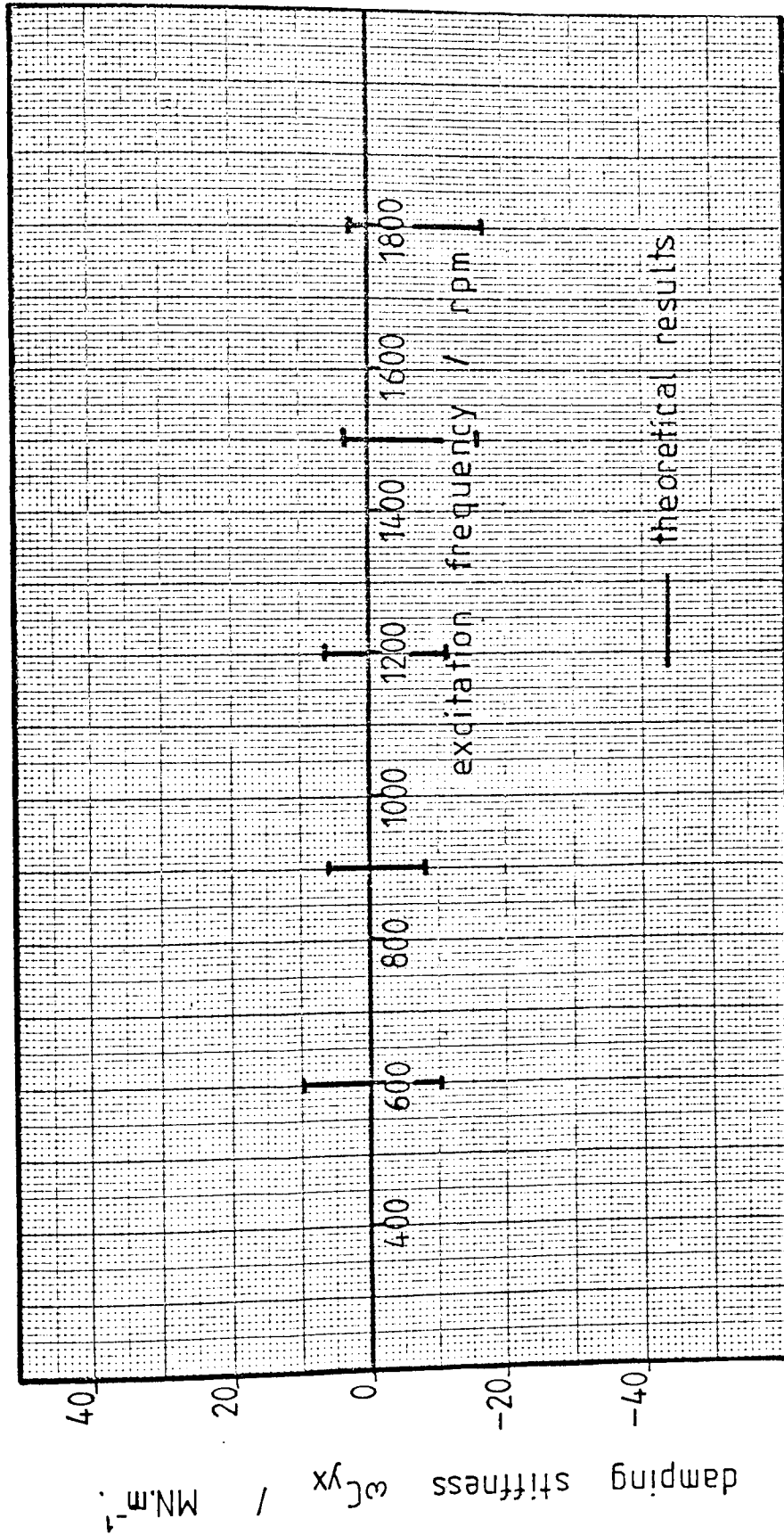


FIG 6.48 VARIATION OF HYDROSTATIC BEARING BUSH DAMPING STIFFNESS  $\omega c_{yx}$  WITH EXCITATION FREQUENCY, ( WITH ACCUMULATORS )

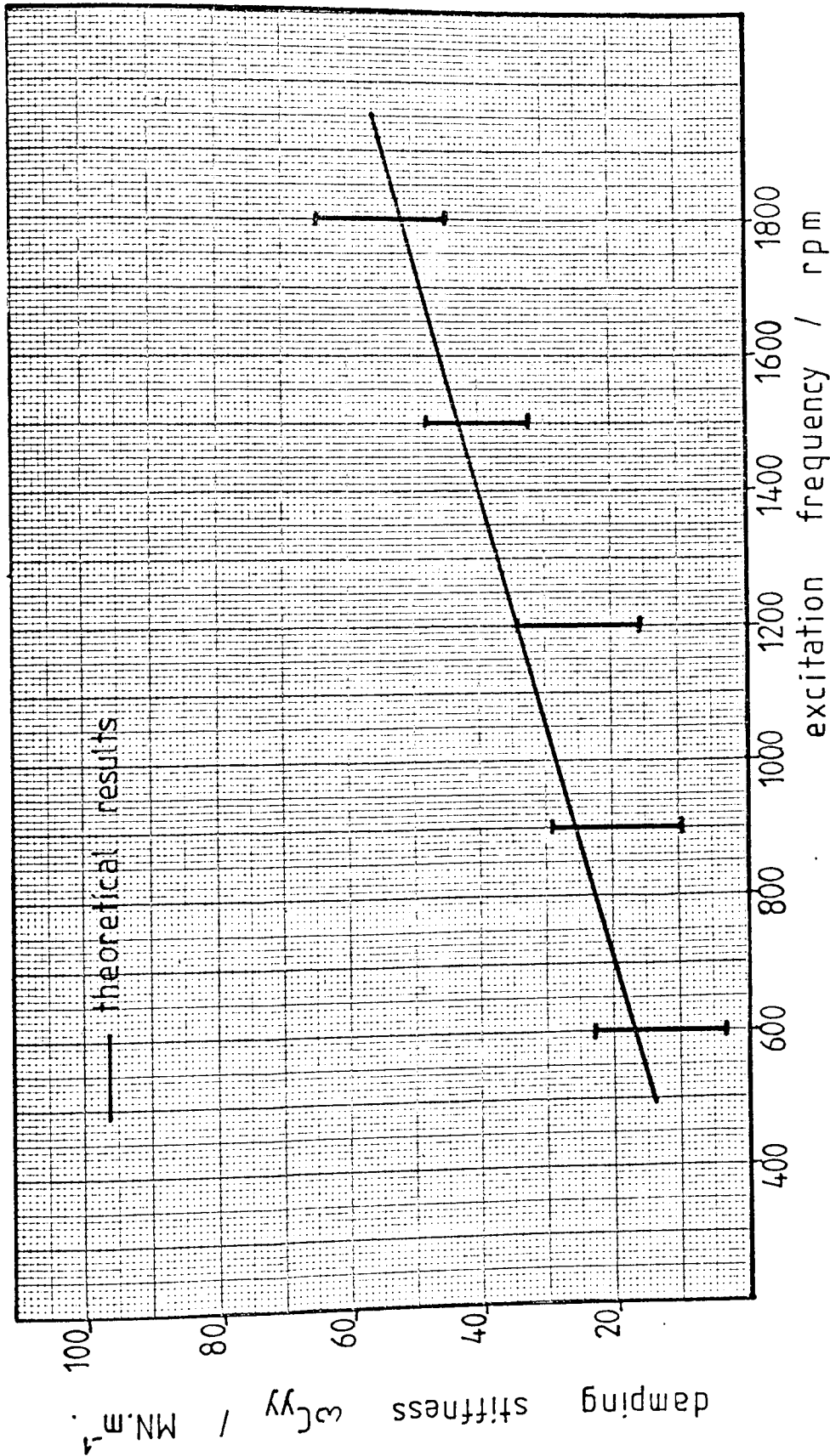


FIG 6.49 VARIATION OF HYDROSTATIC BEARING BUSH DAMPING STIFFNESS  $\omega_{c_{yy}}$  WITH EXCITATION FREQUENCY, ( WITH ACCUMULATORS )

oil-film bearings however.

## 6.6 Dynamic Oil Film Coefficients for the Combined Journal and Hydrostatic Bearing

The theoretical dynamic oil film coefficients for the 'combined' bearing were determined by using the theory in section 4.4 with the 'smoothed' measured journal bearing coefficients of figures 6.5 to 6.12 and the theoretical coefficients for the hydrostatic bearing bush with accumulators connected, figures 6.42 to 6.49. (The case without accumulators connected was not examined because it was desired that a change in overall bearing coefficients be shown, compared to the original journal bearing coefficients. Such an effect using the hydrostatic bearing without the accumulators would not have been obtained since its impedance would have been too large.)

Experimental measurement of amplitude and phase during dynamic excitation of the combined bearing system yielded those values whose means and standard deviations are shown in figures 6.50 and 6.51, for the forward and reverse directions of excitation respectively. These measurements are for excitation frequencies ranging from 400 rpm to 1500 rpm, and again for hydraulic resistance ratio  $R_s/R_a = 10$  and for accumulators whose characteristics correspond to the  $B = 0$  curves of figures 6.18 to 6.21.

Effective overall dynamic oil film coefficients computed from the above mentioned results are shown in figures 6.52 to 6.59 in the form of bars indicating the mean and estimated standard deviation for each excitation frequency examined. Again, the theoretical curves are also presented for comparison.

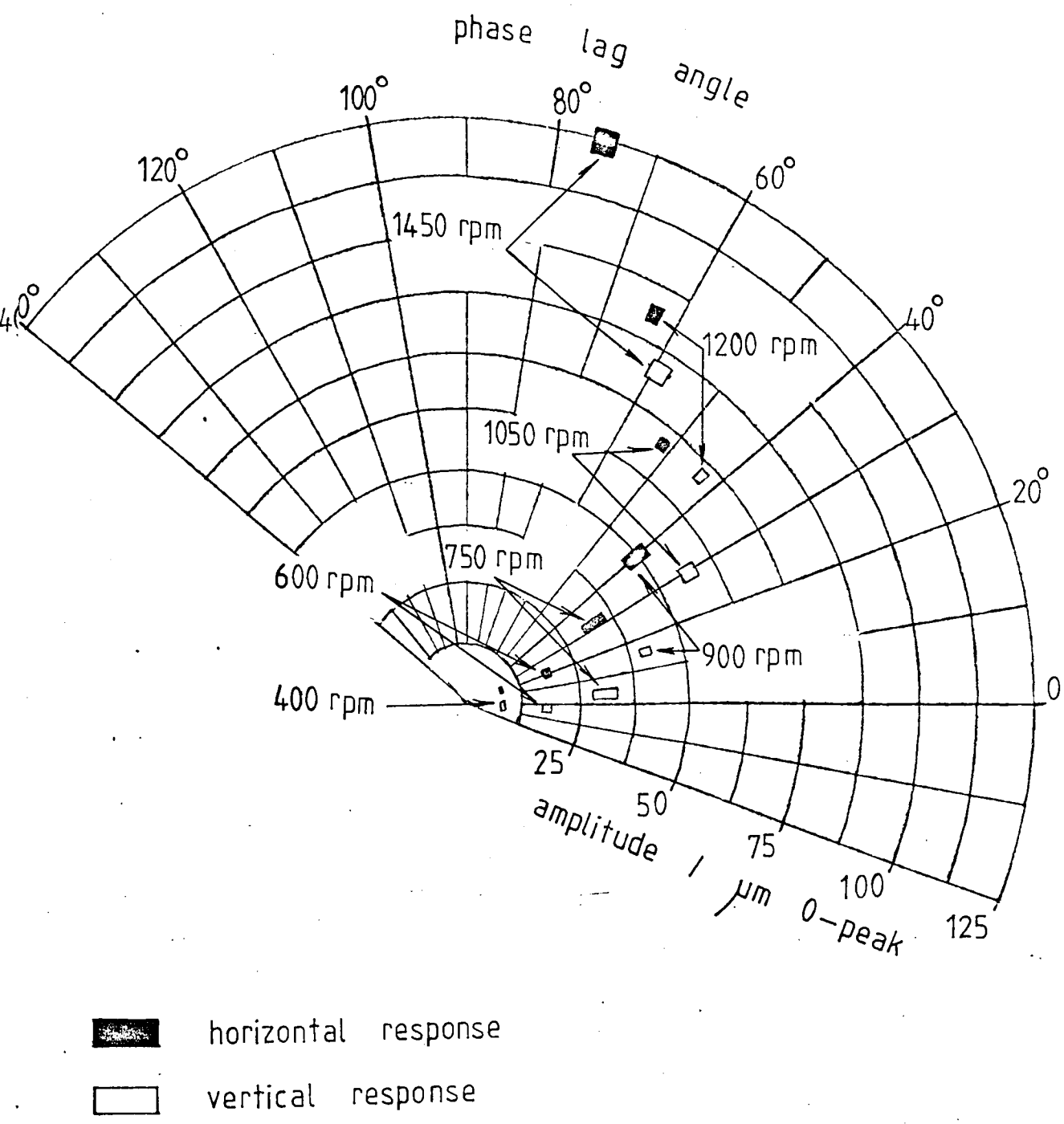
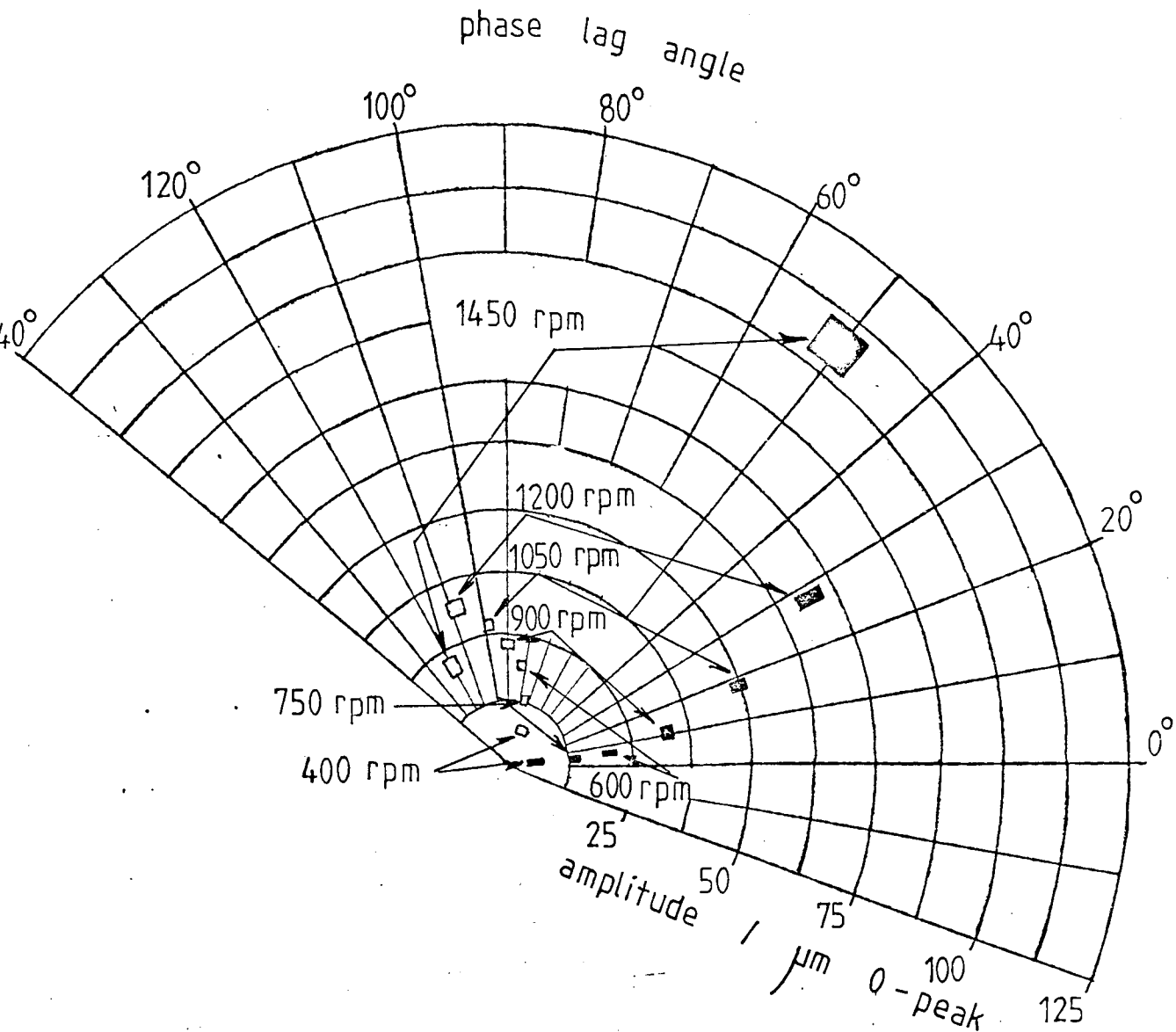


FIG 6.50 NYQUIST DIAGRAM FOR THE COMBINED BEARING, FORWARD EXCITATION




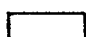
-  horizontal response
-  vertical response

FIG 6.51 NYQUIST DIAGRAM FOR THE COMBINED BEARING, REVERSE EXCITATION

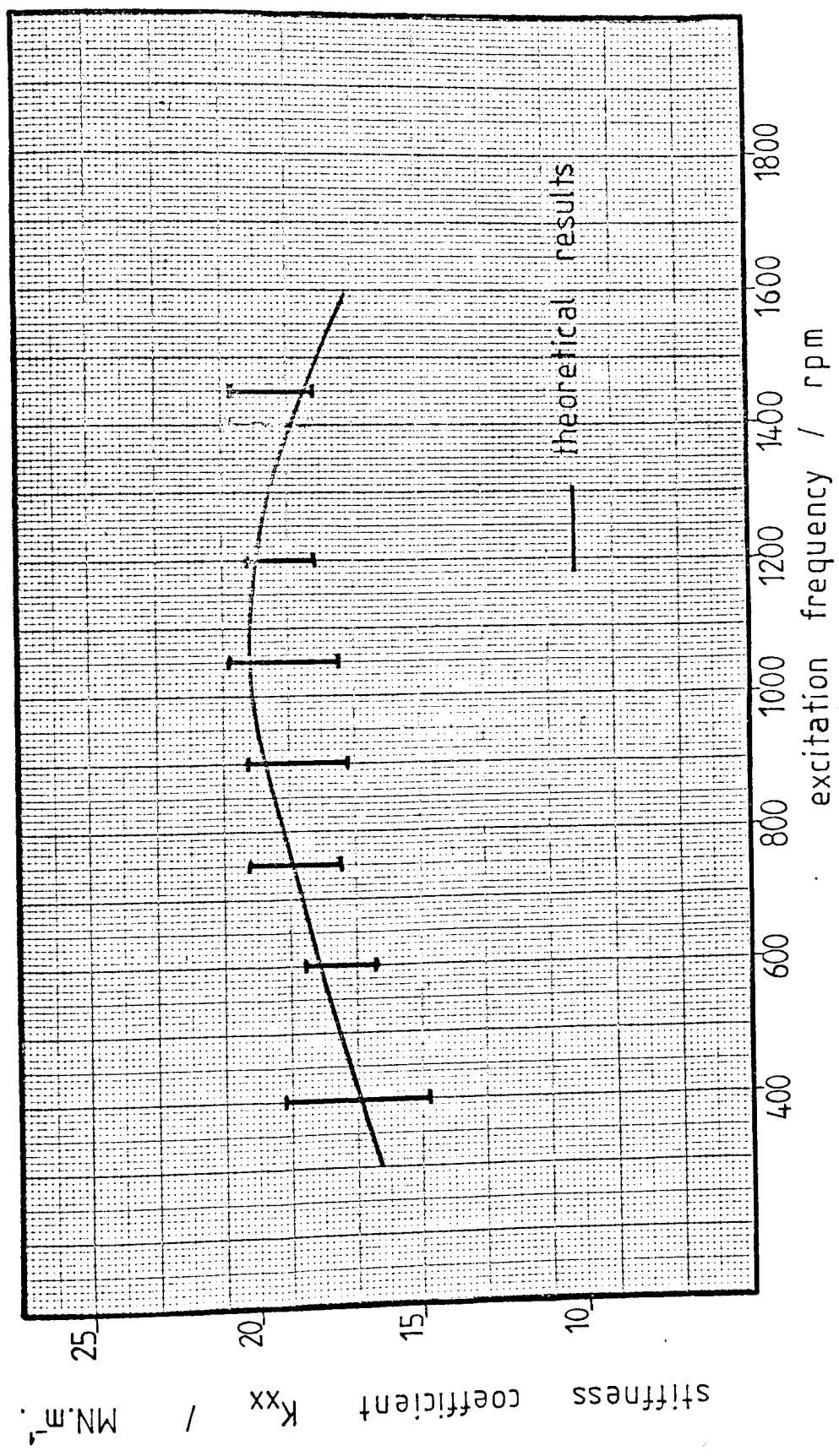


FIG 6.52 VARIATION OF COMBINED BEARING STIFFNESS COEFFICIENT  $K_{xx}$  —  
WITH EXCITATION FREQUENCY

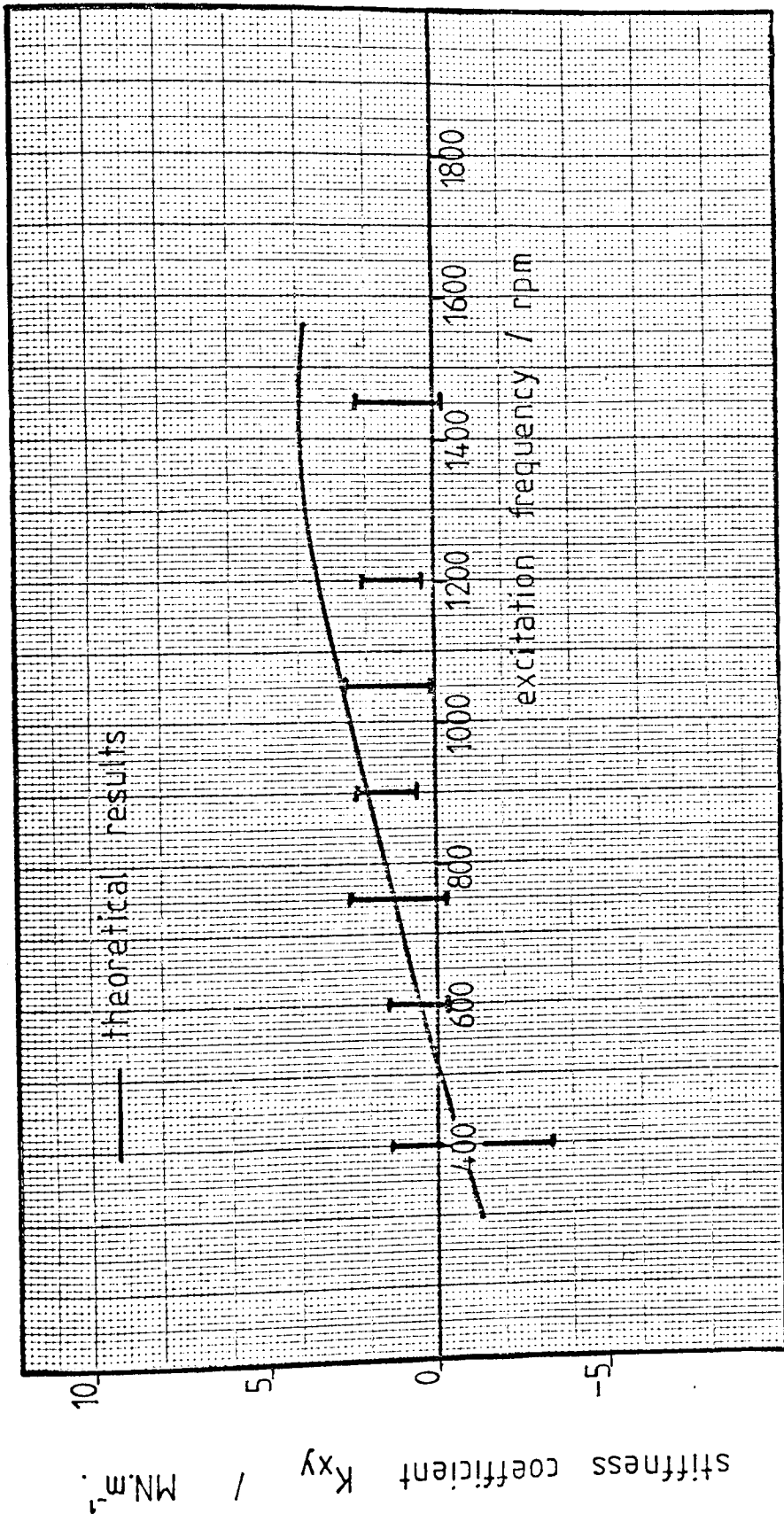


FIG 6.53 VARIATION OF COMBINED BEARING STIFFNESS COEFFICIENT  $K_{xy}$  WITH EXCITATION FREQUENCY

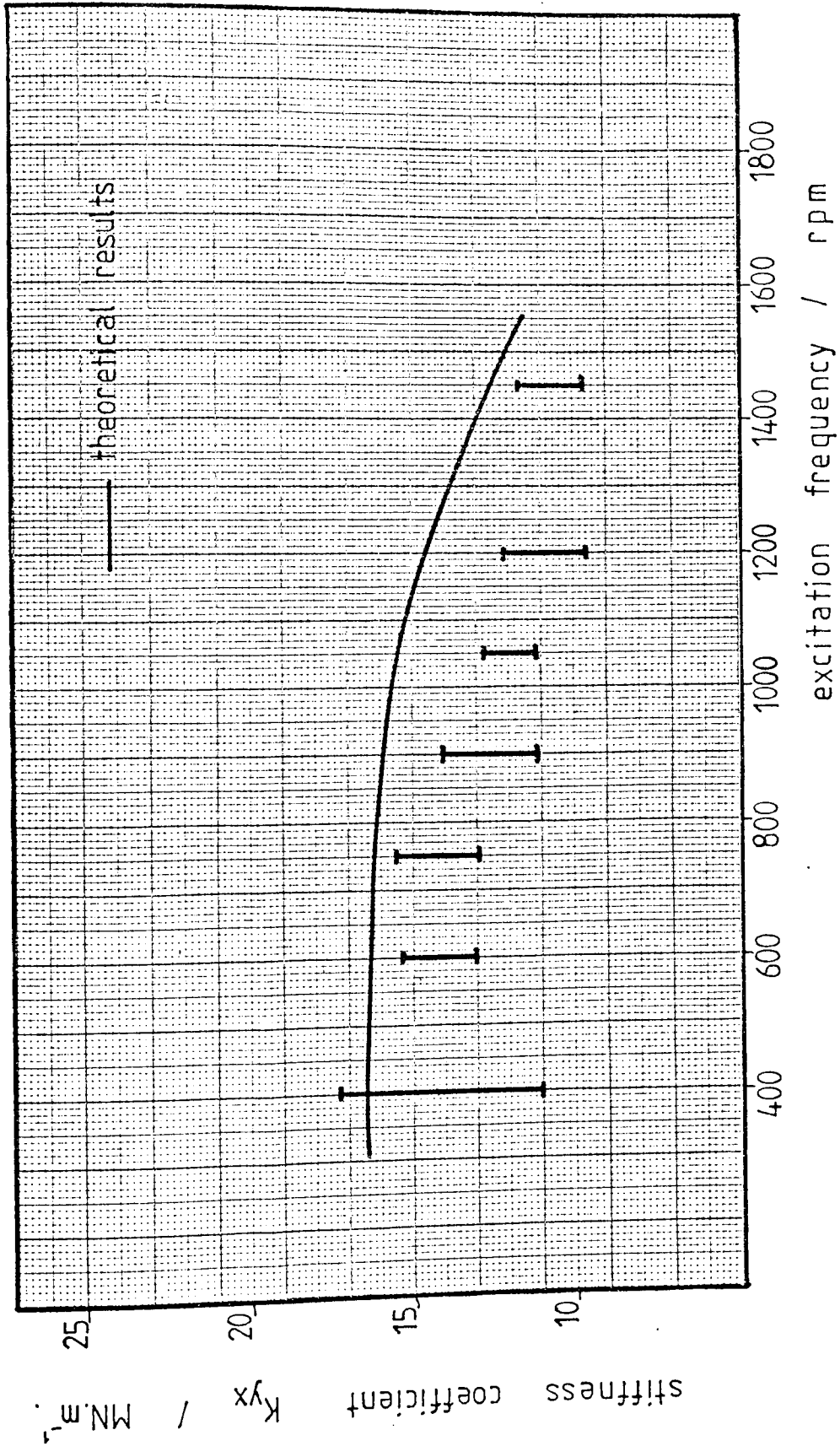


FIG 6.54 VARIATION OF COMBINED BEARING STIFFNESS COEFFICIENT  $K_{yx}$  WITH EXCITATION FREQUENCY



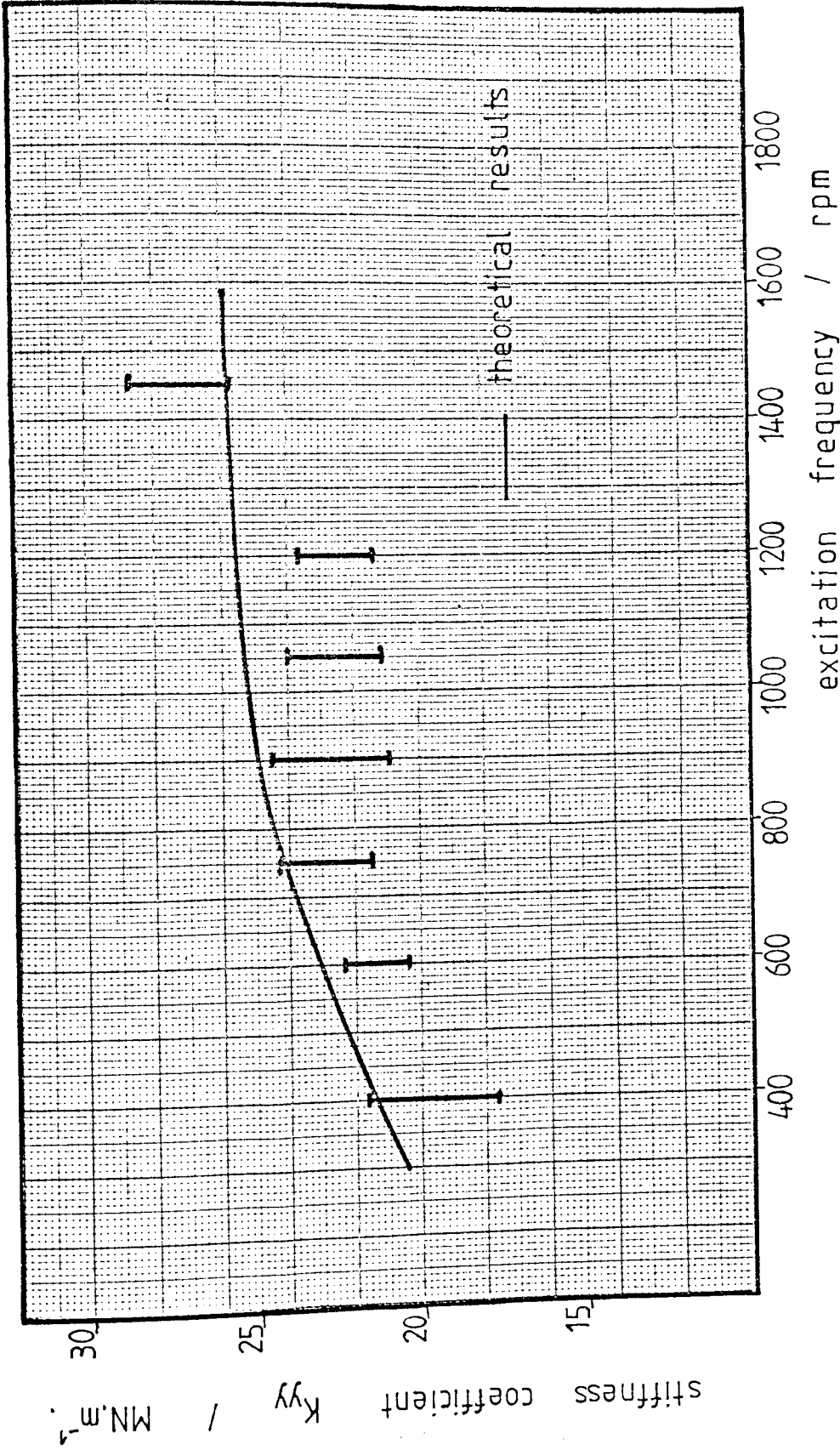


FIG 6.55 VARIATION OF COMBINED BEARING STIFFNESS COEFFICIENT  $K_{yy}$  WITH EXCITATION FREQUENCY

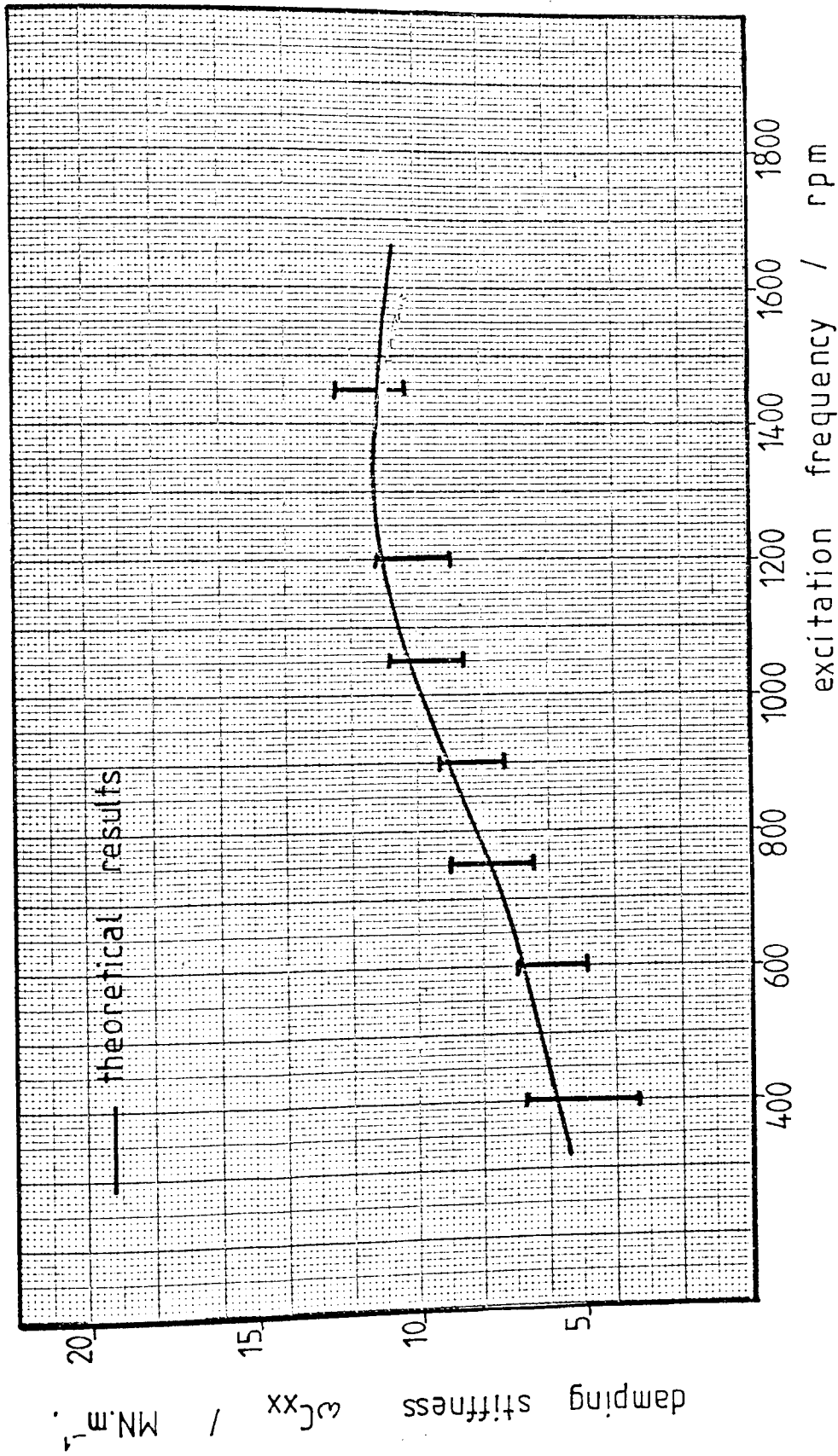


FIG 6.56 VARIATION OF COMBINED BEARING DAMPING STIFFNESS  $\omega c_{xx}$  WITH EXCITATION FREQUENCY

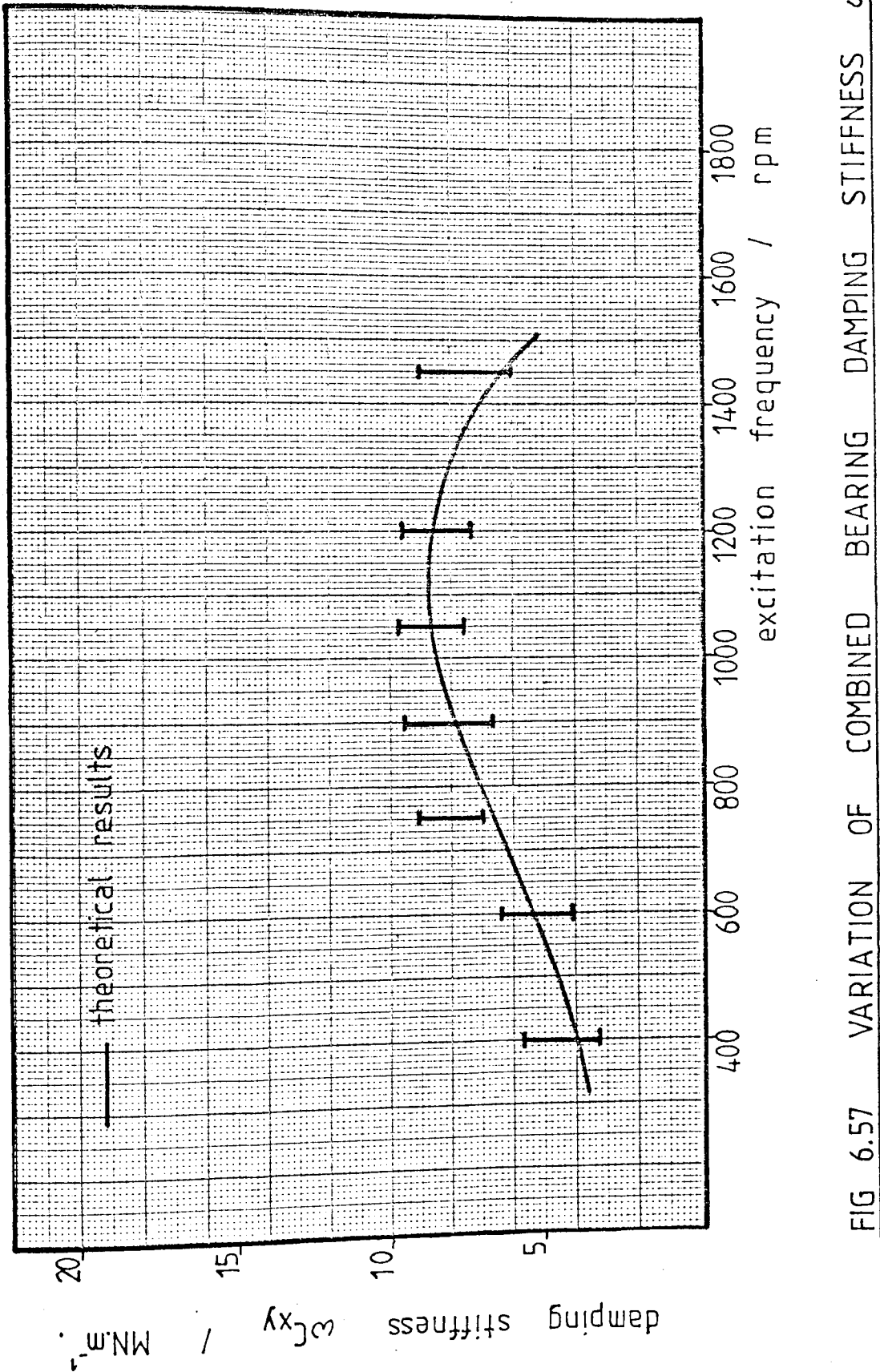


FIG 6.57 VARIATION OF COMBINED BEARING DAMPING STIFFNESS  $\omega c_{xy}$  WITH EXCITATION FREQUENCY

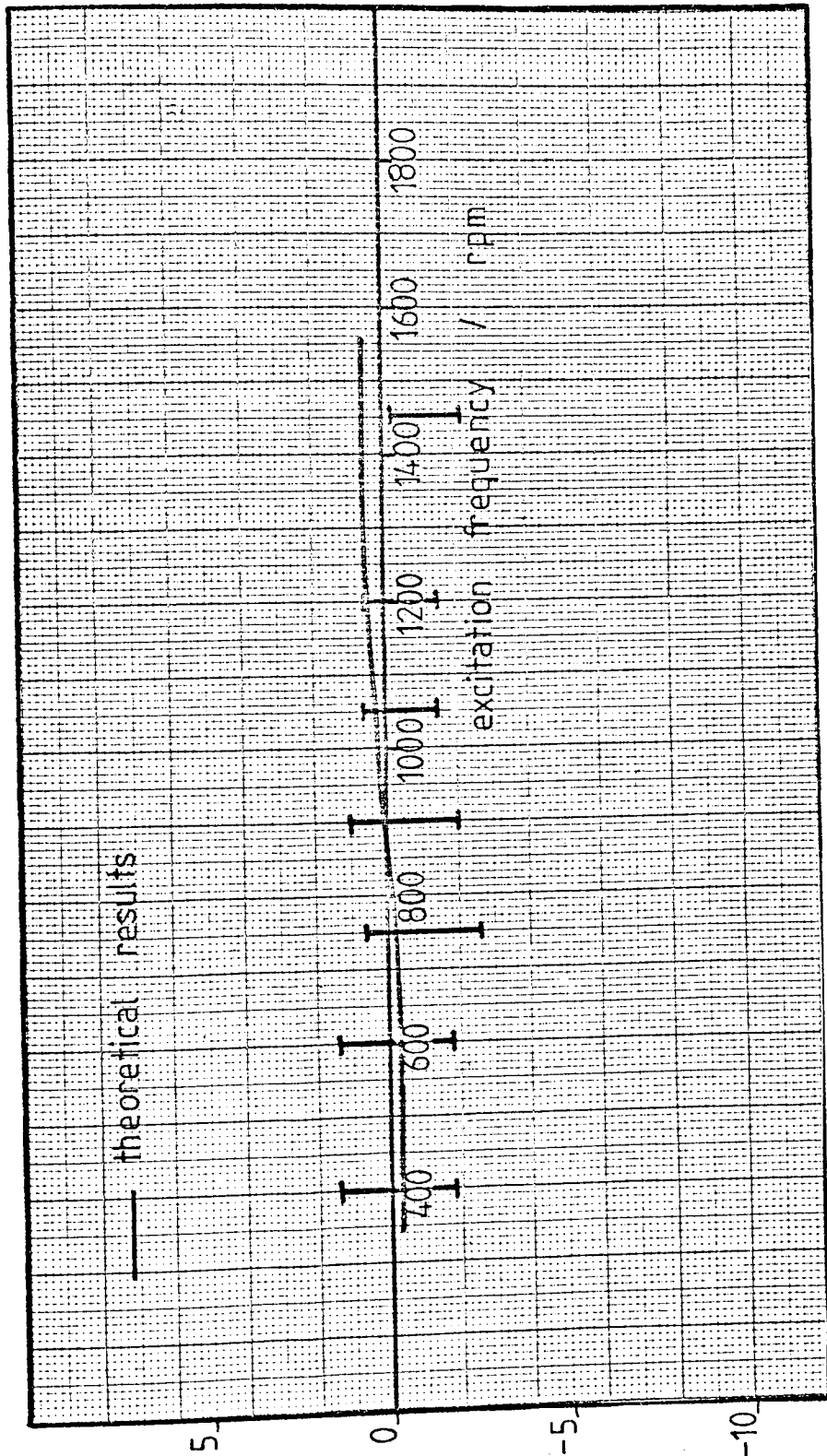


FIG 6.58 VARIATION OF COMBINED BEARING DAMPING STIFFNESS  $\omega c_{yx}$  WITH EXCITATION FREQUENCY

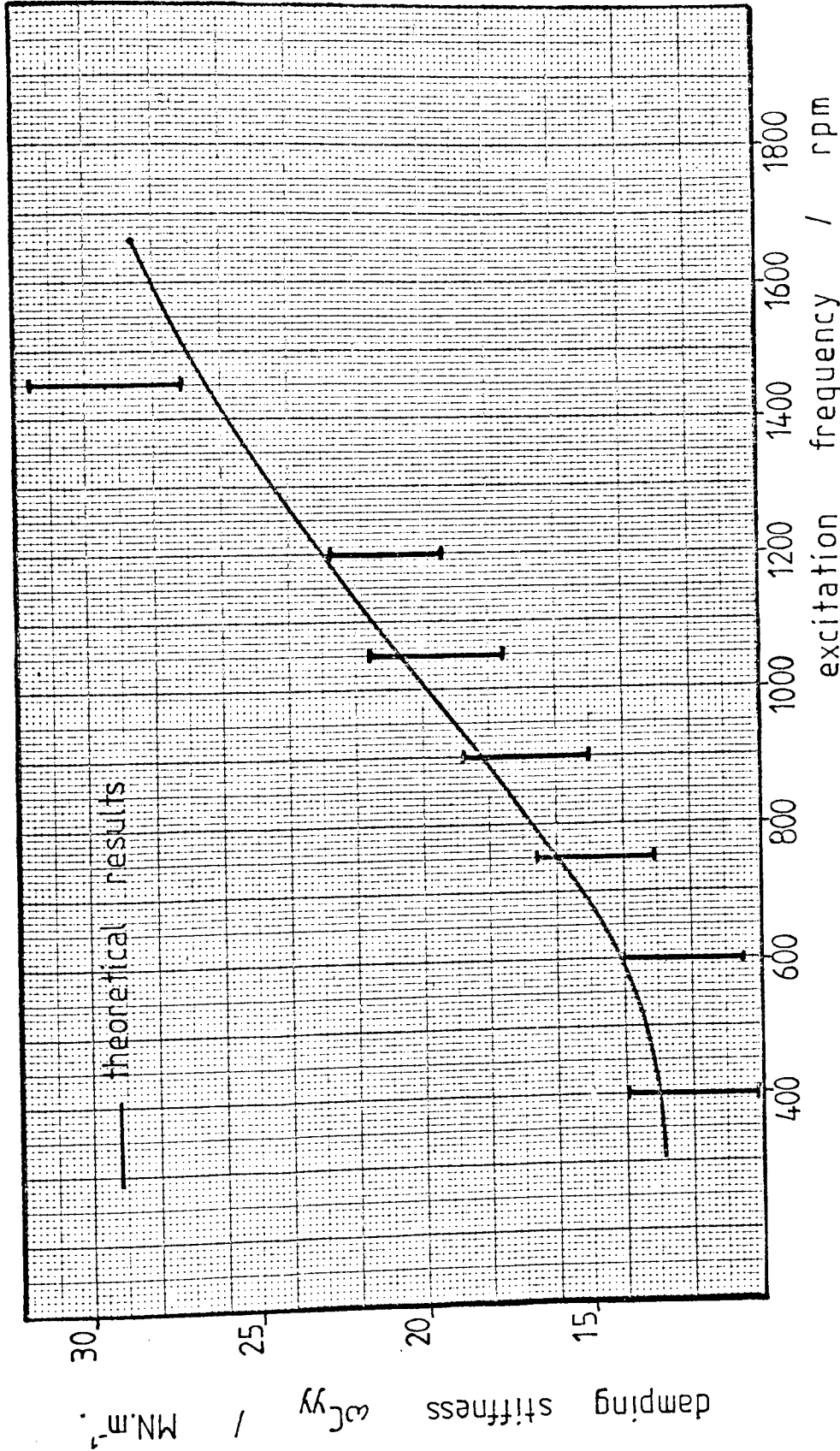


FIG 6.59 VARIATION OF COMBINED BEARING DAMPING STIFFNESS  $\omega_{yy}$  WITH EXCITATION FREQUENCY

## 6.7 Theoretical Amplitude-Frequency Response of a Typical Generator Rotor

In order to establish the influence that the use of the proposed design of combined hydrostatic and journal bearing might have on the vibration of a generator rotor a theoretical investigation of the rotor amplitude response with running speed, for a particular unbalance, was carried out. This involved the use of a computer program which is currently already used in the turbine generator industry and which had been found to give realistic results. The input data for this program consisted partly of the bearing dynamic oil film coefficients. For the rotor selected, the appropriate journal bearing coefficients were input and the rotor response noted. Dynamic oil film coefficients for a hydrostatic bearing design which might have been used for this machine were then determined, using the theory described in chapter 3 with the aid of the computer program in appendix AI, and combined with the journal bearing coefficients, using the methods described in section 4.2 with the aid of the computer program in appendix AII. The rotor response program was then re-run using the combined bearing dynamic oil film coefficients to obtain new rotor response characteristics.

The results of this investigation are summarised by figure 6.60 showing the rotor vibration amplitude at various running speeds. For this particular machine the normal running speed was 1800 rpm and it can be seen that had the rotor exhibited a critical near to this speed, then it could have been moved by using the hydrostatic bearing.

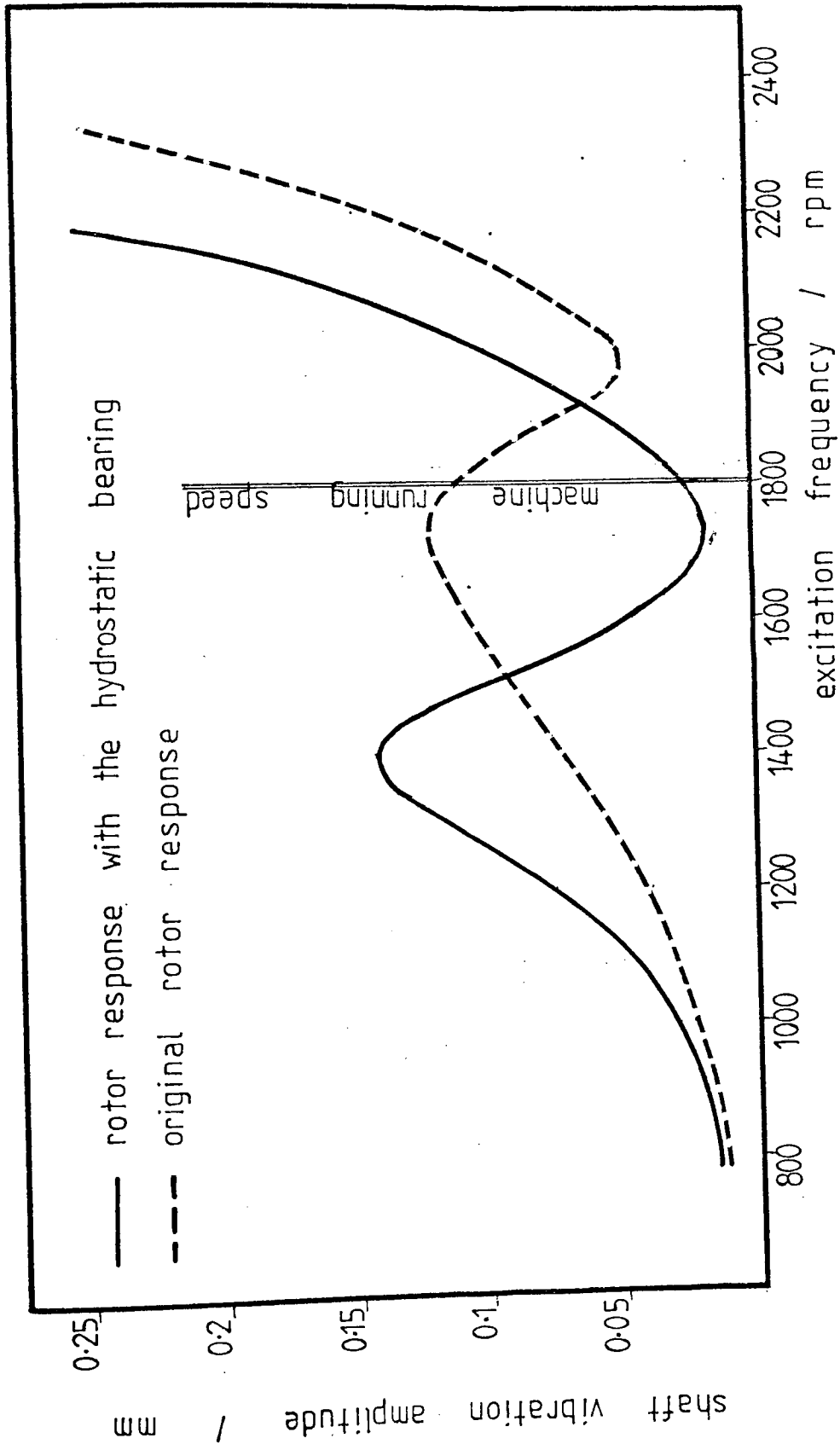


FIG 6.60 THEORETICAL EFFECT OF THE HYDROSTATIC BEARING ON THE RESPONSE OF A GENERATOR ROTOR

## CHAPTER SEVEN

### ACCURACY OF THE EXPERIMENTAL RESULTS



CHAPTER SEVEN

ACCURACY OF THE EXPERIMENTAL RESULTS

7.1 Oil Viscosity

Oil viscosity is temperature and pressure dependent. The variation with temperature for the oil used during the experiments has been examined and is contained in a report by Dwight (51). The temperature measurements of the oil were taken with thermocouples in the flow paths. Experience of using this method indicates that it is accurate to  $\pm 2$  K, using the instrumentation used in the data logging process. This results in a dynamic viscosity measurement to at least  $2.10^{-3}$  Pa s, ie  $\pm 3\%$ . Variation with pressure is insignificant for pressures below 7 MPa ( $\sim 1000$  lb f/in<sup>2</sup>), and so was ignored.

7.2 Journal Speed

This was measured using an inductive probe observing bolt heads on the extension shaft of the main rotor assembly. The signal was read visually at an analogue rpm meter and a digital reading obtained from the data logger voltmeter measuring the voltage across the rpm meter. The accuracy of the rpm meter was  $\pm 4.7\%$  and that of the voltmeter was 0.0035% and hence the logged journal speed was accurate to  $\pm 4.8\%$ .

7.3 Specific Loading

This is dependent on projected bearing area and on the applied static load on the bearing. The bearing area is known almost exactly from the engineering drawings produced during its design. The applied static load is measured using load cells which were specified by the manufacturers as being accurate to  $\pm 0.4\%$  of full scale reading. This meant that ultimately the specific loading examined could be measured to  $\pm 1\%$ .

#### 7.4 Bearing Clearances

Bearing clearances were measured on assembly using proximity probes, to an estimated accuracy of  $\pm 2\%$ . The other potential source of error here is bearing bush elastic or thermal distortion. Work by Dawson, Hudson, Hunter and March (52) and by Hooke, Brighton and O'Donoghue (52) has shown that these effects are insignificant as far as journal bearing operation is concerned. Since the hydrostatic bearing is similar in structure it was assumed that the same conclusions were applicable for it.

Note that for the hydrostatic bearing, the mean effective clearance can be deduced from a measurement of the hydrostatic pocket pressure, and a knowledge of the value of the magnitude of the oil flow out of the pocket. This served to confirm the measured value of clearance.

#### 7.5 Sommerfeld Number

Sommerfeld number is defined as

$$S = \frac{\mu N}{p'} \left(\frac{r}{c}\right)^2$$

where  $\mu$  is the oil dynamic viscosity,  $N$  the journal frequency of rotation,  $p'$  the specific loading on the bearing,  $r$  the journal radius and  $c$  the bearing radial clearance. Using the accuracies determined in sections 7.1 to 7.4 it can be established that Sommerfeld Number may be determined to an accuracy of 15.5%. Such a variation of Sommerfeld Number is likely to affect the journal bearing eccentricity ratio by only 2% of the radial clearance. It may thus be concluded that the effect on journal bearing performance would be negligible.

#### 7.6 Excitation Frequency

The speed of the excitation shaft was measured with an inductive proximity probe observing a bolt head on the shaft. The signal obtained

was fed to an rpm meter giving an analogue indication of speed whilst a parallel connection to the frequency response analyser enabled frequency measurement to  $\pm 1$  rpm. Some instability of the speed of the drive motor meant that the excitation frequency could be guaranteed to only  $\pm 15$  rpm however, for the time interval containing one set of vibration measurements. This is still to 3.8% of the lowest excitation frequency used however (400 rpm).

### 7.7 Excitation Force

This was determined by the amount of out of balance of the excitation shaft and by its speed of rotation. The unbalance moment was calculated, using component dimensions, to an estimated accuracy of 0.5%. For a measurement of shaft speed to 15 rpm, this means that the applied force was known to  $\pm 8.3\%$  for the lowest excitation frequency (400 rpm) and to  $\pm 2\%$  for the highest excitation frequency (2100 rpm).

### 7.8 Sensitivity of the Displacement Transducers

These were calibrated statically and dynamically (see section 6.9) by measuring movement of the target material with a micrometer and measuring the probe output voltage with a digital voltmeter. The micrometer could be read to  $\pm 3 \mu\text{m}$  and the voltmeter was accurate to 1 mV.

Typically, a movement of the target material by 250  $\mu\text{m}$  changed the millivoltmeter reading by 215 mV. This meant that sensitivity could be measured to 1.7%.

Zero drift and change of sensitivity with ambient temperature were assumed to be insignificantly small for the working range. This assumption was based on experience gained with similar transducers prior to the work described in this thesis.

Linearity of each transducer was noted during the calibration procedure and was found to be to  $\pm 5\%$  over the working range, in the worst instance.

## 7.9 Phase Measurement

The specification of the frequency response analyser used to measure phase stated an accuracy of  $\pm 1^\circ$ . The analyser was normally used to measure signals of larger amplitude than were encountered during the work described in this thesis however, and it was estimated that the real accuracy of phase measurements during testing, because of the small signals encountered, was closer to  $\pm 5^\circ$ , indeed it can be seen from the polar plots of measured amplitude and phase in chapter 6 that the standard deviation of phase measurements is significantly greater at low excitation frequencies when the measured vibration amplitude is low. Phase measurement was referenced to a signal pulse corresponding to the passing of the inductive proximity probe by a bolt head on the excitation shaft. An allowance had to be made for the fact that the signal pulse began at some time before the centre of the bolt head coincided with the centre of the probe. It was estimated that the value required to allow for this could be measured, using an oscilloscope to display the signal, to an accuracy of  $\pm 4^\circ$ , so that the nett accuracy of phase measurements was to  $\pm 9^\circ$ .

## 7.10 Pedestal Vibration Measurements

Each velocity probe installed on the test rig to measure pedestal vibration in space, was calibrated beforehand over the working frequency range. It was found that each probe had a natural frequency that affected the probe output signal amplitude, for a considerable part of the frequency range, with a corresponding highly non-linear output with variation in frequency for a given vibration amplitude. (The vibration amplitude was measured with an inductive proximity probe of known sensitivity.) In an attempt to combat the non-linearity bearing testing was conducted at several specific excitation frequencies and

and for each frequency a different copy of probe sensitivities was loaded into the data logger.

Pedestal vibration measurement was further complicated by the fact that velocity probes mounted on the same surface of the pedestal but at different axial positions were found to indicate different pedestal amplitudes and phases. In these instances, mean vector readings were used to determine bearing coefficients.

The net error in pedestal vibration was judged to be of the order of  $\pm 10\%$  for amplitude and 20 percent for phase in the worst instances. effect of these inaccuracies on the measurement of the bearing coefficients was not found to be significant however.

#### 7.11 Measured Oil Film Force Coefficients

The most significant measured variables as far as the determination of the oil film force coefficients is concerned are dynamic force magnitude, vibration amplitude, excitation frequency and phase lag angle. The accuracies to which these values are known has been discussed in the previous sections of this chapter and their effect on the measured oil film force coefficients was determined by using some typical test result data to determine oil film coefficients using the computer program in appendix AIV, and then re-running the program with the appropriate percentage changes in the measured variables. The original data was selected to give the largest change in the measured coefficients, ie the worst possible instance. This was with low frequencies when the original phase lag angle is small, such that any change of phase angle would represent the maximum change of out of phase stiffness.

By using the computer program in this way, to determine the accuracy of the measured oil film force coefficients it was possible to take into account the effects of cross-coupling and errors of pedestal vibration

measurements. It was concluded that any particular stiffness could be measured to within 18% of the net oil film dynamic stiffness in the worst instance. Although this value would appear to be large, it will be remembered that the chances of repeatedly measuring the appropriate variables as inaccurately as possible would be remote, and that the mean measured values of the oil film force coefficients are likely to be much closer to the actual values.

CHAPTER EIGHT

DISCUSSION OF THE THEORETICAL AND EXPERIMENTAL RESULTS

CHAPTER EIGHT

DISCUSSION OF THE THEORETICAL AND EXPERIMENTAL RESULTS

8.1 Static Characteristics of the Journal Bearing

The only static characteristic of the journal bearing that has been investigated is the locus of the shaft centre for variation of Sommerfeld number. This was noted and compared with the theoretical prediction and found to give extremely good correlation, see figures 6.1 and 6.2. In figure 6.2, point A represents the centre of the test journal at zero speed, and point B the same centre for operation at very high speed with negligible static load (a condition which few bearings ever operate under). The locus of the shaft centre is an arc of the shape shown in figure 6.2. For any particular operating conditions the eccentricity ratio and attitude angle are determined by the dimensionless group  $\mu N/p'$ . For  $\mu$  and N large or for  $p'$  very small the eccentricity ratio would tend towards zero. For very small values of the group  $\mu N/p'$  however, the eccentricity ratio would be very large and metal to metal contact would occur under extreme conditions.

The correlation between experiment and theory obtained was taken to be an indication that the journal bearing was operating normally. It was assumed that had there been any significant malfunction, eg misalignment or film cavitation, then this would have manifested itself, to some extent, in a departure of the experimental shaft locus from the well established theoretical shaft locus (references (6), (7), (9) and (10) being some of the authors that have investigated the steady state shaft locus of journal bearings).

This investigation also served to confirm the bearing clearances that had been measured on assembly (since a different locus would have been obtained for a different bearing clearance) and, more importantly, the



steady-state minimum oil film clearance that would exist during dynamic testing (once a particular Sommerfeld number had been selected under which dynamic testing was to be carried out). The latter was particularly important since it helped to establish a safe limit that could be imposed on the maximum vibration amplitudes that could be endured without risking surface to surface contact in the journal bearing bush. The position C on the curve of figure 6.2 represents the operating position at which the dynamic testing on the bearing was carried out.

Knowledge of the journal bearing static characteristics was also necessary in order to predict the static characteristics of the combined hydrostatic and journal bearings. Although the relationship between the two is a straightforward addition of the displacements apparent in the journal and hydrostatic bearings, it was desired that this be confirmed.

### 8.2 Dynamic Oil Film Coefficients for the Journal Bearing

The dynamic oil film coefficients for the journal bearing were required in order to determine the theoretical dynamic oil film coefficients for the combined hydrostatic and journal bearing. They were to be used, then, to demonstrate the accuracy of the theoretical approach to predicting the dynamic behaviour of the combined bearing. The measured bearing coefficients were accepted at their face value (except for the 'smoothed' curves drawn through the plotted points of figures 6.5 to 6.12) without being compared to theoretical predictions. Theory suitable for predicting journal bearing dynamic oil film coefficients is already well developed, for example references (6), (7) and (9) and the author therefore considers that its further development does not constitute a necessary part of the work described in this thesis.

Note that the journal bearing coefficients as measured are effective for

the particular bearing arrangement of the test rig, and for the particular vibration amplitudes and frequencies examined and would probably not agree exactly with those predicted by linear theory. This is because by representing the journal bearing oil film by eight coefficients the assumption has been made that a linear dependence on frequency and amplitude is the case (this, of course, is true in the limit of very small amplitudes but for larger amplitudes the oil film is non-linear). Indeed, the apparent variation of the bearing coefficients with frequency, as measured, may well be symptomatic of the non-linearity. Note also that in the analytical model discussed in section 4.2, the oil film was given zero mass and to this end the bearing dynamic oil film coefficients as measured ignore the fact that oil does have mass. It may also be, then, that some of the variation of the oil coefficients as measured, is in fact attributable to the oil film inertia and not entirely to oil film non-linearity. The oil film inertia would become more significant at higher excitation frequencies since it would have to vibrate faster and would therefore require larger accelerating forces.

### 8.3 Static Characteristics of the Hydrostatic Bearing

Theoretical results for the test hydrostatic bearing bush were obtained from a computer program which was based on the theory described in sections 3.1 to 3.3. This section discusses the static characteristics of the hydrostatic bearing bush and their implications as far as the design of the bush is concerned.

The theoretical static characteristics of the hydrostatic bearing bush are shown in figures 6.13, 6.15 and 6.17. Under most operating conditions the floating ring will have zero horizontal displacement and hence only theoretical results for that case are discussed below. Because of the symmetry of the bearing these results are the same as those for zero

vertical displacement. Figure 6.13 shows the variation of vertical displacement of the floating ring relative to the hydrostatic bush with applied vertical load, for various values of operating parameter  $\beta$  ( $\beta$  being common for all hydrostatic bearing pads in the bush, for this particular case). For the zero displacement position the supported load is zero, whatever the value of  $\beta$ . Away from the zero displacement position, however, the loads for different  $\beta$  values rise with different gradients to different maximum values. Note that for low values of  $\beta$  the maximum load supported (at the maximum displacement) takes a higher value than for high  $\beta$  values. This is because, at the maximum displacement, downwards for example, the bottom hydrostatic bearing pad will have a film clearance tending to zero (we will not consider the case of zero film thickness because that implies surface to surface contact in the bearing in which case all loading is not necessarily transmitted by the oil film) and then the bearing pocket oil pressure tends to the supply pressure because the flow resistance across the bearing land will tend to infinity. This is the case with the bottom bearing pad for all values of  $\beta$ . For the top bearing pad, however, the smaller  $\beta$  is, the smaller the top bearing pocket oil pressure is, and so the downward force applied directly to the floating ring by the top pad is smaller. This means that the external downward load that can be applied to the bearing is larger because the gross load on the bottom bearing pad comprises that provided by the top pad plus the external loading. Similarly, for high  $\beta$  values, the load carried by the bearing bush as a whole is smaller.

More local to the zero displacement position, curves for values of  $\beta$  close to 0.5 have the steepest gradient. This is because  $\beta$  close to 0.5 necessarily implies that the flow resistance over the bearing lands has a value close to that through the capillary restrictors, and so any

change of film clearance resulting from displacement of the floating ring, significantly affects the hydrostatic bearing pocket pressure and hence the load transmitted by the bearing pad. This is not the case for high  $\beta$  values where the flow resistance over the bearing lands is already large, and most of the pressure drop already occurs here and not across the capillary. Neither is it the case for small  $\beta$  values where most of the pressure drop occurs across the capillary, and changes in the resistance to flow across the lands do not significantly affect the total flow resistance.

In designing a hydrostatic bearing bush to be used on a generator set, selection of the  $\beta$  value would depend on two considerations. Namely, the maximum static load that is likely to be applied to the bearing and the accuracy to which that load can be predicted. The designer would aim to operate on a section of the curve showing a steep gradient such that any departure of the load from the design load would not result in too significant a change in film clearances at the bearing pads. Typically,  $\beta = 0.5$  is a value used in the design of hydrostatic bearings generally. This value is often chosen because it gives a more or less constant static stiffness (ie gradient of the load versus displacement curve) in the operating region (up to about  $50 \mu\text{m}$  for the curve on figure 6.13). Figure 6.13 shows, however, that if the load on the bearing is likely to be such that displacement takes a non-zero value, or cannot be predicted accurately then there is an argument for selecting a different  $\beta$  value, say  $\beta = 0.175$  on figure 6.13 which for a static load of about 10 kN would result in a more or less constant static stiffness if this load was known only to within  $\pm 6$  kN. Furthermore, this stiffness is higher than that for  $\beta = 0.5$ . Generally then the  $\beta$  value selected will lie within the range  $0.15 < \beta < 0.5$ .

It is relevant at this stage to discuss the potential significance of

machining inaccuracies as far as the hydrostatic bearing static characteristics are concerned. Such inaccuracies are particularly significant when the nominal design clearance is small (of the order of 125  $\mu\text{m}$  or 0.005") such that a tolerance of say 12.5  $\mu\text{m}$  (0.0005") would result in a significant change in the resistance to oil flow over the bearing lands (remembering that flow resistance is inversely proportional to the cube of the clearance). Such a machining inaccuracy is likely to significantly affect the effective  $\beta$  value at which the bearing operates. Note that with lower  $\beta$  values being more desirable than higher  $\beta$  values, because of the points raised in the previous paragraph, it is better to oversize the bearing clearances rather than to undersize them, giving a higher maximum static load and the probability of a higher static stiffness.

Having decided upon the  $\beta$  value required, the designers next task is that of selecting the required oil supply pressure. This is related to the size of the hydrostatic bearings pads by the load carrying requirements. Normally, a particular supply pressure will be convenient or alternatively the size of the hydrostatic pads will be restricted by the available space and supply pressure will be selected to suit.

Note that the hydrostatic bearing could have been designed to operate with no displacement of the floating ring from its concentric position when the typical specific load is applied, but this would have meant a negative (i.e. upwards) displacement for smaller downward loads on the test bearing. This modification could have been brought about by, for example, applying a smaller oil supply pressure to the top hydrostatic bearing pad at the expense of total support stiffness for the floating ring in the vertical direction. Obviously such a design modification is of little, if any, advantage for a test bearing of this nature, but may be considered when the static load is constant, as in an actual machine.

The experimental static load versus displacement curve is shown in figure 6.14. It can be seen that the agreement with theory is very good and that what small discrepancies do exist can be easily explained by experimental error, and by the accuracy of the mid-land approximation used. It may, therefore, be deduced that the theory is most acceptable as far as the prediction of the static load-displacement characteristics are concerned. Note that were the geometry of the hydrostatic bearing pads such that greater inaccuracies in the theoretical static characteristics were apparent, due to the use of the mid-land approximation, an improvement in accuracy could be obtained by incorporating in the theory a factor which allowed for the inaccuracy of the approximation. The magnitude of such a factor would have to be determined by, for example, the finite difference method discussed in section 3.5.

Figure 6.15 shows the variation of total oil flow to the hydrostatic bearing bush as the floating ring is displaced in the vertical direction. For zero displacement there is a higher oil flow for higher  $\beta$  values because, since flow resistance through the capillaries is low (to make  $\beta$  high), the total flow resistance through the bearing is low. As displacement is increased, for high  $\beta$  values the oil flow rate is increased. This is because for high  $\beta$  values the capillary flow resistance is small and so the bearing pocket pressures are more constant and equal as the inner ring is displaced. Since, for a given change in clearance, the resultant change in flow resistance is larger for a larger clearance, the nett oil flow through the bearing increases with displacement (the pressure drops through the clearances being similar for high values of  $\beta$ ). For lower  $\beta$  values, as the floating ring is displaced downwards in the hydrostatic bush, the most significant contribution to the flow resistance at the top pad is provided by the capillary. This

becomes more so for greater displacements, and so the rate of increase in flow rate at the top pad becomes smaller. At the bottom pad the opposite is the case and the flow resistance over the bearing lands becomes more significant. The conditions at the bottom pad do not result in a significant drop in flow rate, however, because the flow there becomes small anyway as the clearance becomes small. Because the form of the pads is curved, vertical displacement results in an increase in flow through the side pads as flow resistance over the lands is decreased. The overall effect results in a slight increase in total oil flow for large displacement (eg  $\beta = 0.5$ ). Generally, then, for  $\beta$  less than or equal to 0.5 flow rate remains more constant as displacement changes.

As far as the designer is concerned, the most favoured  $\beta$  values to select are again those for  $\beta = 0.5$  and below. For values of  $\beta$  higher than 0.5 the designer would be forced to ensure that there was a significantly greater oil supply available than he is really likely to require. For example, in the extreme case of  $\beta = 0.9$ , if the design operating position was at 40  $\mu\text{m}$  displacement then the nominal oil flow requirement would be  $1.56 \text{ l.s}^{-1}$ , for a bearing similar to the test hydrostatic bearing. In practice, however, the static load, because of possible bearing misalignments for example, may only be predicted to such an accuracy that the actual displacement could possibly be 80  $\mu\text{m}$  in which case the flow requirement would be  $2 \text{ l.s}^{-1}$ , representing a 28% possible increase in the flow requirement. For larger hydrostatic bearings the corresponding possible increase in flow requirement would be even greater with a consequently larger and more expensive oil pump and tank than might really be required. It can be seen that the advantages offered by  $\beta$  values less than 0.5 are that the flow displacement curve is roughly flat over the entire bearing clearance so that whatever displacement the bearing operates at in service, the same oil

supply will suffice and there is no necessity to provide what could be an unnecessary reserve in capacity. Furthermore the nominal values of oil flow are significantly lower for the lower  $\beta$  values representing a further potential saving in the cost of the oil pump and tank.

The experimental oil flow-displacement characteristics are shown in figure 6.16 for the test hydrostatic bearing bush where  $\beta = 0.175$ . The appropriate theoretical curve is reproduced for comparison. It can be seen that the correlation between theory and experiment is extremely good and that the discrepancies are small enough to be explained by experimental error. Note that some of the discrepancy is again due to use of the mid-land approximation which indicates a slightly smaller oil flow than is actually the case. It may be concluded from figure 6.16, then, that the theory presented in sections 3.1 to 3.3 is easily accurate enough for the designer to predict oil flow in a hydrostatic bearing bush similar to that of the design proposed.

Figure 6.17 shows the theoretical variation of the required oil pumping power with vertical displacement of the floating ring in the hydrostatic bush, again for zero horizontal displacement (or vice-versa). These are identical in form to those of the oil flow (figure 6.15) because pumping power is given by the product of oil flow rate and supply pressure (constant in this case), and therefore, require no further explanation. They are presented here to indicate the order of magnitude of pumping power required for the test hydrostatic bearing bush.

#### 8.4 Dynamic Oil Film Coefficients for the Hydrostatic Bearing Bush

##### 8.4a Effect of Hydraulic Resistance Ratio $R_s/R_a$ and Accumulator Operating Parameter, B.

This section discusses the theoretical dynamic oil film coefficients of the test hydrostatic bearing bush, as predicted by the theory contained



in sections 3.1 to 3.3. The results were limited to being applicable to the test hydrostatic bearing bush because the finite amount of time available to conduct the research described in this thesis meant that some rationalisation was necessary, and that it was not possible to investigate theoretically and experimentally the full range of values that all of the parameters could take. Although this means that the actual results recorded are specific to the test hydrostatic bearing, the conclusions, discussed in chapter 9, are more general. Results discussed in this chapter, then, apply to the test hydrostatic bearing bush, and in this section in particular for an excitation frequency of 3000 rpm and various values of accumulator operating parameter,  $B$ , and hydraulic resistance ratio,  $R_s/R_a$ . The experimental results are also discussed in this section with relation to the variables  $B$  and  $R_s/R_a$ . Figures 6.18 to 6.21 show the variation of the direct stiffness and damping of the hydrostatic bearing, ie the floating ring in its bush, with oil line hydraulic resistance ratio and accumulator operating parameter. Note that both the resistance ratio and the accumulator operating parameter influence the operating characteristics of the hydrostatic bearing.

For low resistance ratios,  $R_s/R_a$ , the accumulator operating parameter,  $B$ , has little effect on the operating characteristics. This is expected because as the capillary resistance to the accumulator is increased and tends to infinity, so the accumulator is effectively shut off from the hydrostatic bearing system and so cannot influence it.

Figures 6.18 and 6.19 show that for higher resistance ratios, ie when the accumulator is connected to the system, the accumulator operating parameter does influence the operating dynamic stiffness of the hydrostatic bearing. For lower accumulator operating parameters (ie lower accumulator stiffnesses, giving a lower pressure rise for a given volume

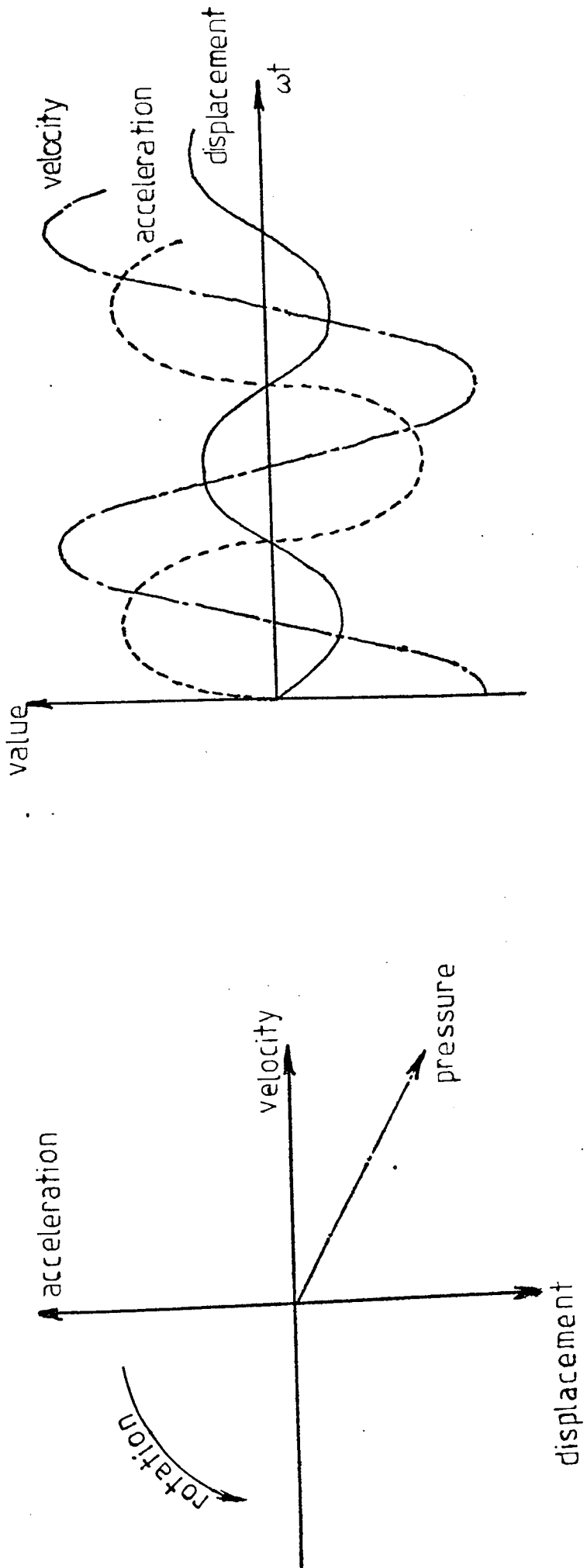
of oil flow into the accumulator) the dynamic stiffness of the hydrostatic oil film is low. This is because when the two hydrostatic bearing surfaces close together the oil between them can easily escape into the accumulator (since there is little oil line resistance - high resistance ratio, and little resistance to flow into the accumulator - low accumulator operating parameter) and so there is little resistance to movement of the bearing surfaces together and a low dynamic stiffness prevails. For larger values of accumulator operating parameter,  $B$ , there is still little resistance of flow to the accumulator but since pressure rises considerably as oil flows into the accumulator so the operating dynamic stiffness of the bearing increases. If the curves of figures 6.18 and 6.19 were extended towards resistance ratios tending to infinity, then for high accumulator operating parameters, also tending to a value of infinity, the dynamic stiffness would tend towards the stiffness obtained at very low resistance ratios. This is because the resistance to flow between hydrostatic pocket and accumulator tends to zero and the accumulator can be imagined to become the lower part of the hydrostatic pocket. This, then, is the same as not having an accumulator connected to the system and the coefficients would tend towards the values for  $R_s/R_a$  tending to zero. This case may be argued for both the stiffness and the damping curves. The curves of figures 6.20 and 6.21 show that for higher hydraulic resistance ratios the damping coefficients for the hydrostatic bearing are reduced, for all accumulator operating parameters. Since the damping is an out of phase stiffness then obviously connecting an accumulator to the system should give a reduced resistance to relative motion of the hydrostatic bearing surfaces. It is expected that damping should be reduced, then, for the same reasons that stiffness is reduced. The curves of figures 6.18 to 6.21 may be explained also in terms of

pressure amplitudes and phase angles. For an oscillating body ie the floating ring, maximum displacement is reached at a point in its cycle of motion which is a quarter of a cycle behind the point where maximum velocity is reached. This in turn is a quarter of a cycle behind the point where maximum acceleration is reached. This may be shown diagrammatically by representing displacement, velocity, and acceleration as vectors, assumed to be rotating in a counter-clockwise direction in figure 8.1(a). Also shown is a vector representing pocket oil pressure for a given hydrostatic pad. Figure 8.1(b) shows how displacement, velocity, and acceleration vary with time for the body.

There is, initially without any accumulator connected to the system, a phase lag of pressure amplitude behind the velocity vector since some of the pressure build up in the hydrostatic pockets is due to the velocity of the floating ring, trying to push oil out of its path, and some is due to the displacement position of the floating ring, ie we have both a stiffness and a damping force.

When the accumulator is introduced to the system the pressure amplitude in the hydrostatic pocket decreases since there is an additional exit provided for oil to flow out of the hydrostatic pocket. This gives rise to a reduced stiffness and damping. For low values of accumulator operating parameter, the greater the resistance ratio (ie the more we reduce flow resistance between hydrostatic pocket and accumulator) the smaller the pressure amplitudes become and hence for very high resistance ratios the stiffness and damping level out at a value determined by the accumulator impedance - the more flexible the accumulator, the lower the pressure amplitudes.

For high values of accumulator operating parameter, figures 6.18 and 6.19 show that as resistance ratio increases, stiffness, having first decreased, rises again to a value that may be higher than the stiffness



(a) vector diagram

(b) value - time relationship

FIG. 8.1 ACCELERATION, VELOCITY, & DISPLACEMENT PHASE RELATIONSHIP FOR AN OSCILLATING BODY.

reached as resistance ratio tends to zero. The explanation for this characteristic is that the flow resistance between hydrostatic pocket and accumulator becomes small enough to allow passage of sufficient oil, in the appropriate fraction of a vibration cycle, into the "stiff" accumulator and thus increase the pressure in the accumulator, hence the pressure in the hydrostatic pocket will build up to a maximum. Because there is resistance to flow into the accumulator, however, there has been a phase lag as far as pressure build up in the hydrostatic pocket is concerned and the pressure vector for the hydrostatic pocket becomes more in phase with the displacement vector in figure 8.1(a). This represents an increase in stiffness and a decrease in damping. Note from figure 6.21 that this phase lag can result in negative damping for high resistance ratios  $R_s/R_a$ , and low accumulator operating parameter B.

For very high accumulator impedances tending to infinity, and resistance ratios tending to infinity (ie little or no resistance to flow between hydrostatic pocket and accumulator) there is no additional phase lag introduced and accumulator and pocket pressures rise and fall almost simultaneously. Because there is now no phase lag, stiffness and damping become equal to the values where resistance ratio tends to zero, as we now effectively have no accumulator in the system again.

From the performance curves for stiffness, figures 6.18 and 6.19, it can be seen that only values of accumulator operating parameter high enough to be of the order of  $10^{12} \text{ N.m}^{-5}$  give a change in stiffness coefficient for a given high resistance ratio (say 100). This is because below this value of accumulator operating parameter the pressure rises in the accumulator are insignificantly small and so the "resistance" to flow into the accumulator is small compared with the "resistance" to flow back through the supply line. Hence pressure rises

in the hydrostatic pocket remain small. When accumulator operating parameter  $B$  is small it does not influence stiffness very much, for example,  $B = 10^4$  and  $B = 10^5 \text{ N.m}^{-5}$  would both give similar stiffnesses. This is because in each case the pressure rises in the accumulator remain small enough, compared with pressure rises in the hydrostatic pocket, to ensure that the main limitation to flow into the accumulator is due to viscous resistance in the capillary and not to a significantly decreasing pressure drop across the capillary.

Note that for zero horizontal displacement of the floating ring, all cross coupling coefficients for the whole bearing are zero at all resistance ratios. This is because at zero horizontal displacement the top and bottom hydrostatic pads offer their highest vertical force. Hence the rate of change of vertical force with horizontal displacement is zero at zero displacement, for these pads; then  $K_{yx}$  and  $C_{yx}$  are zero.  $K_{xy}$  and  $C_{xy}$  take zero values because, for zero horizontal displacement, both left and right hydrostatic pads offer the same load, and the nett horizontal load on the floating ring is zero, for all vertical displacements.

The curves shown in figures 6.17 to 6.20 show different values of stiffness and damping in the horizontal direction than in the vertical direction. The reason for this is that the results apply for a static load of 3.6 kN on the hydrostatic bush which results in a corresponding displacement of the floating ring, from the position where it is concentric with the hydrostatic bush, of 20  $\mu\text{m}$ . The resultant changes in bearing clearances at the top and bottom hydrostatic pads result in an overall increased vertical dynamic stiffness for the hydrostatic bush. Note that this effect is less marked for higher values of the resistance ratio  $R_s/R_a$  because the implication is that the accumulator is more closely connected to the hydrostatic pockets by the smaller hydraulic

resistances. Under such circumstances the dynamic characteristics become more influenced by the accumulator characteristics than by the geometry of the hydrostatic pads.

Experimental results are presented in figures 6.32 to 6.39 for the case where resistance ratio  $R_s/R_a = 0$  and in figures 6.42 to 6.49 for the case where  $R_s/R_a = 10$  and the accumulator operating characteristics are similar to those described by the  $B = 0$  curves. A range of excitation frequencies were investigated in each case. Agreement between theoretical and experimental results is generally very good and therefore confirms the effect of resistance ratio  $R_s/R_a$ , and accumulator operating parameter  $B$ , on the dynamic oil film force coefficients as predicted by the theory. These results are discussed in more detail in section 8.4(c).

At this stage it is relevant to discuss the implications of the curves in figures 6.18 to 6.21 as far as the designer is concerned. The nominal hydrostatic bearing dynamic characteristics, without the accumulators connected, are those values indicated at values of resistance ratio  $R_s/R_a$  tending to zero. (In practice these will not be dissimilar to those where  $R_s/R_a = 0.1$ ). If the impedance indicated by these values is low enough to ensure a suitable rotor critical speed shift when the hydrostatic bearing is introduced to the rotor-bearing system, then all is satisfactory. (The likely critical speed shift would be determined by evaluating the nett effective bearing coefficients, as described in section 4.4 of this thesis, and then examining the rotor response using the new rotor support characteristics. Methods of determining rotor response have been investigated by several authors, and are well documented, references (5), (12) and (13) being some). In the unlikely event of the hydrostatic bearing dynamic stiffness being too low, giving too large a change in rotor support characteristics or rotor critical

speed, then its value may be increased by either increasing the oil supply pressure, increasing the effective area of the hydrostatic pads, changing the pressure ratio  $\beta$ , or decreasing the bearing film clearance. Note that any of these steps would necessitate re-consideration of the hydrostatic bearing bush static characteristics. The most likely case, however, is that the dynamic stiffness will be too large and in this instance the designer would select the value required by reading the appropriate value of resistance ratio  $R_s/R_a$ , and accumulator operating parameter  $B$ , off the design curves of the type shown in figures 6.18 to 6.21. Under most circumstances, the case for accumulator operating parameter  $B$  equal to zero would apply since this corresponds to the typical gas-bag type accumulator that can normally be bought out. If higher values of  $B$  were selected then these would normally represent special accumulators. Note that the actual value of  $B$  that is effective for a given accumulator depends on the accumulator volume and on the gas pre-charge pressure, and should be checked and specified by the designer.

To summarise, then, it is evident that the theory presented in chapter 3 is able to accurately predict hydrostatic bearing dynamic characteristics, and that these characteristics can be tuned, by careful selection of the bearing geometry, accumulators, and hydraulic resistances, to almost any value desired by the designer.

#### 8.4b Effect of Oil Inertia

So far only characteristics for the case where fluid inertia in the oil capillary restrictors is considered to be insignificantly small have been examined. In practice this may be obtained by using capillary of very small diameter and length but with a suitably large length/diameter ratio to ensure that they do not act as orifice restrictors. Under these conditions, however, turbulent flow through the restrictor



may well prevail and the equations describing the bearing operation would have to be re-appraised. Alternatively the designer could accept a switch to orifice compensated hydrostatic bearings which would again show different characteristics. If capillaries having a large active volume are used, however, then inertia effects would have to be considered.

The effect of inertia on the dynamic characteristics may be described in terms of pocket pressure vectors discussed earlier. Consider the part of the vibration cycle where the floating ring is moving downwards say, towards the bottom hydrostatic pad. Normally, the bearing pocket pressure would not reach its peak until after the accumulator was charged with oil, thus restricting further flow out of the pocket into the accumulator. With fluid inertia, the opposite will apply, whereby the hydrostatic pocket pressure must rise in order to accelerate the oil out of the pocket and into the accumulator, thus allowing the floating ring to move. Thus the effect of inertia is to introduced more of a phase lead of the pocket pressure over the displacement vector. This means that there is a tendency for damping to increase while stiffness decreases if there is no change in the magnitude of the pressure vector.

For a given value of accumulator operating parameter and resistance ratio, the variation of bearing coefficients with oil inertia is shown in figures 6.24 to 6.27. ( $B = 0$ ,  $R_S/R_a = 10$ ). These curves show that the effect of oil inertia in the supply line only is small, whilst that of oil inertia in the accumulator line or in both lines is significant if the inertia coefficient is large enough.

The effect of oil inertia in the supply line only is small because with a resistance ratio of ten, the bearing dynamic characteristics are determined mainly by the accumulator characteristics. High oil inertia in the accumulator line only, however, results in an increase of

stiffness and damping because flow to the accumulator becomes more resisted and the dynamic characteristics tend to values corresponding to the case where the accumulator is not connected to the system. When both lines have high inertia coefficients damping has its highest value because the pressure amplitude vector exhibits a phase lead, as described earlier, compared with the case of inertia in the accumulator line only. There is a corresponding decrease of stiffness as compared with the case of oil inertia in the accumulator line only.

Figures 6.24 to 6.27 show that the damping in the system always increases with increase of inertia coefficient, while stiffness first decreases and then increases. This is explained with the aid of figure 8.2. Initially, the pressure rise vector leads the floating ring displacement vector by  $\theta_1$  resulting in stiffness  $S_1$  and damping  $D_1$ . If the inertia of the oil becomes larger, a phase lead is added to the pocket pressure amplitude, as described earlier, and because the pressure vector leads displacement by a bigger angle  $\theta_2$ , stiffness decreases and damping increases. As inertia increases still further, the magnitude of the pressure rise vector increases because of the greater force required to accelerate the fluid. The effect is that of an increase in stiffness to  $S_3$  and damping  $D_3$  even for the larger lead of phase angle  $\theta_3$ .

Note that whether it is the increase in pressure amplitude that most affects dynamic stiffness or whether it is the phase lead introduced will depend on the particular bearing, geometry and operating conditions being considered. Another influencing factor is the bearing clearance.

Figure 6.28 shows the variation of bearing stiffness coefficient  $K_{yy}$  with vertical displacement of the floating ring. The curves show that for zero displacement a smaller decrease in stiffness coefficient is obtained for an increase in inertia coefficient than is obtained

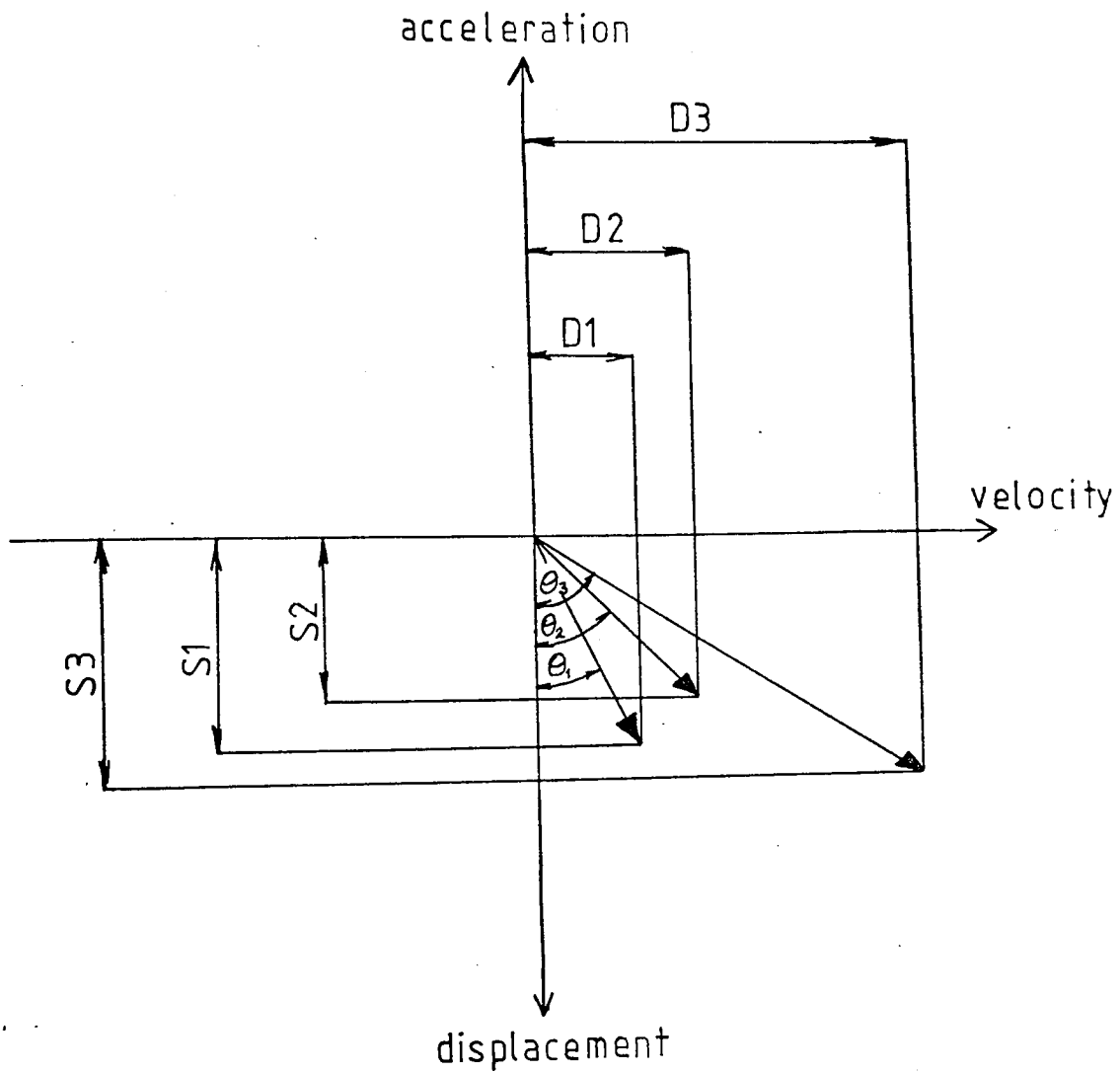


FIG 8.2 EFFECT OF OIL INERTIA ON THE PRESSURE RISE VECTOR IN A HYDROSTATIC POCKET

away from the zero displacement position. This may be explained by the fact that at zero displacement both top and bottom hydrostatic pad film clearances offer the same relatively high resistance to flow over the lands. For a given displacement downwards however, there is a greater decrease in resistance to flow over the top lands than there is an increase in resistance to flow over the bottom lands. The net effect of a larger resistance to flow at the zero displacement position means that it is at this position that the increase in pocket pressure amplitude, discussed above, is most likely. The corresponding damping profile is shown in figure 6.29.

As far as the experimental results are concerned, the inertia coefficient applicable to the accumulator capillary resistances was calculated to be about  $0.003 \times 10^9 \text{ kg.m}^{-4}$ . On inspection of figures 6.24 to 6.27 it can be seen that the resulting influence of oil inertia on the bearing dynamic characteristics was predicted to be negligible. A relatively short capillary was used to connect the accumulators to the hydrostatic bearings so as to minimise the effects of oil inertia in the experimental work. Thus it was possible to more confidently attribute the change in bearing characteristics, obtained by connecting the accumulators to the bearing system (ie comparing the results in figures 6.32 to 6.39 with those of figures 6.42 to 6.49) to the accumulator characteristics and to the capillary resistance as predicted by the theory (ie the effect of changing one variable at a time was considered, so as not to confuse matters).

The significance of oil inertia to the designer is that it offers one potential source of increased damping, see figures 6.26 and 6.27. A large amount of damping is often desirable because it generally promotes lower peak rotor vibration amplitudes local to rotor critical speeds than is the case for lower values of damping. Unless the static load on

151

the hydrostatic bearing, and hence static displacement, can be very accurately predicted, however, then every effort should be made by the designer to minimise the magnitude of the oil inertia. This recommendation is made with the effect of oil inertia on the stiffness profile for the hydrostatic bearing in mind, as shown in figure 6.28, (the corresponding damping profile being shown in figure 6.29). For increased oil inertia, with the test hydrostatic bearing bush arrangement considered, the effect is not only to reduce the nominal value of stiffness at a particular displacement, say 20  $\mu\text{m}$  for example, but also produce a negative stiffness at larger displacements. If the static load were to be larger than predicted, and the bearing operated at the larger displacement then the probability of instability and large vibration amplitudes arising would be very high. Furthermore, there is an advantage to be obtained in using low values of rotor support damping in that the resulting resonance curves tend to be more 'peaky' with vibration amplitude magnification large only in a smaller frequency bandwidth close to the critical speed. In any instance, large peak vibration amplitudes at rotor critical speeds may not be too important because of the possibility, discussed in more detail in chapter 10, that it may not be necessary to run through critical speeds at all.

#### 8.4c Effect of Excitation Frequency

It is important, if the proposed design of bearing is to be used on turbine generators, that the performance be satisfactory over the entire operating frequency range of the generator. Figures 6.22 and 6.23 show the theoretical variation of the test hydrostatic bearing dynamic oil film coefficients with excitation frequency.

The trend is for stiffness to decrease and for damping to increase as exciting frequency increases. This trend can be explained as an increase in phase lead of the pressure pulse, in the hydrostatic

pockets, over the displacement of the floating ring due to resistance to oil flow out of the pockets. The most important point is that stiffness is reduced, by the accumulator action, to a value considerably below the static stiffness, even for very low frequencies. This means that the proposed bearing design will be effective over the entire operational frequency range of generators. (As frequency tends to zero the bearing stiffness tends to the higher static stiffness).

Experimental measurement of the hydrostatic bearing dynamic oil film coefficients, for excitation frequencies in the range 400 r.p.m. to 2000 r.p.m. yielded the values shown in figures 6.32 to 6.39 for resistance ratio  $R_s/R_a = 0$ , and in figures 6.42 to 6.49 for  $R_s/R_a = 10$  and accumulator operating parameter B close to zero.

Theoretical curves are super-imposed in each case for comparison and the same trends discussed in the above paragraph are evident. Note that there is a significant decrease in the magnitude of the bearing coefficients brought about by the introduction of the accumulator to the bearing system. This change is effective for the entire frequency range investigated, as predicted by the theory. Agreement between theoretical and experimental results is very good, the maximum discrepancy being of the order of about 16% of the net dynamic stiffness. These differences can all be explained as being a result of experimental error.

### 8.5 Static Characteristics of the Combined Journal and Hydrostatic Bearing

As has been discussed already in section 6.5, the static load-displacement characteristics of the combined bearing are determined by the vector sum of the displacements appropriate to the individual hydrostatic and journal bearings. The point was also made in section 6.5 that the effect

of the force on the anti-rotation peg of the floating ring (journal bearing bush) on the static displacement should be checked in the design process, but would normally be negligible.

The significance of the above is that the journal bearing Sommerfeld number can no longer be used to completely define the bearing static operating position. This is because, for the component of shaft static displacement attributable to the journal bearing bush displacement inside the hydrostatic bush, the operating position is determined solely by the static load and not by the relationship between load and shaft speed indicated by the Sommerfeld number (assuming oil viscosity to be constant for a particular bearing), as is the case for the journal bearing. For a given static load on the combined bearing then, the shaft locus as its speed changes is described by an arc as is normally the case for journal bearings, for example that shown in figure 6.2. For a larger downward static load, however, that locus is displaced downwards by an amount which depends on the static stiffness of the hydrostatic bearing bush. For all shaft speeds and loads, this means that the shaft locus is given not by an arc but by an area.

#### 8.6 Dynamic Oil Film Coefficients For the Combined Journal and Hydrostatic Bearing

The dynamic oil film coefficients for the combined journal and hydrostatic bearing (with resistance ratio  $R_s/R_a = 10$  and accumulator operating parameter  $B \approx 0$ ) are shown in figures 6.52 to 6.59. The measured oil film coefficients agree well with the corresponding theoretical values and all discrepancies are small enough to be attributable to experimental error.

The effect of introducing the hydrostatic bearing as a means of support for the journal bearing bush has been to significantly reduce the dynamic stiffness of the overall (combined) bearing as compared with

that of the journal bearing alone, see figures 6.5 to 6.12.

Some variation of effective oil film coefficients with excitation frequency exists but it is difficult to suggest the reason for this for any particular single oil film coefficient. Clearly, the exact variation will depend on the variation of oil film coefficients for the two individual bearings with excitation frequency, and on the relationship between the two sets of coefficients described in section 4.2.

The agreement between theoretical and experimental results in figures 6.5 to 6.12 for the combined bearing is evidence that the relationship between the two individual bearings described in section 4.2 is correct. Thus further use of this theory, together with that in sections 3.1 to 3.3 in the design of future combined hydrostatic and journal bearings can be confidently undertaken. If this relatively straight forward theory is already accepted, then the results shown in figures 6.52 to 6.59 reaffirm the theory in chapter 3 describing the hydrostatic bearing characteristics.

The dynamic characteristics of journal bearings are sometimes described as being a function of the bearing Sommerfeld number. This cannot be the case for the dynamic oil film coefficients for the combined hydrostatic and journal bearing because of the dependence of the hydrostatic bearing dynamic oil film coefficients on the static displacement of the floating ring (ie the journal bearing bush), and, therefore, on the static load. This is in accordance with what has already been said in section 8.5 for the static shaft locus. Note also that the combined bearing dynamic characteristics now depend also on the details of the accumulator connections to the hydrostatic bearing.



8.7 Predicted Effect of the Hydrostatic Bearing On the  
Amplitude-Frequency Response Of A Generator Rotor

Theoretical rotor response plots, for a rotor with and without a hydrostatic bearing included in the rotor support, are shown in figure 6.60. The effect of the hydrostatic bearing has been to move the critical speed that was originally at 1750 r.p.m. to 1400 r.p.m. with a consequent reduction of rotor vibration amplitude at the machines normal running speed, by over 80%. Such a reduction in rotor vibration amplitude would significantly reduce stresses in the rotor, improve bearing life, and reduce noise output. Compared with these benefits, the increase of vibration amplitude at the critical speed of 13% is insignificant as the rotor would not normally run for more than several seconds at a time at the new critical speed.

As can be seen from figure 6.60, the effect of the hydrostatic bearing has been to also move the critical speed that would exist above the machines normal running speed, indeed all critical speeds would be moved to some extent because of their dependence on the rotor support dynamic characteristics. The amount by which the critical speeds are shifted would be controlled by selecting a suitable value of resistance ratio  $R_s/R_a$  for the hydrostatic bearing.

CHAPTER NINE

CONCLUSIONS

CHAPTER NINE

CONCLUSIONS

9.1 The Current Situation

The machine power rating of turbine generators has increased significantly over the past 30 years, changing from, typically, less than 100 MW in the early 1950's to up to 1200 MW in the 1980's. With this trend in machine rating has come a tendency for the generator rotor length/diameter ratio to be increased and as a consequence of this, many machines now operate with several critical speeds below their normal running speed. This has led to a problem for the designer in that he must ensure that the normal machine running speed is not close to a critical speed, thereby ensuring that the high vibrations that would otherwise result are avoided. When critical speeds do occur close to a machine's normal running speed, present methods of dealing with the problem are unsatisfactory; the development of the combined journal and hydrostatic bearing described in this thesis offers the possibility of eliminating the problem completely, however.

Examination of the current state of the art reveals that investigations of the static and dynamic characteristics of journal bearings are relatively well documented, references (6), (7), (8), (9), (11) being some. The same may be said of papers dealing with the dynamics of rotors supported in elastic bearings, for example references (5), (12) and (13). So far as hydrostatic bearing development is concerned, the author is able to offer a contribution to knowledge of the dynamic characteristics, there being few papers available which deal with this subject. The static characteristics, on the other hand, are well documented, some references being (15), (19), (20), (21) and (22). Use of the proposed hydrostatic bearing bush to support the journal bearing and rotor is,

of course, completely original so far as the author is aware. There have, however, been several attempts to similarly combine two journal bearings, references (28), (29) and (30), with marginal success. Several authors have investigated the use of a squeeze-film damper around rolling element bearings, references (31) to (37), but these were concerned with different applications, and in any instance the work was on a much smaller scale.

### 9.2 Static Characteristics of the Journal Bearing

Examination of the shaft centre locus for varying Sommerfeld number showed extremely good correlation with that predicted by existing theory. It may thus be concluded that existing theory is satisfactory.

### 9.3 Dynamic Oil Film Coefficients for the Journal Bearing

The work described in this thesis was not concerned with the prediction of journal bearing dynamic behaviour, since much work has already been done in this subject. However, during the experimental work it was necessary to measure the journal bearing effective dynamic oil film coefficients and the results, discussed in section 6.2, showed that there was some variation of these coefficients with exciting frequency. It has further been suggested that this variation with frequency may well be attributable to a combination of the effects of oil film non-linearity with variation of excitation frequency and amplitude, and oil film inertia.

### 9.4 Static Characteristics of the Hydrostatic Bearing

The experimental results discussed in section 6.3 show extremely good correlation with theory for both the load-displacement relationship and the flow-displacement relationship. It may therefore be considered that the theory is satisfactory.

Theoretical results show that a variation in the load-displacement relationship may be obtained by changing the effective pressure ratio  $\beta$  for the bearing. Furthermore, it has been shown that greater static loads may be supported by the hydrostatic bearing bush with smaller values of  $\beta$  than with larger values, and that the higher static stiffnesses will be obtained with values of  $\beta$  between 0.15 and 0.5. Because of these advantages of operating at lower  $\beta$  ratios, future drawings should show dimensions toleranced such that bearing clearances will be oversize (giving a lower value of  $\beta$ ) rather than undersize.

The hydrostatic bearing has been analysed with the aid of a mid-land type of approximation. This approximation becomes less accurate for large bearing land widths compared with the length and breadth of the hydrostatic pad. For the dimensions of the hydrostatic pads used in the test rig discussed in chapter 5, ie 4 cm by 7 cm, including 1 cm land width, the mid-land type of approximation has been found to be accurate to within less than 2%.

Results show that oil flow to the hydrostatic bearing bush varies more significantly for higher values of pressure ratio  $\beta$  than for smaller values, and that the magnitude of the oil flow is larger for high  $\beta$  ratios. These features of the hydrostatic bearing bush again indicate that a design utilising a value of pressure ratio  $\beta$  less than 0.5 would be more advantageous than one utilising a higher value. These conclusions, drawn out of consideration of the bearing oil flows, are also applicable on consideration of the bearing oil pumping power requirements since pumping power is directly proportional to flow rate.

## 9.5 Dynamic Oil Film Coefficients for the Hydrostatic Bearing

Theoretical results for the hydrostatic bearing show that both the stiffness and damping of the oil film can be significantly affected by the presence of an accumulator connected to the hydrostatic pocket. The actual values of oil film stiffness and damping will be determined by both the flow resistance offered by the capillary connecting the accumulator to the hydrostatic bearing, and by the operating characteristics of the accumulator itself. (The dynamic characteristics will also be influenced by parameters such as supply pressure, pressure ratio  $\beta$  etc but these factors also affect the bearings static characteristics and so would not normally be used to tune the dynamic characteristics.) The lowest oil film stiffness and damping is obtained by using a low flow resistance to the accumulator and a low accumulator stiffness (ie low pressure increase per unit volume of oil flow into the accumulator). Experimental results show that the accumulator can be used to drop the hydrostatic bearing oil film stiffness and damping by over 60%, and theoretical results predict that greater reductions can be obtained if required. Under most circumstances a standard gas bag type accumulator would be suitable; these can be bought out and are physically small enough to be neatly included in a bearing-pedestal assembly.

As the excitation frequency is increased, there is a slight reduction in hydrostatic bearing oil film stiffness, whilst the damping stiffness,  $\omega C$ , becomes greater (although the damping coefficient itself,  $C$ , does not change significantly). This stiffness change, however, is not generally of the order of magnitude of the change brought about with the accumulator, and would not adversely affect the operation of the hydrostatic bearing for the proposed use. The same could be said for the damping coefficient.

Experimental results have been obtained for the cases with (resistance

ratio  $R_s/R_a = 10$ ) and without the accumulators connected to the hydrostatic bearing bush and agreement with theory, for a range of excitation frequencies, is very good. There is no reason to believe that equally satisfactory results cannot be obtained for a larger version of the proposed combined bearing design since no scaling problems are envisaged.

The effect of oil inertia has been found to be insignificant for the bearing arrangement examined experimentally, thereby agreeing with the theoretical prediction. It is thought that this will be the case under most circumstances. In the event of oil inertia being significantly large, its effect has been shown theoretically to lead to an increase in the oil film damping coefficient, and to either a decrease or an increase of the oil film stiffness. It is recommended that capillaries providing a low oil inertia coefficient, as defined in section 3.2, be used whenever possible to reduce the risk of a negative oil film stiffness leading to bearing instability.

#### 9.6 Static Characteristics of the Combined Journal and Hydrostatic Bearing

The static load-displacement characteristics for the combined bearing are determined from the vector sum of the individual displacements attributable to each bearing. It is noted that one duty parameter, eg the bearing Sommerfeld number, can no longer be used to determine the operating position of the combined bearing since the load must be specified in order to determine the operating position of the hydrostatic bearing, whilst the speed must also be known before that of the journal bearing can be decided upon. For a given variation in load and speed the shaft centre locus, for the combined bearing, is described by an area rather than an arc (as is the case for the journal bearing) or a straight line (as is normally the case for the hydrostatic bearing).

## 9.7 Dynamic Oil Film Coefficients for the Combined Journal and Hydrostatic Bearing

The individual dynamic oil film coefficients for the journal bearing and for the hydrostatic bearing may be used to determine the net effective dynamic oil film coefficients for the combined journal and hydrostatic bearing. This has been done for the case where hydraulic resistance ratio  $R_s/R_a = 10$  and where accumulator operating parameter  $B \approx 0$  and the results have been found to agree very well with those measured experimentally. This shows that the theory for combining the two sets of oil film coefficients, as presented in section 4.4, is accurate. The discrepancy was typically about 10% and this was attributable to experimental error.

Comparison of the measured oil film coefficients of the combined bearing with those of the journal bearing shows that a reduction of the net effective bearing coefficient, of about 30% generally, has been obtained by the introduction of the hydrostatic bearing with accumulators connected. This is in agreement with theoretical predictions. A greater reduction could have been obtained by using a shorter length of capillary to connect the accumulators to the hydrostatic bearing.

Because the theory for combining the two sets of bearing coefficients has been proved for one set of operating conditions, it follows that the theory is equally applicable to other operating conditions, eg bearing static load or journal speed, since none of these parameters affects the way in which the oil films of the two bearings interact, and does not therefore appear in the theory in section 4.4.



## 9.8 Influence of the Hydrostatic Bearing on the Rotor Amplitude

### Frequency Response

It has been shown theoretically that a hydrostatic bearing with connected accumulators can be used to move rotor critical speeds by over 350 rpm and reduce rotor vibration amplitudes at running speed by over 80%. It will be suggested further, in section 10.2, how further development of the proposed combined bearing might result in making running through rotor critical speeds completely unnecessary, thereby significantly improving noise reduction, rotor stresses and bearing life. The proposed method of modifying the rotor support dynamic characteristics, ie by introducing the hydrostatic bearing around the journal bearing, offers advantages over other methods of (i) independent control of static and dynamic characteristics, (ii) independent control over horizontal and vertical support impedances, (iii) the possibility, with further development, of automatically controlled bearing tuning with varying speed (see section 10.2).

CHAPTER TEN

RECOMMENDATIONS

### 10.1 Further Testing of the Hydrostatic Bearing

This section deals with further testing which could be carried out using the design of hydrostatic bearing that formed part of the test rig. The suggestions deal mostly with testing of the hydrostatic bearing because this is the new part as far as the concept of a combined journal and hydrostatic bearing bush is concerned. Further tests are discussed for different values of resistance ratio  $R_s/R_a$ , different values of accumulator operating parameter B, different values of oil inertia coefficient, and for different journal speeds and static loads.

Whilst the experimental results contained in chapter 6 offer considerable support for the theory concerning the dynamic characteristics of hydrostatic bearings, as developed in chapter 3, tests have been carried out using only two values of resistance ratio  $R_s/R_a$  and only one value of accumulator operating parameter B. Whilst these tests confirm the trend in the variation of hydrostatic bearing dynamic stiffness with change in resistance ratio, the appropriate design curves, such as those in figures 6.17 to 6.20, could be used with more confidence if theoretical results for a number of other different resistance ratios,  $R_s/R_a$ , were confirmed experimentally.

The argument for repeating tests with accumulators having different operating parameters B is less convincing. This is because most of the standard designs of accumulator that can be purchased have operating parameters giving hydrostatic bearing performance curves close to the  $B = 0$  lines in figures 6.17 to 6.20. The operating parameter B is to some extent dependent on the pre-charge pressure of the accumulator but this would provide only a relatively fine control over the value of

B, compared with an accumulator specially designed to be 'stiff' with a very high value of operating parameter B. Since suitable reductions in hydrostatic bearing impedance can be obtained using currently available accumulators there appears to be little point in carrying out tests with special accumulators having high values of operating parameter B; indeed the theoretical results, figures 6.17 to 6.20, indicate that a smaller change in bearing impedance would be obtained anyway.

In section 8.4b it was indicated that a certain amount of lubricant inertia might be beneficial in that it could offer an increase in magnitude of the damping coefficients of the hydrostatic bearing. If this represents a potential improvement in the dynamic performance of the hydrostatic bearing, then the theoretical results should be confirmed experimentally either by using lubricant of different density, or using fluid restrictors of different design.

The dynamic test results discussed in chapters 6 and 8 have been carried out for a journal speed of 1500 rpm and a specific loading of 350 kPa (50 lb/in<sup>2</sup>). The theory developed in section 3 deals with the dynamic characteristics of the hydrostatic bearing and as far as its development and proving by experiment are concerned the journal speed is insignificant. A similar case might be argued for the way in which the combined bearing dynamic oil film coefficients are determined from sets of coefficients for the two individual bearings. The fact that one set of coefficients is affected by journal speed does not affect the way in which the theory is used to determine the combined bearing coefficients. There is an argument for repeating testing at higher journal speeds however, not because the hydrostatic bearing theory that applies is different, but because other problems, the nature of which may be unforeseen, may emerge. Some of the problems which could occur are discussed in section 10.5. Similarly, it might be argued that testing should also

be repeated with a range of static loads.

## 10.2 Possible Improvements in Restrictor Design

The flow restrictors used throughout the work described in this thesis were all of the standard capillary type. Whilst it was not within the scope of the project to investigate the usefulness of other more specialised restrictors, it is pertinent to discuss some of those which might offer advantages. These include those which can be made to provide an infinite static stiffness, and those which might be referred to as variable restrictors.

The use of a restrictor that would provide an infinite static stiffness would be that for any given static load on the hydrostatic bearing, its operating position (in terms of displacement) would stay the same. Some restrictors offering these characteristics are discussed in references (18), (19) and (27). This is important because although the static loading on the hydrostatic bearing might not be predicted very accurately, the operating displacements of the hydrostatic bearing can, thus allowing a more confident prediction of the operating displacements of the journal. This would be useful where there are significantly different loads on different bearings of a turbine-generator shaft line-out and it was desired that hydrostatic bearing design be standardised. On the other hand it might not be useful where it was considered that there was a possibility of a significant amount of bearing misalignment with the generator shaft. Under these circumstances the presence of a finite hydrostatic bearing static stiffness might result in a degree of automatic alignment of the journal bearing bush with its journal.

The restrictor that was discussed in the above paragraph, to modify the hydrostatic bearing static stiffness would be the one which would be placed in the oil supply line. Modification of the restrictor placed

in the accumulator oil line could offer an improvement of bearing dynamic characteristics. One such modification might be the inclusion of a two-position open or closed valve. With reference to figure 6.60 showing the alternative rotor vibration responses with and without the hydrostatic bearing, the response without the hydrostatic bearing would be very similar to that with the hydrostatic bearing but with no accumulators connected (since it is the accumulators that are responsible for a significantly reduced bearing impedance). The presence of an open or closed position valve in the accumulator line then would allow the generator rotor response to be switched from one form to another as the machine speed is changed thus taking advantage of the troughs in each response curve. This idea could be taken a stage further with the design of a variable restrictor whose effective capillary length could be changed from infinity to close to zero, either by having a number of capillaries connecting the hydrostatic bearing to the accumulators and switching their respective valves to the open or closed positions as necessary, or by using a 'screw-thread' type of restrictor similar to that mentioned in reference (19). The advantages offered would be that now, rather than switching between say the two response curves shown in figure 6.60, there would be any number of such curves to choose from, all with their troughs at different speeds. The result of this would be that now it might not be necessary to ever run through a critical speed!

From the variable restrictor mentioned above it is evident that the switching, ie the operation of a valve for instance, would be done remotely. Further development of this theme might include an automatic control whereby the mere running of the generator shaft at a certain speed would ensure that the correct restrictors were connecting the accumulators and hydrostatic bearing bush.

### 10.3 Possible Improvements in Hydrostatic Bearing Design

The development of the hydrostatic bearing bush might be furthered in several ways. These include the use of flat hydrostatic pads, removable hydrostatic pads, methods of introducing more damping if required, and the elimination of the need for an oil supply.

The use of flat hydrostatic pads could offer an advantage over the design used in the test rig described in chapter 5, which were of part cylindrical form for simplicity of manufacture. The advantage to be offered by flat pads is that for a given displacement of the journal bearing bush in one direction, the horizontal for example, the total clearance in the direction perpendicular to it, the vertical in this case, would remain unaltered, meaning permissible vibration amplitudes in that direction would not have to be reduced. This would also eliminate the presence of cross-coupling oil film coefficients for the hydrostatic bearing, under all operating conditions.

The use of removable hydrostatic pads also has certain advantages to offer. For the case where the hydrostatic bearing was designed to have a very small nominal clearance, then, rather than depend on accurate manufacturing to give the clearance required, this could be set on assembly by separate adjustment of each pad. This might be done by clamping the pad to the bush by means of screws but by designing a facility to position any required thickness of shim material between the pad and its seating on the hydrostatic bush. The other advantage to be obtained from using hydrostatic pads is that they need not be installed until after assembly of the rest of the bearing and rotor, thus reducing the chance of damage to the ground surfaces on the lands.

The amount of damping present in a rotor support will affect the peak value of vibration amplitude at the rotor critical speed, and the

'peakiness' of the vibration amplitude-frequency response plot. (More damping tends to smooth out the response plot such that the vibration amplitude away from the critical speed is still quite high whereas a lower amount of damping gives sharp well-defined critical speeds but with a higher peak vibration amplitude.) Some control over the support damping then, may provide an improved rotor dynamic response. One way in which additional damping might be introduced is by ensuring that the effect of oil inertia is more evident, possibly by using longer capillary tubes. This has already been discussed in section 8.4b. Another way in which hydrostatic bearing damping might be increased is by increasing the bearing land area, thereby increasing the amount of squeeze-film damping at the lands. The relationship between squeeze-film damping and land area has been discussed in section 3.4. Note that an alternative might be to manufacture the hydrostatic pads such that rather than have a pocket area as such, they merely had an oil distribution groove running around what would have been the perimeter of the pocket and still is the inner edge of the lands. The area contained inside this distribution groove would be machined to the same level as the bearing lands and would thus provide squeeze film damping. The advantage of this alternative is that it would not lower the load carrying capacity of the hydrostatic pad, unlike the case where the land width is increased (since the oil pressure decreases across the lands).

Further development of the hydrostatic bearing could examine the possibility of eliminating the need for an oil supply and hence supply capillary tube. Instead the same oil would stay trapped in the pockets of the bearing pads and in the accumulator and capillary connection to the pads. In this instance a reliable sealing mechanism would be positioned where the lands originally were around each oil pocket. Once assembled, the system would be filled with oil and pressurised. Static



stiffness would be obtained merely by the high incompressibility of the oil whilst the dynamic stiffness would be adjusted using the capillary connecting the accumulator to the bearing, as before. Such an arrangement would significantly simplify the bearing design, since there would be no need for oil feeds and drains. Furthermore, the initial expenditure and running costs of the feed oil pump would be eliminated.

#### 10.4 Testing on a Full Size Machine

Once suitable test results have been accumulated for a range of running conditions, and any improvements in the system as described in sections 10.2 and 10.3 been made, then testing of the new combined bearing system on a full size machine should be carried out. Only when this has been done will the full capabilities of the bearing be proved.

At this stage it should be possible to observe a further advantage of the combined bearing support system. Most turbine generator rotors exhibit different critical speeds in the horizontal and vertical directions due to different journal bearing and pedestal impedances in these directions. The hydrostatic bearing system could be tuned such that the overall support impedances in the horizontal and vertical directions were similar, thereby halving the number of critical speeds for the designer to concern himself with.

#### 10.5 Possible Complications which should be Investigated

Any complications which might arise as a result of using the combined bearing of the proposed design might be more easily dealt with if prior consideration has been given to them. Such complications might include instability of the rotor-bearing system, bearing misalignment and bearing reliability.

Journal bearing instability sometimes occurs with lightly loaded bearings

operating at high speeds, with the result that large journal vibrations occur. A more detailed examination of this field might reveal how the conditions for the onset of journal instability are affected by the hydrostatic bearing. Furthermore, the stability of the journal bearing bush supported between the hydrodynamic and hydrostatic oil films is now a new consideration; large vibrations of this would again lead to high noise and rapid bearing wear even if the absolute shaft vibrations relative to space were acceptable.

Under normal running conditions both journal and hydrostatic bearing bushes would operate with their axes parallel to the axis of the journal. Misalignment of the bearings on assembly, such that this was no longer the case, may result in different static and dynamic characteristics for both the journal and hydrostatic bearings. Whilst some investigations of the effects of misalignment have been carried out for journal bearings, references (9) and (44), and for hydrostatic bearings, reference (26), these analyses need extending to consider different directions of misalignment and to the particular application of the combined journal and hydrostatic bearing design discussed in this thesis. This would lead to the determination of acceptable tolerances for alignment.

The question of bearing reliability has not yet been considered. With the introduction of a hydrostatic bearing and its associated fittings there are more potential weaknesses in the design. Particular attention might be paid to the possibility of hydrostatic bearing oil pump failure and accumulator failure. Reliability of the oil supply might be improved by having a reserve oil pump automatically switch on should the first fail. Alternatively, an arrangement might be considered whereby if the hydrostatic oil supply failed, then the journal bearing bush was automatically clamped rigidly to the hydrostatic bearing bush,

and the generator shaft would run on the journal bearing alone.

Accumulators sometimes fail by losing gas pressure; this might be allowed for by having a back-up accumulator set permanently connected to the hydrostatic bearing bush, and regularly checking the pre-change pressures.

## LIST OF REFERENCES

LIST OF REFERENCES

1. O. Reynolds "On the Theory of Lubrication and its Application to Mr. B. Towers Experiments" Philosophical Trans. of Royal Society. V.177. Pt.1. 1886.
2. B. Towers "Frictional Experiments with Bearings" Report No's. I and II. Minutes Inst. Mech. Eng. 1884.
3. A. Stodola "Critical Shaft Perturbations As a Result of the Elasticity of the Oil Cushion in the Bearings" Schweizerische Bauzeitung 85. No.21. May 1925.
4. A.C. Hagg and G.O. Sankey. "Elastic and Damping Properties of Oil Film Journal Bearings for Application to Unbalance Vibration Calculations" Jour. App. Mech. Trans. ASME. 1958. p.141.
5. J.W. Lund and B. Sternlicht. "Rotor - Bearing Dynamics with Emphasis on Attenuation" ASME J. Basic Eng. V.84.No.4. Dec.1962. p.491.
6. P.C. Warner "Static and Dynamic Properties of Partial Journal Bearings" ASME J. Basic Eng. V.85. No.2. June 1963. p.247.
7. F.K. Orcutt "The Steady-State and Dynamic Characteristics of the Tilting Pad Journal Bearing in Laminar and Turbulent Flow Regimes" Trans. ASME. J.Lub. Tech. V.89. No.3. July 1967. p.392.

8. J. Glienecke "Experimental Investigation of the Stiffness and Damping Coefficients of Turbine Bearings and their Application to Instability Prediction"  
Proc. Inst. Mech. Eng. 1967. V.181. Pt.3B.  
p.122.
9. R.H. Bannister "Non-Linear Oil Film Force Coefficients for a Journal Bearing Operating Under Aligned and Misaligned Conditions"  
Ph.D. Thesis. 1972. Univ. of Aston in Birmingham.
10. A.A. Raimondi and J. Boyd. "A Solution for the Finite Journal Bearing and its Application to Analysis and Design"  
Trans. ASLE. V.1. No.1. 1958.
11. F.A. Martin and D.R. Garner. "Plain Journal Bearings Under Steady Loads: Design Guidance for Safe Operation"  
Proc. I.Mech.E. 1973. Paper No. LB371/73.
12. R.G. Kirk and E.J. Gunter. "Effect of Support Flexibility and Damping on the Dynamic Response of a Single Mass Flexible Rotor in Elastic Bearings"  
NASA Report No. CR-2082. July 1972.
13. R. Gasch "Vibration of Large Turbo-Rotors in Fluid-Film Bearings on an Elastic Foundation"  
J. Sound and Vibration (1976). 47(1). 53-73.
14. A.A. Raimondi and J. Boyd. "An Analysis of Orifice and Capillary - Compensated Hydrostatic Journal Bearings"  
Lubrication Engineering. Jan. 1957.

15. H.C. Rippel "Design of Hydrostatic Bearings"  
Machine Design 10 Pts. Aug.-Nov. 1963.
16. J.P. O'Donoghue, "Computer Analysis of Externally  
W.B. Rowe & Pressurized Journal Bearings"  
C.J. Hooke. Proc. Inst. Mech. Eng. 1969-70. V.184. Pt.3L.
17. J.K. Royle, "Applications of Automatic Control to  
R.B. Howarth and Pressurized Oil Film Bearings.  
A.L. Caseley-Hayford. Proc. Inst. Mech. Eng. V.176. No.22. 1962.
18. J.P. O'Donoghue and "Hydrostatic Bearing Design"  
W.B. Rowe. Tribology. Feb. 1969.
19. P.B. Davies "Investigation of An All-Metallic Flexible  
Hydrostatic Thrust Bearing"  
ASLE/ASME Lub. Conf. Paper (Atlanta.  
Georgia. Oct. 16-18. 1973).
20. R. Bassani "A New Opposed-Pad Hydrostatic Bearing:  
The Flow Self-Regulating Bearing"  
Meccanica. June 1975. V.10.No.2. p.107.
21. C.K. Singh and "Stiffness Optimization of a Variable  
D.V. Singh Restrictor-Compensated Hydrostatic Thrust  
Bearing System"  
Wear 44.No.2. 1977. p.223-230.
22. G.M. Brown "The Dynamic Characteristics of a Hydro-  
Static Thrust Bearing"  
Int. J. Mach. Tool Des. Res. V.1. p.157-171.
23. L. Licht and "Dynamics of Externally-Pressurized Sliders  
J.W. Cooley With Incompressible and Compressible Films"  
Trans. ASME June 1964. p.396.

24. G. Kh. Ingerter "Dynamic Characteristics of Hydrostatic Bearings"  
Machines and Tooling. V. XL111. No.9.
25. M.J. Newton and R.B. Howarth. "Predicting Changes in Operating Variables for Hydrostatic Thrust Pads Subjected to Tilt and Dynamic Action"  
Proc. 1. Mech.E. V.188. 31/74. 1974.
26. N. Tully "Static and Dynamic Performance of an Infinite Stiffness Hydrostatic Thrust Bearing"  
Trans. ASME. Jan. 1977. p.106.
27. C. Heathcote "Improvements in or Relating to Bearing Assemblies for the Shafts of Alternating Current Generators"  
Patent Specification 1302896. The Patent Office, London.
28. R. Taylor "A Numerical Solution of the Dynamic Characteristics of an Aerostatic, Porous Thrust Bearing Having a Uniform Film Subjected to Linear Axial Load Variations"  
J.Mech. Eng. Sci. V.19. No.3. 1977. p.122.
29. D.A. Boffey "A Study of the Stability of an Externally-Pressurized Gas-Lubricated Thrust Bearing With a Flexible Damped Support"  
Trans. ASME. V.100. July 1978. p.364.
30. B.C. Majumdar "Dynamic Characteristics of Externally Pressurized Rectangular Porous Gas Thrust Bearings"  
J.Lub. Tech. ASME Paper No. 76-Lub-A. 1976.6p.



31. M.C. Shaw and T.J. Nussdorfer, Jr. "An Analysis of the Full-Floating Journal Bearing"  
N.A.C.A. Report No. 866. 1947.
32. C.F. Kettleborough "Frictional Experiments on Lightly-Loaded Fully Floating Journal Bearings"  
Australian J. Applied Sci. Sept. 1954.
33. F.K. Orcutt and C.W. Ng. "Steady-State and Dynamic Properties of the Floating Ring Journal Bearing"  
J. Lub . Tech. Jan. 1968. p.243.
34. K.K. Thomsen and H. Anderson "Experimental Investigation of a Simple Squeeze Film Damper"  
J. Eng. Industry. May 1974. p.427.
35. S. Mohan and E.J. Hahn. "Design of Squeeze Film Damper Supports for Rigid Rotors"  
Trans. ASME. Aug. 1974. p.976.
36. M. Botman "Experiments on Oil-Film Dampers for Turbo-Machinery"  
J. Eng. Power. July 1976.
37. S. Simandiri and E.J. Hahn. "Effect of Pressurization on the Vibration Isolation Capability of Squeeze Film Bearings"  
J.E. Eng. Industry. Feb. 1976. p.109.
38. M.D. Rabinowitz and E.J. Hahn. "Stability of Squeeze-Film-Damper Supported Flexible Rotors"  
J. Eng. Power. Oct. 1977. p.545.

39. E.J. Gunter, "Design and Application of Squeeze Film  
L.E. Barrett and Dampers for Turbomachinery Stabilization"  
P.E. Allaire. Turbo. Mach. Symp. 4th. Proc. Tex. A and M  
Univ. College Station. Oct. 14-16. 1975.  
p.127-141.
40. D.L. Taylor and "Non-linear Response of Short Squeeze-Film  
B.R.K. Kumar. Dampers"  
J. Lub. Tech. Jan. 1980. V.102. p.51.
41. R.A. Cookson and "The Effectiveness of Squeeze-Film Damper  
S.S. Kossa. Bearings Supporting Flexible Rotors  
Without a Centralising Spring"  
Int. J. Mech. Sci. V.22. p.313-324.
42. J.L. Nikolajsen and "Investigation of Squeeze-Film Isolators  
R. Holmes. for the Vibration Control of a Flexible  
Rotor"  
J. Mech. Eng. Sci. V.21. No. 4. 1979.
43. J.L. Nikolajsen, "Investigation of an Electromagnetic Damper  
R. Holmes and for Vibration Control of a Transmission Shaft"  
V. Gondhalekar. Proc. Inst. Mech. Eng. V.193. 1979. No.31.
44. J.P. O'Donoghue, "Design of Hydrostatic Bearings Using an  
W.B. Rowe and Operating Parameter"  
C.J. Hooke. Wear, V. 14. 1969.
45. P.B. Davies "A General Analysis of Multi-Recess Hydro-  
static Journal Bearings"  
Proc. I.Mech.E. 1969-70. V.184. Pt.1. No.43.
46. J.P. O'Donoghue and "Hydrostatic Journal Bearing (Exact  
W.B. Rowe. Procedure)"  
Tribology Nov. 1968. p.230.

47. M.K. Ghosh and B.C. Majumdar. "Plane Vibration Characteristics of Multi-recess Externally Pressurized Oil Journal Bearings"  
Tribology Int. June 1977. p.170.
48. S. Heller "Static and Dynamic Performance of Externally Pressurized Fluid Film Journal Bearings in the Turbulent Regime"  
J. Lub. Tech. July 1974.
49. S.M. Rohde and H.A. Ezzat. "On the Dynamic Behaviour of Hybrid Journal Bearings"  
Trans. ASME. Jan. 1976.
50. R.B. Stambaugh "Vibration Properties of Rubberlike Materials"  
Ind. Eng. Chem. 1942. V.34. p.1358-1365.
51. P.R. Dwight "Some Properties of Oils Used in Bearing Design"  
Unpublish Report No. S/CD u 476. G.E.C.  
Turbine Generators Ltd., Stafford.
52. D. Dawson, J.D. Hudson, B. Hunter and C.N. March. "An Experimental of the Thermal Equilibrium of Steadily Loaded Journal Bearings"  
I.Mech.E. Proc. 1966/67. V.181. Pt.3B.
53. C. Hooke, D. Brighton and J.P. O'Donoghue. "The Effect of Elastic Distortion on the Performance of Thin Shell Bearings"  
I.Mech.E. Lub and Wear Proc. 1967/68  
V.181. Pt.3B.

BIBLIOGRAPHY

- A. Cameron "Basic Lubrication Theory"  
J. Wiley & Sons (1st. edition  
Longmans).
- A. Cameron "Principles of Lubrication"  
Longmans, (London).
- O. Pinkus and "Theory of Hydrodynamic Lubrication"  
B. Sternlicht. McGraw-Hill Book Co.
- N. Tipei "Theory of Lubrication"  
Stanford Univ. Press.  
London: Oxford Univ. Press.
- M.C. Shaw and "Analysis and Lubrication of Bearings"  
E.F. Macks. McGraw-Hill Book Co. Inc. New York,  
Toronto, London.
- P.R. Trumpler "Design of Fluid Film Bearings"  
MacMillan Co., (New York).  
Colliery MacMillan Co., (London).
- M.D. Hersey "Theory and Research in Lubrication"  
J. Wiley & Sons.
- F.M. Stansfield "Hydrostatic Bearings"  
Machinery Publishing Co. Ltd.,  
Brighton.
- J.P. Den Hartog "Mechanical Vibrations"  
McGraw-Hill Book Co., Inc., New York,  
Toronto, London.

J. Morris

"The Strength of Shafts in Vibration"

Crosby Lockwood & Son, Ltd.

D. Fuller

"Theory and Practice of Lubrication  
for Engineers"

J. Wiley & Sons, Inc., New York,  
London, Sydney.

A. Hohn

"Bearings for Steam Turbosets"

Brown Boveri Review. 3-75. p.72-83.

V.J. Vickers

"Recent Trends in Turbogenerators"

Proc. I.E.E. V.121. No.11R. Nov. 1974.

APPENDIX A

DESIGN PROCEDURE FOR THE HYDROSTATIC BEARING

APPENDIX A

DESIGN PROCEDURE FOR THE HYDROSTATIC BEARING

Before the design of the hydrostatic bearing can be finalised, the design of the journal bearing should be complete and the values of its dynamic oil film coefficients for various running speeds should be known. (Literature on journal bearing design is already abundant and has been discussed in chapter 2). The journal bearing characteristics are required in order to determine the operating characteristics for the combined journal and hydrostatic bearing. The design procedure for the hydrostatic bearing is set out below.

1. Determine the static load to be carried by the hydrostatic bearing, (from knowledge of the weight of the rotor, and experience of changes of static loading that may be brought about by other factors eg bearing misalignment). Consideration must be given to any horizontal loads that might occur as well as vertical loads.
2. Determine the hydrostatic bearing geometry. Normally the available space to accommodate the hydrostatic bearing will be restricted and this will determine the maximum size of the hydrostatic bearing bush, and consequently of the hydrostatic pads. The hydrostatic pad land widths will usually be chosen to be about one fifth of the hydrostatic pad dimension (if they are too large then the pad becomes inefficient as a load bearing surface, if they are too small then oil flow will be excessive), and once this is established then the effective pad area (defined by the centre-line of the lands) may be determined.
3. Select the bearing clearances, operating pressure ratio  $\beta$ , and determine the required supply pressure. A bearing clearance of about  $125 \mu\text{m}$  (0.005") is probably close to the optimum value for

most applications. If the clearance becomes significantly larger then oil flow becomes excessive and, if hydrostatic bearings are fitted to the generator, say, and not the turbine, then higher bending stresses at the coupling may result when the oil supply is turned off. If the clearance is too small, however, the effects of bearing misalignment, machining tolerances, and surface contours become too significant and it becomes more difficult to predict bearing behaviour.

Having decided on a particular bearing clearance it is possible to determine the length and diameter of capillary tube required to form the restrictor in the oil supply line for any particular pressure ratio ( $\beta$ ) selected. The value selected will depend on the accuracy to which the static load is known (see also section 8.3).  $\beta = 0.4$  might be typical. Then the required supply pressure may be calculated from equations 3.15 and 3.16 which are combined below in equation A-1.

$$F = \frac{A \cdot P_s \frac{\beta}{1 - \beta} (4 r \alpha + 2 L)}{\frac{\beta}{1 - \beta} (4 R \alpha + 2 L) + f(x, y)} \quad \dots \quad A.1.$$

where the symbols are as defined in chapter 3.

4. Determine the bearing dynamic oil film coefficients for the hydrostatic bearing, according to the theory in chapter 3.
  5. Determine the combined journal and hydrostatic bearing effective dynamic oil film coefficients, as shown in section 3.3. Using the resulting coefficients the theoretical amplitude frequency response for the generator rotor may be determined, (some papers dealing with rotor dynamic response are discussed in chapter 2) and compared with that for journal bearing rotor supports only.
- Note in this first instance the hydrostatic bearing will be assumed



to have no accumulators connected to it. It will probably be found that the hydrostatic bearing without accumulators connected to it has too high an impedance to lower rotor critical speeds by any significant amount. (If, on the other hand, too much change in rotor response has been effected, then the hydrostatic bearing impedance has to be increased by increasing the supply oil pressure, effective bearing pad areas, or changing  $\beta$ ). A further significant change in overall bearing impedance may be brought about by re-calculating the bearing coefficients for the case with accumulators connected to the hydrostatic bearing and re-calculating the new rotor response. A value of resistance ratio  $R_s/R_a = 10$  will normally give a significant critical speed change.

6. Check the stability of the resulting combined journal and hydrostatic bearing in the same way that the stability of the journal bearing alone would be investigated (ie using the combined bearing dynamic oil film coefficients). Bearing stability analysis is already documented, for example, in Cameron's text book "Principles of Lubrication". Note that, in a similar manner, the stability of the journal bearing bush as it floats between the hydrodynamic and hydrostatic oil films should also be checked. If, in either instance, some instability is apparant then an alternative design configuration should be considered. Stability can usually be improved by increasing support damping; methods of increasing hydrostatic bearing damping have been discussed in section 10.3.

#### Sample Calculations

A symmetrical rotor weighing 1.33 MN (133 tons.f.) is supported in two journal bearings, and the positions of the bearings on the rotor are such that the rotor exhibits a critical speed close to its normal running speed of 1800 r.p.m. It is impractical to

change the position of the bearings, and so it is required that a hydrostatic bearing bush be designed to house the journal bearings such that the rotor critical speed is moved away from the machines running speed.

a) The nominal static vertical load on the bearings is given by half of the rotor static weight, ie 0.665 MN. The nominal static horizontal load is negligible but it is known from past experience that both nominal static loads on the bearing could vary by up to 0.2 MN.

b) The journal bearings on the rotor concerned have a bush bore of 47 cm (18.5") and a length/diameter ratio of unity. Since the hydrostatic bearing bush is to be designed to consist of a set of hydrostatic pockets at each end of the bearing, and must not take up any more axial space along the rotor, the dimensions of each pocket will be chosen to be 75 cm x 30 cm. A 30 cm axial length will leave sufficient room for drain areas and journal bearing oil parts. Of these dimensions, 7 cm in each case, at each edge of the pocket, will be occupied by land. Then the net effective area of the hydrostatic pocket is given by

$$A = (75 - 7) \times 10^{-2} \times (30 - 7) \times 10^{-2} = 0.1564 \text{ m}^2$$

c) A hydrostatic bearing pad film clearance of 125  $\mu\text{m}$  (0.005") will be selected to be effective for the zero displacement position of the journal bearing bush in the hydrostatic bearing bush. Because of the high tolerance on the static load, the hydrostatic bearing will be designed with a pressure ratio  $\beta = 0.4$ . For a hydrostatic bush consisting of opposed hydrostatic pads, as shown in figure A.1., the load in that direction is determined by applying equation A.1. for each pad such that

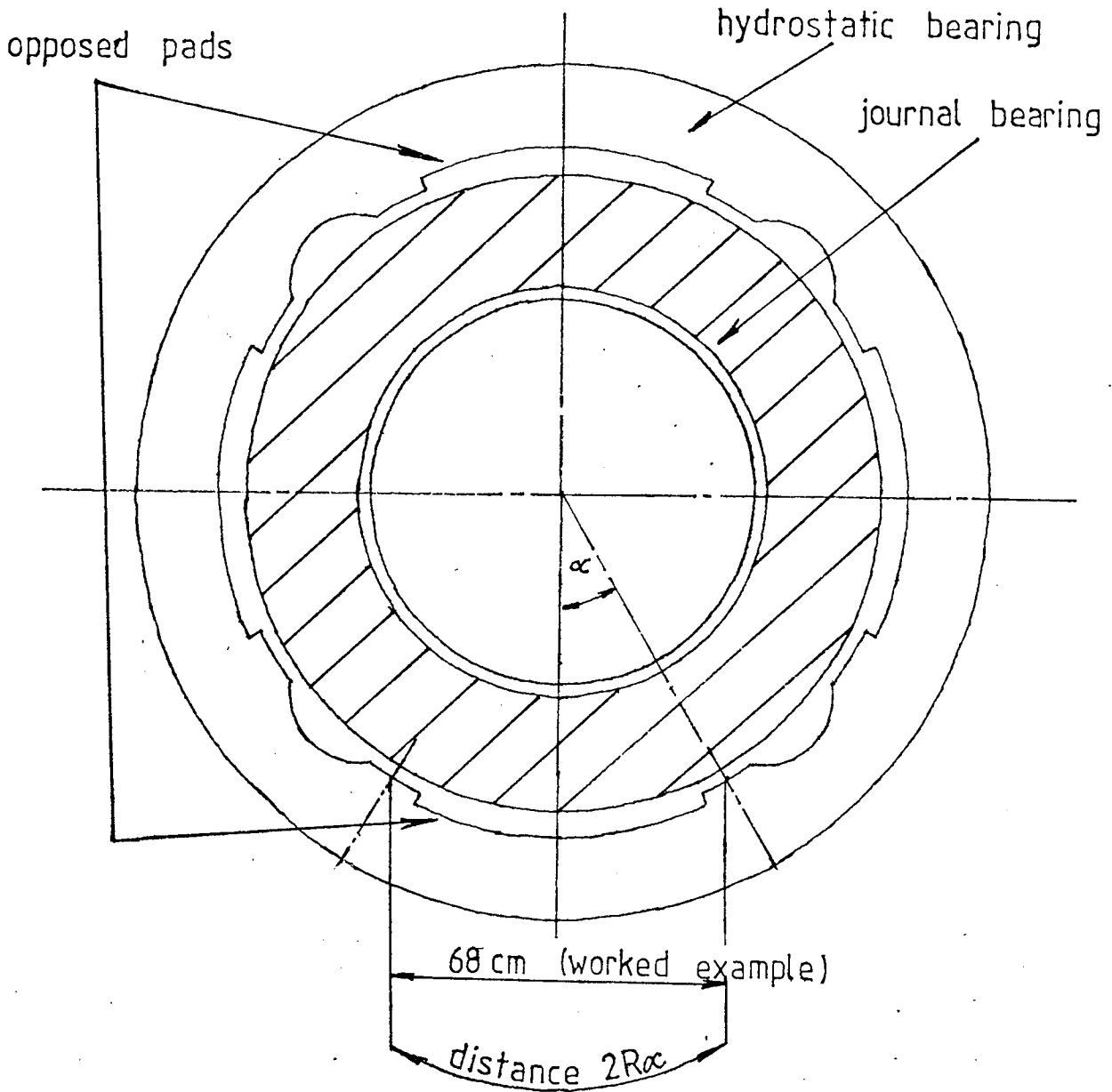


FIG A-1 DIAGRAM OF A HYDROSTATIC BEARING BUSH

$$F = \left\{ \frac{A p_s \frac{\beta}{1 - \beta} (4 R \alpha + 2 L)}{\frac{\beta}{1 - \beta} (4 R \alpha + 2 L) + f(x, y)} \right. \\ \left. \frac{A p_s \frac{\beta}{1 - \beta} (4 R \alpha + 2 L)}{\frac{\beta}{1 - \beta} (4 R \alpha + 2 L) + f(-x, -y)} \right\} \dots A-2$$

where the symbols have the meanings as defined in chapter 3. Since there are two axial sets of hydrostatic pockets in the proposed design of hydrostatic bearing bush, each set has to support only half of the total bearing load. It will be assumed that for the applied static load, a static displacement of 50  $\mu\text{m}$  is acceptable; this leaves a further 75  $\mu\text{m}$  to be taken up by any unforeseen static load, and by vibration amplitudes. Then the supply pressure required is given by

$$p_s = \frac{F}{A} \left\{ \frac{\frac{\beta}{1 - \beta} (4 R \alpha + 2 L)}{\frac{\beta}{1 - \beta} (4 R \alpha + 2 L) + f(x, y)} \right. \\ \left. \frac{\frac{\beta}{1 - \beta} (4 R \alpha + 2 L)}{\frac{\beta}{1 - \beta} (4 R \alpha + 2 L) + f(-x, -y)} \right\}^{-1} \dots A-3$$

Substituting into equation A-3 values of  $F = 0.3325 \text{ MN}$ ,  $A = 0.1564 \text{ m}^2$ ,  $\beta = 0.4$ ,  $R = 0.6 \text{ m}$ ,  $\alpha = 0.61 \text{ rad.}$ ,  $L = 1.91 \text{ m}$ ,  $x = 0$ ,  $y = -50 \mu\text{m}$  gives  $P_s = 4.39 \text{ MPa}$  (640  $\text{lb f/in}^2$ ).

Having selected a pressure ratio  $\beta$ , and a bearing film clearance  $C_o$ , the details of the capillary restrictor may be evaluated from the ratio of the required oil flow through the capillary/the pressure drop across it. This ratio is defined by  $K_s$  in equation 3.14.

- d) The geometry and operating conditions of the hydrostatic bearing bush have been decided, and it now remains only to tune the

dynamic characteristics of the rotor support to optimum values. The computer program in section B-I, based on the theory in chapter 3, was used to give dynamic oil film coefficients for the operating conditions determined in the previous sections (a) to (e). It was assumed that no accumulators were connected to the hydrostatic bearing bush in this instance.

- e) It was found that the magnitude of the hydrostatic bearing oil film coefficients was large relative to the journal bearing oil film impedance, at machine normal running speed. For this reason the program in appendix B-I was re-run for the case where accumulators are connected to the hydrostatic pockets, using a restrictor resistance ratio  $R_s/R_a = 10$ . The resulting bearing coefficients are shown in figure A-2 on an output sheet from the computer program used to combine the hydrostatic bearing oil film coefficients with the journal bearing oil film coefficients (see section B-II). Substitution of these combined bearing coefficients for the journal bearing coefficients as input data to a computer program which predicted rotor dynamic response showed that the critical speed was moved away from the machines normal running speed, in a manner similar to that shown in figure 6.60.
- f) Using the resulting combined bearing dynamic oil film coefficients, a stability analysis of the new rotor bearing system using conventional methods would be carried out to show that the proposed combined bearing was likely to run in a stable mode of operation.

2 - OIL - FILM BEARING PROGRAM

THIS PROGRAM IS USED TO 'ADD' TOGETHER SETS OF HYDRODYNAMIC BEARING OIL FILM COEFFICIENTS AND HYDROSTATIC BEARING OIL FILM COEFFICIENTS, BOTH SETS OF COEFFICIENTS BEING INPUT DATA, AND PRODUCE AN OVERALL SET OF BEARING COEFFICIENTS, WHICH IS APPLICABLE TO THE COMBINED 2-OIL-FILM BEARING

SELECT THE FORM OF OUTPUT THAT YOU REQUIRE BY TYPING THE APPROPRIATE NUMBER:--

- 1 : TABULAR OUTPUT
- 2 : GRAPHICAL OUTPUT

SELECT THE PARAMETER WITH WHICH THE SETS OF COEFFICIENTS VARY BY TYPING THE APPROPRIATE NUMBER :--

- 1 : LOAD / KN.
- 2 : FREQUENCY / rad.s^-1.

INPUT THE HYDRODYNAMIC BEARING COEFFICIENTS IN THE FOLLOWING FORMAT :--

LOAD (OR FREQUENCY),  $K_{yy}$ ,  $K_{xx}$ ,  $K_{xy}$ ,  $C_{yy}$ ,  $C_{xx}$ ,  $C_{xy}$ ,  $C_{yx}$ ,  $C_{xy}$ ,  $C_{yx}$ ,  $C_{xx}$ . EACH ITEM OF DATA SHOULD BE SEPARATED BY A COMMA. UNITS ARE : LOAD/N., FREQUENCY /rad.s^-1.,  $K_{ij}$ /N.m^-1.,  $C_{ij}$ /N.s.m^-1.. INPUT THE DATA ONE LINE AT A TIME, BEGINNING EACH LINE WITH A NEW LOAD (OR FREQUENCY).

USING THE FOLLOWING JOURNAL BEARING DATA :--

FREQUENCY/rad.s^-1.	$K_{yy}$ /N.m^-1.	$K_{xx}$ /N.m^-1.	$K_{xy}$ /N.m^-1.	$K_{yx}$ /N.m^-1.	$C_{yy}$ /N.s.m^-1.	$C_{xx}$ /N.s.m^-1.	$C_{xy}$ /N.s.m^-1.	$C_{yx}$ /N.s.m^-1.
5.20E+01	6.33E+09	5.04E+09	1.46E+08	1.81E+09	4.11E+07	2.70E+07	4.11E+07	2.70E+07
1.05E+02	5.24E+09	4.41E+09	-1.78E+08	1.89E+09	1.90E+07	1.57E+07	1.90E+07	1.57E+07
1.57E+02	4.23E+09	4.01E+09	-7.11E+08	1.96E+09	1.08E+07	1.24E+07	1.08E+07	1.24E+07
2.09E+02	3.96E+09	4.20E+09	-1.22E+09	2.09E+09	7.36E+06	1.20E+07	7.36E+06	1.20E+07
2.62E+02	3.96E+09	4.43E+09	-1.95E+09	2.28E+09	3.94E+07	1.25E+07	4.14E+06	1.25E+07

FIG A-2a OUTPUT FROM THE TWO-OIL-FILM BEARING PROGRAM

INPUT THE HYDROSTATIC BEARING OIL FILM COEFFICIENTS IN THE SAME FORMAT AS THAT WITH WHICH THE JOURNAL BEARING OIL FILM COEFFICIENTS WERE INPUT, BEGINNING EACH LINE WITH A NEW VALUE OF LOAD (OR FREQUENCY)

USING THE FOLLOWING HYDROSTATIC BEARING DATA :-

FREQUENCY/rad.s <sup>-1</sup>	Kyy/N.m <sup>-1</sup>	Kyx/N.m <sup>-1</sup>	Kxy/N.m <sup>-1</sup>	Kxx/N.m <sup>-1</sup>
5.20E+01	2.42E+09	0.00E+00	0.00E+00	2.47E+09
1.05E+02	2.42E+09	0.00E+00	0.00E+00	2.47E+09
1.57E+02	2.42E+09	0.00E+00	0.00E+00	2.47E+09
2.09E+02	2.42E+09	0.00E+00	0.00E+00	2.47E+09
2.62E+02	2.42E+09	0.00E+00	0.00E+00	2.47E+09

FREQUENCY/rad.s <sup>-1</sup>	Cyy/N.s.m <sup>-1</sup>	Cyx/N.s.m <sup>-1</sup>	Cxy/N.s.m <sup>-1</sup>	Cxx/N.s.m <sup>-1</sup>
5.20E+01	1.74E+08	0.00E+00	0.00E+00	1.72E+08
1.05E+02	1.74E+08	0.00E+00	0.00E+00	1.72E+08
1.57E+02	1.74E+08	0.00E+00	0.00E+00	1.72E+08
2.09E+02	1.74E+08	0.00E+00	0.00E+00	1.72E+08
2.62E+02	1.74E+08	0.00E+00	0.00E+00	1.72E+08

2 - OIL - FILM BEARING COEFFICIENTS

FREQUENCY/rad.s <sup>-1</sup>	Kyy/N.m <sup>-1</sup>	Kyx/N.m <sup>-1</sup>	Kxy/N.m <sup>-1</sup>	Kxx/N.m <sup>-1</sup>
5.20E+01	1.99E+09	1.71E+09	-1.90E+08	1.12E+09
1.05E+02	2.48E+09	2.33E+09	-3.65E+08	1.41E+09
1.57E+02	2.50E+09	2.59E+09	-6.71E+08	1.60E+09
2.09E+02	2.59E+09	2.97E+09	-1.04E+09	1.77E+09
2.62E+02	2.69E+09	3.25E+09	-1.55E+09	1.98E+09

FREQUENCY/rad.s <sup>-1</sup>	Cyy/N.s.m <sup>-1</sup>	Cyx/N.s.m <sup>-1</sup>	Cxy/N.s.m <sup>-1</sup>	Cxx/N.s.m <sup>-1</sup>
5.20E+01	8.65E+07	2.71E+07	1.63E+07	1.90E+07
1.05E+02	5.69E+07	1.67E+07	1.10E+07	1.33E+07
1.57E+02	4.16E+07	1.02E+07	7.00E+06	1.19E+07
2.09E+02	3.42E+07	7.27E+06	4.92E+06	1.09E+07
2.62E+02	3.21E+07	4.44E+06	2.54E+06	1.13E+07

FIG A-2b OUTPUT FROM THE TWO-OIL-FILM BEARING PROGRAM

APPENDIX B

COMPUTER PROGRAMS



APPENDIX B

COMPUTER PROGRAMS

B-1 Hydrostatic Bearing Design Program

This program is based on the theory developed in chapter 3, and determines both the static and dynamic characteristics for a hydrostatic bearing, the geometry and oil supply details being input data.

```

10 PRINT
20 OPTION BASE 1
30 DIM Sh(4,4),Ss(4,4),St(4,4),Ish(4,4),Iss(4,4),Ist(4,4),A(1:12)
40 REM START BLOCK A
50 REM : START BLOCK AA
60 PRINT "HYDROSTATIC BEARING RING THEORETICAL ANALYSIS USING RAIMONDI & BOYD AP
PROXIM'H.:";
70 PRINT "-----";
80 PRINT " THIS PROGRAM ASSUMES TWO PLANES OF HYDROSTATIC BEARINGS, WITH FOUR
HYDROSTATICPADS PER PLANE ARRANGED AROUND A STEEL RING. IN EACH PLANE THERE ";
90 PRINT "IS ONE TOP, ONEBOTTOM, ONE LEFT, AND ONE RIGHT PAD. IN THE CENTRE OF T
HE STEEL RING IS ASSUMED TO BE A JOURNAL BEARING. THE PROGRAM DETERMINES THE";
100 PRINT " EIGHT BEARING COEFFICIENTS FOR THE HYDROSTATIC BEARING RING, AND, I
F REQUIRED, ADDS THESE, IN A SUITABLE MANNER, TO THE EIGHT COEFFICIENTS OF ";
110 PRINT "THE JOURNAL BEARING WHICH MUST BE INPUT.:";
120 PRINT
130 PRINT
140 PRINT "SELECT PROGRAM OUTPUT REQUIRED BY TYPING THE APPROPRIATE NUMBER:-";LI
NK(1);
150 PRINT "1 : OUTPUT FOR INDIVIDUAL PADS ONLY";LINK(1);
160 PRINT "2 : OUTPUT FOR COMPLETE HYDROSTATIC RING ONLY";LINK(1);
170 PRINT
180 PRINT
190 INPUT Cv1
200 IF Cv1>2 THEN 140
210 IF Cv1<1 THEN 140
220 PRINT "SELECT FORM OF OUTPUT DESIRED BY TYPING THE APPROPRIATE NUMBER:-";LIN
K(1)
230 PRINT "1 : TABULATED OUTPUT";LINK(0)
240 PRINT "2 : GRAPHICAL OUTPUT";LINK(1)
250 INPUT Cv2
260 IF Cv2<1 THEN 220
270 IF Cv2>2 THEN 220
280 REM : END OF BLOCK AA
290 REM : START BLOCK AB
300 DISP "MIN. VALUE OF STEADY X DISPLACEMENT TO BE EXAMINED";
310 INPUT Xmin
320 DISP "MAX. VALUE OF STEADY X DISPLACEMENT TO BE EXAMINED";
330 INPUT Xmax

```

```

340 DISP "STEP IN X REQUIRED";
350 INPUT Xstep
360 DISP "MIN. VALUE OF STEADY Y DISPLACEMENT TO BE EXAMINED";
370 INPUT Ymin
380 DISP "MAX. VALUE OF STEADY Y DISPLACEMENT TO BE EXAMINED";
390 INPUT Ymax
400 DISP "STEP IN Y REQUIRED";
410 INPUT Ystep
420 REM : END BLOCK AB
430 REM : START BLOCK AC
440 REM : START BLOCK ACA
450 DISP "WHAT VERTICAL VIBRATION AMPLITUDE IN m.";
460 INPUT Y0
470 DISP "WHAT HORIZONTAL VIBRATION AMPLITUDE IN m.";
480 INPUT X0
490 DISP "WHAT PHASE OF HORIZONTAL VIBRATION w.r.t. VERTICAL VIBRATION, IN rad
";
500 INPUT B
510 DISP "WHAT BEARING RADIUS OF CURVATURE, IN m.";
520 INPUT R
530 DISP "WHAT SUPPLY PRESSURE, IN Pa.";
540 INPUT P1
550 DISP "WHAT OIL DYNAMIC VISCOSITY, IN Pa.s.";
560 INPUT U
570 DISP "WHAT FREQUENCY OF VIBRATION, IN rad.s^(-1).";
580 INPUT F
590 REM : END OF BLOCK ACA
600 REM : START BLOCK ACB
610 IMAGE "THESE RESULTS ARE FOR :- VERTICAL VIBRATION AMPLITUDE ="D,DDE"m."
620 PRINT USING 610;Y0
630 IMAGE "
HORIZONTAL VIBRATION AMPLITUDE ="D,DDE"m."
640 PRINT USING 630;X0
650 IMAGE "
HORIZONTAL VIB'N. PHASE w.r.t. VERTICAL VIB'N. ="D,DDE"rad."
660 PRINT USING 650;B
670 IMAGE "
BEARING RADIUS OF CURVATURE ="D,DDE"m."
680 PRINT USING 670;R
690 IMAGE "
BEARING SUPPLY PRESSURE ="D,DDE"Pa."
700 PRINT USING 690;P1
710 IMAGE "
OIL DYNAMIC VISCOSITY ="D,DDE"Pa.s."

```

```

720 PRINT USING 710;U
730 IMAGE "
^(-1)."
FREQUENCY OF VIBRATION ="D.DDE"rad.s
740 PRINT USING 730;F
750 PRINT
760 REM : END OF BLOCK ACB
770 REM : START BLOCK ACC
780 FOR Padno=1 TO 4
790 PRINT "THIS NEXT BLOCK OF INPUT DATA IS FOR PAD NUMBER ";Padno;LIN(1);
800 DISP "WHAT HALF ANGLE FROM C.L. TO LAND CENTRE, IN rad.";
810 INPUT A3(Padno)
820 DISP "WHAT BEARING LENGTH FROM LAND C.L. TO LAND C.L., IN m.";
830 INPUT L(Padno)
840 DISP "WHAT BEARING LAND WIDTH, IN m.";
850 INPUT D(Padno)
860 DISP "WHAT BEARING DESIGN CLEARANCE, IN m.";
870 INPUT C(Padno)
875 IF Padno=1 THEN C(Padno)=C(Padno)*4/3
876 IF Padno=2 THEN C(Padno)=C(Padno)*4/3
880 DISP "WHAT BEARING OPERATING PARAMETER B RATIO, Ø<B<1, B DIMENSIONLESS";
890 INPUT R1(Padno)
900 DISP "WHAT RATIO OF SUPPLY OIL LINE RESISTANCE TO ACCUMULATOR OIL LINE RESI
STANCE";
910 INPUT R2(Padno)
920 DISP "WHAT ACCUMULATOR OPERATING PARAMETER, IN N.m^5.
";
930 INPUT B1(Padno)
940 DISP "WHAT SUPPLY LINE OIL INERTIA COEFFICIENT, IN Kg.m^-4.";
950 INPUT C1(Padno)
960 DISP "WHAT ACCUMULATOR LINE OIL INERTIA COEFFICIENT, IN Kg.m^-4.";
970 INPUT C2(Padno)
980 DISP SPA(100)
990 REM : END OF BLOCK ACC
1000 REM : START BLOCK ACC
1010 IMAGE "PAD NO."D"DESIGN SPEC'N. IS :-"
1020 PRINT USING 1010;Padno
1030 IMAGE "
HALF ANGLE FROM CENTRE LINE TO LAND CENTRE ="D.DDE"rad."
1040 PRINT USING 1030;A3(Padno)
1050 IMAGE "
BEARING LENGTH FROM LAND C.L. TO LAND C.L.="D.DDE"m."
1060 PRINT USING 1050;L(Padno)

```

```

1070 IMAGE "
1080 PRINT USING 1070;D(Padno)
1090 IMAGE "
1100 PRINT USING 1090;C(Padno)
1110 IMAGE "
1120 PRINT USING 1110;R1(Padno)
1130 IMAGE "
1140 PRINT USING 1130
1150 IMAGE "
1160 PRINT USING 1150;R2(Padno)
1170 IMAGE "
"
1180 PRINT USING 1170;B1(Padno)
1190 IMAGE "
-4."
1200 PRINT USING 1190;C1(Padno)
1210 IMAGE "
-4."
1220 PRINT USING 1210;C2(Padno)
1230 PRINT LIN(1)
1240 REM : END OF BLOCK ACD
1250 NEXT Padno
1260 FOR Xj=Xmin TO Xmax STEP Xstep
1270 IF CV2=2 THEN GOSUB 4330
1280 FOR Yj=Ymin TO Ymax STEP Ystep
1290 REM : START BLOCK HE
1300 REM : START BLOCK HEA
1310 REM : NOW CALCULATE STEADY X & Y DISPLACEMENTS VALID FOR EACH INDIVIDUAL PA
D.
1320 Y(1)=-Yj
1330 X(1)=-Xj
1340 Y(3)=-Xj
1350 X(3)=Yj
1360 Y(2)=Yj
1370 X(2)=Xj
1380 Y(4)=Xj
1390 X(4)=-Yj
1400 REM : DETERMINE VIBRATION AMPLITUDES VALID FOR EACH INDIVIDUAL PAD
1410 X0(1)=X0(2)=Y0(3)=Y0(4)=X0
1420 Y0(1)=Y0(2)=X0(3)=X0(4)=Y0

```

```

LAND WIDTH ="D.DDE"m."
BEARING DESIGN CLEARANCE ="D.DDE"m."
OPERATING PARAMETER B RATIO ="D.DDE
RATIO OF OIL SUPPLY LINE RESISTANCE "
TO ACCUMULATOR OIL LINE RESISTANCE ="D.DDE
ACCUMULATOR OPERATING PARAMETER ="D.DDE"H.m^5
SUPPLY LINE OIL INERTIA COEFFICIENT ="D.DDE"Kg.m^4
ACCUMULATOR LINE OIL INERTIA COEFFICIENT ="D.DDE"Kg.m^4

```

```
1430 REM : DETERMINE PHASE OF X VIB'N. w.r.t. Y VIB'N. VALID FOR EACH INDIVIDUAL
PAD.
1440 B(1)=B(2)=B
1450 B(3)=B(4)=B
1460 REM : END OF BLOCK AEA
1470 REM : START OF BLOCK AEB
1480 REM : SETTING VARIABLES OF EQUATIONS TO CORRECT VALUE FOR PAD
1490 FOR Padno=1 TO 4
1500 X=X(Padno)
1510 Y=Y(Padno)
1520 X0=X0(Padno)
1530 Y0=Y0(Padno)
1540 A=As(Padno)
1550 L=L(Padno)
1560 D=D(Padno)
1570 C=C(Padno)
1580 R1=R1(Padno)
1590 R2=R2(Padno)
1600 B1=B1(Padno)
1610 B=B(Padno)
1620 C1=C1(Padno)
1630 C2=C2(Padno)
1640 REM : END OF BLOCK AEB
1650 REM : START BLOCK AEC
1660 REM : START BLOCK AEA
1670 REM : EVALUATION OF FUNCTIONS OF THE SIMULTANEOUS EQUATIONS TO BE SOLVED
1680 REM : SETTING MARKER TO 1 TO SHOW THAT PRESSURE AMPLITUDES AND PHASE ANGLES
CORRESPONDING TO INPUT DATA ARE BEING CALCULATED
1690 M=0
1700 REM : END OF BLOCK AEA
1710 REM : START BLOCK AEB
1720 M=M+1
1730 REM : END OF BLOCK AEB
1740 REM : START BLOCK AEC
1750 REM : FIRST, SET X VIBRATION COMPONENTS TO CORRECT VALUE
1760 X01=X0*Cos(B)
1770 X02=X0*SIN(B)
1780 REM : NEXT DETERMINE MAGNITUDE OF F(x,y) USED TO DESCRIBE FLOW OUT OF POCKET
OVER LANDS
```

```

1790 Fxy=C^3/12/U/D*(4*R*A+2*L+6*Y/C*(2*R*SIN(A)+L*COS(A))+1/C^2*((X^2+Y^2)*R*A*
6+3*R*SIN(2*A)*(Y^2-X^2)+6*Y^2*L*COS(A)^2+6*X^2*L*SIN(A)^2))
1800 Fxy=Fxy+1/12/U/D*(4*R*Y^3*(SIN(A)-SIN(A)^3/3)+12*R*X^2*Y*SIN(A)^3/3+2*L*Y^3
*COS(A)^3+6*L*X^2*Y*SIN(A)^2*COS(A))
1810 REM : NOW CALCULATE PPO, THE STEADY BEARING POCKET PRESSURE
1820 Ppo=P1*(R1/(1-R1))*(2*L+4*R*A)/(R1/(1-R1))*(2*L+4*R*A)+12*U*D/C^3*Fxy)
1830 REM : NOW CALCULATE Q( I ), THE OIL FLOW FOR PAD NO. I
1840 Q(Padno)=Ppo*Fxy
1850 REM : DETERMINE TOTAL EFFECTIVE PAD AREA, Ap.
1860 Ap=R*2*A*L
1870 F(Padno)=Ap*Ppo
1880 REM : F( I ) IS LOAD ON PAD NO. I
1890 P(Padno)=Q(Padno)*P1
1900 REM : P( I ) IS PUMPING POWER REQUIRED FOR PAD NO. I
1910 REM : EVALUATE THE DIFFERENTIAL OF Fxy w.r.t. X
1920 Fx=C^3/12/U/D*(1/C^2*(12*R*A*X-6*R*X*SIN(2*A)+12*X*L*SIN(A)^2)+1/C^3*(24*R*
X*Y*SIN(A)^3/3+12*L*X*Y*SIN(A)^2*COS(A)))
1930 REM : EVALUATE THE DIFFERENTIAL OF Fxy w.r.t. Y
1940 Fy=C^3/12/U/D*(1/C*(12*R*SIN(A)+6*L*COS(A))+1/C^2*(12*Y*R*A+6*R*Y*SIN(2*A)+
12*L*Y*COS(A)^2)+1/C^3*(12*R*Y^2*(SIN(A)-SIN(A)^3/3)))
1950 Fy=Fy+1/12/U/D*(12*R*X^2*SIN(A)^3/3+6*L*Y^2*COS(A)^3+6*L*X^2*SIN(A)^2*COS(A
))
1960 REM : DETERMINE INVERSE SUPPLY OIL LINE RESISTANCE
1970 Ks=C^3*(2*L+4*R*A)/12/U/D*R1/(1-R1)
1980 REM : DETERMINE INVERSE ACCUMULATOR OIL LINE RESISTANCE
1990 Ka=R2*Ks
2000 REM : DETERMINE COEFFICIENTS OF SIMULTANEOUS EQUATIONS
2010 V(1,1)=V(2,2)=V(3,5)=V(4,6)=V(7,7)=V(8,8)=-1
2020 V(1,2)=V(1,5)=V(1,6)=V(1,7)=V(1,8)=V(2,1)=V(2,5)=V(2,6)=V(2,7)=V(2,8)=0
2030 V(3,2)=V(3,3)=V(3,4)=V(3,5)=V(4,1)=V(4,3)=V(4,4)=V(4,5)=V(5,1)=V(5,2)=V(5,3
)=V(5,4)=V(5,5)=V(5,8)=V(6,1)=V(6,2)=V(6,3)=V(6,4)=V(6,6)=V(6,7)=V(7,2)=0
2040 V(7,4)=V(7,5)=V(7,6)=V(7,8)=V(8,1)=V(8,3)=V(8,5)=V(8,7)=0
2050 V(1,3)=V(2,4)=-1/Ks
2060 V(1,4)=C1*F
2070 V(2,3)=-C1*F
2080 V(3,1)=V(4,2)=V(7,3)=V(8,4)=1
2090 V(3,7)=V(4,8)=-1/Ka
2100 V(3,8)=F*D2
2110 V(4,7)=-F*D2
2120 V(5,6)=-F

```

```
2130 V(5,7)=V(6,8)=-B1
2140 V(6,5)=F
2150 V(7,1)=V(8,2)=-Fxy
2160 V(1,9)=V(2,9)=V(3,9)=V(4,9)=V(5,9)=V(6,9)=0
2170 V(7,9)=Ppo*Fx*X01+Ppo*Fy*Y0
2180 V(8,9)=Ap*F*Y0+Ppo*Fx*X02
2190 REM : N IS THE NO. OF EQU'NS. (AND UNKNOWNS)
2200 N=8
2210 REM : BEGIN SOLN. OF SIMULTANEOUS EQUATIONS
2220 GOSUB 3870
2230 REM : END OF SIMULTANEOUS EQU'N. SOL'N.
2240 E=SQR(A(1)^2+A(2)^2)
2250 A(9)=ABS(A(1))
2260 A(10)=ABS(A(2))
2270 IF A(9)=0 THEN 2300
2280 De=ATN(A(10)/A(9))
2290 GOTO 2310
2300 De=PI/2
2310 IF A(2)>0 THEN 2330
2320 De=-De
2330 IF A(1)>0 THEN 2350
2340 De=PI-De
2350 G=SQR(A(5)^2+A(6)^2)
2360 A(11)=ABS(A(5))
2370 A(12)=ABS(A(6))
2380 IF A(11)=0 THEN 2410
2390 S=ATN(A(12)/A(11))
2400 GOTO 2420
2410 S=PI/2
2420 IF A(6)>0 THEN 2440
2430 S=-S
2440 IF A(5)>0 THEN 2470
2450 S=PI-S
2460 REM : END OF BLOCK RECC
2470 IF M>1 THEN 2550
2480 REM : START BLOCK RECD
2490 E(Padno)=E
2500 De(Padno)=De
2510 G(Padno)=G
2520 S(Padno)=S
```



```

2530 REM : END OF BLOCK RECD
2540 REM : START BLOCK RECE
2550 REM :PUTTING X VIBRATION AMPLITUDE TO 0 IN ORDER TO CALCULATE Kyy AND Cyy
2560 X0=0
2570 Y0=1.0E-5
2580 REM : END OF BLOCK RECE
2590 IF M<2 THEN 1720
2600 IF M=3 THEN 2660
2610 REM : START BLOCK RECF
2620 Kyy=-Ap*A(1)/Y0
2630 Cyy=-Ap*A(2)/Y0/F
2640 REM : END OF BLOCK RECF
2650 REM : START BLOCK RECG
2660 REM :ASSIGNING A VALUE TO X VIBRATION AMPLITUDE IN ORDER TO CALCULATE Kyy A
ND Cyy
2670 X0=1.0E-5
2680 Y0=0
2690 REM : END OF BLOCK RECG
2700 IF M<3 THEN 1720
2710 REM : START BLOCK RECH
2720 Kyx=Ap*E*(SIN(B)^2+COS(B)*COS(De))/X0
2730 Cyx=Ap*E*SIN(De-B)/F/X0
2740 REM : END OF BLOCK RECH
2750 REM : START OF BLOCK RECI
2760 Kyy(Padno)=Kyy
2770 Cyy(Padno)=Cyy
2780 Kyx(Padno)=Kyx
2790 Cyx(Padno)=Cyx
2800 REM : END OF BLOCK RECI
2810 REM : END OF BLOCK REC
2820 NEXT Padno
2830 REM : END OF BLOCK REB
2840 IF Cv1=2 THEN 3180
2850 REM : START BLOCK REC
2860 IF Cv2=1 THEN GOTO 2920
2870 REM : (THUS STARTING BLOCK RECA)
2880 REM : START BLOCK RECB
2890 GOSUB 7320
2900 REM : END C BLOCK RECB
2910 GOTO 3720

```

```

2920 REM : START BLOCK AECA
2930 IF Xj>Xmin THEN 2970
2940 IF Yj>Ymin THEN 2970
2950 PRINT LIN(1)
2960 PRINT "INDIVIDUAL PAD PERFORMANCE CHARACTERISTICS - FOR THESE COEFFICIENTS
THE Y DIRECTION IS THE DIRECTION NORMAL TO THAT PAD : -";LIN(0)
2970 PRINT LIN(1)
2980 IMAGE "THIS OUTPUT FOR HYDROSTATIC RING DISPLACEMENTS X="MD.DDE" m. & Y="M
D.DDE" m."
2990 PRINT USING 2980;Xj,Yj
3000 PRINT LIN(0)
3010 PRINT "BEARING PARAMETER PAD 1 PAD 2 PAD 3
PAD 4";LIN(1)
3020 IMAGE 5X"Kyy"6X"/ N.m^-1."4X,MD.DDDE,3X,MD.DDDE,3X,MD.DDDE,3X,MD.DDDE
3030 IMAGE 5X"Kyx"6X"/ N.m^-1."4X,MD.DDDE,3X,MD.DDDE,3X,MD.DDDE,3X,MD.DDDE
3040 IMAGE 5X"Cyy"6X"/ N.s.m^-1."2X,MD.DDDE,3X,MD.DDDE,3X,MD.DDDE,3X,MD.DDDE
3050 IMAGE 5X"Cyx"6X"/ N.s.m^-1."2X,MD.DDDE,3X,MD.DDDE,3X,MD.DDDE,3X,MD.DDDE
3060 IMAGE "PUMPING POWER / W."9X,MD.DDDE,3X,MD.DDDE,3X,MD.DDDE,3X,MD.DDDE
3070 IMAGE "OIL FLOW / m^3.s^-1."2X,MD.DDDE,3X,MD.DDDE,3X,MD.DDDE,3X,MD.DDDE
E
3080 IMAGE "LOAD / N."9X,MD.DDDE,3X,MD.DDDE,3X,MD.DDDE,3X,MD.DDDE
3090 PRINT USING 3020;Kyy(1);Kyy(2);Kyy(3);Kyy(4)
3100 PRINT USING 3030;Kyx(1);Kyx(2);Kyx(3);Kyx(4)
3110 PRINT USING 3040;Cyy(1);Cyy(2);Cyy(3);Cyy(4)
3120 PRINT USING 3050;Cyx(1);Cyx(2);Cyx(3);Cyx(4)
3130 PRINT USING 3060;P(1);P(2);P(3);P(4)
3140 PRINT USING 3070;Q(1);Q(2);Q(3);Q(4)
3150 PRINT USING 3080;F(1);F(2);F(3);F(4)
3160 REM : END OF BLOCK AECA
3170 GOTO 3720
3180 REM : START BLOCK AED
3190 Kxxh=(Kyy(3)+Kyy(4))*2
3200 Kxyh=(Kyx(3)+Kyx(4))*-2
3210 Kyyh=(Kyy(1)+Kyy(2))*2
3220 Kyxh=(Kyx(1)+Kyx(2))*2
3230 Cxxh=(Cyy(3)+Cyy(4))*2
3240 Cxyh=(Cyx(3)+Cyx(4))*-2
3250 Cyyh=(Cyy(1)+Cyy(2))*2
3260 Cyxh=(Cyx(1)+Cyx(2))*2
3270 Oh=(O(1)+O(2)+O(3)+O(4))*2

```

```

3280 Ph=(P(1)+P(2)+P(3)+P(4))*2
3290 Fyh=(F(1)-F(2))*2
3300 Fxh=(F(3)-F(4))*2
3310 REM : END OF BLOCK AED
3320 REM : START BLOCK AEE
3330 IF Cv2=2 THEN GOTO 3680
3340 REM : START BLOCK AEEA
3350 IMAGE 5X"Kyy / N.m^-1."27X,MD.DDDE
3360 IMAGE 5X"Kyx / N.m^-1."27X,MD.DDDE
3370 IMAGE 5X"Kxx / N.m^-1."27X,MD.DDDE
3380 IMAGE 5X"Kxy / N.m^-1."27X,MD.DDDE
3390 IMAGE 5X"Cyy / N.s.m^-1."25X,MD.DDDE
3400 IMAGE 5X"Cyx / N.s.m^-1."25X,MD.DDDE
3410 IMAGE 5X"Cxx / N.s.m^-1."25X,MD.DDDE
3420 IMAGE 5X"Cxy / N.s.m^-1."25X,MD.DDDE
3430 IMAGE 5X"DOWNWARD LOAD / N."22X,MD.DDDE
3440 IMAGE 5X"SIDWAYS LOAD (from pad 4 to 3) / N."4X,MD.DDDE
3450 IMAGE 5X"PUMPING POWER / W."22X,MD.DDDE
3460 IMAGE 5X"OIL FLOW / m^3.s^-1."20X,MD.DDDE
3470 PRINT LINK(1)
3480 IMAGE "THIS OUTPUT FOR X="MD.DDE" m. & Y="",MD.DDE" m."
3490 PRINT USING 3480;Xj,Yj
3500 PRINT LINK(0)
3510 PRINT "HYDROSTATIC BEARING PARAMETER
3520 PRINT "-----"
3530 PRINT USING 3350;Kyyh
3540 PRINT USING 3360;Kyxh
3550 PRINT USING 3370;Kxxh
3560 PRINT USING 3380;Kxyh
3570 PRINT USING 3390;Cyyh
3580 PRINT USING 3400;Cyxh
3590 PRINT USING 3410;Cxxh
3600 PRINT USING 3420;Cxyh
3610 PRINT USING 3430;-Fyh
3620 PRINT USING 3440;Fxh
3630 PRINT USING 3450;Ph
3640 PRINT USING 3460;Qh
3650 REM : END OF BLOCK AEEA
3660 REM : END OF BLOCK ADG
3670 GOTO 3720

```

```

VALUE";LIN(0)
-----";LIN(0)

```

```

3680 REM : START BLOCK AEEB
3690 GOSUB 7520
3700 REM : END OF BLOCK AEEB
3710 REM : END OF BLOCK AEE
3720 NEXT Yj
3730 IF CV2=1 THEN GOTO 3830
3740 REM : START BLOCK AF
3750 DUMP GRAPHICS
3760 EXIT GRAPHICS
3770 REM : END OF BLOCK AF
3780 REM : START BLOCK AG
3790 IF CV1=1 THEN GOSUB 7790
3800 IF CV1=2 THEN GOSUB 8100
3810 PRINT PAGE
3820 REM : END OF BLOCK AG
3830 NEXT Xj
3840 BEEP
3850 DISP "PROGRAM RUN COMPLETE";
3860 END
3870 REM : SUBROUTINE FOR SIMULTANEOUS EQUATION SOLUTION
3880 REM : THE COEFFICIENTS OF THE N EQUATIONS ARE THE MATRIX V(N,N+1)
3890 REM : THE ANSWERS ARE THE MATRIX A(N)
3900 REM : THE SUFFICES i ARE TO DISTINGUISH SUB-VARIABLES OF SIMULTANEOUS EQUATI
ON SOL'N. FROM MAIN VARIABLES OF PROGRAM - THE TWO ARE NOT RELATED
3910 FOR Qi=1 TO N-1
3920 Bi=V(Qi,Qi)
3930 Di=0
3940 FOR Ii=Qi+1 TO N
3950 Gi=V(Ii,Qi)
3960 IF ABS(Gi)>ABS(Bi) THEN 3980
3970 GOTO 4040
3980 Xi=Xi
3990 Di=1
4000 Mi=Ii
4010 Bi=Gi
4020 REM : Di IS 1 IF A ROW INTERCHANGE IS REQUIRED
4030 REM : Mi IS THE ROW WITH THE LARGEST ELEMENT
4040 NEXT Ii
4050 IF Di<>1 THEN 4130
4060 REM : INTERCHANGE ROWS IF NECESSARY

```

```

4070 FOR Zi=Qi TO N+1
4080 Ci=V(Mi,Zi)
4090 REM :Ci IS AN INTERMEDIATE VARIABLE
4100 V(Mi,Zi)=V(Qi,Zi)
4110 V(Qi,Zi)=Ci
4120 NEXT Zi
4130 Xi=0
4140 FOR Pi=Qi+1 TO N
4150 IF V(Pi,Qi)=0 THEN 4210
4160 Fi=V(Pi,Qi)/V(Qi,Qi)
4170 FOR Ni=Qi+1 TO N+1
4180 V(Pi,Ni)=V(Pi,Ni)-Fi*V(Qi,Ni)
4190 Xi=Xi
4200 NEXT Ni
4210 NEXT Pi
4220 NEXT Qi
4230 REM :CALCULATE ANSWERS BY BACK SUBSTITUTION
4240 FOR Ii=N TO 1 STEP -1
4250 Ai=0
4260 FOR Ji=Ii+1 TO N
4270 Ai=Ai+V(Ii,Ji)*A(Ji)
4280 NEXT Ji
4290 A(Ii)=(V(Ii,N+1)-Ai)/V(Ii,Ii)
4300 NEXT Ii
4310 REM :END OF SIMULTANEOUS EQU'N. SOL'N.
4320 RETURN
4330 REM : START BLOCK AD
4340 IF Cv1=1 THEN GOTO 4600
4350 REM : START BLOCK ADB
4360 PRINT "THE CHOICE OF PARAMETERS TO BE PLOTTED AGAINST EACH OTHER IS: -";LINK
0)
4370 PRINT " 1 : Kyx";LIN(0)
4380 PRINT " 2 : Kyx";LIN(0)
4390 PRINT " 3 : Kxy";LIN(0)
4400 PRINT " 4 : Kxx";LIN(0)
4410 PRINT " 5 : Cyx";LIN(0)
4420 PRINT " 6 : Cyx";LIN(0)
4430 PRINT " 7 : Cxy";LIN(0)
4440 PRINT " 8 : Cxx";LIN(0)
4450 PRINT " 9 : Y DISPLACEMENT FOR RING";LIN(0)

```

```

4460 PRINT "10 : LOAD IN Y DIRECTION";LIN(0)
4470 PRINT "11 : TOTAL OIL FLOW";LIN(0)
4480 PRINT "12 : TOTAL PUMPING POWER";LIN(0)
4490 PRINT "SELECT OUTPUT DESIRED BY TYPING IN THE APPROPRIATE NUMBERS";LIN(1)
4500 DISP "WHICH X AXIS VARIABLE DO YOU REQUIRE";
4510 INPUT Vxpn
4520 IF Vxpn<1 THEN GOTO 4500
4530 IF Vxpn>12 THEN GOTO 4500
4540 DISP "WHICH Y AXIS VARIABLE DO YOU REQUIRE ";
4550 INPUT Vyprn
4560 IF Vyprn<1 THEN GOTO 4500
4570 IF Vyprn>12 THEN GOTO 4500
4580 REM : END OF BLOCK ADA
4590 GOTO 4830
4600 PRINT "THE CHOICE OF PARAMETERS TO BE PLOTTED AGAINST EACH OTHER IS:-";LINK
0)
4610 PRINT " 1 : Kyx";LIN(0)
4620 PRINT " 2 : Kyx";LIN(0)
4630 PRINT " 3 : Cyx";LIN(0)
4640 PRINT " 4 : Cyx";LIN(0)
4650 PRINT " 5 : Y DISPLACEMENT FOR RING";LIN(0)
4660 PRINT " 6 : LOAD ON HYDROSTATIC PAD";LIN(0)
4670 PRINT " 7 : OIL FLOW FOR PAD";LIN(0)
4680 PRINT " 8 : PUMPING POWER FOR PAD";LIN(0)
4690 PRINT "SELECT OUTPUT DESIRED BY TYPING IN THE APPROPRIATE NUMBERS";LIN(1)
4700 DISP "WHICH X AXIS VARIABLE DO YOU REQUIRE";
4710 INPUT Vxpn
4720 IF Vxpn<1 THEN GOTO 4700
4730 IF Vxpn>8 THEN GOTO 4700
4740 DISP "WHICH Y AXIS VARIABLE DO YOU REQUIRE";
4750 INPUT Vyprn
4760 IF Vyprn<1 THEN GOTO 4740
4770 IF Vyprn>8 THEN GOTO 4740
4780 DISP "INPUT THE PAD NUMBER FOR THE PAD THAT YOU WISH TO EXAMINE";
4790 INPUT Vpn
4800 IF Vpn<1 THEN GOTO 4780
4810 IF Vpn>4 THEN GOTO 4780
4820 REM : END OF BLOCK ADA
4830 REM : START BLOCK ADC
4840 DISP "WHAT MIN. VALUE OF X SCALE DO YOU REQUIRE";

```

```
4850 INPUT Sxmin
4860 DISP "WHAT MAX. VALUE OF X SCALE DO YOU REQUIRE";
4870 INPUT Sxmax
4880 IF Sxmax<=Sxmin THEN GOTO 4840
4890 DISP "WHAT MIN. VALUE OF Y SCALE DO YOU REQUIRE";
4900 INPUT Symin
4910 DISP "WHAT MAX. VALUE OF Y SCALE DO YOU REQUIRE";
4920 INPUT Symax
4930 IF Symax<=Symin THEN GOTO 4890
4940 PRINT PAGE
4950 GRAPHICS
4960 PLOTTER IS 13,"GRAPHICS"
4970 SCALE Sxmin,Sxmax,Symin,Symax
4980 Xint=0
4990 IF Sxmin>0 THEN Xint=Sxmin
5000 IF Sxmax<0 THEN Xint=Sxmax
5010 Yint=0
5020 IF Symin>0 THEN Yint=Symin
5030 IF Symax<0 THEN Yint=Symax
5040 AXES (Sxmax-Sxmin)/40,(Symax-Symin)/40,Xint,Yint,5,5
5050 FRAME
5060 REM : END OF BLOCK ADD
5070 REM : START BLOCK ADD
5080 REM : START BLOCK ADDA
5090 LDIR 0
5100 CSIZE 2
5110 IF Xint<(Sxmax+Sxmin)/2 THEN GOTO 5220
5120 IF Yint<(Symax+Symin)/2 THEN GOTO 5170
5130 MOVE Xint+(Sxmax-Sxmin)/5,Yint+(Symax-Symin)/40
5140 LORG 1
5150 Xgraph=1
5160 GOTO 5300
5170 MOVE Xint+(Sxmax-Sxmin)/5,Yint-(Symax-Symin)/40
5180 LORG 3
5190 Xgraph=2
5200 GOTO 5300
5210 REM : START BLOCK ADD
5220 IF Yint<(Symax+Symin)/2 THEN GOTO 5270
5230 MOVE Xint-(Sxmax-Sxmin)/5,Yint+(Symax-Symin)/40
5240 LORG 7
```

```
5250 Xgraph=3
5260 GOTO 5300
5270 MOVE Xint-(Sxmax-Sxmin)/5,Yint-(Symax-Symin)/40
5280 LORG 9
5290 Xgraph=4
5300 REM : END OF BLOCK ADDA
5310 IF Cv1=1 THEN GOTO 5590
5320 REM : START BLOCK ADDB
5330 IF Vxrn<>1 THEN GOTO 5350
5340 LABEL USING "17A";"Kyy<(ring)/N.m^-1."
5350 IF Vxrn<>2 THEN GOTO 5370
5360 LABEL USING "17A";"Kyx<(ring)/N.m^-1."
5370 IF Vxrn<>3 THEN GOTO 5390
5380 LABEL USING "17A";"Kxy<(ring)/N.m^-1."
5390 IF Vxrn<>4 THEN GOTO 5410
5400 LABEL USING "17A";"Kxx<(ring)/N.m^-1."
5410 IF Vxrn<>5 THEN GOTO 5430
5420 LABEL USING "17A";"Cyy<(ring)/N.s.m^-1."
5430 IF Vxrn<>6 THEN GOTO 5450
5440 LABEL USING "17A";"Cyx<(ring)/N.s.m^-1."
5450 IF Vxrn<>7 THEN GOTO 5470
5460 LABEL USING "17A";"Cxy<(ring)/N.s.m^-1."
5470 IF Vxrn<>8 THEN GOTO 5490
5480 LABEL USING "17A";"Cxx<(ring)/N.s.m^-1."
5490 IF Vxrn<>9 THEN GOTO 5510
5500 LABEL USING "10A";"Y<(ring)/m."
5510 IF Vxrn<>10 THEN GOTO 5530
5520 LABEL USING "16A";"Y LOAD (ring)/N."
5530 IF Vxrn<>11 THEN GOTO 5550
5540 LABEL USING "24A";"OIL FLOW/m^3.s^-1.<(ring)"
5550 IF Vxrn<>12 THEN GOTO 5570
5560 LABEL USING "22A";"PUMPING POWER/W.<(ring)"
5570 REM : END OF BLOCK ADDB
5580 GOTO 5850
5590 REM : START BLOCK ADDC
5600 IF Vxpn<>1 THEN GOTO 5620
5610 LABEL USING "4A,D,9A";"Kyy<;Ypn;">/N.m^-1."
5620 IF Vxpn<>2 THEN GOTO 5640
5630 LABEL USING "4A,D,9A";"Kyx<;Ypn;">/N.m^-1."
5640 IF Vxpn<>3 THEN GOTO 5660
```



```
5650 LABEL USING "4A,D,9A";"Kxy("<";Vpn;")>/N.m^-1."  
5660 IF Vxpn<>4 THEN GOTO 5680  
5670 LABEL USING "4A,D,9A";"Kxx("<";Vpn;")>/N.m^-1."  
5680 IF Vxpn<>5 THEN GOTO 5700  
5690 LABEL USING "4A,D,9A";"Cyy("<";Vpn;")>/N.s.m^-1."  
5700 IF Vxpn<>6 THEN GOTO 5720  
5710 LABEL USING "4A,D,9A";"Cyx("<";Vpn;")>/N.s.m^-1."  
5720 IF Vxpn<>7 THEN GOTO 5740  
5730 LABEL USING "4A,D,9A";"Cxy("<";Vpn;")>/N.s.m^-1."  
5740 IF Vxpn<>8 THEN GOTO 5760  
5750 LABEL USING "4A,D,9A";"Cxx("<";Vpn;")>/N.s.m^-1."  
5760 IF Vxpn<>9 THEN GOTO 5780  
5770 LABEL USING "10A";"Y(ring)/m."  
5780 IF Vxpn<>10 THEN GOTO 5800  
5790 LABEL USING "7A";"LOAD/N."  
5800 IF Vxpn<>11 THEN GOTO 5820  
5810 LABEL USING "18A";"OIL FLOW/m^3.s^-1."  
5820 IF Vxpn<>12 THEN GOTO 5840  
5830 LABEL USING "22A";"PUMPING POWER/W."  
5840 REM : END OF BLOCK ADDC  
5850 REM : START BLOCK ADDC  
5860 LDIR PI/2  
5870 IF Xgraph=1 THEN GOTO 6060  
5880 IF Xgraph=3 THEN GOTO 6060  
5890 IF Sxmin<>Xint THEN GOTO 5930  
5900 MOVE Xint+(Sxmax-Sxmin)/8,Yint-(Symax-Symin)/40  
5910 LORG 8  
5920 LABEL USING "MD.DDE";Sxmin+(Sxmax-Sxmin)/8  
5930 IF Sxmax<>Xint THEN GOTO 5970  
5940 MOVE Xint-(Sxmax-Sxmin)/8,Yint-(Symax-Symin)/40  
5950 LORG 8  
5960 LABEL USING "MD.DDE";Sxmax-(Sxmax-Sxmin)/8  
5970 IF Sxmax=Xint THEN GOTO 6010  
5980 MOVE Sxmax-(Sxmax-Sxmin)/40,Yint-(Symax-Symin)/40  
5990 LORG 9  
6000 LABEL USING "MD.DDE";Sxmax  
6010 IF Sxmin=Xint THEN GOTO 6050  
6020 MOVE Sxmin+(Sxmax-Sxmin)/40,Yint-(Symax-Symin)/40  
6030 LORG 7  
6040 LABEL USING "MD.DDE";Sxmin
```

```
6050 GOTO 6220
6060 IF Sxmin<>Xint THEN GOTO 6100
6070 MOVE Xint+(Sxmax-Sxmin)/8,Yint+(Symax-Symin)/40
6080 LORG 2
6090 LABEL USING "MD,DDE";Sxmin+(Sxmax-Sxmin)/8
6100 IF Sxmax<>Xint THEN GOTO 6140
6110 MOVE Xint-(Sxmax-Sxmin)/8,Yint+(Symax-Symin)/40
6120 LORG 2
6130 LABEL USING "MD,DDE";Sxmax-(Sxmax-Sxmin)/8
6140 IF Sxmax=Xint THEN GOTO 6180
6150 MOVE Sxmax-(Sxmax-Sxmin)/40,Yint+(Symax-Symin)/40
6160 LORG 3
6170 LABEL USING "MD,DDE";Sxmax
6180 IF Sxmin=Xint THEN GOTO 6220
6190 MOVE Sxmin+(Sxmax-Sxmin)/40,Yint+(Symax-Symin)/40
6200 LORG 1
6210 LABEL USING "MD,DDE";Sxmin
6220 REM : END OF BLOCK ADDE
6230 REM : START BLOCK ADDE
6240 LDIR PI/2
6250 IF Xgraph<>1 THEN GOTO 6290
6260 MOVE Xint+(Sxmax-Sxmin)/40,Yint+(Symax-Symin)/5
6270 LORG 3
6280 GOTO 6390
6290 IF Xgraph<>2 THEN GOTO 6330
6300 MOVE Xint+(Sxmax-Sxmin)/40,Yint-(Symax-Symin)/5
6310 LORG 9
6320 GOTO 6390
6330 IF Xgraph<>3 THEN GOTO 6370
6340 MOVE Xint-(Sxmax-Sxmin)/40,Yint+(Symax-Symin)/5
6350 LORG 1
6360 GOTO 6390
6370 MOVE Xint-(Sxmax-Sxmin)/40,Yint-(Symax-Symin)/5
6380 LORG 7
6390 REM : END OF BLOCK ADDE
6400 IF CV1=1 THEN GOTO 6480
6410 REM : START BLOCK ADDE
6420 IF Vyrn<>1 THEN GOTO 6440
6430 LABEL USING "17A";Kyy<ring>/N.m^-1."
6440 IF Vyrn<>2 THEN GOTO 6460
```

```

6450 LABEL USING "17A";"Kyx(ring)/N.m^-1."
6460 IF Vyrn<>3 THEN GOTO 6480
6470 LABEL USING "17A";"Kxy(ring)/N.m^-1."
6480 IF Vyrn<>4 THEN GOTO 6500
6490 LABEL USING "17A";"Kxx(ring)/N.m^-1."
6500 IF Vyrn<>5 THEN GOTO 6520
6510 LABEL USING "17A";"Cyy(ring)/N.s.m^-1."
6520 IF Vyrn<>6 THEN GOTO 6540
6530 LABEL USING "17A";"Cyx(ring)/N.s.m^-1."
6540 IF Vyrn<>7 THEN GOTO 6560
6550 LABEL USING "17A";"Cxy(ring)/N.s.m^-1."
6560 IF Vyrn<>8 THEN GOTO 6580
6570 LABEL USING "17A";"Cxx(ring)/N.s.m^-1."
6580 IF Vyrn<>9 THEN GOTO 6600
6590 LABEL USING "10A";"Y(ring)/m."
6600 IF Vyrn<>10 THEN GOTO 6620
6610 LABEL USING "16A";"Y LOAD (ring)/N."
6620 IF Vyrn<>11 THEN GOTO 6640
6630 LABEL USING "24A";"OIL FLOW/m^3.s^-1.(ring)"
6640 IF Vyrn<>12 THEN GOTO 6660
6650 LABEL USING "22A";"PUMPING POWER/W.(ring)"
6660 REM : END OF BLOCK ADDE
6670 GOTO 6940
6680 REM : START BLOCK ADDG
6690 IF Vyrn<>1 THEN GOTO 6710
6700 LABEL USING "4A,D,9A";"Kyy(";Vpn;")/N.m^-1."
6710 IF Vyrn<>2 THEN GOTO 6730
6720 LABEL USING "4A,D,9A";"Kyx(";Vpn;")/N.m^-1."
6730 IF Vyrn<>3 THEN GOTO 6750
6740 LABEL USING "4A,D,9A";"Kxy(";Vpn;")/N.m^-1."
6750 IF Vyrn<>4 THEN GOTO 6770
6760 LABEL USING "4A,D,9A";"Kxx(";Vpn;")/N.m^-1."
6770 IF Vyrn<>5 THEN GOTO 6790
6780 LABEL USING "4A,D,9A";"Cyy(";Vpn;")/N.s.m^-1."
6790 IF Vyrn<>6 THEN GOTO 6810
6800 LABEL USING "4A,D,9A";"Cyx(";Vpn;")/N.s.m^-1."
6810 IF Vyrn<>7 THEN GOTO 6830
6820 LABEL USING "4A,D,9A";"Cxy(";Vpn;")/N.s.m^-1."
6830 IF Vyrn<>8 THEN GOTO 6850
6840 LABEL USING "4A,D,9A";"Cxx(";Vpn;")/N.s.m^-1."

```

```
6850 IF Vypn<>9 THEN GOTO 6870
6860 LABEL USING "10A";"Y(ring)/m."
6870 IF Vypn<>10 THEN GOTO 6890
6880 LABEL USING "7A";"LOAD/N."
6890 IF Vypn<>11 THEN GOTO 6910
6900 LABEL USING "18A";"OIL FLOW/m^3.s^-1."
6910 IF Vypn<>12 THEN GOTO 6930
6920 LABEL USING "16A";"PUMPING POWER/W."
6930 REM : END OF BLOCK ADDS
6940 REM : START BLOCK ADDH
6950 LIIR 0
6960 IF Xgraph>2 THEN GOTO 7140
6970 IF Symax<>Yint THEN GOTO 7010
6980 MOVE Xint+(Sxmax-Sxmin)/40,Symax-(Symax-Symin)/8
6990 LORG 2
7000 LABEL USING "MD.DDE";Symax-(Symax-Symin)/8
7010 IF Symin<>Yint THEN GOTO 7050
7020 MOVE Xint+(Sxmax-Sxmin)/40,Symin+(Symax-Symin)/8
7030 LORG 2
7040 LABEL USING "MD.DDE";Symin+(Symax-Symin)/8
7050 IF Symax=Yint THEN GOTO 7090
7060 MOVE Xint+(Sxmax-Sxmin)/40,Symax-(Symax-Symin)/40
7070 LORG 3
7080 LABEL USING "MD.DDE";Symax
7090 IF Symin=Yint THEN GOTO 7130
7100 MOVE Xint+(Sxmax-Sxmin)/40,Symin+(Symax-Symin)/40
7110 LORG 1
7120 LABEL USING "MD.DDE";Symin
7130 GOTO 7300
7140 IF Symax<>Yint THEN GOTO 7180
7150 MOVE Xint-(Sxmax-Sxmin)/40,Symax-(Symax-Symin)/8
7160 LORG 8
7170 LABEL USING "MD.DDE";Symax-(Symax-Symin)/8
7180 IF Symin<>Yint THEN GOTO 7220
7190 MOVE Xint-(Sxmax-Sxmin)/40,Symin+(Symax-Symin)/8
7200 LORG 8
7210 LABEL USING "MD.DDE";Symin+(Symax-Symin)/8
7220 IF Symax=Yint THEN GOTO 7260
7230 MOVE Xint-(Sxmax-Sxmin)/40,Symax-(Symax-Symin)/40
7240 LORG 9
```

```
7250 LABEL USING "MD.DDE";Symax
7260 IF Symin=Yint THEN GOTO 7300
7270 MOVE Xint-(Sxmax-Sxmin)/40,Symint+(Symax-Symmin)/40
7280 LORG 7
7290 LABEL USING "MD.DDE";Symin
7300 REM : END OF BLOCK ADDH
7310 RETURN
7320 REM : START BLOCK RECB
7330 IF Vxpn=1 THEN Vx=Kyy(Vpn)
7340 IF Vxpn=2 THEN Vx=Kyx(Vpn)
7350 IF Vxpn=3 THEN Vx=Cyy(Vpn)
7360 IF Vxpn=4 THEN Vx=Cyx(Vpn)
7370 IF Vxpn=5 THEN Vx=Yj
7380 IF Vxpn=6 THEN Vx=F(Vpn)
7390 IF Vxpn=7 THEN Vx=0(Vpn)
7400 IF Vxpn=8 THEN Vx=P(Vpn)
7410 IF Vypn=1 THEN Vy=Kyy(Vpn)
7420 IF Vypn=2 THEN Vy=Kyx(Vpn)
7430 IF Vypn=3 THEN Vy=Cyy(Vpn)
7440 IF Vypn=4 THEN Vy=Cyx(Vpn)
7450 IF Vypn=5 THEN Vy=Yj
7460 IF Vypn=6 THEN Vy=F(Vpn)
7470 IF Vypn=7 THEN Vy=0(Vpn)
7480 IF Vypn=8 THEN Vy=P(Vpn)
7490 PLOT Vx,Vy
7500 REM : END OF BLOCK RECB.
7510 RETURN
7520 REM : START BLOCK REEB
7530 IF Vxpn=1 THEN Vx=Kyyh
7540 IF Vxpn=2 THEN Vx=Kyxh
7550 IF Vxpn=3 THEN Vx=Kxyh
7560 IF Vxpn=4 THEN Vx=Kxxh
7570 IF Vxpn=5 THEN Vx=Cyyh
7580 IF Vxpn=6 THEN Vx=Cyxh
7590 IF Vxpn=7 THEN Vx=Cxvh
7600 IF Vxpn=8 THEN Vx=Cxxh
7610 IF Vxpn=9 THEN Vx=Yj
7620 IF Vxpn=10 THEN Vx=Fyh
7630 IF Vxpn=11 THEN Vx=0h
7640 IF Vxpn=12 THEN Vx=Ph
```

```

7650 IF Vyrn=1 THEN Vy=Kyxx
7660 IF Vyrn=2 THEN Vy=Kyxx
7670 IF Vyrn=3 THEN Vy=Kyxx
7680 IF Vyrn=5 THEN Vy=Cyxx
7690 IF Vyrn=6 THEN Vy=Cyxx
7700 IF Vyrn=7 THEN Vy=Cyxx
7710 IF Vyrn=8 THEN Vy=Cxxx
7720 IF Vyrn=9 THEN Vy=Yj
7730 IF Vyrn=10 THEN Vy=Fyh
7740 IF Vyrn=11 THEN Vy=Qh
7750 IF Vyrn=12 THEN Vy=Ph
7760 PLOT Vx,Vy
7770 REM : END OF BLOCK REEB
7780 RETURN
7790 REM : BEGIN SUBROUTINE, WITHIN BLOCK AG, FOR SINGLE PAD OUTPUT.
7800 PRINT
7810 IMAGE "THIS GRAPH IS FOR :- "
7820 IMAGE "
7830 IMAGE "          HYDROSTATIC BEARING PAD NUMBER : "D
          "          HALF ANGLE FROM CENTRE LINE TO LAND CENTRE ="D.DDE"rad.
7840 IMAGE "          BEARING PAD LENGTH FROM LAND CENTRE TO LAND CENTRE ="D.DDE"m."
7850 IMAGE "          BEARING LAND WIDTH ="D.DDE"m."
7860 IMAGE "          BEARING DESIGN CLEARANCE ="D.DDE"m."
7870 IMAGE "          OPERATING PARAMETER B RATIO ="D.DDE
7880 IMAGE "          RATIO OF SUPPLY/ACCUMULATOR OIL LINE FLOW RESISTANCE ="D.DDE
7890 IMAGE "          ACCUMULATOR OPERATING PARAMETER ="D.DDE"N.m^
-5."
7900 IMAGE "          BEARING RADIUS OF CURVATURE ="D.DDE"m."
7910 IMAGE "          BEARING SUPPLY PRESSURE ="D.DDE"Pa."
7920 IMAGE "          OIL DYNAMIC VISCOSITY ="D.DDE"Pa.s
."
7930 IMAGE "          FREQUENCY OF VIBRATION ="D.DDE"rad.
s<-1."
7940 IMAGE "          RING X DISPLACEMENT ="D.DDE"m."
7950 PRINT USING 7810
7960 PRINT USING 7820;Vpn
7970 PRINT USING 7830;Ra(Vpn)
7980 PRINT USING 7840;L(Vpn)
7990 PRINT USING 7850;D(Vpn)
8000 PRINT USING 7860;C(Vpn)

```

```
8010 PRINT USING 7870;R1(Vpn)
8020 PRINT USING 7880;R2(Vpn)
8030 PRINT USING 7890;B1(Vpn)
8040 PRINT USING 7900;R
8050 PRINT USING 7910;P1
8060 PRINT USING 7920;U
8070 PRINT USING 7930;F
8080 PRINT USING 7940;Xj
8090 RETURN
8100 REM : BEGIN SUBROUTINE, WITHIN BLOCK AG, FOR HYDROSTATIC RING OUTPUT.
8110 PRINT
8120 IMAGE "THIS GRAPH IS FOR :--"
8130 IMAGE "      BEARING RADIUS OF CURVATURE ="D.DDE"m."
8140 IMAGE "      BEARING OIL SUPPLY PRESSURE ="D.DDE"Pa."
8150 IMAGE "      OIL DYNAMIC VISCOSITY ="D.DDE"Pa.s."
8160 IMAGE "      FREQUENCY OF VIBRATION ="D.DDE"rad.s^-1."
8170 IMAGE "      RING X DISPLACEMENT ="D.DDE"m."
8180 PRINT USING 8120
8190 PRINT USING 8130;R
8200 PRINT USING 8140;P1
8210 PRINT USING 8150;U
8220 PRINT USING 8160;F
8230 PRINT USING 8170;Xj
8240 RETURN
```

B-11 Two-Oil-Film Bearing Program

This program accepts as input data bearing dynamic oil film coefficients for two individual bearings positioned in series with each other in a manner similar to the journal and hydrostatic bearings of the proposed design. The program then determines net oil film coefficients for the combined bearing and these are output in tabular form. The method of analysis used is described in section 4.4.



```

10 OPTION BASE 1
20 DIM Hdbm(1:4,1:4),Hsbm(1:4,1:4),Invj(1:4,1:4),Invh(1:4,1:4),
Obsm(1:4,1:4)
30 REM : START BLOCK A
40 REM : START BLOCK AA
50 PRINT "2 - OIL - FILM BEARING PROGRAM";LIN(0)
60 PRINT "-----";LIN(1)
70 PRINT " THIS PROGRAM IS USED TO 'ADD' TOGETHER SETS OF HYDRODYNAMIC BEAR
ING OIL FILM COEFFICIENTS AND HYDROSTATIC BEARING OIL FILM COEFFICIENTS, BOTH ";
80 PRINT "SETS OF";LIN(0)
90 PRINT "COEFFICIENTS BEING INPUT DATA, AND PRODUCE AN OVERALL SET OF BEARING
";LIN(0)
100 PRINT "COEFFICIENTS, WHICH IS APPLICABLE TO THE COMBINED 2-OIL-FILM BEARING
";LIN(0)
110 PRINT
120 PRINT "SELECT THE FORM OF OUTPUT THAT YOU REQUIRE BY TYPING THE APPROPRIATE
NUMBER: -";LIN(1)
130 PRINT "1 : TABULAR OUTPUT";LIN(0)
140 PRINT "2 : GRAPHICAL OUTPUT";LIN(1)
150 INPUT Cv1
160 IF Cv1<1 THEN GOTO 120
170 IF Cv1>2 THEN GOTO 120
180 REM : END OF BLOCK AA
190 REM : START BLOCK AB
200 DISP "HOW MANY SETS OF COEFFICIENTS DO YOU WISH TO PROCESS";
210 INPUT Ncoeff
220 IF Ncoeff<1 THEN GOTO 200
230 PRINT "SELECT THE PARAMETER WITH WHICH THE SETS OF COEFFICIENTS VARY BY TYP
ING THE";LIN(1);"APPROPRIATE NUMBER : -";LIN(1)
240 PRINT "1 : LOAD / KN.";LIN(0)
250 PRINT "2 : FREQUENCY / rad.s^-1.";LIN(1)
260 INPUT Cv2
270 IF Cv2<1 THEN GOTO 230
280 IF Cv2>2 THEN GOTO 230
290 IF Cv2=2 THEN GOTO 350
300 DISP "INPUT THE FREQUENCY (IN rad.s^-1.) TO WHICH THE INPUT COEFFICIENTS AP
PLY";
310 INPUT F
320 IMAGE "USING FREQUENCY ="MD.DDE"rad.s^-1"
330 PRINT USING 320;F

```

```

340 PRINT "-----";LIN(2)
350 PRINT "INPUT THE HYDRODYNAMIC BEARING COEFFICIENTS IN THE FOLLOWING FORMAT
: ";LIN(0)
360 PRINT "LOAD (OR FREQUENCY), Kyy, Kyx, Kxy, Kxx, Cyy, Cyx, Cxx.";LIN(0)
370 PRINT "EACH ITEM OF DATA SHOULD BE SEPARATED BY A COMMA. UNITS ARE : LOAD/N
, FREQUENCY/rad.s^-1., Kij/N.m^-1., Cij/N.s.m^-1..INPUT THE DATA ONE LINE AT";
380 PRINT " A TIME, ";LIN(1);"BEGINNING EACH LINE WITH A NEW LOAD (OR FREQUENCY)
.";LIN(2)
390 FOR I=1 TO Nocoef
400 INPUT Jbsm(I,1),Jbsm(I,2),Jbsm(I,3),Jbsm(I,4),Jbsm(I,5),Jbsm(I,6),Jbsm(I,7)
,Jbsm(I,8),Jbsm(I,9)
410 NEXT I
420 REM : END OF BLOCK AB
430 REM : START BLOCK AC
440 PRINT "USING THE FOLLOWING JOURNAL BEARING DATA : -";LIN(0)
450 PRINT "-----";LIN(1)
460 IF Cv2=2 THEN GOTO 620
470 IMAGE 4X"LOAD / N."7X"Kyy/N.m^-1."4X"Kyx/N.m^-1."4X"Kxy/N.m^-1."4X"Kxx/N.m^-1."
480 PRINT USING 470
490 FOR I=1 TO Nocoef
500 IMAGE 3X,MD.DDE,6X,MD.DDE,6X,MD.DDE,6X,MD.DDE,6X,MD.DDE,6X,MD.DDE
510 PRINT USING 500;Jbsm(I,1);Jbsm(I,2);Jbsm(I,3);Jbsm(I,4);Jbsm(I,5)
520 NEXT I
530 PRINT LIN(0)
540 IMAGE 4X"LOAD/N."8X"Cyy/N.s.m^-1."2X"Cyx/N.s.m^-1."2X"Cxy/N.s.m^-1."2X"Cxx/
N.s.m^-1."
550 PRINT USING 540
560 FOR I=1 TO Nocoef
570 IMAGE 3X,MD.DDE,6X,MD.DDE,6X,MD.DDE,6X,MD.DDE,6X,MD.DDE
580 PRINT USING 570;Jbsm(I,1);Jbsm(I,6);Jbsm(I,7);Jbsm(I,8);Jbsm(I,9)
590 NEXT I
600 PRINT LIN(2)
610 GOTO 760
620 IMAGE "FREQUENCY/rad.s^-1."1X"Kyy/N.m^-1."4X"Kyx/N.m^-1."4X"Kxy/N.m^-1."4X"
Kxx/N.m^-1."
630 PRINT USING 620
640 FOR I=1 TO Nocoef
650 IMAGE 3X,MD.DDE,6X,MD.DDE,6X,MD.DDE,6X,MD.DDE,6X,MD.DDE,6X,MD.DDE
660 PRINT USING 650;Jbsm(I,1);Jbsm(I,2);Jbsm(I,3);Jbsm(I,4);Jbsm(I,5)

```

```

670 NEXT I
680 PRINT LIN(0)
690 IMAGE "FREQUENCY/rad.s^-1."1X"Cyy/N.s.m^-1."2X"Cxy/N.s.m^-1."2X"Cxx/N.s.m^-1."
700 PRINT USING 690
710 FOR I=1 TO Nocoef
720 IMAGE 3X,MD.DDE,8X,MD.DDE,6X,MD.DDE,6X,MD.DDE,6X,MD.DDE,6X,MD.DDE
730 PRINT USING 570;Jbsm(I,1);Jbsm(I,6);Jbsm(I,7);Jbsm(I,8);Jbsm(I,9)
740 NEXT I
750 PRINT LIN(1)
760 REM : END OF BLOCK AC
770 REM : START BLOCK AD
780 PRINT "INPUT THE HYDROSTATIC BEARING OIL FILM COEFFICIENTS IN THE SAME FORM
AT AS THAT WITH WHICH THE JOURNAL BEARING OIL FILM COEFFICIENTS WERE ";LIN(0)
790 PRINT "INPUT, BEGINNING EACH LINE WITH A NEW VALUE OF LOAD (OR FREQUENCY)";
LIN(1)
800 FOR I=1 TO Nocoef
810 INPUT Hbsm(I,1),Hbsm(I,2),Hbsm(I,3),Hbsm(I,4),Hbsm(I,5),Hbsm(I,6),Hbsm(I,7)
,Hbsm(I,8),Hbsm(I,9)
820 NEXT I
830 REM : END OF BLOCK AD
840 REM : START BLOCK AE
850 PRINT "USING THE FOLLOWING HYDROSTATIC BEARING DATA :-";LIN(0)
860 PRINT "-----";LIN(1)
870 IF CV2=2 THEN GOTO 1030
880 IMAGE 4X"LOAD / N."7X"Kyy/N.m^-1."4X"Kyx/N.m^-1."4X"Kxy/N.m^-1."4X"Kxx/N.m^-1."
890 PRINT USING 880
900 FOR I=1 TO Nocoef
910 IMAGE 3X,MD.DDE,8X,MD.DDE,6X,MD.DDE,6X,MD.DDE,6X,MD.DDE,6X,MD.DDE
920 PRINT USING 910;Hbsm(I,1);Hbsm(I,2);Hbsm(I,3);Hbsm(I,4);Hbsm(I,5)
930 NEXT I
940 PRINT LIN(0)
950 IMAGE 4X"LOAD / N."6X"Cyy/N.s.m^-1."2X"Cyx/N.s.m^-1."2X"Cxy/N.s.m^-1."2X"Cx
x/N.s.m^-1."
960 PRINT USING 950
970 FOR I=1 TO Nocoef
980 IMAGE 3X,MD.DDE,8X,MD.DDE,6X,MD.DDE,6X,MD.DDE,6X,MD.DDE,6X,MD.DDE
990 PRINT USING 980;Hbsm(I,1);Hbsm(I,6);Hbsm(I,7);Hbsm(I,8);Hbsm(I,9)
1000 NEXT I

```

```
1010 PRINT LIN(1)
1020 GOTO 1170
1030 IMAGE "FREQUENCY/rad.s^-1. "1X"Kyy/N.m^-1. "4X"Kyx/N.m^-1. "4X"Kxy/N.m^-1. "4X"
Kxx/N.m^-1."
1040 PRINT USING 1030
1050 FOR I=1 TO Nocoef
1060 IMAGE 3X,MD.DDE,6X,MD.DDE,6X,MD.DDE,6X,MD.DDE,6X,MD.DDE
1070 PRINT USING 1060;Hbsm(I,1);Hbsm(I,2);Hbsm(I,3);Hbsm(I,4);Hbsm(I,5)
1080 NEXT I
1090 PRINT LIN(0)
1100 IMAGE "FREQUENCY/rad.s^-1. "1X"Cyy/N.s.m^-1. "2X"Cyx/N.s.m^-1. "2X"Cxy/N.s.m^-
1. "2X"Cxx/N.s.m^-1."
1110 PRINT USING 1100
1120 FOR I=1 TO Nocoef
1130 IMAGE 3X,MD.DDE,6X,MD.DDE,6X,MD.DDE,6X,MD.DDE,6X,MD.DDE
1140 PRINT USING 570;Hbsm(I,1);Hbsm(I,6);Hbsm(I,7);Hbsm(I,8);Hbsm(I,9)
1150 NEXT I
1160 PRINT LIN(1)
1170 REM : END OF BLOCK RE
1180 IF CV1=1 THEN GOTO 3280
1190 REM : START BLOCK AF
1200 REM : START BLOCK AFA
1210 PRINT "THE CHOICE OF PARAMETERS TO BE PLOTTED AGAINST EACH OTHER IS : -";LIN
(1)
1220 PRINT "1 : Kyy";LIN(1)
1230 PRINT "2 : Kyx";LIN(1)
1240 PRINT "3 : Kxy";LIN(1)
1250 PRINT "4 : Kxx";LIN(1)
1260 PRINT "5 : Cyy";LIN(1)
1270 PRINT "6 : Cyx";LIN(1)
1280 PRINT "7 : Cxy";LIN(1)
1290 PRINT "8 : Cxx";LIN(1)
1300 PRINT "9 : LOAD ( OR FREQUENCY )";LIN(1)
1310 PRINT "SELECT OUTPUT DESIRED BY TYPING IN THE APPROPRIATE NUMBER";LIN(1)
1320 DISP "WHICH X AXIS VARIABLE DO YOU REQUIRE";
1330 INPUT Vxn
1340 IF Vxn<1 THEN GOTO 1310
1350 IF Vxn>9 THEN GOTO 1310
1360 DISP "WHICH Y AXIS VARIABLE DO YOU REQUIRE";
1370 INPUT Vyn
```

```
1380 IF Vyn<1 THEN GOTO 1310
1390 IF Vyn>9 THEN GOTO 1310
1400 REM : END OF BLOCK AFA
1410 REM : START BLOCK AFB
1420 DISP "WHAT MINIMUM VALUE OF X SCALE DO YOU REQUIRE";
1430 INPUT Sxmin
1440 DISP "WHAT MAXIMUM VALUE OF X SCALE DO YOU REQUIRE";
1450 INPUT Sxmax
1460 IF Sxmax<=Sxmin THEN GOTO 1420
1470 DISP "WHAT MINIMUM VALUE OF Y SCALE DO YOU REQUIRE";
1480 INPUT Symin
1490 DISP "WHAT MAXIMUM VALUE OF Y SCALE DO YOU REQUIRE";
1500 INPUT Symax
1510 IF Symax<=Symin THEN GOTO 1470
1520 PRINT PAGE
1530 GRAPHICS
1540 PLOTTER IS 13,"GRAPHICS"
1550 SCALE Sxmin,Sxmax,Symin,Symax
1560 Xint=0
1570 IF Sxmin>0 THEN Xint=Sxmin
1580 IF Sxmax<0 THEN Xint=Sxmax
1590 Yint=0
1600 IF Symin>0 THEN Yint=Symin
1610 IF Symax<0 THEN Yint=Symax
1620 AXES (Sxmax-Sxmin)/40,(Symax-Symin)/40,Xint,Yint,5,5
1630 FRAME
1640 REM : END OF BLOCK AFB
1650 REM : START BLOCK AFC
1660 REM : START BLOCK AFCA
1670 LDIR 0
1680 CSIZE 2
1690 IF Xint>(Sxmax+Sxmin)/2 THEN GOTO 1790
1700 IF Yint>(Symax+Symin)/2 THEN GOTO 1750
1710 MOVE Xint+(Sxmax-Sxmin)/5,Yint+(Symax-Symin)/40
1720 LORG 1
1730 Xgraph=1
1740 GOTO 1890
1750 MOVE Xint+(Sxmax-Sxmin)/5,Yint-(Symax-Symin)/40
1760 LORG 3
1770 Xgraph=2
```

```
1780 GOTO 1890
1790 IF Yint<(Symax+Symin)/2 THEN GOTO 1840
1800 MOVE Xint-(Sxmax-Sxmin)/5,Yint+(Symax-Symin)/40
1810 LORG 7
1820 Xgraph=3
1830 GOTO 1890
1840 MOVE Xint-(Sxmax-Sxmin)/5,Yint-(Symax-Symin)/40
1850 LORG 9
1860 Xgraph=4
1870 REM : END OF BLOCK AFCA
1880 REM : START BLOCK AFCA
1890 IF Vxn<>1 THEN GOTO 1910
1900 LABEL USING "13A";"Kyy / N.m^-1."
1910 IF Vxn<>2 THEN GOTO 1930
1920 LABEL USING "13A";"Kyx / N.m^-1."
1930 IF Vxn<>3 THEN GOTO 1950
1940 LABEL USING "13A";"Kxy / N.m^-1."
1950 IF Vxn<>4 THEN GOTO 1970
1960 LABEL USING "13A";"Kxx / N.m^-1."
1970 IF Vxn<>5 THEN GOTO 1990
1980 LABEL USING "15A";"Cyy / N.s.m^-1."
1990 IF Vxn<>6 THEN GOTO 2010
2000 LABEL USING "15A";"Cyx / N.s.m^-1."
2010 IF Vxn<>7 THEN GOTO 2030
2020 LABEL USING "15A";"Cxy / N.s.m^-1."
2030 IF Vxn<>8 THEN GOTO 2050
2040 LABEL USING "15A";"Cxx / N.s.m^-1."
2050 IF Vxn<>9 THEN GOTO 2100
2060 IF Cv2<>1 THEN GOTO 2080
2070 LABEL USING "9A";"LOAD / N."
2080 IF Cv2<>2 THEN GOTO 2100
2090 LABEL USING "21A";"FREQUENCY / rad.s^-1."
2100 REM : END OF BLOCK AFCA
2110 REM : START BLOCK AFCA
2120 LDIR PI/2
2130 IF Xgraph=1 THEN GOTO 2320
2140 IF Xgraph=3 THEN GOTO 2320
2150 IF Sxmin<>Xint THEN GOTO 2190
2160 MOVE Xint+(Sxmax-Sxmin)/8,Yint-(Symax-Symin)/40
2170 LORG 8
```

```
2180 LABEL USING "MD,DDE";Sxmin+(Sxmax-Sxmin)/8
2190 IF Sxmax<>Xint THEN GOTO 2230
2200 MOVE Xint-(Sxmax-Sxmin)/8,Yint-(Symax-Symin)/40
2210 LORG 8
2220 LABEL USING "MD,DDE";Sxmax-(Sxmax-Sxmin)/8
2230 IF Sxmax=Xint THEN GOTO 2270
2240 MOVE Sxmax-(Sxmax-Sxmin)/40,Yint-(Symax-Symin)/40
2250 LORG 9
2260 LABEL USING "MD,DDE";Sxmax
2270 IF Sxmin=Xint THEN GOTO 2310
2280 MOVE Sxmin+(Sxmax-Sxmin)/40,Yint-(Symax-Symin)/40
2290 LORG 7
2300 LABEL USING "MD,DDE";Sxmin
2310 GOTO 2500
2320 IF Sxmin<>Xint THEN GOTO 2360
2330 MOVE Xint+(Sxmax-Sxmin)/8,Yint+(Symax-Symin)/40
2340 LORG 2
2350 LABEL USING "MD,DDE";Sxmin+(Sxmax-Sxmin)/8
2360 IF Sxmax<>Xint THEN GOTO 2400
2370 MOVE Xint-(Sxmax-Sxmin)/8,Yint+(Symax-Symin)/40
2380 LORG 2
2390 LABEL USING "MD,DDE";Sxmax-(Sxmax-Sxmin)/8
2400 IF Sxmax=Xint THEN GOTO 2440
2410 MOVE Sxmax-(Sxmax-Sxmin)/40,Yint+(Symax-Symin)/40
2420 LORG 3
2430 LABEL USING "MD,DDE";Sxmax
2440 IF Sxmin=Xint THEN GOTO 2500
2450 MOVE Sxmin+(Sxmax-Sxmin)/40,Yint+(Symax-Symin)/40
2460 LORG 1
2470 LABEL USING "MD,DDE";Sxmin
2480 REM : END OF BLOCK AFCC
2490 REM : START BLOCK AFCD
2500 LDIR PI/2
2510 IF Xgraph<>1 THEN GOTO 2550
2520 MOVE Xint+(Sxmax-Sxmin)/40,Yint+(Symax-Symin)/5
2530 LORG 3
2540 GOTO 2670
2550 IF Xgraph<>2 THEN GOTO 2590
2560 MOVE Xint+(Sxmax-Sxmin)/40,Yint-(Symax-Symin)/5
2570 LORG 9
```

```
2580 GOTO 2670
2590 IF Xgraph<>3 THEN GOTO 2630
2600 MOVE Xint-(Sxmax-Sxmin)/40, Yint+(Symax-Symin)/5
2610 LORG 1
2620 GOTO 2670
2630 MOVE Xint-(Sxmax-Sxmin)/40, Yint-(Symax-Symin)/5
2640 LORG 7
2650 REM : END OF BLOCK AFCD
2660 REM : START BLOCK AFCE
2670 IF Vym<>1 THEN GOTO 2690
2680 LABEL USING "13A";"Kyy / N.m^-1."
2690 IF Vym<>2 THEN GOTO 2710
2700 LABEL USING "13A";"Kyx / N.m^-1."
2710 IF Vym<>3 THEN GOTO 2730
2720 LABEL USING "13A";"Kxy / N.m^-1."
2730 IF Vym<>4 THEN GOTO 2750
2740 LABEL USING "13A";"Kxx / N.m^-1."
2750 IF Vym<>5 THEN GOTO 2770
2760 LABEL USING "15A";"Cyy / N.s.m^-1."
2770 IF Vym<>6 THEN GOTO 2790
2780 LABEL USING "15A";"Cyx / N.s.m^-1."
2790 IF Vym<>7 THEN GOTO 2810
2800 LABEL USING "15A";"Cxy / N.s.m^-1."
2810 IF Vym<>8 THEN GOTO 2830
2820 LABEL USING "15A";"Cxx / N.s.m^-1."
2830 IF Vym<>9 THEN GOTO 2900
2840 IF Cv2<>1 THEN GOTO 2860
2850 LABEL USING "9A";"LOAD / N."
2860 IF Cv2<>2 THEN GOTO 2900
2870 LABEL USING "21A";"FREQUENCY / rad.s^-1."
2880 REM : END OF BLOCK AFCE
2890 REM : START BLOCK AFCE
2900 LDIR 0
2910 IF Xgraph>2 THEN GOTO 3090
2920 IF Symax<>Yint THEN GOTO 2960
2930 MOVE Xint+(Sxmax-Sxmin)/40, Symax-(Symax-Symin)/8
2940 LORG 2
2950 LABEL USING "MD.IDE";Symax-(Symax-Symin)/8
2960 IF Symin<>Yint THEN GOTO 3000
2970 MOVE Xint+(Sxmax-Sxmin)/40, Symin+(Symax-Symin)/8
```



```

2980 LORG 2
2990 LABEL USING "MD.DDE";Symin+(Symax-Symin)/8
3000 IF Symax=Yint THEN GOTO 3040
3010 MOVE Xint+(Sxmax-Sxmin)/40,Symax-(Symax-Symin)/40
3020 LORG 3
3030 LABEL USING "MD.DDE";Symax
3040 IF Symin=Yint THEN GOTO 3080
3050 MOVE Xint+(Sxmax-Sxmin)/40,Symin+(Symax-Symin)/40
3060 LORG 1
3070 LABEL USING "MD.DDE";Symin
3080 GOTO 3270
3090 IF Symax<>Yint THEN GOTO 3130
3100 MOVE Xint-(Sxmax-Sxmin)/40,Symax-(Symax-Symin)/8
3110 LORG 8
3120 LABEL USING "MD.DDE";Symax-(Symax-Symin)/8
3130 IF Symin<>Yint THEN GOTO 3170
3140 MOVE Xint-(Sxmax-Sxmin)/40,Symin+(Symax-Symin)/8
3150 LORG 8
3160 LABEL USING "MD.DDE";Symin+(Symax-Symin)/8
3170 IF Symax=Yint THEN GOTO 3210
3180 MOVE Xint-(Sxmax-Sxmin)/40,Symax-(Symax-Symin)/40
3190 LORG 9
3200 LABEL USING "MD.DDE";Symax
3210 IF Symin=Yint THEN GOTO 3270
3220 MOVE Xint-(Sxmax-Sxmin)/40,Symin+(Symax-Symin)/40
3230 LORG 7
3240 LABEL USING "MD.DDE";Symin
3250 REM : END OF BLOCK AFCF
3260 REM : END OF BLOCK AFC
3270 REM : END OF BLOCK AF
3280 FOR M=1 TO 2
3290 IF M=1 THEN GOTO 3310
3300 IF Cv1=2 THEN GOTO 4480
3310 FOR I=1 TO Ncoeff
3320 REM START BLOCK AG
3330 REM : START BLOCK AGA
3340 IF Cv2=2 THEN F=Jbsm(I,1)
3350 Hdbm(1,1)=Hdbm(2,3)=Jbsm(I,5)
3360 Hdbm(1,2)=Jdbm(2,4)=Jbsm(I,4)
3370 Hdbm(1,3)=-Jbsm(I,9)*F

```

```
3380 Hdbm(1,4)=-Jbsm(I,8)*F
3390 Hdbm(2,1)=Jbsm(I,9)*F
3400 Hdbm(2,2)=Jbsm(I,8)*F
3410 Hdbm(3,1)=Hdbm(4,3)=Jbsm(I,3)
3420 Hdbm(3,2)=Hdbm(4,4)=Jbsm(I,2)
3430 Hdbm(3,3)=-Jbsm(I,7)*F
3440 Hdbm(3,4)=-Jbsm(I,6)*F
3450 Hdbm(4,1)=Jbsm(I,7)*F
3460 Hdbm(4,2)=Jbsm(I,6)*F
3470 Dvj=DET(Hdbm)
3480 REM : END OF BLOCK AGA
3490 REM : START BLOCK AGB
3500 Hsbm(1,1)=Hsbm(2,3)=Hsbm(I,5)
3510 Hsbm(1,2)=Hsbm(2,4)=Hsbm(I,4)
3520 Hsbm(1,3)=-Hsbm(I,9)*F
3530 Hsbm(1,4)=-Hsbm(I,8)*F
3540 Hsbm(2,1)=Hsbm(I,9)*F
3550 Hsbm(2,2)=Hsbm(I,8)*F
3560 Hsbm(3,1)=Hsbm(4,3)=Hsbm(I,3)
3570 Hsbm(3,2)=Hsbm(4,4)=Hsbm(I,2)
3580 Hsbm(3,3)=-Hsbm(I,7)*F
3590 Hsbm(3,4)=-Hsbm(I,6)*F
3600 Hsbm(4,1)=Hsbm(I,7)*F
3610 Hsbm(4,2)=Hsbm(I,6)*F
3620 Dth=DET(Hsbm)
3630 REM : END OF BLOCK AGB
3640 IF Dvj=0 THEN GOTO 3820
3650 IF Dth=0 THEN GOTO 3820
3660 REM : START BLOCK AGC
3670 MAT Invj=INV(Hdbm)
3680 MAT Invhs=INV(Hsbm)
3690 MAT Invo=Invj+Invhs
3700 MAT Obsm=INV(Invo)
3710 REM : END OF BLOCK AGC
3720 REM : START BLOCK AGD
3730 Obm(I,2)=Obsm(4,4)
3740 Obm(I,3)=Obsm(4,3)
3750 Obm(I,4)=Obsm(1,2)
3760 Obm(I,5)=Obsm(1,1)
3770 Obm(I,6)=Obsm(4,2)/F
```

```

3780 Obm(I,7)=Obsm(4,1)/F
3790 Obm(I,8)=Obsm(2,2)/F
3800 Obm(I,9)=Obsm(2,1)/F
3810 REM : END OF BLOCK AGD
3820 REM : END OF BLOCK AG
3830 REM : START BLOCK AH
3840 IF Dtk<>0 THEN GOTO 3890
3850 REM : START BLOCK AHA
3860 IMAGE MD,DDE,3X"JOURNAL BEARING STIFFNESS MATRIX HAS ZERO DETERMINANT"
3870 PRINT USING 3860;Jbsm(I,1)
3880 REM : END OF BLOCK AHA
3890 IF Dtk<>0 THEN GOTO 3940
3900 REM : START BLOCK AHB
3910 IMAGE MD,DDE,3X"HYDROSTATIC BEARING STIFFNESS MATRIX HAS ZERO DETERMINANT"
3920 PRINT USING 3910;Jbsm(I,1)
3930 REM : END OF BLOCK AHB
3940 IF Dkj=0 THEN GOTO 4450
3950 IF Dth=0 THEN GOTO 4450
3960 IF Cv1=2 THEN GOTO 4260
3970 REM : START BLOCK AHC
3980 IF M=2 THEN GOTO 4020
3990 IF I>1 THEN GOTO 4020
4000 PRINT "2 - OIL - FILM BEARING COEFFICIENTS";LIN(0)
4010 PRINT "-----";LIN(1)
4020 IF I>1 THEN GOTO 4170
4030 IF Cv2=2 THEN GOTO 4110
4040 IMAGE 4X"LOAD / N."7X"Kyy/N.m^-1."4X"Kyx/N.m^-1."4X"Kxy/N.m^-1."4X"Kxx/N.m^-1."
-1."
4050 IMAGE 4X"LOAD / N."6X"Cyy/N.s.m^-1."2X"Cyx/N.s.m^-1."2X"Cxy/N.s.m^-1."2X"Cx
x/N.s.m^-1."
4060 IF M=2 THEN GOTO 4090
4070 PRINT USING 4040
4080 GOTO 4170
4090 PRINT USING 4050
4100 GOTO 4170
4110 IMAGE "FREQUENCY/rad.s^-1."1X"Kyy/N.m^-1."4X"Kyx/N.m^-1."4X"Kxy/N.m^-1."4X"
Kxx/N.m^-1."
4120 IMAGE "FREQUENCY/rad.s^-1."1X"Cyy/N.s.m^-1."2X"Cyx/N.s.m^-1."2X"Cxy/N.s.m^-
1."2X"Cxx/N.s.m^-1."
4130 IF M=2 THEN GOTO 4160

```

```
4140 PRINT USING 4110
4150 GOTO 4170
4160 PRINT USING 4120
4170 REM : END OF BLOCK AF
4180 IF CV1=2 THEN GOTO 4260
4190 IMAGE 3X,MD,DDE,8X,MD,DDE,6X,MD,DDE,6X,MD,DDE,6X,MD,DDE
4200 IF M=2 THEN GOTO 4230
4210 PRINT USING 4190;Jbzm(I,1);Obm(I,2);Obm(I,3);Obm(I,4);Obm(I,5)
4220 GOTO 4240
4230 PRINT USING 4190;Jbzm(I,1);Obm(I,6);Obm(I,7);Obm(I,8);Obm(I,9)
4240 REM : END OF BLOCK AHC
4250 GOTO 4440
4260 REM : START BLOCK AHD
4270 IF Vxn=1 THEN Vx=Obm(I,2)
4280 IF Vxn=2 THEN Vx=Obm(I,3)
4290 IF Vxn=3 THEN Vx=Obm(I,4)
4300 IF Vxn=4 THEN Vx=Obm(I,5)
4310 IF Vxn=5 THEN Vx=Obm(I,6)
4320 IF Vxn=6 THEN Vx=Obm(I,7)
4330 IF Vxn=9 THEN Vx=Jbzm(I,1)
4340 IF Vyn=1 THEN Vy=Obm(I,2)
4350 IF Vyn=2 THEN Vy=Obm(I,3)
4360 IF Vyn=3 THEN Vy=Obm(I,4)
4370 IF Vyn=4 THEN Vy=Obm(I,5)
4380 IF Vyn=5 THEN Vy=Obm(I,6)
4390 IF Vyn=6 THEN Vy=Obm(I,7)
4400 IF Vyn=7 THEN Vy=Obm(I,8)
4410 IF Vyn=8 THEN Vy=Obm(I,9)
4420 IF Vyn=9 THEN Vy=Jbzm(I,1)
4430 PLOT Vx,Vy
4440 REM : END OF BLOCK AHD
4450 REM : END OF BLOCK AH
4460 NEXT I
4470 PRINT LIN(0)
4480 NEXT M
4490 PRINT LIN(0)
4500 IF CV1=2 THEN GOTO 4520
4510 PRINT LIN(1)
4520 IF CV1=1 THEN GOTO 4610
4530 REM : START BLOCK AI
```

4540 DUMP GRAPHICS  
4550 EXIT GRAPHICS  
4560 PRINT LINK(1)  
4570 IMAGE 22X"OUTPUT FOR 2 - OIL - FILM BEARING"  
4580 PRINT USING 4570  
4590 PRINT PAGE  
4600 REM : END OF BLOCK RI  
4610 END

B-III Finite Difference Program

This program is discussed briefly in section 3.5 and was used to determine the accuracy of the mid-land type of approximation used in the theoretical analysis. The input data required is the bearing geometry, the oil pocket and drain pressures, and the node spacing required for the analysis. The program calculates the net bearing supported load which can then be compared with the value computed using the mid-land approximation.

```

10 OPTION BASE 1
20 DIM V(1:78,1:79),A(1:78)
30 REM : START BLOCK AA
40 IMAGE "FINITE DIFF. PROGRAM TO SOLVE FOR PRESSURE DISTRIBUTION IN A HYDROST
ATIC BEARING"
50 IMAGE "-----"
60 PRINT USING 40
70 PRINT USING 50
80 IMAGE "THIS PROGRAM SOLVES A FINITE DIFFERENCE MESH, WHOSE NODAL SPACING IN
THE X AND Y DIRECTIONS IS I AND J RESPECTIVELY, AND WHICH IS 'L' SHAPED, FOR"
90 IMAGE "PRESSURE AT EACH NODE. FOR MORE INFORMATION ABOUT MESH GEOMETRY SEE P
ROGRAM DOCUMENTATION."
100 IMAGE "*** WARNING *** - THIS PROGRAM ONLY SUITABLE FOR MESHES HAVING LESS
THAN 79 NODES WHEN USED WITH HP9845A"
110 PRINT USING 80
120 PRINT USING 90
130 PRINT LIN(1)
140 PRINT USING 100
150 PRINT LIN(1)
160 REM : END OF BLOCK AA
170 REM : START BLOCK AB
180 IMAGE "INPUT THE HYDROSTATIC BEARING DETAILS IN THE FOLLOWING ORDER, SEPAR
ATING EACH ITEM OF DATA WITH A COMMA :- LENGTH OF BEARING (OUTSIDE LANDS), "
190 IMAGE "WIDTH OF BEARING (OUTSIDE LANDS), LAND WIDTH, POCKET PRESSURE, AND D
RAIN PRESSURE. ALL DIMENSIONS IN cm. END Pa. AS APPROPRIATE."
200 PRINT USING 180
210 PRINT USING 190
220 PRINT LIN(1)
230 INPUT Ls,B,W,Pp,Pd
240 IF Ls<0 THEN 200
250 IF B<0 THEN 200
260 IF W<0 THEN 200
270 IF W>Ls/2 THEN 200
280 IF W>B/2 THEN 200
290 IF Pd>Pp THEN 200
300 IMAGE "USING FOLLOWING DATA :-"
310 IMAGE "LENGTH OF BEARING = "MD.DDE"cm."
320 IMAGE "WIDTH OF BEARING = "MD.DDE"cm."
330 IMAGE "LAND WIDTH = "MD.DDE"cm."

```

```
340 IMAGE "POCKET PRESSURE = "MD,DDE"Pa."
350 IMAGE "DRAIN PRESSURE = "MD,DDE"Pa."
360 PRINT USING 300
370 PRINT USING 310;Le
380 PRINT USING 320;B
390 PRINT USING 330;W
400 PRINT USING 340;Pp
410 PRINT USING 350;Pd
420 PRINT LIN(2)
430 X2=Le/2
440 X1=X2-W
450 Y2=B/2
460 Y1=Y2-W
470 REM : END OF BLOCK AB
480 REM : START BLOCK AC
490 IMAGE "NOTE : NODE SPACING MUST BE SUCH THAT AN INTEGER NUMBER OF NODE SPAC
ES CAN FIT INTO THE MESH AREA PRECISELY. VULGAR FRACTIONS ARE NOT ALLOWED"
500 PRINT USING 490
510 DISP "WHAT X DIRECTION NODE SPACING DO YOU REQUIRE";
520 INPUT H
530 DISP "WHAT Y DIRECTION NODE SPACING DO YOU REQUIRE";
540 INPUT K
550 Nn=(Y2/K+1)*(X2/H+1)-X1/H*Y1/K
560 REDIM V(1:Nn,1:Nn+1),A(1:Nn)
570 L=0
580 REM : END OF BLOCK AC
590 FOR X=H TO X2-H STEP H
600 FOR Y=K TO Y2-K STEP K
610 IF Y>Y1 THEN 640
620 IF X>X1 THEN 640
630 GOTO 940
640 REM : START BLOCK AD
650 I=X/H
660 J=Y/K
670 L=L+1
680 Ii=I-1
690 Ji=J
700 Yi=Y
710 GOSUB 4700
720 V(L,In)=K^2
```



```
730 Ii=I
740 Ji=J
750 Yi=Y
760 GOSUB 4700
770 V(L,In)=-2*K^2-2*H^2
780 Ii=I+1
790 Ji=J
800 Yi=Y
810 GOSUB 4700
820 V(L,In)=K^2
830 Ii=I
840 Ji=J-1
850 Yi=Y-K
860 GOSUB 4700
870 V(L,In)=H^2
880 Ii=I
890 Ji=J+1
900 Yi=Y+K
910 GOSUB 4700
920 V(L,In)=H^2
930 REM : END OF BLOCK AD
940 NEXT Y
950 NEXT X
960 REM : START BLOCK AE
970 Y=0
980 FOR X=X1+H TO X2-H STEP H
990 I=X/H
1000 J=0
1010 L=L+1
1020 Ii=I-1
1030 Ji=J
1040 Yi=Y
1050 GOSUB 4700
1060 V(L,In)=K^2
1070 Ii=I
1080 Ji=J
1090 Yi=Y
1100 GOSUB 4700
1110 V(L,In)=-2*K^2-2*H^2
1120 Ii=I+1
```

```
1130 Ji=J
1140 Yi=Y
1150 GOSUB 4700
1160 V(L,In)=K^2
1170 Ii=I
1180 Ji=J+1
1190 Yi=Y+K
1200 GOSUB 4700
1210 V(L,In)=2*H^2
1220 NEXT X
1230 X=X+1
1240 FOR Y=Y1+K TO Y2-K STEP K
1250 I=0
1260 J=Y/K
1270 L=L+1
1280 Ii=I
1290 Ji=J
1300 Yi=Y
1310 GOSUB 4700
1320 V(L,In)=-2*K^2-2*H^2
1330 Ii=I+1
1340 Ji=J
1350 Yi=Y
1360 GOSUB 4700
1370 V(L,In)=2*K^2
1380 Ii=I
1390 Ji=J-1
1400 Yi=Y-K
1410 GOSUB 4700
1420 V(L,In)=H^2
1430 Ii=I
1440 Ji=J+1
1450 Yi=Y+K
1460 GOSUB 4700
1470 V(L,In)=H^2
1480 NEXT Y
1490 X=X+1
1500 FOR Y=0 TO Y1 STEP K
1510 I=X/H
1520 J=Y/K
```

```
1530 L=L+1
1540 I=I
1550 J=J
1560 Y=Y
1570 GOSUB 4700
1580 V(L,In)=I
1590 V(L,In+1)=Pp
1600 NEXT Y
1610 Y=Y+1
1620 FOR X=0 TO X1-H STEP H
1630 I=X/H
1640 J=Y/K
1650 L=L+1
1660 I=I
1670 J=J
1680 Y=Y
1690 GOSUB 4700
1700 V(L,In)=I
1710 V(L,In+1)=Pp
1720 NEXT X
1730 X=X+2
1740 FOR Y=0 TO Y2 STEP K
1750 I=X/H
1760 J=Y/K
1770 L=L+1
1780 I=I
1790 J=J
1800 Y=Y
1810 GOSUB 4700
1820 V(L,In)=I
1830 V(L,In+1)=Pd
1840 NEXT Y
1850 Y=Y+2
1860 FOR X=0 TO X2-H STEP H
1870 I=X/H
1880 J=Y/K
1890 L=L+1
1900 I=I
1910 J=J
1920 Y=Y
```

```

1930 GOSUB 4700
1940 V(L,In)=1
1950 V(L,Nn+1)=Pd
1960 NEXT X
1970 REM : END OF BLOCK RE
1980 REM : START BLOCK AF
1990 REM : SUBROUTINE TO SOLVE SIMULTANEOUS EQUATIONS
2000 REM : THE COEFFICIENTS OF THE N EQUATIONS ARE THE MATRIX V(N,N+1)
2010 REM : THE ANSWERS ARE THE MATRIX A(N)
2020 REM : THE SUFFICES S ARE TO DISTINGUISH SUB-VARIABLES OF THIS SUBROUTINE FR
OM MAIN VARIABLES OF PROGRAM - THE TWO ARE NOT RELATED
2030 Xs=0
2040 N=Nn
2050 FOR Qs=1 TO N-1
2060 Bs=V(Qs,Qs)
2070 Ds=0
2080 FOR Is=Qs+1 TO N
2090 Gs=V(Is,Qs)
2100 IF ABS(Gs)>ABS(Bs) THEN 2120
2110 GOTO 2180
2120 Xs=Xs
2130 Ds=1
2140 Ms=Is
2150 Bs=Gs
2160 REM : Ds IS 1 IF A ROW INTERCHANGE IS REQUIRED
2170 REM : Ms IS THE ROW WITH THE LARGEST ELEMENT
2180 NEXT Is
2190 IF Ds<>1 THEN 2270
2200 REM : INTERCHANGE ROWS IF NECESSARY
2210 FOR Zs=Qs TO N+1
2220 Cs=V(Ms,Zs)
2230 REM : Cs IS AN INTERMEDIATE VARIABLE
2240 V(Ms,Zs)=V(Qs,Zs)
2250 V(Qs,Zs)=Cs
2260 NEXT Zs
2270 Xs=0
2280 FOR Ps=Qs+1 TO N
2290 IF V(Ps,Qs)=0 THEN 2350
2300 Ps=V(Ps,Qs)/V(Qs,Qs)
2310 FOR Ns=Qs+1 TO N+1

```

```
2320 V(Ps,Ns)=V(Ps,Ns)-Fs*V(Qs,Ns)
2330 Xs=Xs
2340 NEXT Ns
2350 NEXT Ps
2360 NEXT Qs
2370 REM : CALCULATE ANSWERS BY BACK SUBSTITUTION
2380 FOR Is=N TO 1 STEP -1
2390 Rs=0
2400 FOR Js=Is+1 TO N
2410 Rs=Rs+V(Is,Js)*R(Js)
2420 NEXT Js
2430 R(Is)=(V(Is,N+1)-Rs)/V(Is,Is)
2440 NEXT Is
2450 REM : END OF SIMULTANEOUS EQUATION SOLUTION
2460 REM : END OF BLOCK AF
2470 REM : OUTPUTTING PRESSURES NOW
2480 IMAGE "NODE PRESSURES"
2490 IMAGE "-----"
2500 PRINT LIN(2)
2510 PRINT USING 2480
2520 PRINT USING 2490
2530 PRINT LIN(1)
2540 FOR I=1 TO NM
2550 IMAGE "PRESSURE AT NODE ",2D,"=",MD,DDE
2560 PRINT USING 2550;I,A(I)
2570 PRINT LIN(0)
2580 NEXT I
2590 Load=0
2600 FOR X=H TO X2-H STEP H
2610 FOR Y=K TO Y2-K STEP K
2620 IF Y>Y1 THEN GOTO 2650
2630 IF X>X1 THEN GOTO 2650
2640 GOTO 2740
2650 REM : START BLOCK AG
2660 I=X/H
2670 J=Y/K
2680 Ii=I
2690 Ji=J
2700 Yi=Y
2710 GOSUB 4700
```

```
2720 Load=Load+A(In)*H*K
2730 REM : END OF BLOCK AG
2740 NEXT Y
2750 NEXT X
2760 REM : START BLOCK AH
2770 Y=0
2780 FOR X=X1+H TO X2-H STEP H
2790 I=X/H
2800 J=0
2810 Ii=I
2820 Ji=J
2830 Yi=Y
2840 GOSUB 4700
2850 Ln1=A(In)
2860 Ii=I
2870 Ji=J+1
2880 Yi=Y+K
2890 GOSUB 4700
2900 Ln2=A(In)
2910 Load=Load+((Ln1-Ln2)*.75+Ln2)*H*K/2
2920 NEXT X
2930 X=X2
2940 FOR Y=K TO Y2-K STEP K
2950 I=X/H
2960 J=Y/K
2970 Ii=I
2980 Ji=J
2990 Yi=Y
3000 GOSUB 4700
3010 Ln1=A(In)
3020 Ii=I-1
3030 Ji=J
3040 Yi=Y
3050 GOSUB 4700
3060 Ln2=A(In)
3070 Load=Load+((Ln1-Ln2)*.75+Ln2)*H*K/2
3080 NEXT Y
3090 Y=Y2
3100 FOR X=H TO X2-H STEP H
3110 I=X/H
```

```
3120 J=Y/K
3130 I=I
3140 J=J
3150 Y=Y
3160 GOSUB 4700
3170 Ln1=A(In)
3180 I=I
3190 J=J-1
3200 Y=Y-K
3210 GOSUB 4700
3220 Ln2=A(In)
3230 Load=Load+((Ln1-Ln2)*.75+Ln2)*H*K/2
3240 NEXT X
3250 X=X+1
3260 FOR Y=Y1+K TO Y2-K STEP K
3270 I=0
3280 J=Y/K
3290 I=I
3300 J=J
3310 Y=Y
3320 GOSUB 4700
3330 Ln1=A(In)
3340 I=I+1
3350 J=J
3360 Y=Y
3370 GOSUB 4700
3380 Ln2=A(In)
3390 Load=Load+((Ln1-Ln2)*.75+Ln2)*H*K/2
3400 NEXT Y
3410 Y=Y1
3420 FOR X=H TO X1-H STEP H
3430 I=X/H
3440 J=Y/K
3450 I=I
3460 J=J
3470 Y=Y
3480 GOSUB 4700
3490 Ln1=A(In)
3500 I=I
3510 J=J+1
```

```
3520 Yi=Y+K
3530 GOSUB 4700
3540 Ln2=R(In)
3550 Load=Load+((Ln1-Ln2)*.75+Ln2)*H*K/2
3560 NEXT X
3570 X=X+1
3580 FOR Y=K TO Y1-K STEP K
3590 I=X/H
3600 J=Y/K
3610 Ii=I
3620 Ji=J
3630 Yi=Y
3640 GOSUB 4700
3650 Ln1=R(In)
3660 Ii=I+1
3670 Ji=J
3680 Yi=Y
3690 GOSUB 4700
3700 Ln2=R(In)
3710 Load=Load+((Ln1-Ln2)*.75+Ln2)*H*K/2
3720 NEXT Y
3730 REM : NOW CALCULATE LOADS SUPPORTED AT CORNER NODES
3740 X=X+1
3750 Y=0
3760 I=X/H
3770 J=Y/K
3780 Ii=I
3790 Ji=J
3800 Yi=Y
3810 GOSUB 4700
3820 Ln1=R(In)
3830 Ii=I+1
3840 Ji=J+1
3850 Yi=Y+K
3860 GOSUB 4700
3870 Ln2=R(In)
3880 Load=Load+((Ln1-Ln2)*.75+Ln2)*H*K/4
3890 X=X+2
3900 Y=0
3910 I=X/H
```



3920 J=Y/K  
3930 I=I  
3940 J=J  
3950 Y=Y  
3960 GOSUB 4700  
3970 Ln1=R(In)  
3980 I=I-1  
3990 J=J+1  
4000 Y=Y+K  
4010 GOSUB 4700  
4020 Ln2=R(In)  
4030 Load=Load+((Ln1-Ln2)\*.75+Ln2)\*H\*K/4  
4040 X=X2  
4050 Y=Y2  
4060 I=X/H  
4070 J=Y/K  
4080 I=I  
4090 J=J  
4100 Y=Y  
4110 GOSUB 4700  
4120 Ln1=R(In)  
4130 I=I-1  
4140 J=J-1  
4150 Y=Y-K  
4160 GOSUB 4700  
4170 Ln2=R(In)  
4180 Load=Load+((Ln1-Ln2)\*.75+Ln2)\*H\*K/4  
4190 X=X0  
4200 Y=Y2  
4210 I=X/H  
4220 J=Y/K  
4230 I=I  
4240 J=J  
4250 Y=Y  
4260 GOSUB 4700  
4270 Ln1=R(In)  
4280 I=I+1  
4290 J=J-1  
4300 Y=Y-K  
4310 GOSUB 4700

```
4320 Ln2=R(In)
4330 Load=Load+((Ln1-Ln2)*.75+Ln2)*H*K/4
4340 X=X0
4350 Y=Y1
4360 I=X/H
4370 J=Y/K
4380 Ii=I
4390 Ji=J
4400 Yi=Y
4410 GOSUB 4700
4420 Ln1=R(In)
4430 Ii=I+1
4440 Ji=J+1
4450 Yi=Y+K
4460 GOSUB 4700
4470 Ln2=R(In)
4480 Load=Load+((Ln1-Ln2)*.75+Ln2)*H*K/4
4490 X=X1
4500 Y=Y1
4510 I=X/H
4520 J=Y/K
4530 Ii=I
4540 Ji=J
4550 Yi=Y
4560 GOSUB 4700
4570 Ln1=R(In)
4580 Ii=I+1
4590 Ji=J+1
4600 Yi=Y+K
4610 GOSUB 4700
4620 Ln2=R(In)
4630 Load=Load+((Ln1-Ln2)*.75+Ln2)*H*K*3/4
4640 REM : END OF BLOCK AH
4650 PRINT
4660 IMAGE "NO. OF NODES =",30," LOAD =",D,DDE,"N."
4670 PRINT USING 4660;Nn,Load*4E-4+((Le-2*W)*(B-2*W))*Pp*1E-4
4680 PRINT
4690 END
4700 REM : SUBROUTINE TO DETERMINE NODE NUMBER RELATING TO COORDINATE OF A PARTI
      CULAR NODE
```

```
4710 IF Y1<Y1 THEN M=X1/H*(Ji+1)
4720 IF Y1>Y1 THEN M=X1/H*Y1/K
4730 I=(X2/H+1)*Ji+(Ii+1)-M
4740 RETURN
```

B-1Y Bearing Dynamic Oil Film Coefficient Program

This program was used in the analysis of experimental results. It accepts details of the experimentally measured vibrations of the test rig rotor as input data, and gives the dynamic oil film stiffness and damping coefficients that correspond to those vibrations as output. The theory appropriate to this program has been discussed in chapter 4.

```

10 OPTION BASE 1
20 DIM Y(1:8,1:8),Yt(1:8,1:8),B(1:8),An(1:8)
30 PRINTER IS 0
40 PRINT
50 PRINT
60 PRINT TAB(10),"BEARING COEFFICIENT CALCULATIONS"
70 PRINT
80 INPUT "PED. FORWARD X VIB'N. AMP. & PHASE ( m & Degrees ) ?",Xpf0,Gf1
90 INPUT "PED. FORWARD Y VIB'N. AMP. & PHASE ( m & Degrees ) ?",Ypf0,Gf2
100 INPUT "SHAFT FORWARD X VIB'N. AMP. & PHASE ( m & Degrees ) ?",Xf0,Af1
110 INPUT "SHAFT FORWARD Y VIB'N. AMP. & PHASE ( m & Degrees ) ?",Yf0,Af2
120 INPUT "PED. REVERSE X VIB'N. AMP. & PHASE ( m & Degrees ) ?",Xpr0,Gr1
130 INPUT "PED. REVERSE Y VIB'N. AMP. & PHASE ( m & Degrees ) ?",Ypr0,Gr2
140 INPUT "SHAFT REVERSE X VIB'N. AMP. & PHASE ( m & Degrees ) ?",Xr0,Ar1
150 INPUT "SHAFT REVERSE Y VIB'N. AMP. & PHASE ( m & Degrees ) ?",Yr0,Ar2
160 INPUT "ROTOR MASS IN Kg. ?",M
170 INPUT "EXCITATION FREQUENCY IN rad./s. ?",F
180 INPUT "HORIZONTAL FORCE AMPLITUDE IN N.?",Fx0
190 INPUT "VERTICAL FORCE AMPLITUDE IN N.?",Fy0
200 DEG
210 Y(1,1)=Y(2,3)=Y(3,5)=Y(4,7)=Xf0*SIN(Af1)
220 Y(1,2)=Y(2,4)=Yf0*COS(Af2)
230 Y(3,6)=Y(4,8)=-Yf0*COS(Af2)
240 Y(1,5)=Y(2,7)=Xf0*COS(Af1)
250 Y(3,1)=Y(4,3)=-Xf0*COS(Af1)
260 Y(1,6)=Y(2,8)=Y(3,2)=Y(4,4)=Yf0*SIN(Af2)
270 Y(5,1)=Y(6,3)=Xp0*SIN(Ap1)
280 Y(7,5)=Y(8,7)=-Xp0*SIN(Ap1)
281 Y(7,6)=Y(8,8)=Yp0*COS(Ap2)
290 Y(5,2)=Y(6,4)=Yp0*COS(Ap2)
300 Y(5,5)=Y(6,7)=Y(7,1)=Y(8,3)=-Xp0*COS(Ap1)
310 Y(5,6)=Y(6,8)=-Yp0*SIN(Ap2)
320 Y(7,2)=Y(8,4)=Yp0*SIN(Ap2)
330 B(1)=-M*F^2*Xpf0*SIN(Gf1)
340 B(2)=Fy0+M*F^2*Ypf0*COS(Gf2)
350 B(3)=Fx0+M*F^2*Xpf0*COS(Gf1)
360 B(4)=M*F^2*Ypf0*SIN(Gf2)
370 B(5)=-M*F^2*Xpr0*SIN(Gr1)
380 B(6)=Fy0+M*F^2*Ypr0*COS(Gr2)
390 B(7)=Fx0+M*F^2*Xpr0*COS(Gr1)
400 B(8)=M*F^2*Ypr0*SIN(Gr2)

```

```

410 MAT Yt=INV(Y)
420 MAT An=Yt*B
430 Kxx=-An(1)+M*F^2
440 Kxy=An(2)
450 Kyx=-An(3)
460 Kyy=An(4)+M*F^2
470 Cxx=An(5)/F
480 Cxy=An(6)/F
490 Cyx=An(7)/F
500 Cyy=An(8)/F
510 PRINT TAB(10), "INPUT DATA WAS :--"
520 PRINT
530 PRINT USING "55A,MD,DDE,5A,MDDD";"PED. FORWARD X VIB'N. AMP. & PHASE (m. &
degrees.) = ",Xpf0," & ",Gf1
540 PRINT USING "55A,MD,DDE,5A,MDDD";"PED. FORWARD Y VIB'N. AMP. & PHASE (m. &
degrees.) = ",Ypf0," & ",Gf2
550 PRINT USING "55A,MD,DDE,5A,MDDD";"SHAFT FORWARD X VIB'N. AMP. & PHASE (m. &
degrees.) = ",Xf0," & ",Rf1
560 PRINT USING "55A,MD,DDE,5A,MDDD";"SHAFT FORWARD Y VIB'N. AMP. & PHASE (m. &
degrees.) = ",Yf0," & ",Rf2
570 PRINT
580 PRINT USING "55A,MD,DDE,5A,MDDD";"PED. REVERSE X VIB'N. AMP. & PHASE (m. &
degrees.) = ",Xpr0," & ",Gr1
590 PRINT USING "55A,MD,DDE,5A,MDDD";"PED. REVERSE Y VIB'N. AMP. & PHASE (m. &
degrees.) = ",Ypr0," & ",Gr2
600 PRINT USING "55A,MD,DDE,5A,MDDD";"SHAFT REVERSE X VIB'N. AMP. & PHASE (m. &
degrees.) = ",Xr0," & ",Rr1
610 PRINT USING "55A,MD,DDE,5A,MDDD";"SHAFT REVERSE Y VIB'N. AMP. & PHASE (m. &
degrees.) = ",Yr0," & ",Rr2
620 PRINT
630 PRINT USING "38A,DDDD";"ROTOR MASS ( Kg ) = ",M
640 PRINT USING "38A,DDDD";"EXCITATION FREQUENCY ( rad./s. ) = ",F
650 PRINT USING "38A,DDDD";"HORIZONTAL FORCE AMPLITUDE ( N. ) = ",Fx0
660 PRINT USING "38A,DDDD";"VERTICAL FORCE AMPLITUDE ( N. ) = ",Fy0
670 PRINT LIN(2)
680 PRINT USING "27A";"BEARING COEFFICIENTS ARE :--"
690 PRINT
700 PRINT USING "21A,MD,DDE";"Kyy ( N./m. ) = ",Kyy
710 PRINT USING "21A,MD,DDE";"Kyx ( N./m. ) = ",Kyx
720 PRINT USING "21A,MD,DDE";"Kxy ( N./m. ) = ",Kxy

```

```
730 PRINT USING "21A, MD. DDE"; "Kxx < N./m. > " = " , Kxx
740 PRINT
750 PRINT USING "21A, MD. DDE"; "Cyy < N.s./m. > " = " , Cyy
760 PRINT USING "21A, MD. DDE"; "Cyx < N.s./m. > " = " , Cyx
770 PRINT USING "21A, MD. DDE"; "Cxy < N.s./m. > " = " , Cxy
780 PRINT USING "21A, MD. DDE"; "Cxx < N.s./m. > " = " , Cxx
790 PRINT LIN(3)
800 END
```